International School for Advanced Studies - SISSA

Neurobiology Sector

Hypoglossal motoneurons: a model to investigate physiological and pathophysiological properties of brainstem motoneurons

Thesis submitted for the degree of

"Doctor Philosophiae"

Candidate:

Alessandra Cifra

Supervisor:

Prof. Andrea Nistri

SISSA, Via Bonomea 265, 34136 Trieste, Italy

Notes:

The work described in this thesis was carried out at the International School for Advanced Studies, Trieste, between November 2007 and August 2011. Data reported in the present thesis have been published in the following articles:

1) A. Cifra, F. Nani, E. Sharifullina and A. Nistri (2009) A repertoire of rhythmic bursting produced by hypoglossal motoneurones in physiological and pathological conditions. Philos Trans R Soc Lond B Biol Sci. 364: 2493-50.

2) F. Nani, A. Cifra, and A. Nistri (2010) Transient oxidative stress evokes early changes in the functional properties of neonatal rat hypoglossal motoneurons in vitro. Eur J Neurosci. 31: 951-66.

3) A. Cifra, F. Nani, and A. Nistri (2011a) Riluzole is a potent drug to protect neonatal rat hypoglossal motoneurons in vitro from glutamate-mediated excitotoxicity. Eur J Neurosci. 33: 899-913.

4) A. Cifra, F. Nani, and A. Nistri (2011b) Respiratory motoneurons and pathological conditions: lessons from hypoglossal motoneurons challenged by excitotoxic or oxidative stress. Respir Physiol Neurobiol. Epub ahead of print.

5) A. Cifra, G.L. Mazzone, F. Nani, A. Nistri and M. Mladinic (2011c) Postnatal developmental profile of neurons and glia in motor nuclei of the brainstem and spinal cord, and its comparison with organotypic slice cultures. In press.

Data reported in Cifra et al. (2009 and 2011 a,b) arises from my own experiments and data analysis (electrophysiology) and in collaboration with Dr. Francesca Nani (immunohistochemistry). As concerning the work by Nani et al. (2010) I performed and analyzed the immunohistochemical experiments on the effects of transient oxidative stress on hypoglossal motoneurons in collaboration with Dr. Francesca Nani who has collected all the electrophysiological data. Finally, I collaborated with Dr. Francesca Nani, Dr. Miranda Mladinic and Dr. Graciela L. Mazzone on the work named “Postnatal developmental profile of neurons and glia in motor nuclei of the brainstem and spinal cord” of which I performed the experiments on brainstem slices.

I thank my supervisor, Andrea Nistri, and all our collaborators for all the work which has

been done. It was a very important scientific experience, hard work but, at the end, also a pleasure.

Contents

Abbreviations

AHP, afterhyperpolarization;

ALS, amyotrophic lateral sclerosis;

AMPA, α-amino-3-hydroxy-5-methyl-4-isoxazoleproprionic acid;

APV, D-amino-phosphonovalerate;

ATF-3, activating transcription factor 3;

CHMP2B, charged multivesicular body protein 2B

CNQX, 6-cyano-7-nitroquinoxaline-2,3-dione;

CPGs, central pattern generators;

CREB, cAMP responsive element binding protein;

CSF, cerebrospinal fluid;

DHR 123, dihydrorhodamine 123;

DMRC; dorsal medullary reticular column;

EAAT2, excitatory amino acid transporter 2;

FALS, familial amyotrophic lateral sclerosis;

FUS / TLS, fused-in-sarcoma/translated-in-liposarcoma;

GABA, γ-aminobutyric acid;

GDNF, glial cell line-derived neurotrophic factor;

GFAP, glial fibrillary acidic protein;

GLT-1, glutamate transporter-1;

GluR2, glutamate receptor subunit 2;

HM, hypoglossal motoneuron;

H_2O_2, hydrogen peroxide;

HSP, heat shock protein;

5-HT, serotonin;

HVA, high-threshold activated;

IEG, immediate-early gene;

I_h, hyperpolarization-activated cationic current;

I_{CaP}, persistent calcium current;

I_{NaP}, persistent sodium current;

LVA, low-threshold activated;

mGluR, metabotrobic glutamate receptor;

NE, norepinephrine;

NGF, nerve growth factor;

NMDA, N-methyl-D-aspartate;

NO, nitric oxide;

NTS; nucleus of the solitary tract;

P0-P4, postnatal day 0-5;

PIC, persistent inward current;

REM, rapid-eye-movement;

Rho 123, rhodamine 123;

ROS, reactive oxygen species;

SALS, sporadic amyotrophic lateral sclerosis;

SOD1, superoxide dismutase 1;

SP, substance P;

TASK, TWIK-Related Acid-Sensitive K^+ channel;

TBOA, threo-β-benzyloxyaspartate;

TDP-43, TAR DNA-binding protein 43;

TRH, thyrotropin-releasing hormone;

TTX, tetrodotoxin;

VAPB, vesicle-associated membrane protein B.

Abstract

Hypoglossal motoneurons (HMs) are brainstem neurons that command rhythmic contraction of the tongue muscles during breathing as well as a variety of non-respiratory functions such as sleep, vocalization, suckling and swallowing. Neurodegenerative diseases like amyotrophic lateral sclerosis (ALS; Lou-Gehrig disease) often damage HMs with distressing symptoms like dysarthria, dysphagia and breathing failure. In addition, HM activity and its neuromodulation are crucial for the proper control of upper airway flow during sleep, whose obstruction is associated with the neurological disorder known as obstructive sleep apnea. *In vitro* preparations of the neonatal rat brainstem slice represent a useful model to investigate functional properties of HMs in physiological and pathological conditions. However, studies with these preparations need, as a prerequisite, a detailed description of the relative type (and number) of neurons and glia normally present in the tissue as well as of the effects that the experimental procedure itself (tissue slicing and maintenance *in vitro*) may have on *in vitro* cell survival, before assessing the consequences of any cell-selective/experimentally-induced damage and potential neuroprotection.

Thus, the present study investigated the cell populations of the brainstem nucleus hypoglossus during postnatal development (postnatal days 0 and 4, P0 and P4) reporting that motoneurons are the largest neuronal population and make up almost half of all cells, with the rest being mainly astroglia. Preparing brainstem slices unavoidably affected both HMs and astrocytes, with an initial loss of HM number (35 %) which, however, remained stable for up to 4 h of *in vitro* incubation in control Krebs solution. The same procedure induced time-dependent changes in the expression of the astroglial marker S100 (which labels a Ca^{2+} binding protein), as the early slicing-related fall of this signal was replaced by gradual recovery during *in vitro* incubation. Subsequent exposure of brainstem slices to excitotoxic stress (believed to occur at ALS onset) elicited by the block of glutamate uptake via threo-β-benzyloxyaspartate (TBOA, 50 μM), evoked sustained HM bursting, early (1 h) enhancement of the S100 immunostaining of astrocytes, and activated the motoneuronal stress factor ATF-3 (activating transcription factor 3), with loss (30 %) of motoneuron staining appearing after 4 h of TBOA treatment. Conversely, oxidative stress (another putative actor in ALS pathogenesis), elicited via application of hydrogen peroxide (H_2O_2, 1 mM, 30 min), induced HM membrane depolarization accompanied by an increase in input resistance, augmented

firing and depressed spontaneous synaptic events. Moreover, despite H_2O_2 enhanced intracellular oxidative processes (as shown by increased oxidation of the membrane permeable biomarker dihydrorhodamine 123), there was no early (1 h) change in HM numbers (although most cells became immunopositive for ATF-3) nor changes in S100 immunoreactivity.

With the TBOA model, early application of 5 μM riluzole (the only drug currently licensed for symptomatic ALS treatment) inhibited bursting, reversed TBOA-evoked changes in S100 immunostaining and prevented late loss of motoneuron staining.

These data show that brainstem slices are a suitable *in vitro* preparation to assess cell-specific alterations of motoneuron and glia evoked by excitotoxicity and oxidative stress. These two factors triggered distinct effects in terms of HM electrophysiological responses (long-lasting bursting and strong facilitation of network synaptic transmission versus slow depolarization and inhibition of network synaptic transmission, respectively) and cell specific alterations to motoneuron and glia; however, both induced early expression of ATF-3 distress factor. Therefore, these results suggest that excitotoxic and oxidative challenges may share a common early biochemical hallmark of distress, opening the possibility to target downstream effectors of neuronal damage for potential neuroprotection.

Introduction

1. Hypoglossal motoneurons: location, function and intrinsic properties

1.1 Location: the hypoglossal nucleus

The hypoglossal nucleus (XII cranial nucleus) is located in the medulla oblongata close to the midline immediately beneath the base of the fourth ventricle (Krammer et al., 1979). It innervates the tongue intrinsic and extrinsic muscles. The extrinsic muscles have bone attachment, and include genioglossus, styloglossus, hyoglossus, and geniohyoid muscles, whose activity control protrusion, retraction, depression and elevation of the tongue; intrinsic muscles are not attached to the bone, they are located within the body of the tongue and they are composed of vertical, transversal, superior and inferior longitudinal muscles that alter the shape of the tongue (Lowe, 1980). In the rat, HMs are somatotopically organized (Fig. 1): the ventrolateral subdivision of XII nucleus innervates the tongue protractor muscles, while the dorsal part innervates retractor muscles; HMs controlling tongue intrinsic muscles, instead, are mainly located in the medial region of the XII nucleus with the exception of the longitudinal ones, located in the ventro- and dorsolateral regions (Krammer et al, 1979; Lowe, 1980, Sokoloff and Deacon, 1992; Dobbins and Feldman, 1995). Such XII nucleus organization allows the fine control of various tongue movements during respiration, mastication, sucking and swallowing (Lowe, 1980).

Two distinct neuronal populations have been found in the hypoglossal nucleus of cats, rats and monkeys (Cooper, 1981; Boone and Aldes, 1984 ; Takasu and Hashimoto, 1988 ; Takata, 1993): motoneurons (type I) comprising the largest population, are large (25-50 μm) multipolar cells, whereas group II neurons are smaller (10-20 μm), round to oval shaped cells (Boone and Aldes, 1984). Motoneurons spread their dendrites extensively within the XII nucleus and the neighboring reticular formation (Viana et al., 1990; Altschuler et al., 1994), while group II neurons have few dendritic processes and are located at the ventral or dorsolateral regions of the nucleus (Boone and Aldes, 1984; Takasu and Haschimoto, 1988).

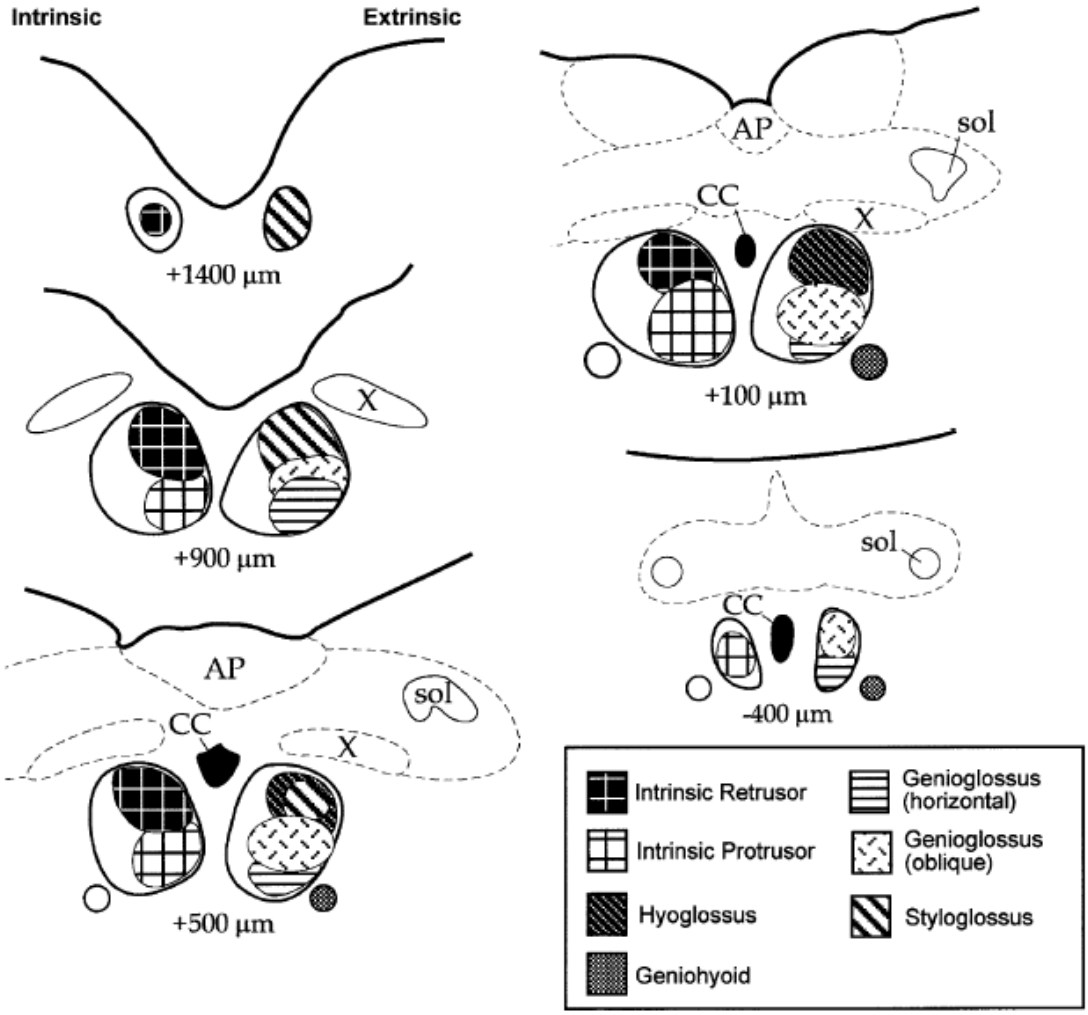

Fig. 1. Myotopic organization of the rat XII motor nucleus. Schematic drawings of the dorsomedial medulla at five distinct levels (top to bottom: rostral to caudal) expressed in mm relative to the obex (or calamus scriptorius). They represent approximate location of XII motoneurons supplying both the intrinsic (left side) and extrinsic (right side) tongue muscles. Abbreviations: X, dorsal motor nucleus of the vagus; sol, tractus solitarius; AP, area postrema; CC, central canal (modified from Gestreau et al., 2005).

According to neuroanatomical (Cooper, 1981; Boone and Aldes, 1984 ; Takasu and Hashimoto, 1988; Takata, 1993) and electrophysiological studies (Green and Negishi, 1963; Sumi, 1969; Takata,1993; Peever et al., 2002), type II hypoglossal neurons are likely to be GABAergic interneurons.

Axons of the HMs emerge from the ventrolateral aspect of the medulla and course, via the hypoglossal nerve (XII cranial nerve; Fig. 2), to innervate intrinsic and extrinsic

muscles of the tongue (Berger et al., 1996).

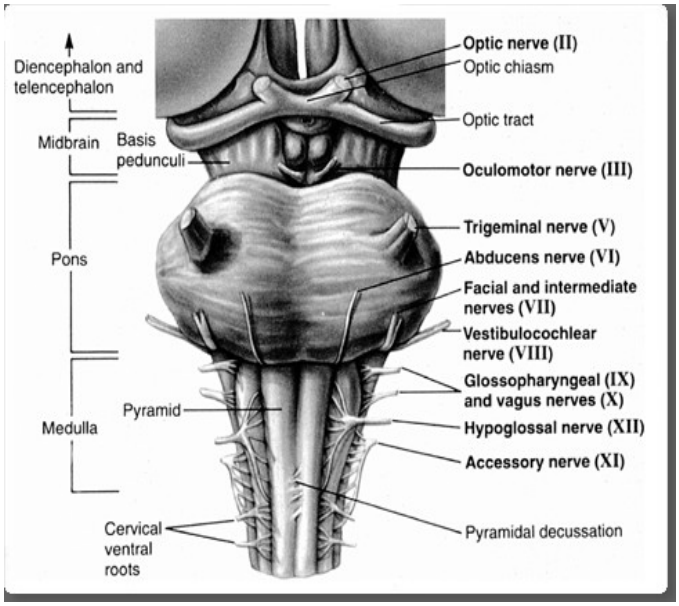

Fig. 2. Ventral view of human brainstem. The brainstem is composed of three major divisions: medulla, pons, and midbrain. The hypoglossal nerve (XII cranial nerve) originates in the medulla (adapted from Kandel et al., 1991).

Premotoneurons to the XII nucleus are located in the reticular formation, the spinal V complex, the nucleus of the solitary tract (NTS) (Borke et al., 1983), the pre-Bötzinger complex (Smith et al., 2007) and other brainstem and higher-order regions of the brain (Dobbins and Feldman, 1995; Rekling et al., 2000; Peever et al., 2002; see also Table 1). Another source of premotorneurons is represented by inspiratory interneurons within the XII nucleus itself, participating to the transmission of the respiratory drive to HMs, as demonstrated by cross-correlation analysis (Peever et al., 2002). However, the primary source of the inputs to the XII nucleus arises from the caudal reticular formation immediately ventral to the nucleus of the solitary tract (NTS), which is termed dorsal medullary reticular column (DMRC; Cunningham and Sawchenko, 2000; Fig. 3). Projections from the DMRC are largely bilateral, distributed to both dorsal and ventral subdivisions of XII nucleus, and, therefore, can simultaneously innervate both tongue protractor and retractor muscles. This arrangement shows an independent, albeit coordinated activation of antagonist muscles of the tongue (Dobbins and Feldman, 1995; Fay and Norgren, 1997; Cunningham and Sawchenko, 2000).

Motor Nuclei	Reticular Formation/ Spinal Gray	NTS	Spinal V Complex	Vestibular Nuclei	Peri-ambigual Region	Raphe Nuclei	Locus Coeruleus/ A7, A5	Pontine Nuclei	PH/ riMLF/ NIC	PAG	Location of Premotor Neuron Unknown*
XII	+ GABA, Gly	+	+ GABA, Gly		+	+ 5HT, SP,Enk	+ NE	+		+	ACh;adenosine; ADH; angiotensins II, III IV; ATP; DA; CRF; endothelin; NT; prostaglandin;PTHRP; somatostatin-28; TRH

Table 1. Major afferents input to the hypoglossal nucleus. +, Projection from premotoneurons to motoneurons; CRF, corticotropin-releasing factor; DA, dopamine; Gly, glycine; INC, interstitial nucleus of Cajal; Met-Enk, methionine-enkephalin; NKA, neurokinin A; NT, neurotensin; PTHRP, parathyroid hormone-related peptide; PAG, periaquaductal gray; PH, prepositus hypoglossi; riMLF, rostral interstitial nucleus of the medial longitudinal fasciculus; SP, substance P; TRH, thyrotropin-releasing hormone; ADH, vasopressin. Periambigual region is defined here as a region around and within the ambiguus nucleus in the ventrolateral medulla; locus coeruleus is defined as locus coeruleus and subcoeruleus nucleus; pontine nuclei include nucleus of the Kölliker-Fuse, parabrachial nucleus, pontine medial reticular formation.

* Column indicates receptor expression, immunoreactivity, or physiological effect of putative transmitters within a motor nucleus, but with unknown location of the premotor neuron somata (modified from Rekling et al., 2000).

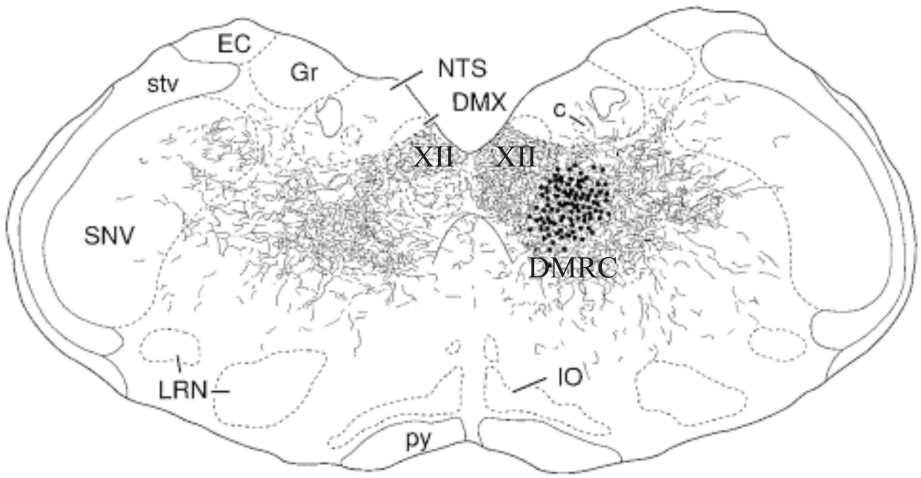

Fig. 3. Schematic representation of XII nucleus innervation. Anterograde labeling shows that hypoglossal nuclei (XII) receive inputs from dorsomedial reticular column (DMRC), where the Phaseolus vulgaris-leucoagglutinin (PHA-L) labeling dye was injected. DMRC innervates both contralateral and ipsilateral XII nuclei. Abbreviations: NTS, nucleus tractus solitarius; DMX, dorsal

motor nucleus of the vagus nerve; Gr, gracile nucleus; EC, external cuneate nucleus; stv, spinal tract of the trigeminal nucleus; SNV, spinal trigeminal nucleus; LRN, lateral reticular nucleus; py, pyramidal tract; IO, inferior olive (modified from Cunningham and Sawchenko, 2000).

1.2 Hypoglossal motoneuron function

HMs innervate tongue muscles and participate in several oropharyngeal behaviours that must be functional from birth including breathing, mastication, swallowing, suckling and protective reflexes such as coughing (Gestreau et al., 2005). Tongue muscles form (together with laryngeal and pharyngeal muscles and soft tissues) the upper airways, which subserve valve or airway stability functions during breathing and respiration-related activities (Berger, 2000; Feldman and Del Negro, 2006): these behaviours require rhythmic contractions with appropriate muscle coordination to allow dynamic changes in airway size without obstruction of the upper airways by the tongue (Horner, 2008). HMs are not endowed with spontaneous activity: their rhythmic discharges are provided by groups of functionally connected neurons, termed central pattern generators (CPGs) located at the level of the brainstem. CPGs are neurons wired together able to produce rhythmic motor patterns even in the absence of the commands from higher centres or from sensory afferents (Marder and Calabrese, 1996). CPGs for breathing (Suzue, 1984; Smith et al., 1991; Rekling and Feldman, 1998), swallowing (Jean, 2001) and mastication (Nakamura and Katakura, 1995) have been identified. A single CPG can have divergent synaptic inputs on distinct pools of HMs and subset of HMs can receive convergent excitatory and inhibitory synaptic drives arising from different CPGs. Indeed Roda and collaborators (2002) analysed the discharge patterns of cat HMs and changes in their membrane potentials during breathing, swallowing and coughing *in vivo*, revealing that some cells were concerned with only one behaviour (swallowing), some received a synaptic drive during breathing and swallowing, and some others exhibited membrane potential changes in relation to the three tested behaviours (Fig. 4). These results suggest that common subsets of HMs are activated during multiple behaviours and that multifunctional XII premotor neurons exist, shared by several CPGs (Fig. 5).

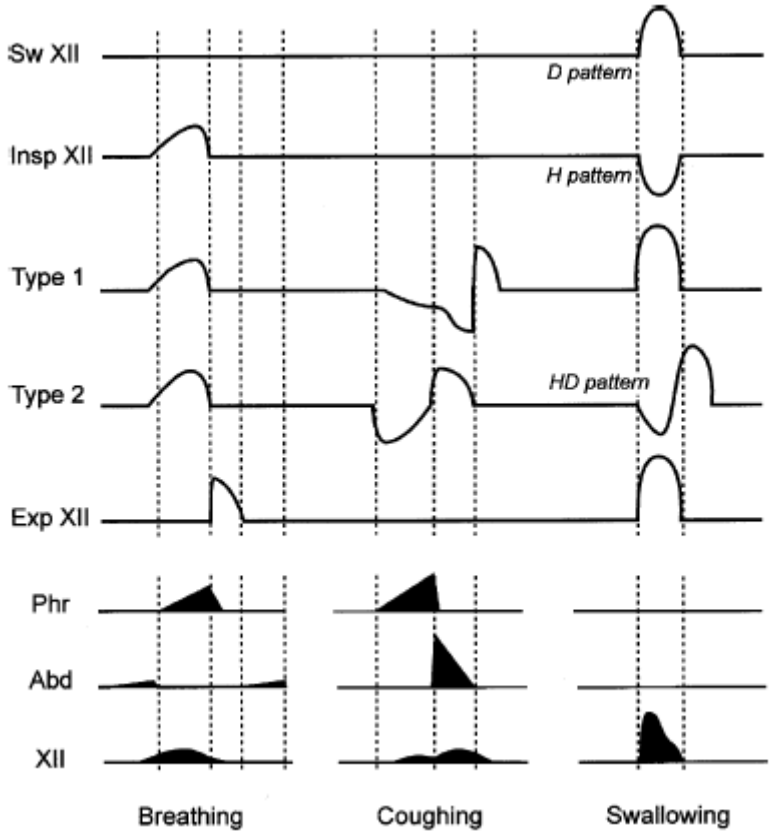

Fig. 4. Schematic drawings showing nerve activities (bottom traces) and changes in membrane potentials (upper traces) of subsets of XII motoneurons (XII Mn) during breathing, coughing and swallowing in non-vagotomized, artificially ventilated decerebrate cats. One group of XII Mn was activated only during swallowing (Sw XII). Three groups of inspiratory XII Mn (Insp XII) had different membrane trajectories during coughing and swallowing (see text for detailed patterns). Expiratory XII Mn (Exp XII) were not involved in coughing but were depolarized during swallowing. Abbreviations: XII, hypoglossal nerve; Abd, abdominal nerve; Phr, phrenic nerve (from Gestreau et al., 2005).

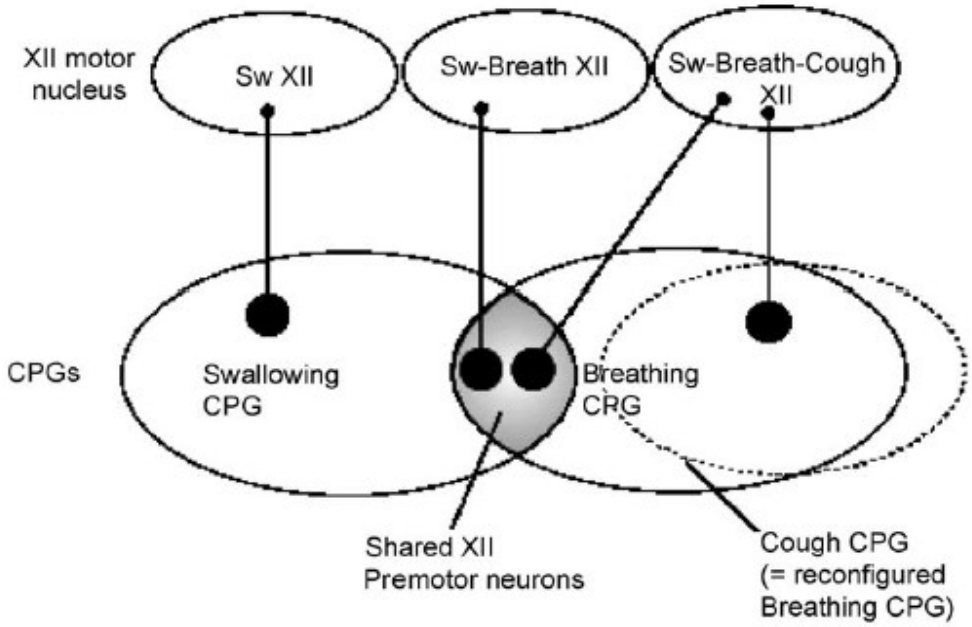

Fig. 5. Output patterns of lingual muscles are achieved by activation of various subsets of XII motoneurons. Brainstem neural networks (or central pattern generators, CPGs) producing breathing, swallowing and coughing motor activities form neural ensembles including XII premotor neurons (black circles). The latter send convergent and divergent projections onto the subsets of motoneurons. Several results suggest the existence of multifunctional (or shared) premotor neurons (see overlapping CPGs). The cough motor pattern is likely generated by reconfiguration of the breathing CPG (modified from Gestreau et al., 2005).

In vitro brainstem preparations from newborn rodents comprising intact CPGs are useful models to study network mechanisms subserving rhythmic motor behaviours and their modulation, overcoming the technical limitations of *in vivo* experiments. Moreover, in experimental models the afferent inputs to brainstem circuits can be activated precisely, while output, in the form of motor activity recorded from cranial nerves or target organ responses, can be measured directly (Nicholls and Paton, 2009), allowing fine analysis of the input-output network integration. For example, en-block and *in situ* brainstem-spinal cord preparations, which maintain respiratory-related rhythmic activity comparable to the one recorded from intact animals (Suzue, 1984; Smith and Feldman, 1987; Smith et al., 1990; Paton, 1996; Dutschmann and Paton, 2003), are useful for elucidating reflex and synaptic mechanisms responsible for the generation and control of respiratory rhythm. Also brainstem slices, despite representing a reduced and simplified model of brainstem circuit, retain rhythmic activity and allow higher accessibility in

terms of single cell recordings and pharmacological approach: in these preparations, whole cell from single HMs or XII nerve recordings are useful to monitor the motor output of the respiratory centres and examine functional changes in respiratory rhythm generation and its modulation (Smith et al., 1991; Paton et al., 1994; Funk et al., 1993; Ramirez et al., 1997; Telgkamp and Ramirez, 1999; Shao and Feldman, 2005; Fig. 6).

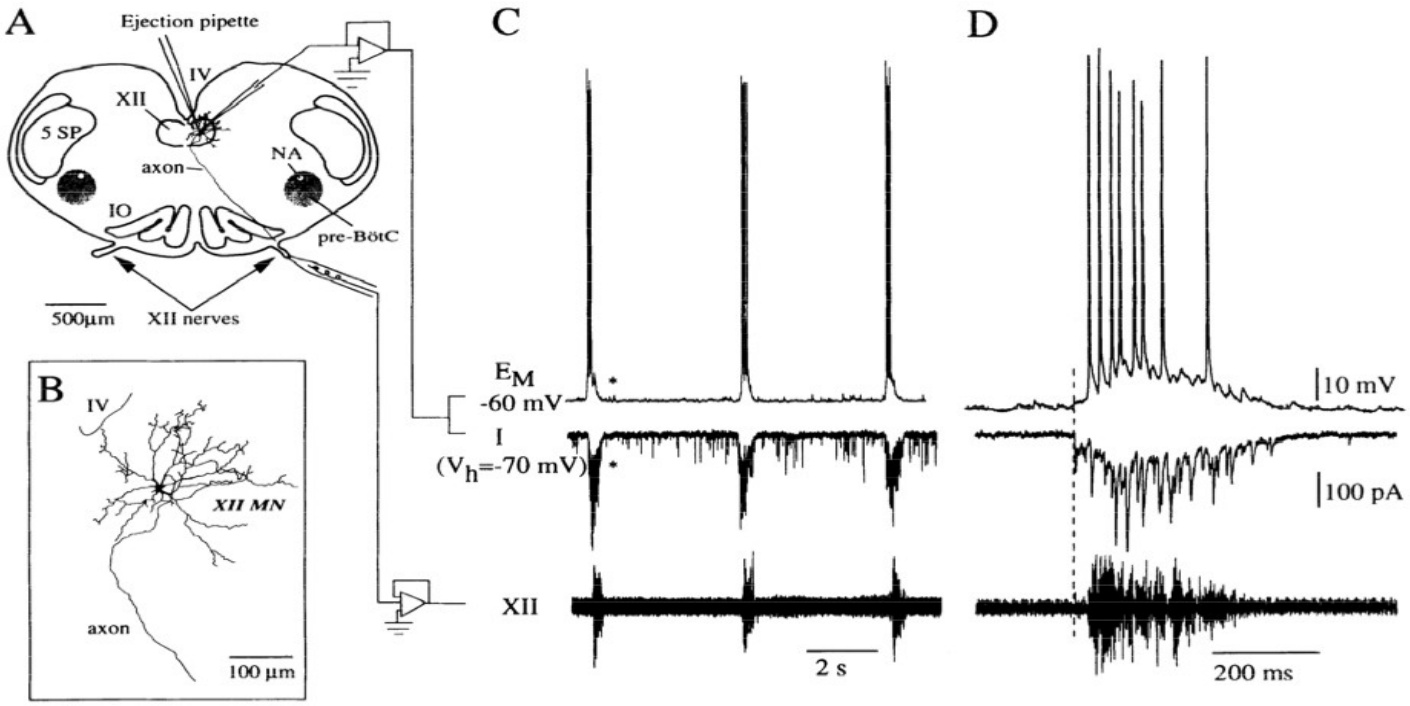

Fig. 6. Medullary slice preparation of the neonatal rat. (A) Scheme of the neonatal rat medullary slice preparation illustrating arrangement of electrodes for whole-cell recording of hypoglossal (XII) motoneuron and nerve activity. Local application of drugs is accomplished with pressure ejection pipette over one XII motor nucleus. (B) Camera lucida reconstruction of Lucifer yellow-filled XII motoneuron showing multipolar cell soma and processes extending outside the margins of the XII motor nucleus. (C) Whole-cell current- and voltage-clamp recordings showing characteristics of inspiratory-modulated synaptic drive potentials and currents of a typical XII motoneuron. Potentials and currents occur in phase with population activity in XII nerve recorded with extracellular suction electrodes (XII, bottom trace). (D) Time scale expanded for 1 burst (C, *). IV, 4th ventricle; 5 SP, spinal trigeminal nucleus; IO, inferior olive; NA, nucleus ambiguus (From Funk et al., 1993).

HM activity is also important during sleep. Sleep, especially REM (rapid-eye-movement) sleep, causes fundamental modifications in the activity and tone of respiratory muscles (in particular the dilator genioglossus muscle innervated by the nucleus hypoglossus) leading to airway narrowing and increased resistance to breathing

(Horner, 2008). In individuals with an already anatomically narrow upper airways the effects of sleep on pharyngeal muscle tone can predispose to obstructive sleep apnea (Remmers et al., 1978), a disorder affecting approximately 4% of adults caused by repeated episodes of pharyngeal airway obstruction in part due to a sleep related reduction in the activity of upper airway dilator muscles (Jordan and White, 2008). Current information, obtained from intact naturally sleeping animal models, demonstrate that tonic excitatory drives to the hypoglossal motor nucleus (mediated principally by noradrenergic and glutamatergic inputs) are prominent in wakefulness and withdrawn in sleep when also tonic inhibitory GABA inputs predominates, thus contributing to the suppression of respiratory muscle activity (Horner, 2009). Again, studies regarding the mechanisms acting at the hypoglossal motor nucleus to modulate motor output to the genioglossus muscle, are fundamental to clarify the transition from wakefulness to natural sleep states as well as the pathogenesis of obstructive sleep apnea (Horner et al., 1994; Horner, 2007).

In summary, HMs subserve a variety of fundamental functions, some of which are established early during development, whose mechanisms in physiological and pathological conditions can be investigated experimentally *in vivo* and *in vitro*.

1.3 Hypoglossal motoneuron receptors and intrinsic properties

Motoneurons do not participate to the generation of motor programs but they contribute to the patterning of motor outputs, for the expression of various oropharyngeal behaviours, through their endogenous properties (Berger, 2000). In the next section, receptors and intrinsic properties of HMs will be briefly reviewed.

1.3.1 Receptors

The primary respiratory synaptic drive to respiratory motoneurons, including HMs, is due to the release of glutamate from synaptic terminals apposed to these motoneurons (Berger, 2000). *In vitro* recordings from neonatal rats (Greer et al. 1991; Funk et al., 1993; O'Brien et al., 1997) as well as immunocytochemistry studies (Williams et al., 1996; García Del Caño et al., 1999) show that HMs express both N-methyl-D-aspartate (NMDA) and non-NMDA (α-amino-3-hydroxy-5-methyl-4-isoxazoleproprionic acid, AMPA, and kainate) ionotropic receptors at synaptic sites. However, transmission of the respiratory drive to XII motoneurons is mainly dependent on and modulated by endogenously released excitatory amino acids acting at non-NMDA receptors with

activation of NMDA receptors representing only a relatively small component (Greer et al., 1991; Funk et al., 1993). Likewise, recordings from HM embryonic organotypic cultures (Launey et al., 1999) suggest that on brainstem motoneurons NMDA receptors are not directly involved in synaptic transmission, and could be located either extrasynaptically or at silent synapses; however, activation of these receptors evokes sustained bursting in a subset of HMs (Sharifullina et al., 2008). Finally, HMs express also metabotrobic glutamate receptors (mGluRs; Hay et al., 1999; Laslo et al., 2001a) whose activation on neonatal HMs influences motoneuron excitability (Donato et al., 2003) and facilitates glycinergic inhibitory transmission (Donato and Nistri, 2000).

HMs receive GABAergic and glycinergic inputs originating mostly from the reticular formation (Li et al., 1997), and the respiratory centers (the pre-Bötzinger complex in the ventrolateral medulla) (Paton and Richter 1995); in addition hypoglossal interneurons may represent a source of GABAergic inhibition (see previous sections). The neurotransmitters GABA and glycine operate by activating Cl^- channels. GABA receptors mainly belong to the $GABA_A$ class and are reversibly blocked by bicuculline, while glycine receptors are blocked by strychnine (Barnard et al., 1993; Kuhse et al., 1995; Donato and Nistri, 2000). On HMs from neonatal rats, $GABA_A$ and glycine receptors are present on the same neuron with the two neurotransmitters being co-released from the same presynaptic terminals (O'Brien and Berger, 1999). However, glycinergic and GABAergic events differ in kinetics, frequency and amplitude with the former being faster, larger in amplitude and occurring at higher frequency (O'Brien and Berger, 1999; Donato and Nistri, 2000). Both neurotransmitters, despite eliciting depolarization of HM membrane potential, always inhibit neonatal HMs, probably by shunting their membrane resistance (via a large increase in Cl^- permeability) to make them less responsive to excitatory signals (Marchetti et al., 2002). During postnatal development, instead, inhibitory synaptic transmission (particularly glycinergic neurotransmission) to rat HMs becomes faster and hyperpolarizing with age (Singer and Berger, 2000).

In addition, HMs express receptors for a variety of neuromodulators, including: norepinephrine (NE; Parkis et al., 1995), thyrotropin-releasing hormone (TRH; Rekling, 1990, 1992; Bayliss et al., 1994a), serotonin (5-HT; Berger et al., 1992; Umemiya and Berger, 1995b; Singer et al., 1996) and substance P (SP; Yasuda et al., 2001), which all modulate motoneuronal excitability via complex postsynaptic as well as presynaptic mechanisms. These effects are postnatally regulated (Selvaratnam et al., 1998 for NE;

Bayliss et al., 1994a for TRH; Talley et al., 1997 for 5-HT; Adachi et al., 2010 for SP) and share some effectors pathways (for instance, converging on a resting leak K^+ current, namely TASK-1; Talley et al., 2000). Also cholinergic modulation has multiple effects on the XII nucleus, acting via nicotinic (Quitadamo et al., 2005; Pagnotta et al., 2005; Lamanauskas and Nistri, 2006) or muscarinic receptors (Bellingham and Berger, 1996; Bellingham and Funk, 2000; Pagnotta et al., 2005), affecting both excitatory and inhibitory transmission to HMs.

1.3.2 Intrinsic properties

Synaptic inputs to HMs are a major determinant of HM motor output. Those inputs are, however, integrated by HM intrinsic passive (e.g., resting membrane potential, input resistance) and active membrane properties (determined for the most part by the specific type, location and density of ion channels present on cell membranes) to generate the firing behaviour of such motoneurons (Berger, 2000). Table 2 summarizes the main type of currents mediated by voltage-activated ion channels expressed by HMs and responsible for HM sub-threshold and spike-firing behaviour. Besides the sodium and potassium channels that generate the action potential (Mosfeldt Laursen and Rekling, 1989; Viana et al., 1993 a,b; Lape and Nistri, 1999, 2001), HMs express both low-threshold activated (LVA; T-type) and high-threshold activated (HVA; N-, P/Q- and L-types) calcium channels (Umemiya and Berger, 1994; Viana et al., 1993a) as well as different types of K^+ conductances some of which are responsible for two types of afterhyperpolarization (AHP) following the action potential (Viana et al., 1993b; Lape and Nistri, 2000). HMs also possess a mixed cationic Na^+/K^+ hyperpolarization-activated current (I_h , Bayliss et al. 1994b) and persistent inward currents mediated by Na^+ and/or Ca^{2+} channels (I_{NaP} and I_{CaP}; Powers and Binder, 2003; Del Negro et al., 2005; Lamanauskas and Nistri, 2008).

HMs display characteristic firing patterns following membrane depolarization: in response to current step injection the majority of neonatal HMs exhibits a steady pattern of repetitive firing which is reached after a single, fast period of frequency adaptation; a smaller subgroup actually shows an incrementing firing pattern with a progressive acceleration of firing to steady state level (Viana et al., 1995). Conversely, adult (>P21) HMs initially exhibit high-frequency firing which is followed by three different phases of adaptation (Sawczuk et al. 1995), even though they fire at a higher rate than neonatal HMs (Viana et al., 1995).

Table 2. Main membrane currents in hypoglossal motoneurons and their proposed function.

Current	Abbreviation	Description and function	References
Fast Na^+ current	I_{Na}	TTX-sensitive, fast activating and inactivating, responsable for the depolarizing phase of the AP	Mosfeldt Laursen and Rekling, 1989; Haddad et al., 1990; Lape and Nistri, 2001
Delayed rectifer K^+ current	I_{KDR}, I_{slow}	TEA-sensitive, AP repolarization, fAHP	Mosfeldt Laursen and Rekling, 1989; Haddad et al., 1990, Viana et al., 1993a; Lape and Nistri 1999
Fast K^+ current	A-type, I_{fast}	4-AP-sensitive,initial spike frequency adaptation, fAHP	Mosfeldt Laursen and Rekling, 1989; Viana et al., 1993a; Lape and Nistri 1999
Ca^{2+}-activated K^+ current (two types of channels: BK=large conductance; SK=small conductance)	$I_{K\ Ca(BK)}$; $I_{K\ Ca(SK)}$	mAHP ($I_{K\ Ca(SK)}$), repetitive firing properties, AP repolarization ($I_{K\ Ca(BK)}$)	Mosfeldt Laursen and Rekling, 1989; Viana et al., 1993a; Umemiya and Berger, 1994; Lape and Nistri, 2000; Rekling et al., 2000
Low-threshold Ca^{2+} current	I_{CaLVA}	Rebound depolarization, bursting behaviour,AP repolarization(via activation of $I_{K\ Ca(BK)}$), ADP	Viana et al., 1993b; Umemiya and Berger, 1994;
High-threshold Ca^{2+} current	I_{CaHVA}	ADP, mAHP(via activation of $I_{K\ Ca(SK)}$)	Viana et al., 1993b; Umemiya and Berger, 1994;
Na^+/K^+ hyperpolarization-activated current	I_h	Rebound potentials, stabilize V_m around rest, reduces mAHPs as well as response to inibitory synaptic inputs	Bayliss et al., 1994b; Viana et al., 1994
Persistent inward currents (Na^+ and Ca^{2+})	I_{NaP}; I_{CaP}	Integration of synaptic inputs, rythmic discharges	Powers and Binder, 2003; Zeng et al., 2005; Moritz et al., 2007

TTX, tetrodotoxin; AP, action potential; TEA, tetraethylammonium; fAHP, fast afterhyperpolarization; 4-AP, 4-aminopyridine; mAHP, medium AHP; ADP, afterdepolarization; V_m, membrane potential.

Difference in the firing pattern of HMs during development are likely due to changes in some conductances. In fact, results from *in vitro* studies of rat HMs have shown that properties of HMs change during the postnatal period (Haddad et al., 1990; Núñez-Abades et al., 1993; Bayliss et al. 1994b; Viana et al., 1994; Viana et al., 1995, Berger et al., 1995), including a decrease in the duration of AHP (Viana et al., 1994; Viana et al., 1995) a decline in LVA calcium current (Viana et al.1993a; Umemiya and Berger, 1994), and a higher expression of I_h (Bayliss et al. 1994b; Viana et al. 1994). Also passive membrane properties are affected by the postnatal development: an approximate 10 mV hyperpolarization of the resting membrane potential and a decrease in input resistance with associated increase in rheobase (defined as the amplitude of injected depolarizing current that causes a HM to reach firing threshold in about one-half of the trials) have shown to occur postnatally (Haddad et al., 1990; Viana et al., 1994).

Based on the aforementioned data, Purvis and Butera (2005) have developed a single-compartment electrophysiological model for HMs which is able to reproduce the fine features of the HM firing behaviour and its age-dependent changes which have been observed experimentally and reported above. It is likely that the these changes may correlate with the mechanical properties of different motor unit innervated by HMs as already demonstrated for the matching between motoneuron passive properties and muscle unit properties in the rat medial gastrocnemius (Bakels and Kernell, 1993; Gardiner, 1993): for instance, slowly decrementing firing pattern, common during the early postnatal period, may be better matched to the activity of fatigable motor units, whereas the adult pattern, characterized by very high initial firing frequencies and higher steady-state firing rates, would be better tuned to the activity of faster fatigue-resistant motor units (Viana et al., 1995).

In broad terms, transformation of synaptic input to motoneurons for the generation of a motor output (to express specific motor behaviours) will depend on several factors: 1) motor unit type 2) type and location of synaptic terminals, 3) character and distribution of active and passive membrane properties, and 4) effects of neuromodulators on HM synaptic transmission and repetitive firing behaviour (Rekling et al., 2000).

2. Amyotrophic lateral sclerosis

2.1 General features

Amyotrophic lateral sclerosis (ALS) is a relatively common adult-onset

neurodegenerative disease. ALS typically develops between 50 and 60 years of age as a relentless, progressive neuromuscular failure, caused by degeneration of both upper motoneurons in the motor cortex and lower motoneurons connecting the spinal cord and brainstem to skeletal muscle fibers, leading to muscle denervation and atrophy (Cleveland and Rothstein, 2001). The pathological hallmarks of ALS are astrocytic gliosis and the presence of intracellular inclusions (bunina bodies, ubiquitinated inclusions, hyaline conglomerate inclusions and Lewy-like bodies, Rowland and Shneider, 2001; Neumann et al., 2006; Wijesekera and Leigh, 2009) in degenerating neurones and glia. Initial ALS symptoms often present in one motoneuron population, such as only lower motoneurons, upper motoneurons, or bulbar motoneurons (innervating muscles that control speech, chewing, and swallowing), but will spread to contiguous motoneuron groups as the disease progresses: those signs include progressive limb weakness, respiratory insufficiency, spasticity, hyperreflexia, dysarthria and dysphagia (Kühnlein, et al., 2008). However, the pathological process in ALS is today recognized to extend beyond the motor system to other "non motor" regions of the central nervous system and organs (like the skin, liver, bone marrow and the enteric nervous system; Silani et al., 2011a). Moreover, clinical overlap and transition forms between ALS and frontotemporal dementia as well as cognitive and behavioral impairments in ALS patients has been reported (Strong et al., 2009) rather suggesting that ALS is a "multiple system" neurodegenerative disorder (Turner, 2009). The rate of disease progression varies between individuals and can be influenced by the site of onset, but is usually rapid, with an average survival of only 2-3 years from symptoms onset; denervation of the respiratory muscles and diaphragm with respiratory failure and infection is generally the fatal event (Cleveland and Rothstein, 2001).

2.2 Causes of ALS

The disease cause is unknown in the majority of ALS cases, which are described as being sporadic (SALS), while 5-10 % cases are genetic and classified as familial (FALS). The etiology of SALS is largely unknown, and the worldwide incidence of disease in the 1990's is reported to be between 1.5 and 2.7 per 100,000 population/year (average 1.89 per 100,000/ year) in Europe and North America with a uniform incidence across these countries (Wijesekera and Leigh, 2009). The exceptions to this are the Western Pacific island of Guam and the Kii peninsula of Japan, where the incidence has been much higher, possibly linked to an environmental toxin such as β-methylamino-L-

alanine (Cox et al., 2003). The prevalence of ALS has also been reported to be increased among Gulf War veterans (Horner et al., 2003) and in male professional football players engaged by an Italian football team in the period 1970-2001 presumably due to diffusion of illegal drugs among athletes (Chiò et al., 2005). Environmental neurotoxins (Shaw and Höglinger, 2008), viral infections and autoimmunity (Rowland and Shneider, 2001) have been proposed as putative etiological factors for sporadic ALS.

SALS and FALS are clinically indistinguishable and do not usually develop until middle or later life, so identification of genetic cases is not straightforward, as a clear family history needs to be documented. Mutations in several genes have now been identified as leading to ALS, and additional loci have also been linked to the disease (Valdmanis and Rouleau, 2008). The first gene to be identified as being mutated in ALS, which accounts for 10-20 % of autosomal dominant FALS cases, was copper / zinc superoxide dismutase (Cu / Zn SOD, SOD1; Rosen et al., 1993). The SOD1 enzyme normally catalyzes dismutation of superoxide radicals to hydrogen peroxide (H_2O_2) and oxygen in a two-step redox reaction (Barber et al., 2006), protecting cells from the potential toxic damage of reactive oxygen species (ROS) to proteins, lipids and DNA (including changes in protein conformation, oxidation of unsaturated fatty acids and DNA/RNA alterations; Barber et al., 2006). Since more than 140 mutations in the SOD1 gene have been associated to FALS (Boillée et al., 2006), a variety of murine genetic models expressing the ALS mutated human SOD1 protein have been generated (Cleveland and Rothstein, 2001; Gurney et al., 1994). Such transgenic animals develop late neuromuscular symptoms similar to ALS (probably because of the mutated SOD1 gain-of-function leading to motoneuron degeneration; Ferrante et al., 1997), therefore representing important tools to study the mechanisms involved in ALS pathology (Gurney et al., 1994; Cleveland and Rothstein, 2001; Boillée et al., 2006). Because FALS and SALS cases are clinically similar, progress in elucidating the mechanisms underlying FALS may provide insight into both forms of the disease. Apart from the SOD1 gene, other genes, whose mutations have been associated to adult-onset ALS, include fused-in-sarcoma/translated-in-liposarcoma (FUS / TLS; Kwiatkowski et al., 2009), TAR DNA-binding protein (TDP-43; Kabashi et al., 2008), charged multivesicular body protein 2B (CHMP2B; Parkinson et al., 2006), vesicle-associated membrane protein (synaptobrevin-associated protein) B (VAPB; Nishimura et al., 2004), and angiogenin (Greenway et al., 2006). Given the diversity of the physiological functions affected by mutations in these genes, it is generally assumed that the disease classified as “ALS” is the result of defects

in a variety of cellular mechanisms. These include oxidative stress, mitochondrial dysfunction, endoplasmic reticulum stress, protein aggregation, disruption of the neurofilament network and intracellular trafficking along microtubules, defects in RNA processing. Two further majors factors in ALS pathogenesis are excitotoxicity caused by dysregulation of glutamate signaling and involvement of non-neuronal cells neighboring motoneurons (Cleveland and Rothstein, 2000; Shaw, 2005; Fig. 7).

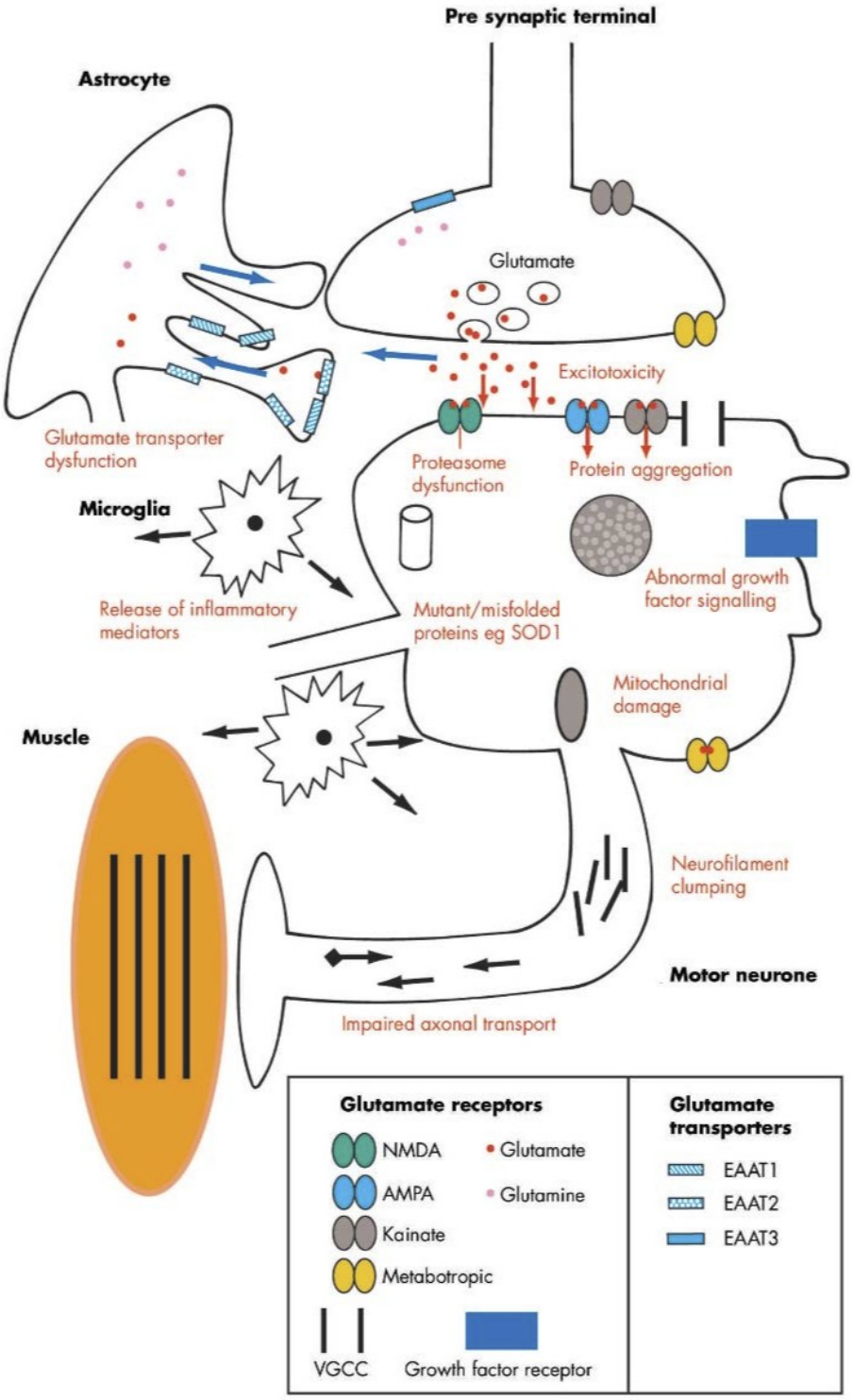

Fig. 7. Schematic representation of putative major mechanisms that may contribute to motor neurone injury in ALS (from Shaw, 2005).

2.2.1 Involvement of non-neuronal cells

The concept that non-neuronal cells could affect the viability of motoneurons stems from the observation that a common characteristic of ALS and other neurodegenerative disorders is the occurrence of a neuroinflammatory reaction consisting of activated glial cells, mainly microglia and astrocytes (Philips and Robberecht, 2011). In postmortem brain and spinal cord from ALS patients both reactive microglia and oligodendroglia were found in the primary motor cortex, motor nuclei of the brainstem, the anterior horns, and the full extent of the corticospinal tract (Kawamata et al., 1992), while astrocytosis was detected in the ventral and dorsal horns from sporadic ALS autoptic tissue (Schiffer et al., 1996), and in the cortical gray matter of non-motor and motor regions from familial and sporadic ALS cases (Nagy et al., 1994).

As findings based on postmortem tissue represent the final stages of the disease, it has been difficult to discern whether the activation of astrogliosis or microgliosis is detrimental or beneficial to motoneurons and whether it is a causative or secondary element in motoneuron degeneration.

Animal models have provided abundant information which helped to clarify the nature of glial contribution to ALS pathogenesis. For instance, Clement and collaborators (2003) generated chimeric mice composed of mixtures of normal cells and cells that express a human mutant SOD1. In these mice, motoneurons expressing transgenic G93A or G37R SOD1 failed to degenerate if they were adjacent to large numbers of supporting cells (such as astrocytes and glia) without the mutant protein. Reciprocally, motoneurons without the transgene demonstrated pathology if surrounded by non-neuronal cells with the mutant SOD1 transgene. Similar results were obtained with humanized ALS models: Di Giorgio et al. (2007) used embryonic stem cells (ESCs) derived from mice carrying normal or mutant transgenic alleles of the human SOD1 gene to generate motoneurons by *in vitro* differentiation. The authors found that motoneurons carrying either the non-pathological human SOD1 transgene or the mutant $SOD1^{G93A}$ allele degenerated when co-cultured with $SOD1^{G93A}$ glial cells. Thus, toxicity to motoneurons was shown to require damage from mutant SOD1 acting within non-neuronal cells.

To determine which type of cell could influence the initiation and propagation of the disease, Boillée et al. (2006) have generated transgenic mice ($LoxSOD1^{G37R}$) that carry a mutated human $SOD1^{G37R}$ gene flanked at both ends by 34-base pair LoxP sequences to allow recognition and regulated deletion by the Cre recombinase in specific cell lines.

The use of such partial and selective gene inactivation technique demonstrated that the expression of the mutated SOD1 transgene within motoneurons is a primary determinant of disease onset and of an early phase of disease progression; conversely, diminishing the levels of expression of mutant SOD1 in microglia has little effect on the early disease phase, but it sharply slows down disease progression (Boillée et al., 2006).

Results from genetic ALS animal models suggest that mutant proteins in motor neurons determine disease onset and early stages of disease, whereas mutant SOD1 in microglia and astrocytes mainly determines disease progression and duration, supporting the hypothesis of "non–cell autonomous" disease mechanisms (Ilieva et al., 2009). Putative factors released by glia cells interfering with motoneuron function and survival have been identified as prostaglandins (Di Giorgio et al., 2007), proinflammatory cytokines and ROS (Marchetto et al., 2008)

Glia cells are also involved in another important process whose disregulation is a prevailing contributor to ALS pathology, i.e. glutamate metabolism. Astrocytes are the main cellular defence against glutamate excitotoxicity as they express a high density of glutamate transporters responsible for accumulating up to 80% of the total glutamate released in the brain (Danbolt, 2001). Detailed aspects concerning the role of excitotoxicity in ALS, also in relation to glia, are provided in the next section.

2.2.2 Glutamate-mediated excitotoxicity

Glutamate is the major excitatory neurotransmitter released from presynaptic nerve terminals, with subsequent diffusion across the synaptic cleft and activation of specific postsynaptic receptors, particularly the ionotropic NMDA and AMPA receptors. The excitatory signal is terminated upon removal of glutamate from the synaptic cleft by specific glutamate transporters (known as "excitatory amino acid transporters", EAATs; Danbolt, 2001) expressed mainly by astrocytes (Danbolt, 2001; Heath and Shaw, 2002). Classic excitotoxicity is due to increased synaptic glutamate concentrations and excessive stimulation of glutamate receptors, which may occurs when the balance between release and re-uptake of glutamate is disturbed (Heath and Shaw, 2002). "Slow" excitotoxicity, instead, refers to a process when neurones become vulnerable to ambient extracellular glutamate because of cellular metabolism impairment (Doble, 1999; Van Den Bosch et al., 2006; Fig 8.). Mechanisms leading to glutamate-mediated neuronal injury involve prolonged depolarization of neurones, changes in intracellular ion concentrations, and activation of enzymatic cascades: ion influx is usually associated

with osmotic swelling and early necrotic events, while increase of intracellular Ca^{2+}, with subsequent activation of Ca^{2+}-dependent enzymatic pathways, may lead to delayed cell death (Doble, 1999).

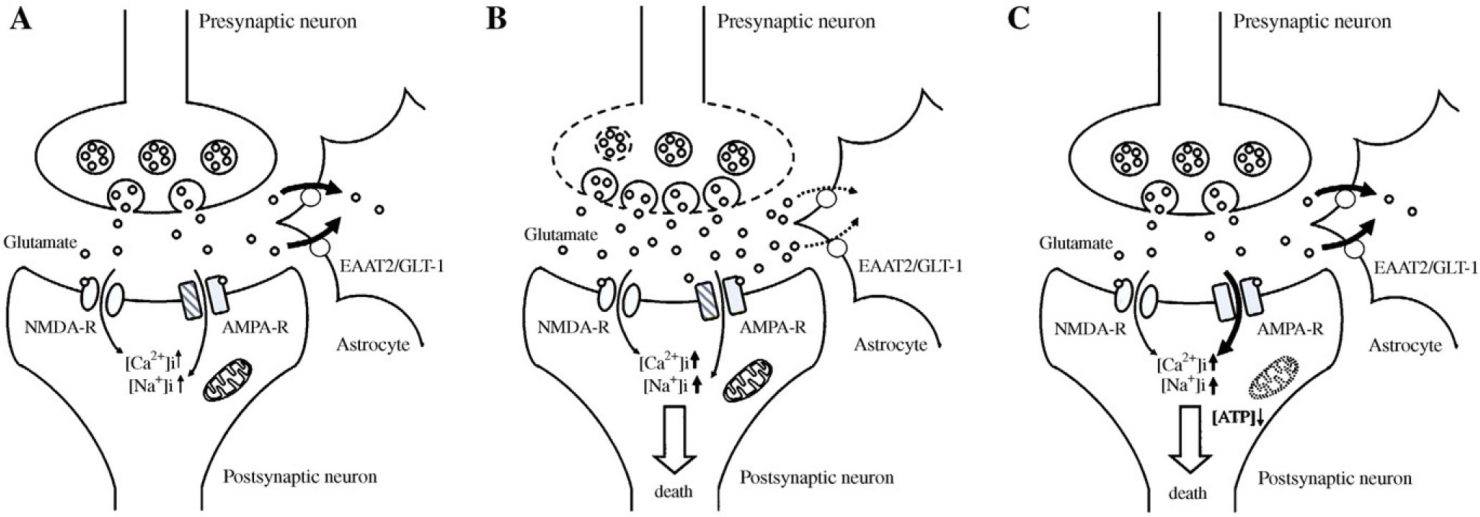

Fig. 8. Glutamatergic neurotransmission and excitotoxicity. (A) Under normal conditions, glutamate released from the presynaptic neuron activates NMDA and AMPA receptors, resulting in Na^+ and Ca^{2+} influx with depolarization of the postsynaptic neuron and generation of an action potential. (B) Classical excitotoxicity is induced by an elevation of the extracellular glutamate concentration. This can be caused by an increased release of glutamate or a deficient re-uptake of glutamate into the astrocytes by the EAAT2/GLT-1 transporter. The excessive stimulation of the glutamate receptors gives rise to an increased intracellular concentration of Na^+ and Ca^{2+} ions and this can result in neuronal death. (C) Slow excitotoxicity refers to neurons becoming more sensitive to glutamate stimulation in normal extracellular glutamate concentration. This sensitization can be caused by changes in the properties of the glutamate receptors (resulting in higher Ca^{2+} permeability) or by mitochondrial distress, leading to energetically compromised neurons (from Van Den Bosch et al., 2006).

Excitotoxicity has been associated with a wide range of acute (hypoxia/ischaemia, hypoglycaemia, status epilepticus and trauma; Ikonomidou and Turski, 1995) and chronic (such as Alzheimer's, Parkinson's, Huntington's diseases; amply reviewed by Doble, 1999 and Sheldon and Robinson, 2007) neurodegenerative disorders. Over the past decades, studies have suggested a potential role for glutamate metabolism disregulation also in ALS: in fact, increased glutamate levels have been found in the

cerebrospinal fluid (CSF) of a subgroup of ALS patients (Rothstein et al., 1990; Shaw et al., 1995a, Spreux-Varoquaux et al., 2002), impaired glutamate transport was reported in synaptosomes from neural ALS patients tissue (Rothstein et al., 1992) and toxic effects of CSF from ALS patients has been demonstrated in rat cultured spinal cord motoneurons due to activation of glutamate receptors and increase in intracellular Ca^{2+} (Sen et al., 2005). Moreover, loss of EAAT2, the main astrocytic glutamate transporter, has been reported in sporadic ALS (Fray et al., 1998; Rothstein et al., 1995; Sasaki et al., 2000) as well as in mutant SOD1 ALS animal models (GLT-1, glutamate transporter-1, is the equivalent of the human EAAT2; Bruijn et al., 1997; Trotti et al., 1999; Howland et al., 2002; Dunlop et al., 2003).

Motoneurons posses several features which may render them more vulnerable to excitotoxicity: first, they express AMPA Ca^{2+}-permeable receptors lacking the functional GluR2 subunit, thereby rendering them more permeable to Ca^{2+} influx (Williams et al., 1997; Shaw et al., 1999; Essin et al., 2002; Van Damme et al., 2002); secondly, they lack the intracellular expression of Ca^{2+} binding proteins parvalbumin and calbindin (Ince et al., 1993) showing a low endogenous Ca^{2+} buffering capacity (Lips and Keller, 1998; Palecek et al., 1999). ALS-resistant motor nuclei (oculomotor, trochlear, and abducens) differ from ALS-vulnerable ones (trigeminal, facial, ambiguus, and hypoglossal) in terms of expression of type I mGluRs (Laslo et al., 2001a) and GluR2-lacking AMPA receptors (Laslo et al., 2001b), expression of glutamate transporters (Medina et al., 1996), Ca^{2+} dynamics and expression of Ca^{2+}-binding proteins (Reiner et al., 1995; Laslo et al., 2000; Vanselow and Keller, 2000; von Lewinski et al., 2008), again suggesting an important link between specific motoneuron features and their vulnerability to excitotoxicity.

Recently, Van Damme et al. (2007) demonstrated a difference in GluR2 expression in motoneurons from two rat strains, which correlated with a difference in vulnerability to AMPA receptor-mediated excitotoxicity, both *in vitro* and *in vivo*. This strain difference was used to study factors regulating GluR2 expression *in vitro* discovering that astrocytes regulate its expression in a region-specific way (i.e., only astrocytes derived from the ventral part of the spinal cord retained this property), and the presence of mutant SOD1 in these cells abolished their GluR2-regulating capacity. These findings suggested that the cross-talk between astrocytes and neurons is paramount to neuronal function and that disturbances in this intercellular communication may contribute to the pathogenesis of motor neuron degeneration (Rao and Weiss, 2004; Van Den Bosch and Robberecht, 2008). Even though disruption of glial transporters could represent a

primary causative event in ALS pathogenesis triggering excitotoxic damage to motoneurons, another possibility is that motoneurons themselves may release factors able to interfere with astrocytic glutamate uptake: for instance, Rao et al. (2003), by using the oxidation-sensitive dyes hydroethidine and dihydrorhodamine, have found that glutamate induces ROS generation in cultured motoneurons. They also found that these ROS appear to leave the motoneurons and to induce oxidation and disruption of glutamate uptake in neighboring astrocytes as assessed with [^{3}H]glutamate uptake (Rao et al., 2003). Thus, these authors suggest that a feedforward cycle may contribute to ALS progression, as increases in extracellular glutamate concentration will result in higher motoneuron ROS generation and severer damage to astrocytic glutamate transport, causing further rises in glutamate levels with selective motoneuron injury (Fig. 9).

Whatever the cause, excitotoxicity seems to play a pivotal role in ALS pathogenesis and several features expressed by motoneurons may preferentially expose them to the deleterious effects of glutamatergic overactivity (Fig. 10).

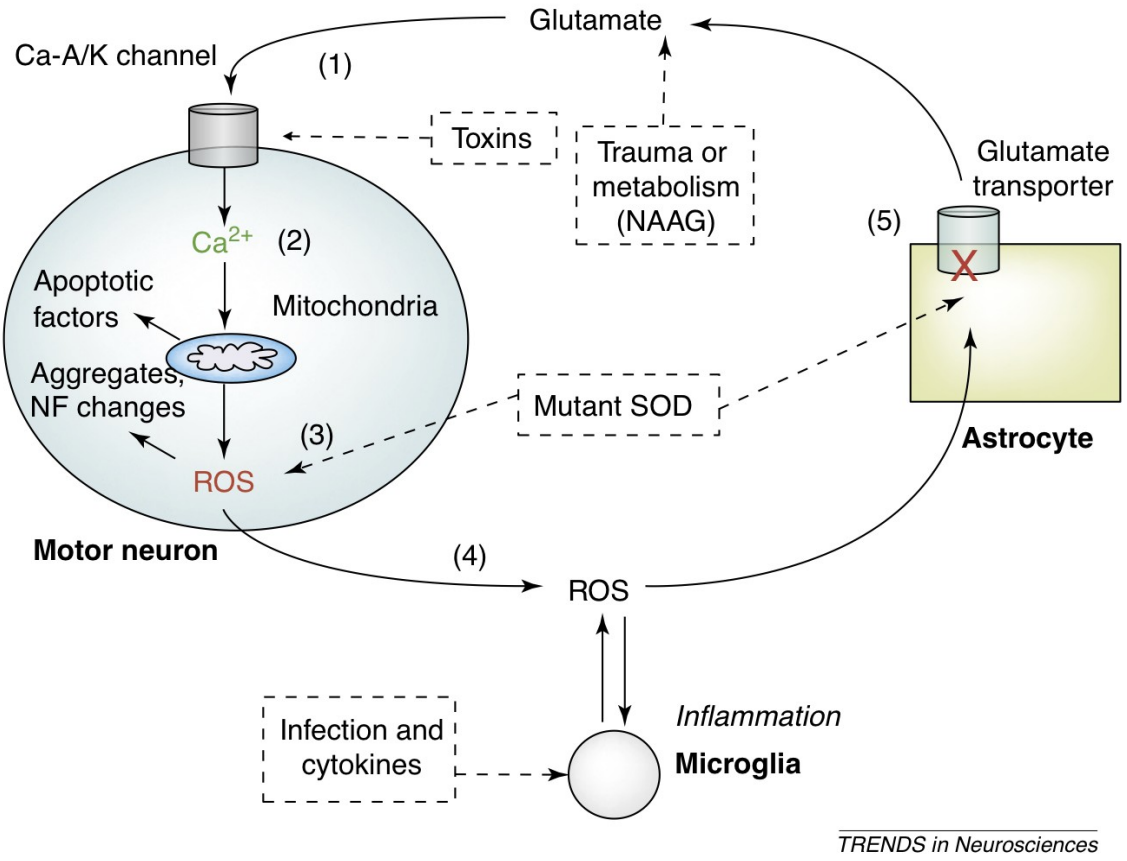

Fig. 9. A feedforward model of amyotrophic lateral sclerosis (ALS) pathogenesis. Basis for a feedforward cycle leading to selective motor neuron injury in ALS. Elevations of extracellular glutamate levels (1) could induce excessive Ca^{2+} entry into motor neurons (2), which would be substantially buffered by mitochondria, with consequent generation of ROS and, possibly, activation of apoptotic pathways (3). ROS could pass across the motor neuron plasma membrane (4) and damage astrocytic glutamate transporters (5), thereby causing further rises in extracellular glutamate levels. Such a cycle could in principle be triggered at different sites (e.g. via glutamate rises or oxidative stress), and thus might be compatible with a multiplicity of mechanisms leading into a common self-propagating disease pathway. For instance, if mutant SOD1 acts through oxidative mechanisms, it could enhance ROS disruption of glial glutamate transporters as well as of the motor neurons themselves. Additionally, inflammation and microglial activation, whether triggered by infection or other cytokine mediated processes, can induce oxidative stress. Alternatively, events including trauma, hydrolysis of the neuropeptide N-acetyl-aspartyl glutamate (NAAG) or ingestion of environmental excitotoxins could increase activation of glutamate receptors (from Rao and Weiss, 2004).

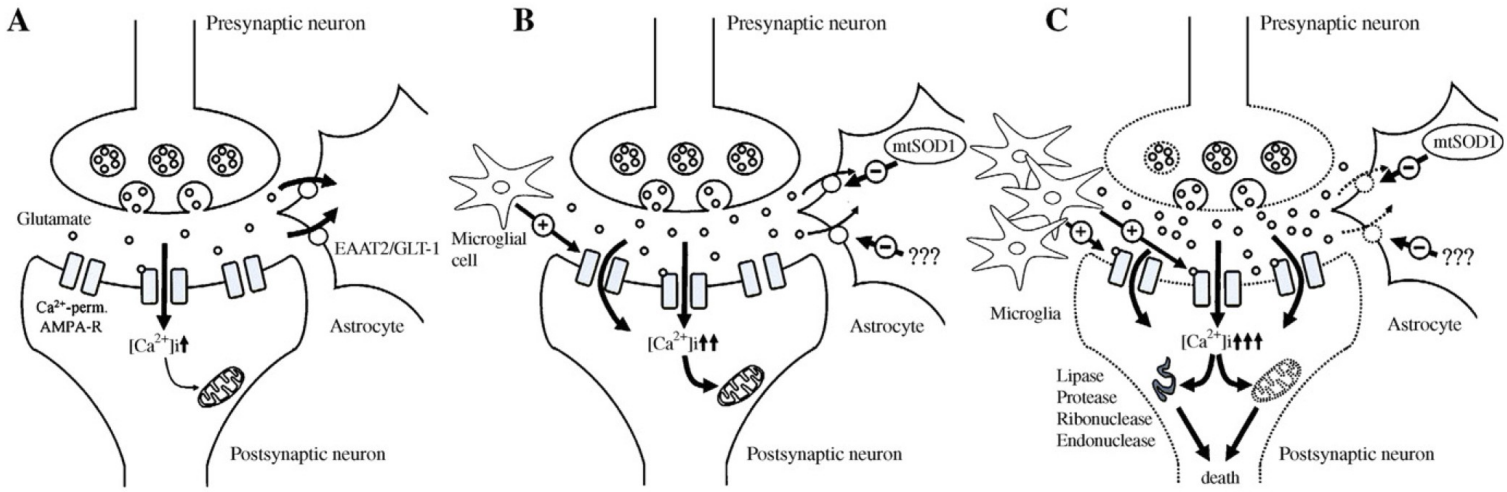

Fig. 10. Putative mechanisms that may account for ALS-related excitotoxic damage to motoneurons. (A) Under normal conditions, glutamate released by the presynaptic neuron activates postsynaptic receptors and then its action is terminated by astrocytic re-uptake via glutamate transporters (EAAT2/GLT1). (B) If glutamate transporters are damaged, glutamate concentration starts to increase, leading to higher (and/or longer) stimulation of receptors, including the Ca^{2+}-permeable AMPA ones. Damage to glial transporters can be due to the presence of mutant (mt) SOD1; however, as the decrease in uptake capacity is also observed in sporadic ALS cases, other unknown factors must be involved. Moreover, activated microglial cells can secrete substances which can in turn increase the glutamatergic stimulation of the postsynaptic neuron. All together, these processes contribute to massive influx of Ca^{2+} which, because of the low calcium buffering capacity of motoneurons, will result in mitochondria overloading. (C) When mitochondrial buffering ability is exceeded, the excessive cytoplasmic Ca^{2+} concentration may increase the probability of generation of toxic reactive oxygen species and also activate different types of Ca^{2+}-dependent enzymes which in turn may trigger neuronal death pathways. Finally, injured neurons will release further glutamate resulting in a dramatic increase in its extracellular concentration and spreading of neurodegeneration (from Van Den Bosch et al., 2006).

2.3 ALS treatments: all roads lead to riluzole

Many putative disease-modifying strategies for ALS have been tested in clinical trials, these include: anti-glutamate drugs, antioxidants, anti-inflammatory and immunomodulatory agents, neurotrophic factors, antiviral agents and energy metabolism-related compounds (Cleveland and Rothstein, 2001; Rowland and Shneider, 2001; Mitchell and Borasio, 2007). To date the only drug licensed for the ALS clinical

treatment is riluzole (Lacomblez et al., 1996), which, however, can only slow down disease progression temporarily (Groeneveld et al., 2008).

2.3.1 The action of riluzole on glutamatergic transmission

Riluzole has neuroprotective, anticonvulsant, anxiolytic and anesthetic qualities, and its mode of action is composite and dependent on its actual concentration. Its neuroprotective effect has been first associated with the block of glutamatergic neurotransmission. Riluzole was shown to inhibit basal glutamate release and release evoked by neuronal activation both *in vivo* in the cat nucleus caudatus (Cheramy et al., 1992) and in the rat spinal cord (Coderre et al., 2007), and *in vitro* in cultured cerebellar granule cells (Doble et al., 1992; Hubert et al., 1994), hippocampal slices (Martin et al., 1993), in rat cerebrocortical synaptosomes (Wang et al., 2004) and HMs (Lamanauskas and Nistri, 2006). On cultured cerebellar granule as well as in cerebrocortical synaptosomes, the inhibition of glutamate release could be blocked by pretreatment of the cells with the G-protein inhibitor pertussis toxin (Doble et al., 1992; Hubert et al., 1994; Wang et al., 2004); on HMs, instead, the effect was occluded by prior treatment with chelerythrin (Lamanauskas and Nistri, 2008), a protein kinase C (PKC) blocker, confirming riluzole ability to directly inhibit PKC as previously demonstrated on mouse cortical cultures (Noh et al., 2000). Thus, it is likely that riluzole may interact with a G-protein-driven presynaptic mechanism to inhibit glutamate release. However, Fumagalli et al. (2008) reported that riluzole can also significantly increase glutamate uptake in a dose-dependent manner, as measured by [^{3}H]glutamate uptake in rat cortical synaptosomes as well as in three different HEK293 line cells individually expressing the three main glutamate transporters GLAST (equivalent of human EAAT1), GLT1 (equivalent of EAAT2) and EAAC1(equivalent of EAAT3). Similarly, Liu et al. (2001) demonstrated that, in the NG108-15 neuroprogenitor cell line, riluzole increased GLT1-reporter and GLT1 protein expression and that this increase was enhanced by heat shock and coincident with the riluzole-induced increased expression of two heat shock proteins (HSP; HSP70 and HSP90). Moreover, riluzole produced an enhancement of spinal cord synaptosomal glutamate uptake in control animals and early-stage disease SOD1^{G93A} rats (Dunlop et al., 2003). The effect of riluzole on glutamate uptake seems to be biphasic and dose dependent, since low (1-10 μM) doses enhances glutamate uptake, while higher (> 100 μM) doses depress it in rat spinal cord synaptosomes (Azbill et al., 2000) and in cortical astrocytes cultures (Frizzo et al., 2004). Also the increase of glutamate uptake

may depend on G-proteins pathways as cholera toxin (known to inhibits G-proteins) could prevent riluzole effect on rat spinal cord synaptosomes (Azbill et al., 2000).

Thus, the mechanisms by which riluzole can affect glutamatergic neurotransmission seem to involve the block of glutamate release and the enhancement of glutamate uptake; in both cases interaction with G-protein pathways may represent a pivotal target for riluzole action. However, other presynaptic and postsynaptic effects of riluzole have been reported which may contribute indirectly to the decrease of neurotransmitter release and/or represent independent mechanisms of neuroprotection acting on different cell processes.

2.3.2 Other mechanisms of action

More recently, the action of riluzole has been attributed to powerful block of persistent inward currents (PICs): on motoneurons, PICs are composed by persistent sodium current (I_{NaP}) and/or persistent calcium current (I_{CaP}), both being important for integrating synaptic inputs, for repetitive firing properties (Crill, 1996; Russo and Housgaard, 1999) and for prolonged rhythmic discharges (Darbon et al., 2004; van Drongelen et al., 2006). Riluzole was reported to block PICs (mainly I_{NaP} , partially I_{caP}) and repetitive firing on spinal motoneurons (Miles et al., 2005; Harvey et al., 2006; Kuo et al., 2006), HMs (Lamanauskas and Nistri, 2008) and cortical neurons (Urbani and Belluzzi, 2000).

In addition, riluzole inhibits both high- and low-voltage-activated calcium currents in cortical neurons (Stefani et al., 1997), dorsal root ganglion neurons (Huang et al., 1997), and rat cerebrocortical synaptosomes (Wang et al., 2004). The drug can also blocks potassium conductances (Zona et al., 1998; Duprat et al., 2000; Ahn et al., 2005) and tetrodotoxin (TTX)-sensitive sodium channels (Song et al., 1997). Finally, it can inhibit glycinergic postsynaptic currents on HMs (Umemiya and Berger, 1995a) and strongly potentiates postsynaptic $GABA_A$ responses both in cultured hippocampal neurons and in Xenopus oocytes expressing recombinant receptors (He et al., 2002).

2.3.3 Neuroprotective action of riluzole

Riluzole is important for neuroprotection both *in vitro* and *in vivo.* In rat motoneuron-enriched cultures riluzole rescued cells from NMDA- and glutamate-mediated excitotoxicity as assessed by 3-(4,5-dimethylthiazol- 2-yl)-2,5-diphenyl tetrazolium bromide (MTT) metabolism (Estevez et al., 1995). Also on rat spinal cord organotypic cultures riluzole could block neuronal excitotoxic damage evoked by a glutamate

transport inhibitor (Rothstein and Kuncl, 1995; Chang et al., 2010), glutamate itself (Guzmán-Lenis et al., 2009) or kainate (Mazzone and Nistri, 2011).

Riluzole is neuroprotective *in vivo* in animal models of neuronal injury, known to involve excitotoxic mechanisms, such as experimentally induced cerebral ischemia. These animal models of stroke involve excitotoxic neuronal loss, following massive release of glutamate in the ischemic area: when ischemia is induced experimentally, riluzole reduces the volume of damaged ischemic area and prevents necrosis (Pratt et al., 1992).

Riluzole has also been suggested for treating spinal cord (Schwartz and Fehlings, 2002) and brain injury (Wahl and Stutzmann, 1999), Huntington's disease (Wu et al., 2006) and epilepsy (Farber et al., 2002).

Despite its important neuroprotective action in experimental models, clinical data are currently available only for ALS, and even in this case riluzole can only slow down disease progression extending patients lifespan for about 3-6 months (Groeneveld et al., 2008). Given that neuroprotective strategies are most warranted at early stages of the disease (while by the time of clinically-detectable ALS symptoms already 30% motoneurons have degenerated; Swash and Ingram, 1988), should a range of reliable biomarkers for the ALS pre-symptomatic stage be available, then the potential disease-modifying effect of riluzole might be tested at the early onset of the disease.

3. ATF-3: a marker for neuronal stress

ATF-3 is a member of the ATF / CREB (cAMP responsive element binding protein) family of transcription factors. This family comprises 20 members of proteins which have a basic region-leucine zipper (bZip) DNA biding domain recognizing the consensus ATF/CRE sequence “TGACGTCA” (Hai and Hartman, 2001). The ATF/CREB proteins form selective homodimers as well as heterodimers with each other and with other bZip proteins (such as the AP-1 and C/EBP proteins) (Hai et al., 1999), expanding their ability to regulate gene expression (Hai and Hartman, 2001). ATF-3 represses transcription as a homodimer (Chen et al., 1994) and activates transcription as a heterodimer with Jun proteins (Hai et al., 1999). Furthermore, it has many characteristics of immediate-early genes (IEGs) (Wolfgang and Chen, 1997) as its expression, relatively low at rest in most cell types, increases immediately (within 2 h) and transiently upon exposure to many stressful stimuli: for instance, ATF-3 mRNA levels rise in rat dorsal root ganglia sensory neurons and in spinal motor neurons after nerve injury (Tsujino et

al., 2000, Huang et al., 2006, 2007) and in the rat hypoglossal nucleus after hypoglossal nerve transection (Nakagomi et al., 2003). Moreover, ATF-3 is strongly expressed in SOD^{G93A} mouse motoneurons prior to neurodegeneration (Vlug *et al*., 2005) as well as in the spinal cord of $SOD1^{G93A}$ rats (Malaspina et al., 2010).

Thus, given its early and transient kinetic of expression in response to extracellular stress signals and its relative specificity for neuronal damage, ATF-3 can be used as a useful marker for early neuronal distress.

4. Hypoglossal motoneurons: a model to study ALS-related pathological factors

HMs are among the most strongly damaged neurons in ALS. HM dysfunction, resulting in dysarthria and dysphagia, is often a very early symptom in ALS patients (Kühnlein et al., 2008) and bulbar deficits are also clearly detectable in ALS animal models in the early phase of the disease (Smittkamp et al., 2010).

The hypoglossal nucleus has been extensively investigated to clarify the basic pathogenetic mechanisms of ALS and to understand its selective vulnerability: studies of the expression of calcium binding proteins, type I mGluRs, GluR2 AMPA receptor subunit (Reiner et al., 1995; Lips and Keller, 1998; Laslo et al., 2000, 2001a,b) and characterization of HM functional changes in mutant SOD1 animals (von Lewinski et al., 2008; van Zundert et al., 2008), indicated how the nucleus hypoglossus is at very high risk of neurodegeneration and may represent a useful *in vitro* model to mimic ALS pathogenesis in experimental conditions.

In our laboratory we have recently used HMs to mimic the effects of a transient oxidative stress (elicited by H_2O_2) on HM properties and survival (Nani et al., 2010). Since oxidative stress is considered a major player in ALS pathogenesis not only in ALS familial cases (as indicated by the host (>140) of SOD1 mutations) but even in the absence of mutated SOD1 (Shaw et al., 1995b; Ferrante et al., 1997; Bogdanov et al., 2000; Ihara et al., 2005), wildtype HMs represented an appropriate model for studying the consequences of a free-radical challenge. We found that H_2O_2 generated a complex chain of events including reduced network activity and enhanced HM firing; moreover, despite these effects were not accompanied by early (1 h) motoneuronal loss, they were associated with activation of the distress factor ATF-3, and no damage to astroglia was observed. Therefore, these results demonstrated that acute oxidative stress induced a

series of functional changes hitherto unreported and potentially relevant to the theory of oxidative damage in ALS (Vucic and Kiernan, 2006).

In the present study we extended our investigation on the effect of excitotoxicity, a second important player in ALS pathogenesis (Van Den Bosch et al., 2006). We had previously (Sharifullina and Nistri, 2006) developed a simple *in vitro* model of excitotoxic stress to HMs by blocking glutamate uptake with the selective inhibitor TBOA: this compound preferentially blocks the glutamate transport system of glial cells and is experimentally advantageous because it is devoid of effects on glutamate receptors and is not transported by the glutamate carrier (Anderson et al., 2001), thus avoiding amino acid hetero-exchange. When TBOA is applied to HMs, about half of the cells exhibits bursting activity accompanied by strong enhancement in excitatory synaptic transmission, neuronal recruitment and massive depolarization: bursts are synchronous between electrically coupled motoneurons and in a subset of cells they are associated to irreversible rise of their Ca^{2+} levels, leading to HM deterioration without recovery (Sharifullina and Nistri, 2006). These observations demonstrated that inhibition of glutamate uptake can have a deadly effect on motoneurons (with TBOA-bursting being the cellular hallmark of the on-going pathological event), that this is not a generalized phenomenon within the nucleus hypoglossus, as only motoneurons displaying large bursts and Ca^{2+} disregulation are likely to be those that later die.

Therefore, despite the limitation of an *in vitro* model, the TBOA protocol represents a good mimicry of ALS-related excitotoxicity at least for the following reasons: excitotoxicity is actually produced by raising endogenous glutamate, rather than by giving a glutamate agonist, resembling its gradual build-up in the cerebrospinal fluid of ALS patients (which is thought to be caused by the down-regulation of glutamate uptake; Rothstein et al., 1992, 1995); in analogy to the human pathology (Swash and Ingram, 1988) the effects of TBOA are patchy and not generalized to all motoneurons, leaving the possibility for testing neuroprotective strategies.

Aims

1) In the present study we used HMs from the neonatal rat brainstem to investigate the ability of riluzole (the only drug currently licensed for ALS treatment; Lacomblez et al., 1996) to change the excitotoxicity consequent to TBOA application in terms of network bursting and survival of motoneurons. We enquired whether riluzole, applied early (~ 15 min) after the onset of the excitotoxic insult, at a concentration similar to the plasma therapeutic concentration in human (5 μM; Wokke, 1996; Cheah et al., 2010), could suppress the deadly bursting of motoneurons and protect their numbers. We also looked for early sign of motoneuron distress investigating the expression of the ATF-3 transcription factor (often associated to neuronal distress; Tsujino et al., 2000; Hai and Hartman, 2001; Vlug et al., 2005) and then, given the important contribution by non-neuronal cells to ALS pathogenesis (Clement et al., 2003; Rao and Weiss, 2004; Boillée et al., 2006; Van Damme et al., 2007; Di Giorgio et al., 2007; Marchetto et al., 2008; Van Den Bosch and Robberecht, 2008; Philips and Robberecht, 2011), we further explored whether TBOA could affect glia and whether riluzole could change this action. These data are reported in Cifra et al. (2011a).

2) Moreover, to better evaluate the nature and specificity of our experimental protocols on the hypoglossal nucleus cell populations, we investigated the numbers and types of neurons and glia present in this brain region during postnatal development and also the effects of the slicing and *in vitro* procedures on cell viability. These results are reported in Cifra et al. (2011c) (see also Cifra et al., 2011a for the effects of slicing and *in vitro* procedures on cell viability).

3) Finally, we analyzed the results obtained with the TBOA-model in relation to those collected in the work by Nani et al., (2010), in order to compare the consequences to HMs of excitotoxicty and oxidative stress, being two major factors in ALS pathogenesis. These data are reported in Cifra et al. (2009) and Cifra et al. (2011b).

For Materials&Methods and Results sections, please see enclosed papers.

PHILOSOPHICAL TRANSACTIONS OF THE ROYAL SOCIETY B BIOLOGICAL SCIENCES

A repertoire of rhythmic bursting produced by hypoglossal motoneurons in physiological and pathological conditions

Alessandra Cifra, Francesca Nani, Elina Sharifullina and Andrea Nistri

Phil. Trans. R. Soc. B 2009 **364**, 2493-2500
doi: 10.1098/rstb.2009.0071

PHILOSOPHICAL TRANSACTIONS OF THE ROYAL SOCIETY B

Phil. Trans. R. Soc. B (2009) **364**, 2493–2500
doi:10.1098/rstb.2009.0071

A repertoire of rhythmic bursting produced by hypoglossal motoneurons in physiological and pathological conditions

Alessandra Cifra†, Francesca Nani†, Elina Sharifullina and Andrea Nistri*

International School for Advanced Studies (SISSA), Via Beirut 2-4, 34014 Trieste, Italy

The brainstem *nucleus hypoglossus* contains motoneurons that provide the exclusive motor nerve supply to the tongue. In addition to voluntary tongue movements, tongue muscles rhythmically contract during a wide range of physiological activities, such as respiration, swallowing, chewing and sucking. Hypoglossal motoneurons are destroyed early in amyotrophic lateral sclerosis (ALS), a fatal neurodegenerative disease often associated with a deficit in the transport system of the neurotransmitter glutamate.

The present study shows how periodic electrical discharges of motoneurons are mainly produced by a neuronal network that drives them into bursting mode via glutamatergic excitatory synapses. Burst activity is, however, modulated by the intrinsic properties of motoneurons that collectively synchronize their discharges via gap junctions to create 'group bursters'. When glial uptake of glutamate is blocked, a distinct form of pathological bursting spontaneously emerges and leads to motoneuron death. Conversely, H_2O_2-induced oxidative stress strongly increases motoneuron excitability without eliciting bursting. Riluzole (the only drug currently licensed for the treatment of ALS) suppresses bursting of hypoglossal motoneurons caused by blockage of glutamate uptake and limits motoneuron death. These findings highlight how different patterns of electrical oscillations of brainstem motoneurons underpin not only certain physiological activities, but also motoneuron death induced by glutamate transporter impairment.

Keywords: brainstem; amyotrophic lateral sclerosis; oscillation; glutamate uptake; oxidative stress; hydrogen peroxide

1. RHYTHMIC ELECTRICAL DISCHARGES ARE NECESSARY FOR STEREOTYPIC MOTOR BEHAVIOUR

Rhythmic electrical oscillations mediate information storage and transfer within neuronal networks (Sejnowski & Paulsen 2006). In addition, repetitive motor commands are required for behaviours based on rhythmic contractions of skeletal muscles, such as respiration (Suzue 1984; Onimaru *et al.* 1987; Ballanyi *et al.* 1999), mastication and swallowing (Jean 2001). These functions demand the coordinated discharges of a network of neurons that initiate and maintain the rhythmic output of motoneurons: hypoglossal motoneurons are driven by pre-motoneurons embedded in a functional ensemble termed 'central pattern generator' (Grillner 2006; Kiehn 2006; Rybak *et al.* 2007; Briggman & Kristan 2008) whose localization is believed to be distributed among several nuclei of the caudal brainstem. Important, yet unresolved, questions are the existence of multiple central pattern generators subserving analogous functions and the extent of their network overlap in anatomical or functional terms.

One major motor output of the brainstem is from the motoneurons of the nucleus hypoglossus that command tongue muscles to contract rhythmically during inspiratory movements, chewing, sucking, swallowing, and vocalization with different, function-related frequencies and properties (Lowe 1980). In neurodegenerative diseases such as the bulbar form of amyotrophic lateral sclerosis (ALS), the nucleus hypoglossus is among the most vulnerable (Krieger *et al.* 1994; Lips & Keller 1999; Laslo *et al.* 2001). In ALS, pathological clonic muscle contractions often precede muscle paralysis. Hence, studying the functional characteristics of hypoglossal motoneurons can provide useful information on the integrative properties of brainstem motor networks in health and disease.

Within this framework, the activity of hypoglossal motoneurons can be considered as the functional readout of information programmed and encoded in pre-motoneuronal networks. This notion is, perhaps, too simple as it does not include the possibility that motoneurons are endowed with intrinsic rhythmogenesis and/or that small local networks lacking distinct nuclear arrangement can potently drive rhythmic discharges of motoneurons. The present study intends

*Author for correspondence (nistri@sissa.it).
†These authors equally contributed to the present study.

One contribution of 17 to a Discussion Meeting Issue 'Brainstem neural networks vital for life'.

to show the complexity of bursting modes generated by hypoglossal motoneurons through a spectrum of mechanisms that range from intrinsic rhythmicity to network-evoked activity via a blend of functional processes related to physiological or pathological conditions.

We have investigated these issues by using, as an experimental tool, a relatively thin (approx. 250 μm) coronal slice of the neonatal rat brainstem in which the nucleus hypoglossus can be readily identified and single living motoneurons can be viewed with infrared microscopy. In our studies, we have employed whole-cell patch clamp recording from hypoglossal motoneurons together with their histochemical analysis (Sharifullina *et al.* 2004, 2005; Lamanauskas & Nistri 2006, 2008). Bursts are defined as large, sustained changes in membrane potential (or holding current) caused by periodic up and down swings of the baseline, while oscillations are more rapid, low-amplitude fluctuations.

2. HETEROGENEITY OF MOTONEURON RHYTHMIC BURSTING EVOKED BY NEUROMODULATORS

Can motoneurons display intrinsic bursting in the absence of a functional network? Membrane depolarization by intracellular current injection or application of high K^+ solution consistently fails to trigger oscillatory activity (Sharifullina *et al.* 2005, 2008). Thus, unlike pre-motoneuronal networks that promptly generate rhythmic oscillations when depolarized with high K^+, hypoglossal motoneurons do not share this property whether residing in an intact slice or isolated from their connections. Nevertheless, such motoneurons can produce persistent bursts (0.43 ± 0.07 Hz) when excited by the glutamate agonist *N*-methyl-D-aspartate (NMDA) (figure 1*a*). This activity is reversibly blocked by inorganic Ca^{2+} channel blockers like Cd^{2+} (Sharifullina *et al.* 2008; figure 1*a*). Conversely, the Na^+ channel blocker tetrodotoxin can suppress bursting in a few motoneurons only.

In the majority of motoneurons recorded from a brainstem slice preparation with intact synaptic transmission, the NMDA-induced bursts tend to wane (despite sustained membrane depolarization), and are readily reinstated when the membrane potential is returned to baseline level by current injection. A significant minority of these neurons do, however, behave like persistent bursters at depolarized membrane potential. Curiously, NMDA-evoked bursts are resistant to elevated concentrations (5–12 mM) of extracellular Mg^{2+}, probably because of the widespread expression of the NR2D receptor subunit that confers poor sensitivity of NMDA receptors to Mg^{2+} (Sharifullina *et al.* 2008). These properties are not generalized to all brainstem motoneurons. For instance, in trigeminal motoneurons, NMDA-evoked bursting develops after the first post-natal week, shows a different Mg^{2+} sensitivity and is powerfully facilitated by serotonin (Hsiao *et al.* 2002). Thus, it appears that the developmental maturation of motoneuron bursting patterns starts very early for hypoglossal motoneurons. It is tempting to speculate that such a bursting represents one mechanism for rhythmic tongue contractions typical of milk sucking (Kutsuwada *et al.* 1996) appearing immediately after birth.

To sum up, hypoglossal motoneurons can produce rhythmic bursting elicited by NMDA through a robust mechanism that is mainly intrinsic to these cells because it is unaffected by blockers of excitatory

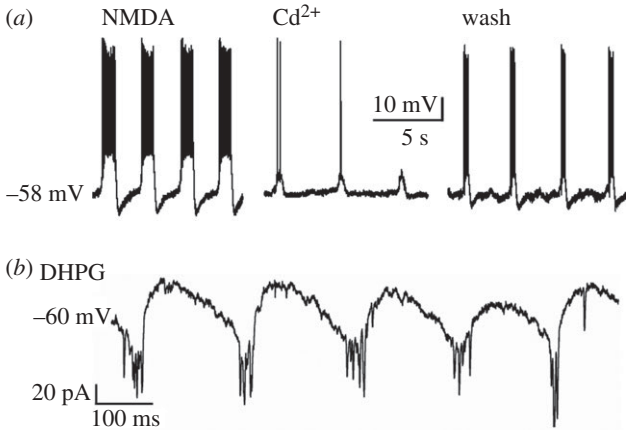

Figure 1. Bursting of hypoglossal motoneurons induced by NMDA or DHPG. (*a*) Under current clamp condition, steady bursting is evoked by 25 μM NMDA. Each depolarization wave comprises a cluster of action potentials. In the presence of Cd^{2+} (400 μM), bursting is suppressed (middle panel) but reinstated during washout (right panel). (*b*) Theta frequency bursting evoked by DHPG (25 μM) applied to a motoneuron voltage clamped at −60 mV. Bursts are observed as inward current (large downward deflections) with superimposed fast oscillations; for further details, see Sharifullina *et al.* (2005, 2008).

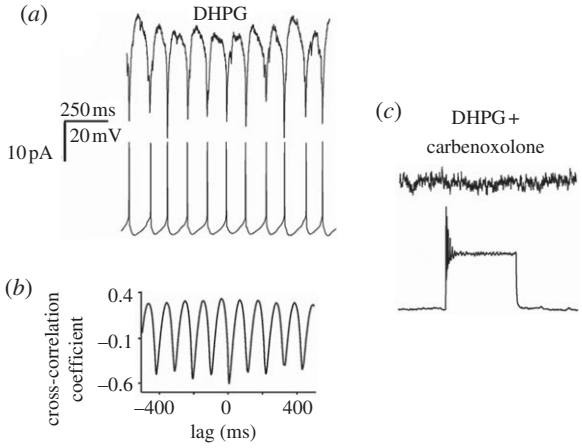

Figure 2. Bursting depends on electrical coupling between motoneurons. (*a*) Example of paired, patch clamp recording from two adjacent motoneurons in voltage (top row) and current (bottom row) conditions during application of DHPG (25 μM). Note the 1 : 1 coupling between burst currents and burst depolarizations. (*b*) Cross correlogram of data shown in A confirm tight coupling between events. (*c*) Carbenoxolone (100 μM) blocks bursting in both cells and prevents depolarization. A depolarizing current (0.6 nA) pulse injected into the current clamped cell evokes transient firing without any response in the voltage-clamped neuron, demonstrating loss of electrical coupling. All data are from the same pair of hypoglossal motoneurons; for further details, see Sharifullina *et al.* (2005).

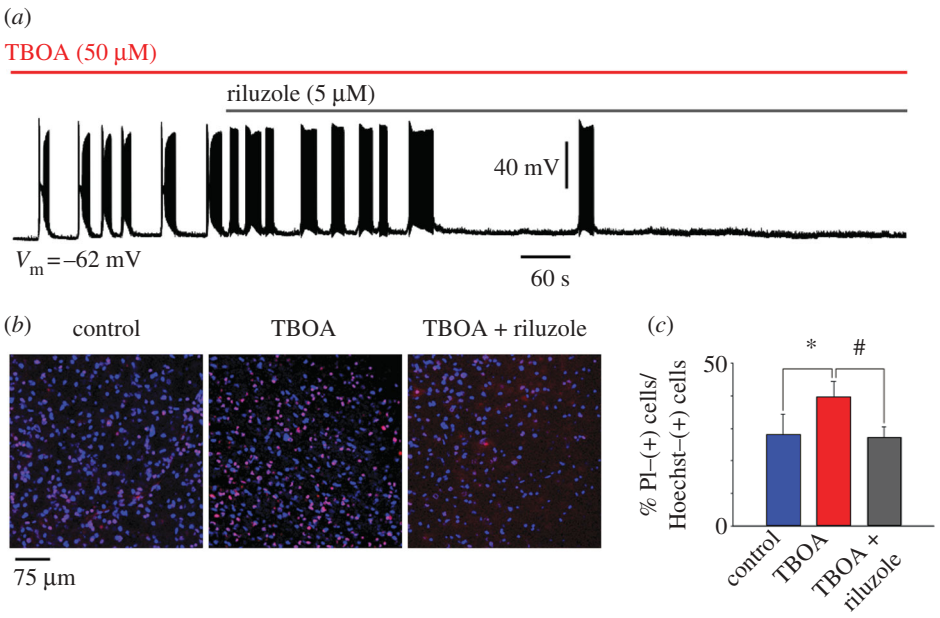

Figure 3. Riluzole inhibits TBOA-evoked bursting. (*a*) Sample trace of current clamp recording from hypoglossal motoneuron exposed to TBOA (50 μM) that, on average, produces 3.0 ± 0.7 mV depolarization ($n = 8$; data not shown). In this example (recorded in the presence of 0.4 μM strychnine and 10 μM bicuculline), bursts emerge with a latency of 60 s. Note that the burst structure is made up of a depolarization envelope with superimposed fast spikes followed by transient inactivation and subsequent return of firing. This pattern confers a 'butterfly' shape to each burst event. Riluzole (5 μM) added after 4.30 min from the start of TBOA application slowly inhibits bursting, which, in this example, is suppressed after 10 min. (*b*) Histochemical demonstration of motoneuron damage produced by 60 min application of TBOA and its antagonism by riluzole (applied 14 min from the start of TBOA application). Cell damage is assessed with propidium iodide (a DNA dye that labels membrane-damaged cells; Sharifullina & Nistri 2006) staining (shown in red) versus staining due to Hoechst 33342 (shown in blue; a cell-permeable DNA dye). (*c*) Histograms quantify increased death of motoneurons after exposure to TBOA ($n = 13$) and its prevention by riluzole ($n = 23$), which preserves the same number of surviving cells found in control conditions ($n = 19$). Data are expressed as percentage of propidium iodide-positive cells versus Hoechst 33342-positive cells and quantified with ImageJ software. $^{*}p = 0.038$ for the difference between control and TBOA, and $^{\#}p = 0.025$ for the difference between TBOA and TBOA plus riluzole. Slices were collected from 10 rats (A. Cifra 2008, unpublished data).

or inhibitory synaptic transmission (Sharifullina *et al.* 2008), and that is preserved despite fluctuations in extracellular Mg^{2+}.

Activation of NMDA receptors is not the only glutamatergic stimulus to induce bursting. In fact, pharmacological stimulation by 3,5-dihydroxyphenylglycine (DHPG) of subtype 1 receptors of group I metabotropic glutamate receptors (mGluR; widely expressed in the brainstem; Del Negro & Chandler 1998) evokes a characteristic pattern of bursting (6.5 ± 0.6 Hz) that falls within the range of the so-called theta oscillations (Sharifullina *et al.* 2005; figure 1*b*). These bursts, which are preceded by a significant rise in cell input resistance and are usually accompanied by fast oscillations (18 ± 8 Hz; see rapid transients in figure 1*b*), are insensitive to NMDA receptor blockers and are due to a large enhancement of AMPA receptor-mediated responses at the network and motoneuron levels (Sharifullina *et al.* 2004). Bursting is apparently paced by the cyclic activation of K_{ATP} conductances, thus linking electrical discharges to the cell energy metabolism. Current clamp recording indicates that, during bursting, motoneuron spikes appear only at the peak of each burst, in contrast to the irregular firing emerging when the same cell is depolarized to a comparable level of membrane potential (Sharifullina *et al.* 2005). Hence, bursts strongly constrain the firing pattern of motoneurons and amplify AMPA receptor-mediated synaptic inputs. While the theta frequency of bursts induced by DHPG is too fast for the normal inspiratory rhythm of *in vivo* normoxic animals, it is likely that mGluR activation (even if not involved in eupnoea) contributes to the expression of the respiratory rhythm (Li & Nattie 1995).

Bursting emerging in the presence of DHPG is, therefore, an example of the mixed origin of such electrical events, namely coincidence of increased excitatory synaptic activity and enhanced sensitivity of motoneurons to these inputs (Nistri *et al.* 2006).

Our studies have indicated that theta frequency bursts can also be generated by an almost exclusively pre-synaptic mechanism of facilitation of glutamate release. Our former experiments have indicated that ambient acetylcholine facilitates glutamate release (Quitadamo *et al.* 2005). When nicotinic receptors are stimulated by nicotine (Lamanauskas & Nistri 2006), bursting (5.6 ± 0.3 Hz) appears with some delay after the initial inward current and is associated with a large increase in the frequency of glutamatergic synaptic events. Thus, oscillations emerge once network excitability is strongly heightened and abruptly disappear when the network excitability falls below threshold. Under these experimental conditions, bursting requires continuous activation of nicotinic receptors, and lasts for approximately 10 min, suggesting that nicotinic

receptor desensitization develops slowly. As in the case of DHPG-elicited bursting, nicotine-evoked bursting transforms the irregular firing of motoneurons into a time-locked pattern in coincidence with the peak of each oscillatory event (Lamanauskas & Nistri 2006). Interestingly, nicotine-evoked bursting is suppressed by AMPA receptor blockers (though insensitive to NMDA receptor antagonism) or by group I mGluR antagonists. These observations suggest that nicotine-induced bursting requires a robust release of endogenous glutamate acting concurrently via AMPA as well as metabotropic receptors.

3. FACTORS RESPONSIBLE FOR MOTONEURON BURSTING

Throughout these investigations, it was apparent that bursting could be observed in the majority of hypoglossal motoneurons, though a significant number of them never generated bursts. For instance, 75 per cent of motoneurons typically exhibit NMDA-induced bursting (Sharifullina *et al.* 2008), while for DHPG- (Sharifullina *et al.* 2005) and nicotine-induced (Lamanauskas & Nistri 2006) bursting the percentage is 40–50%. Although one might assume that the stronger excitation elicited by NMDA versus DHPG or nicotine is an important factor to increase bursting occurrence, other processes are probably implicated as well.

One contributor is synaptic inhibition mediated by gamma-aminobutyric acid (GABA) and glycine (Marchetti *et al.* 2002). In all tests with different protocols to evoke bursts, pharmacological block of $GABA_A$ and glycine receptors consistently raises the likelihood of observing bursts without changing burst properties like frequency or duration. It is noteworthy that, unlike spinal networks (Bracci *et al.* 1996), pharmacological block of synaptic inhibition in the brainstem slice does not elicit bursting of hypoglossal motoneurons.

While diverse bursting patterns are induced with different protocols and show distinctive sensitivity to pharmacological agents, there is one common property consistently shared in every condition tested, namely the dependence on electrical coupling of motoneurons. Previous studies have identified electrical coupling between hypoglossal motoneurons under *in vivo* and *in vitro* conditions using dye coupling or electrophysiological recording (Mazza *et al.* 1992; Rekling *et al.* 2000). Figure 2*a* shows an example of strong, bidirectional coupling between adjacent motoneurons in the brainstem slice preparation (Sharifullina *et al.* 2005) in which, during bursting evoked by DHPG, two hypoglossal motoneurons are simultaneously recorded under voltage (upper record) and current (lower record) conditions. Signal coupling between burst currents and spikes is 1 : 1, with strong cross correlation as indicated by the plot in figure 2*b*. It seems likely that electrical coupling depends on gap junctions sensitive to carbenoxolone (100 μM) as demonstrated in figure 2*c*, in which this agent suppresses electrical coupling between the two motoneurons as well as their synchronous DHPG-induced bursting. The expression of various types of connexins in the neonatal and adult rat brainstem (Solomon *et al.* 2001; Solomon 2003) indicates that the neurons probably synchronize their bursting activity through these membrane proteins specialized in interneuronal communication. The electrical equivalent of this communication is the presence of 'spikelets' and 'burstlets', namely the action potentials and the depolarization waves spread via gap junction that recruit, excite and coordinate motoneuron discharge patterns (Sharifullina *et al.* 2005). Bursts are, therefore, the summated expression of synchronized depolarization and firing occurring in a group of motoneurons. This interpretation accords with the poor voltage sensitivity of bursts (Sharifullina *et al.* 2005, 2008) because their origin comes from functionally interconnected cells rather than from ligand and/or voltage-gated channels of single motoneurons.

To express and support bursting, the interplay among complex conductance mechanisms is necessary. For example, in the case of NMDA, it is proposed that the activity of persistent inward currents, fast Na^+ current activation/inactivation and rhythmic activation and deactivation of K^+ conductances pace the oscillation frequency (Sharifullina *et al.* 2008). Nevertheless, sustained NMDA-dependent bursting detected in the majority of motoneurons requires the drive by a few (electrically coupled) motoneurons that continuously burst (or fire) and, thus, provide strong excitation to the functionally coupled network of motoneurons. This notion is supported by the presence of hypoglossal nerve bursting even when concomitant recording from a single motoneuron shows burst fading (Sharifullina *et al.* 2008).

In networks of similar integrate-and-fire neurons, different network patterns depend on the strength of electrical coupling (Chow & Kopell 2000). Furthermore, this process may amplify the parameter range over which initially uncoupled neurons can start bursting (Soto-Trevinõ *et al.* 2005), especially because a neuromodulator (for example, DHPG or nicotine) can modify intrinsic properties, gap junctions and synaptic inputs, thereby changing the effective compartmental structure of the network (Soto-Trevinõ *et al.* 2005).

4. GROUP BURSTERS

Hypoglossal motoneurons are not endowed with spontaneous rhythmicity. To express synchronous, repeated discharges, several conditions must be met, among which, as shown earlier, the presence of electrical coupling or synchronous excitatory synaptic drive is of paramount importance. Hence, bursting is not due to the activity of pacemakers, but is an emergent property (Del Negro *et al.* 2002) of the pre-motoneuron/motoneuron network where the fundamental unit of oscillation is an ensemble of neurons (with similar intrinsic properties) that become rhythmically active through chemical and electrotonic excitatory synaptic interactions (Rekling & Feldman 1998). These concepts have been applied to brainstem respiratory neurons, leading to the proposal of 'group pacemakers' (Feldman & Del Negro 2006). This model is also useful for interpreting data concerning hypoglossal motoneurons that may be viewed as 'group bursters', bound together in a synchronous oscillatory activity by

neuromodulators that raise motoneuron and pre-motoneuron excitability via facilitation of synaptic inputs and neuronal conductances.

Experimental and theoretical studies of cortical networks (Eytan & Marom 2006) have indicated that a threshold-governed, synchronized population event follows the logistics of neuronal recruitment in an effectively scale-free connected network in which synchronization time does not increase markedly with network size. It is likely that similar principles apply to the group bursters of hypoglossal motoneurons.

5. PATHOPHYSIOLOGICAL BURSTING

Hypoglossal motoneurons are particularly sensitive to neurodegenerative diseases like ALS, whose early symptoms include slurred speech, dysphagia and tongue biting. A large number of patients show abnormally high concentrations of glutamate in their cerebrospinal fluid and impaired glutamate uptake by glia. For these reasons it has been argued that ALS may be caused by excitotoxicity of motoneurons due to their continuous over-stimulation by glutamate (Cleveland & Rothstein 2001; Rowland & Shneider 2001; Bruijn *et al.* 2004; Rao & Weiss 2004). Excitotoxicity is thought to involve production of free oxygen radicals and oxidative stress with depletion of cell energy metabolism (Rao & Weiss 2004). Rare cases of genetically transmitted ALS show a mutation of the enzyme superoxide dismutase 1 (SOD1) that normally scavenges these toxic compounds. Neonatal hypoglossal motoneurons from SOD1 mutant mice show enhanced excitability and synaptic inputs long before the onset of neurological symptoms (van Zundert *et al.* 2008).

Consistent with the view that glutamate can induce excitotoxicity of hypoglossal motoneurons is the demonstration that pharmacological inhibition by DL-threo-β-benzyloxyaspartate (TBOA; 50 μM) of the glutamate transporters elicits a deadly motoneuron bursting pattern that leads to patchy loss of motoneurons as demonstrated by Sharifullina & Nistri (2006). The TBOA-evoked bursting is clearly an emergent property of motoneurons that require efficient network activity to exhibit this pattern accompanied by strong enhancement in excitatory synaptic transmission, neuronal recruitment, massive depolarization and burst firing. Interestingly, TBOA bursts occur even in a minislice of the brainstem, which essentially excludes the reticular formation: this result is consistent with the view of scale-free group bursters synchronized independently from network size.

Unlike bursts observed following the application of neuromodulators, TBOA burst currents are very slow (occurring on average once every 2 min), very long (35 ± 2 s) and much larger than those produced by NMDA or DHPG. However, only approximately one-third of motoneurons show TBOA bursting, though block of synaptic inhibition significantly increases bursting occurrence. TBOA bursts possess certain characteristics similar to those of the less dramatic bursts induced by neuromodulators, namely they are synchronous between electrically coupled motoneurons and are fully suppressed by carbenoxolone and glutamate receptor antagonists.

The spatio-temporal evolution of TBOA bursts can be monitored with patch clamping and intracellular Ca^{2+} imaging (Sharifullina & Nistri 2006). Bursting motoneurons are scattered throughout the nucleus hypoglossus and show gradual elevation in their baseline Ca^{2+} with repeated transients. In a number of them, bursting is replaced by a massive, irreversible inward current and a persistently high level of intracellular Ca^{2+}, suggesting severe cell damage. Histochemical analysis has confirmed significant loss of hypoglossal motoneurons, a phenomenon prevented by carbenoxolone or glutamate receptor blockers.

Our observations suggest that inhibition of glutamate uptake can have a deadly effect on motoneurons, that this is not a generalized phenomenon within the nucleus hypoglossus and that those motoneurons that display large bursts are probably those that later die.

As riluzole is the only drug licensed for delaying ALS disease progression in man, it may be useful to find out if riluzole can block TBOA bursts and motoneuron loss in the brainstem slice model. Furthermore, it is important, for ALS cellular pathophysiology, to understand whether the deleterious effect of TBOA is mediated by free oxygen radicals in analogy with the scenario proposed for SOD1-mutated ALS (Rao & Weiss 2004).

6. A MODEL TO PREDICT IF DRUGS CAN BLOCK THE EXCITOTOXIC DAMAGE OF HYPOGLOSSAL MOTONEURONS

Riluzole has complex pharmacological effects on brainstem motoneurons. At low concentrations (5–10 μM), the main targets of its action are pre-synaptic inhibition of the release of glutamate and suppression of voltage-gated persistent inward currents mediated by Na^+ and Ca^{2+} (Lamanauskas & Nistri 2008). It seems likely that these combined effects contribute to limit motoneuron excitability and, perhaps, to retard the relentless progression of ALS. Although riluzole can block nicotine-evoked bursting (Lamanauskas & Nistri 2008), it seems useful to explore whether riluzole can suppress the much stronger TBOA-evoked bursts. Figure 3*a* shows that, under current clamp conditions, riluzole (5 μM), applied after the onset of bursting, suppresses this phenomenon. Bursts are blocked within 319 ± 138 s without significant change in their period or duration, or in baseline membrane potential. Similarly, motoneuron damage (monitored on the basis of propidium iodide staining) following TBOA application is also limited by applying riluzole after TBOA (figure 3*b*,*c*).

These data suggest that TBOA bursting is a useful *in vitro* model to test the efficiency of neuroprotective drugs to inhibit excitotoxicity and pathological discharges of brainstem motoneurons.

7. ARE EXCITOTOXICITY AND OXIDATIVE STRESS TWO CLOSELY KNITTED PATHWAYS TO MOTONEURON DAMAGE?

The aetiology and pathogenesis of sporadic ALS remain poorly understood in terms of known environmental

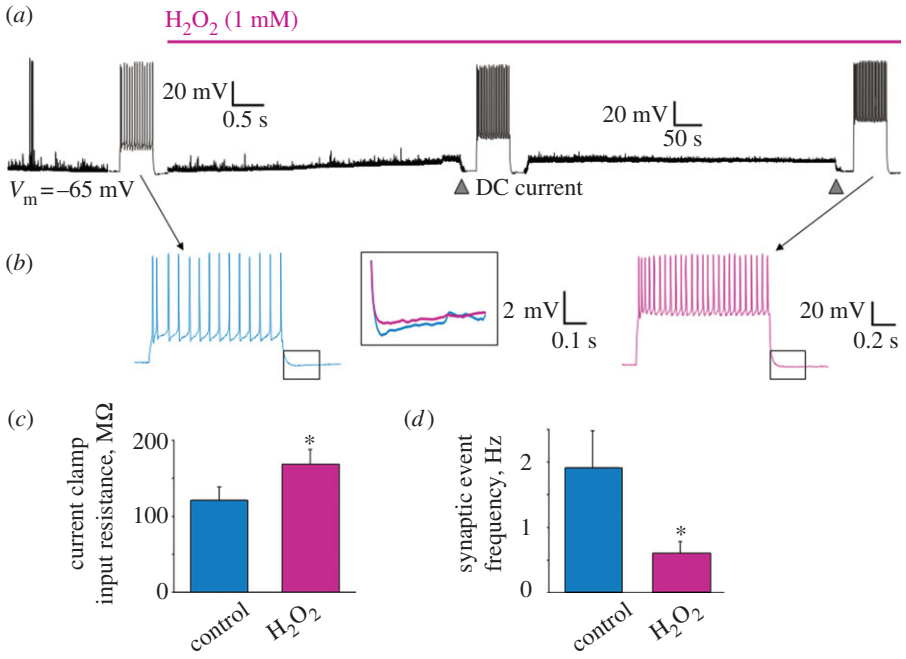

Figure 4. Changes in motoneuron excitability induced by H_2O_2. (*a*) Examples of responses of hypoglossal motoneuron to bath-applied H_2O_2. Trace is a continuous, slow record (in current clamp configuration) of a cell with initial membrane potential of −65 mV (for methods, see Sharifullina *et al.* 2005; Lamanauskas & Nistri 2008). Segments of this trace are also shown on a faster time base to depict spike firing evoked by intracellular injection of 300 pA (500 ms). Note that, following the application of H_2O_2, there is gradual membrane depolarization (8 mV) associated with reduction in global synaptic events (decrease in baseline thickness and noise; see (*d*) for quantification of event frequency) and enhanced spike firing (when the membrane potential is repolarized back to rest). (*b*) Fast time base example of spike activity in control (blue) and during H_2O_2 application (pink). Note the larger number of spikes and the larger amplitude of the membrane voltage response to the same current injection pulse (300 pA). The box section shows (at higher gain) superimposed spike afterhyperpolarizations recorded in control or during H_2O_2 application. Despite the higher number of spikes, the afterhyperpolarization is decreased. (*c*) Change in cell input resistance (measured from voltage response to a hyperpolarizing current pulse of −50 pA) in the presence of H_2O_2. Data are averages from five motoneurons (*$p < 0.01$). (*d*) Reduction in global synaptic event frequency elicited by H_2O_2 (data are from five motoneurons voltage clamped at −70 mV; *$p < 0.04$) (F. Nani 2008, unpublished data).

toxic agents. Current theories favour 'convergence' of excitotoxicity and oxidative stress as the two cell processes concurring to produce motoneuron death in ALS (Cleveland & Rothstein 2001; Bruijn *et al.* 2004; Rao & Weiss 2004). Hence, if a strong excitotoxic stimulus prompts damage via oxidative stress, one may test whether oxidative stress implies excitotoxicity or, at least, changes in motoneuron excitability similar to those evoked by excitotoxicity. Hydrogen peroxide (H_2O_2) is a natural neuromodulator (at low μM concentrations; Kamsler & Segal 2004) as well as a robust donor of free oxygen radicals to evoke severe oxidative stress (at mM concentrations) downstream of SOD1 activity (Kato *et al.* 2004; Nicholls 2004). Figure 4*a* shows that 1 mM H_2O_2 evokes complex effects on hypoglossal motoneurons, which, in most cases, are actually opposite to those elicited by TBOA.

Thus, H_2O_2 induces a slow depolarization (8 mV) accompanied by increased firing in response to current injection from similar baseline membrane potential, probably due to a depression of the spike afterhyperpolarization that normally contributes to spike frequency accommodation (figure 4*b*). In contrast to TBOA bursting, H_2O_2 induces a significant rise in motoneuron input resistance (figure 4*c*) and large depression of all synaptic events without the emergence of any oscillatory activity (figure 4*d*). The effects elicited by H_2O_2 are insensitive to blockers of excitatory or inhibitory synaptic transmission. Hence, oxidative stress paradoxically makes motoneurons more isolated from their network and yet more intrinsically excitable. This condition is indeed associated with oxidative stress damage of motoneurons as shown in figure 5*a*,*b*, where this process is assessed on the basis of the rhodamine 123 marker.

It is interesting to compare the acute action of H_2O_2 with the motoneuron phenotype of the mutated SOD1 mice with aberrant handling of reactive oxygen species (van Zundert *et al.* 2008). In either case, hypoglossal motoneurons fire more intensely: however, in the mutant, the persistent Na^+ current is enhanced without change in input resistance or afterhyperpolarization. The consequence of acute application of H_2O_2 to wild-type motoneurons is, on the other hand, depression of the persistent inward current and increased input resistance. Because data from SOD1 mutant motoneurons have been collected in the pre-symptomatic phase, it seems likely that they indicate compensatory mechanisms to cope with the results of gene mutation before the disease flares up.

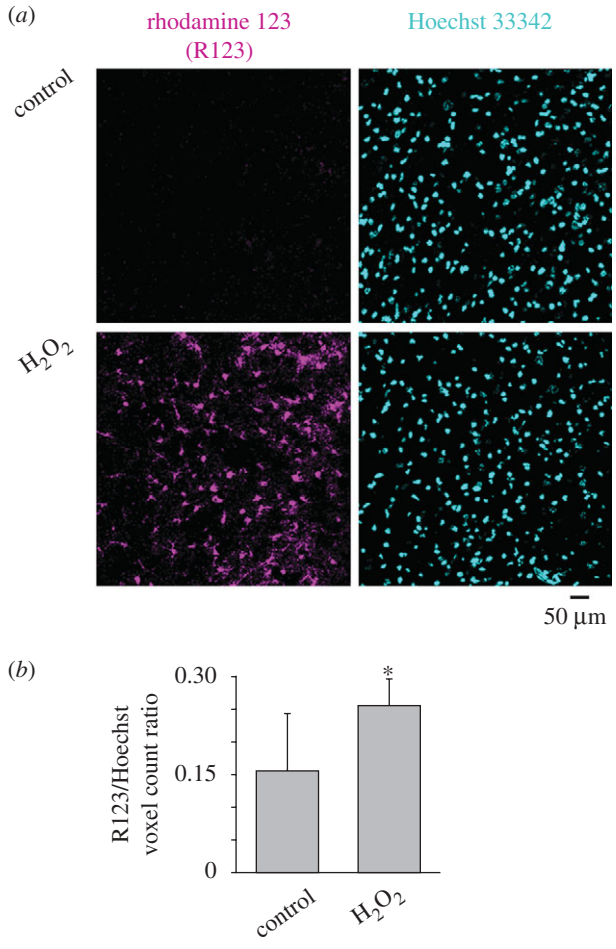

Figure 5. Oxidative stress of hypoglossal motoneurons induced by H_2O_2. (*a*) Histological example of rhodamine 123 staining of cells in hypoglossal slices incubated for 20 min in control solution or in the presence of H_2O_2 (1 mM). After rinsing, cells were stained with rhodamine 123 (5 µM; magenta pseudocolour) to reveal intracellular oxidative processes (Gomes *et al.* 2005; Jiang *et al.* 2006) and Hoechst 33342 (cyan pseudocolour) to show cell nuclei (Sharifullina & Nistri 2006). Note that, notwithstanding the analogous number of Hoechst-positive cells, there is a larger number of rhodamine 123-positive elements following H_2O_2. (*b*) Histograms show the ratio of rhodamine-positive cells over Hoechst-positive cells, indicating a significant rise after H_2O_2. Data are from 11 slices in control conditions and 14 slices after H_2O_2 and are quantified with ImageJ software ($*p < 0.03$). (F. Nani 2008, unpublished data).

8. CONCLUSIONS

In vitro studies of hypoglossal motoneurons have disclosed new properties that, rather than being simple operators of motor programmes generated by central pattern generators, appear to contribute to a variety of repetitive motor patterns essential for physiological functions. Nevertheless, the appearance of deranged motor patterns may indicate impending motoneuron damage and might represent a predictive model to assess potential pharmacological agents against neurodegenerative diseases like ALS.

This work is supported by a PRIN grant from MIUR and by a research grant from the Friuli Venezia Giulia regional government for the project SPINAL. We thank Dr Micaela Grandolfo for her help with histochemical experiments.

REFERENCES

Ballanyi, K., Onimaru, H. & Homma, I. 1999 Respiratory network function in the isolated brainstem–spinal cord of newborn rats. *Prog. Neurobiol.* **59**, 583–634. (doi:10.1016/S0301-0082(99)00009-X)

Bracci, E., Ballerini, L. & Nistri, A. 1996 Spontaneous rhythmic bursts induced by pharmacological block of inhibition in lumbar motoneurons of the neonatal rat spinal cord. *J. Neurophysiol.* **75**, 640–647.

Briggman, K. L. & Kristan, W. B. 2008 Multifunctional pattern-generating circuits. *Annu. Rev. Neurosci* **31**, 271–294. (doi:10.1146/annurev.neuro.31.060407.125552)

Bruijn, L. I., Miller, T. M. & Cleveland, D. W. 2004 Unraveling the mechanisms involved in motor neuron degeneration in ALS. *Annu. Rev. Neurosci.* **27**, 723–749. (doi:10.1146/annurev.neuro.27.070203.144244)

Chow, C. C. & Kopell, N. 2000 Dynamics of spiking neurons with electrical coupling. *Neural Comput.* **12**, 1643–1678. (doi:10.1162/089976600300015295)

Cleveland, D. W. & Rothstein, J. D. 2001 From Charcot to Lou Gehrig: deciphering selective motor neuron death in ALS. *Nat. Rev. Neurosci.* **2**, 806–819. (doi:10.1038/35097565)

Del Negro, C. A. & Chandler, S. H. 1998 Regulation of intrinsic and synaptic properties of neonatal rat trigeminal motoneurons by metabotropic glutamate receptors. *J. Neurosci.* **18**, 9216–9226.

Del Negro, C. A., Morgado-Valle, C. & Feldman, J. L. 2002 Respiratory rhythm: an emergent network property? *Neuron* **34**, 821–830. (doi:10.1016/S0896-6273(02)00712-2)

Eytan, D. & Marom, S. 2006 Dynamics and effective topology underlying synchronization in networks of cortical neurons. *J. Neurosci.* **26**, 8465–8476. (doi:10.1523/JNEUROSCI.1627-06.2006)

Feldman, J. L. & Del Negro, C. A. 2006 Looking for inspiration: new perspectives on respiratory rhythm. *Nat. Rev. Neurosci.* **7**, 232–242. (doi:10.1038/nrn1871)

Gomes, A., Fernandes, E. & Lima, J. L. F. C. 2005 Fluorescence probes used for detection of reactive oxygen species. *J. Biochem. Biophys. Methods* **65**, 45–80. (doi:10.1016/j.jbbm.2005.10.003)

Grillner, S. 2006 Biological pattern generation: the cellular and computational logic of network in motion. *Neuron* **52**, 751–766. (doi:10.1016/j.neuron.2006.11.008)

Hsiao, C. F., Wu, N., Levine, M. S. & Chandler, S. H. 2002 Development and serotonergic modulation of NMDA bursting in rat trigeminal motoneurons. *J. Neurophysiol.* **87**, 1318–1328.

Jean, A. 2001 Brain stem control of swallowing: neuronal network and cellular mechanisms. *Physiol. Rev.* **81**, 929–969.

Jiang, Z. G. *et al.* 2006 A multifunctional cytoprotective agent that reduces neurodegeneration after ischemia. *PNAS* **103**, 1581–1586. (doi:10.1073/pnas.0510573103)

Kamsler, A. & Segal, M. 2004 Hydrogen peroxide as a diffusible signal molecule in synaptic plasticity. *Mol. Neurobiol.* **29**, 167–178. (doi:10.1385/MN:29:2:167)

Kato, S. *et al.* 2004 Histological evidence of redox system breakdown caused by superoxide dismutase 1 (SOD1) aggregation is common to SOD1-mutated motor neurons in humans and animal models. *Acta Neuropathol.* **107**, 149–158. (doi:10.1007/s00401-003-0791-1)

Kiehn, O. 2006 Locomotor circuits in the mammalian spinal cord. *Annu. Rev. Neurosci.* **29**, 279–306. (doi:10.1146/annurev.neuro.29.051605.112910)

Krieger, C., Jones, K., Kim, S. U. & Eisen, A. A. 1994 The role of intracellular free calcium in motor neuron disease. *J. Neurol. Sci.* **124**, 27–32. (doi:10.1016/0022-510X(94)90173-2)

Kutsuwada, T. *et al.* 1996 Impairment of suckling response, trigeminal neuronal pattern formation, and hippocampal LTD in NMDA receptor epsilon 2 subunit mutant mice. *Neuron* **16**, 333–344. (doi:10.1016/S0896-6273(00)80051-3)

Lamanauskas, N. & Nistri, A. 2006 Persistent rhythmic oscillations induced by nicotine on neonatal rat hypoglossal motoneurons *in vitro*. *Eur. J. Neurosci.* **24**, 2543–2556. (doi:10.1111/j.1460-9568.2006.05137.x)

Lamanauskas, N. & Nistri, A. 2008 Riluzole blocks persistent Na^+ and Ca^{2+} currents and modulates release of glutamate via presynaptic NMDA receptors on neonatal rat hypoglossal motoneurons *in vitro*. *Eur. J. Neurosci.* **27**, 2501–2514. (doi:10.1111/j.1460-9568.2008.06211.x)

Laslo, P., Lipski, J., Nicholson, L. F., Miles, G. B. & Funk, G. D. 2001 GluR2 AMPA receptor subunit expression in motoneurons at low and high risk for degeneration in amyotrophic lateral sclerosis. *Exp. Neurol.* **169**, 461–471. (doi:10.1006/exnr.2001.7653)

Li, A. & Nattie, E. E. 1995 Prolonged stimulation of respiration by brain stem metabotropic glutamate receptors. *J. Appl. Physiol.* **79**, 1650–1656.

Lips, M. B. & Keller, B. U. 1999 Activity-related calcium dynamics in motoneurons of the nucleus hypoglossus from mouse. *J. Neurophysiol.* **82**, 2936–2946.

Lowe, A. A. 1980 The neural regulation of tongue movements. *Prog. Neurobiol.* **15**, 975–983. (doi:org/10.1016/0301-0082(80)90008-8)

Marchetti, C., Pagnotta, S., Donato, R. & Nistri, A. 2002 Inhibition of spinal or hypoglossal motoneurons of the newborn rat by glycine or GABA. *Eur. J. Neurosci.* **15**, 975–983. (doi:10.1046/j.1460-9568.2002.01927.x)

Mazza, E., Nunez-Abades, P. A., Spielmann, J. M. & Cameron, W. E. 1992 Anatomical and electrotonic coupling in developing genioglossal motoneurons of the rat. *Brain Res.* **598**, 127–137. (doi:10.1016/0006-8993(92)90176-A)

Nicholls, D. G. 2004 Mitochondrial dysfunction and glutamate excitotoxicity studied in primary neuronal cultures. *Curr. Mol. Med.* **4**, 149–177. (doi:10.2174/1566524043479239)

Nistri, A., Ostroumov, K., Sharifullina, E. & Taccola, G. 2006 Tuning and playing a motor rhythm: how metabotropic glutamate receptors orchestrate generation of motor patterns in the mammalian central nervous system. *J. Physiol.* **572**, 323–334. (doi:10.1113/jphysiol.2005.100610)

Onimaru, H., Arata, A. & Homma, I. 1987 Localization of respiratory rhythm-generating neurons in the medulla of brainstem–spinal cord preparations from newborn rats. *Neurosci. Lett.* **78**, 151–155. (doi:10.1016/0304-3940(87)90624-0)

Quitadamo, C., Fabbretti, E., Lamanauskas, N. & Nistri, A. 2005 Activation and desensitization of neuronal nicotinic receptors modulate glutamatergic transmission on neonatal rat hypoglossal motoneurons. *Eur. J. Neurosci.* **22**, 2723–2734. (doi:10.1111/j.1460-9568.2005.04460.x)

Rao, S. D. & Weiss, J. H. 2004 Excitotoxic and oxidative cross-talk between motor neurons and glia in ALS pathogenesis. *Trends Neurosci.* **27**, 17–23. (doi:10.1016/j.tins.2003.11.001)

Rekling, J. C. & Feldman, J. L. 1998 PreBötzinger complex and pacemaker neurons: hypothesized site and kernel for respiratory rhythm generation. *Annu. Rev. Physiol.* **60**, 385–405. (doi:10.1146/annurev.physiol.60.1.385)

Rekling, J. C., Shao, X. M. & Feldman, J. L. 2000 Electrical coupling and excitatory synaptic transmission between rhythmogenic respiratory neurons in the preBotzinger complex. *J. Neurosci.* **20**, RC113.

Rowland, L. P. & Shneider, N. A. 2001 Amyotrophic lateral sclerosis. *N. Engl. J. Med.* **344**, 1688–1700. (doi:10.1056/NEJM200105313442207)

Rybak, I. A., Abdala, A. P., Markin, S. N., Paton, J. F. & Smith, J. C. 2007 Spatial organization and state-dependent mechanisms for respiratory rhythm and pattern generation. *Prog. Brain. Res.* **165**, 201–220. (doi:10.1016/S0079-6123(06)65013-9)

Sejnowski, T. J. & Paulsen, O. 2006 Network oscillations: emerging computational principles. *J. Neurosci.* **26**, 1673–1676. (doi:10.1523/JNEUROSCI.3737-05d.2006)

Sharifullina, E. & Nistri, A. 2006 Glutamate uptake block triggers deadly rhythmic bursting of neonatal rat hypoglossal motoneurons. *J. Physiol.* **572**, 407–423. (doi:10.1113/jphysiol.2005.100412)

Sharifullina, E., Ostroumov, K. & Nistri, A. 2004 Activation of group I metabotropic glutamate receptors enhances efficacy of glutamatergic inputs to neonatal rat hypoglossal motoneurons *in vitro*. *Eur. J. Neurosci.* **20**, 1245–1254. (doi:10.1111/j.1460-9568.2004.03590.x)

Sharifullina, E., Ostroumov, K. & Nistri, A. 2005 Metabotropic glutamate receptor activity induces a novel oscillatory pattern in neonatal rat hypoglossal motoneurones. *J. Physiol.* **563**, 139–159. (doi:10.1113/jphysiol.2004.079509)

Sharifullina, E., Ostroumov, K., Grandolfo, M. & Nistri, A. 2008 *N*-methyl-D-aspartate triggers neonatal rat hypoglossal motoneurons *in vitro* to express rhythmic bursting with unusual Mg^{2+} sensitivity. *Neuroscience* **154**, 804–820. (doi:10.1016/j.neuroscience.2008.03.010)

Solomon, I. C. 2003 Connexin36 distribution in putative CO_2-chemosensitive brainstem regions in rat. *Respir. Physiol. Neurobiol.* **139**, 1–20. (doi:10.1016/j.resp.2003.09.004)

Solomon, I. C., Halat, T. J., El-Maghrabi, M. R. & O'Neal, M. H. 2001 Localization of connexin26 and connexin32 in putative CO_2-chemosensitive brainstem regions in rat. *Respir. Physiol.* **129**, 101–121. (doi:10.1016/S0034-5687(01)00299-7)

Soto-Trevinõ, C., Rabbah, P., Marder, E. & Nadim, F. 2005 Computational model of electrically coupled, intrinsically distinct pacemaker neurons. *J. Neurophysiol.* **94**, 590–604. (doi:10.1152/jn.00013.2005)

Suzue, T. 1984 Respiratory rhythm generation in the in vitro brain stem–spinal cord preparation of the neonatal rat. *J. Physiol.* **354**, 173–183.

van Zundert, B., Peuscher, M. H., Hynynen, M., Chen, A., Neve, R. L., Brown Jr, R. H., Constantine-Paton, M. & Bellingham, M. C. 2008 Neonatal neuronal circuitry shows hyperexcitable disturbance in a mouse model of the adult-onset neurodegenerative disease yotrophic lateral sclerosis. *J. Neurosci.* **28**, 10 864–10 874. (doi:10.1523/JNEUROSCI.1340-08.2008)

EJN fens EUROPEAN JOURNAL OF NEUROSCIENCE

European Journal of Neuroscience, pp. 1–16, 2010 doi:10.1111/j.1460-9568.2010.07108.x

Transient oxidative stress evokes early changes in the functional properties of neonatal rat hypoglossal motoneurons *in vitro*

Francesca Nani,[1] Alessandra Cifra[1] and Andrea Nistri[1,2]
[1]Neurobiology Sector, International School for Advanced Studies (SISSA), Via Beirut 2-4, 34151 Trieste, Italy
[2]SPINAL (Spinal Person Injury Neurorehabilitation Applied Laboratory), Istituto di Medicina Fisica e Riabilitazione, 33100 Udine, Italy

Keywords: amyotrophic lateral sclerosis, ATF-3, brain stem, hydrogen peroxide, reactive oxygen species

Abstract

Oxidative stress of motoneurons is believed to be an important contributor to neurodegeneration underlying the familial (and perhaps even the sporadic) form of amyotrophic lateral sclerosis (ALS). This concept has generated numerous rodent genetic models with inborn oxidative stress to mimic the clinical condition. ALS is, however, a predominantly sporadic disorder probably triggered by environmental causes. Thus, it is interesting to understand how wild-type motoneurons react to strong oxidative stress as this response might cast light on the presymptomatic disease stage. The present study used, as a model, hypoglossal motoneurons from the rat brainstem slice to investigate how hydrogen peroxide could affect synaptic transmission and intrinsic motoneuron excitability in relation to their survival. Hydrogen peroxide (1 mM; 30 min) induced inward current or membrane depolarization accompanied by an increase in input resistance, enhanced firing and depressed spontaneous synaptic events. Despite enhanced intracellular oxidative processes, there was no death of motoneurons, although most cells were immunopositive for activating transcription factor 3, a stress-related transcription factor. Voltage-clamp experiments indicated increased frequency of excitatory or inhibitory miniature events, and reduced voltage-gated persistent currents of motoneurons. The global effect of this transient oxidative challenge was to depress the input flow from the premotor interneurons to motoneurons that became more excitable due to a combination of enhanced input resistance and impaired spike afterhyperpolarization. Our data show previously unreported changes in motoneuron activity associated with cell distress caused by a transient oxidative insult.

Introduction

Amyotrophic lateral sclerosis (ALS) is a relentless neurodegenerative disease, with loss of motoneurons in the spinal cord and certain brainstem motor nuclei (Laslo *et al.*, 2001a,b; von Lewinski & Keller, 2005). While the cause of most cases of sporadic ALS remains unclear, a minority of ALS cases have genetic origin due to multiple missense mutations in the cytosolic Cu/Zn superoxide dismutase 1 (SOD-1) gene (Rosen *et al.*, 1993). Transgenic mice expressing the ALS mutant human SOD-1 protein develop late neuromuscular symptoms similar to ALS (Gurney *et al.*, 1994), probably because of the SOD gain-of-function leading to motoneuron degeneration (Beal *et al.*, 1997; Ferrante *et al.*, 1997; Ihara *et al.*, 2005). Nonetheless, the electrophysiological phenotype is complex because SOD^{G93A} motoneurons show hyperexcitability because of increased persistent Na^+ current [PIC(Na); Kuo *et al.*, 2005; van Zundert *et al.*, 2008], whereas SOD^{G85R} motoneurons display decreased excitability (Bories *et al.*, 2007).

One theory for the etiopathogenesis of sporadic ALS is based on excitotoxicity, in turn triggering mitochondrial dysfunction, impaired Ca^{2+} homeostasis, neurofilament disruption and protein aggregation (Brown & Robberecht, 2001; Cleveland & Rothstein, 2001; Pasinelli & Brown, 2006). Nevertheless, oxidative stress has also been implicated as a major player, even in the absence of mutated SOD-1 (Shaw *et al.*, 1995; Ferrante *et al.*, 1997; Bogdanov *et al.*, 2000; Ihara *et al.*, 2005). The consequences of an acute oxidative stress to wild-type motoneurons remain, however, unclear.

Are there two distinct pathological processes (excitotoxicity and oxidative stress) leading to motoneuron degeneration? Do their mechanisms of action go through common downstream gateways (Cleveland & Rothstein, 2001)?

We have attempted to clarify some of these questions by using an *in vitro* model of wild-type rat brainstem motoneurons of the nucleus hypoglossus whose dysfunction resulting in dysarthria and dysphagia is often a very early symptom of ALS (Medina *et al.*, 1996; Shaw & Ince, 1997). Indeed, initial bulbar symptoms are diagnosed on the basis of the patient's ability to speak, and manage food and drinks (Kühnlein *et al.*, 2008).

With our model we explored the very early motoneuron response to oxidative stress by focusing on changes in excitatory and inhibitory

Correspondence: Dr A. Nistri, [1]Neurobiology Sector, as above.
E-mail: nistri@sissa.it

Received 23 September 2009, revised 11 December 2009, accepted 16 December 2009

synaptic transmission on wild-type motoneurons and in their intrinsic excitability in relation to intracellular oxidation and survival. We wished to find out if even a transient oxidative stress was sufficient to trigger off electrophysiological alterations associated with expression of the activating transcription factor 3 (ATF-3) typical of neuronal distress (Tsujino *et al.*, 2000; Hai & Hartman, 2001; Vlug *et al.*, 2005). To this end, oxygen-derived free-radical formation was induced by bath-applying 1 mM hydrogen peroxide (H_2O_2) that exerts its toxic effects through the ferrous-iron-dependent (Fenton reaction) and superoxide-driven (Haber–Weiss reaction) generation of the highly reactive hydroxyl radical (Halliwell, 1992). Our data indicated that H_2O_2 depressed premotor interneuron activity and enhanced hypoglossal motoneuron (HM) firing not accompanied by early cell death, yet associated with activation of the stress factor ATF-3.

Materials and methods

Slice preparation

All experiments were carried out in accordance with the regulations of the Italian Animal Welfare act (DL 27/1/92 n.116) following the European Community directives no. 86/609 93/88 (Italian Ministry of Health authorization for the local animal care facility in Trieste D 69/98-B), and approved by the local authority veterinary service. As full details of the experimental methods have been published earlier (Quitadamo *et al.*, 2005; Lamanauskas & Nistri, 2006, 2008), only a brief account is provided hereafter. Brainstem slices (250 μm thick) from neonatal (P1–P5 day old) urethane – anaesthetized Wistar rats were cut in ice-cold, oxygenated (95% O_2/5% CO_2) Krebs solution, containing (in mM): NaCl, 130; KCl, 3; NaH_2PO_4, 1.5; $CaCl_2$, 1; $MgCl_2$, 5; $NaHCO_3$, 25; glucose, 100 (pH 7.4; 300–320 mOsm). After 40 min recovery at 32°C and 1 h at room temperature, they were used for recording.

Electrophysiological recordings

HMs were identified within the nucleus hypoglossus with an infrared video-camera. All cell recordings were obtained, at ambient temperature, under whole-cell patch-clamp conditions. For voltage-clamp experiments, patch electrodes had 3–4 MΩ resistance, whereas for current-clamp experiments they had 8–10 MΩ resistance. Cells were clamped at values between −60 and −70 mV holding potential (V_h), as close as possible to initial resting potential. Cells were used for analysis when series resistance increases did not exceed 10%. Voltage-activated currents were measured in response to slow (21 mV/s) triangular voltage-clamp commands from −80 mV to +20 mV and back (Lamanauskas & Nistri, 2008), in accordance with the studies by Schwindt & Crill (1980). In current-clamp mode, neurons were kept at their initial resting level of membrane potential (V_m) while the bridge was routinely balanced throughout the experiment. Intracellular DC currents (200–500 pA; 500 ms) were injected into HMs to study firing properties and afterhyperpolarization (AHP) amplitude.

Voltage and current pulse generation and data acquisition were performed using pCLAMP 10.0 software (Axon Instruments, Molecular Devices, Sunnyvale, CA, USA). Patch pipettes were filled with intracellular solution containing (in mM): CsCl, 130; NaCl, 5; $MgCl_2$, 2; $CaCl_2$, 1; HEPES, 10; EGTA, 10; ATP-Mg, 2; sucrose, 2 (pH 7.2 with CsOH; 280–300 mOsm) for voltage-clamp experiments. Intracellular CsCl, that minimized the leak current of the recorded cell, was used to enable larger changes in V_h. For current-clamp experiments, 130 mM KCl always replaced CsCl.

Solutions and drugs

Slices were superfused (2–3 mL/min) with a gassed solution containing (in mM): NaCl, 130; KCl, 3; NaH_2PO_4, 1.5; $CaCl_2$, 1.5; $MgCl_2$, 1; $NaHCO_3$, 25; glucose, 10 (pH 7.4; 300–320 mOsm). The following drugs were used: 6-cyano-7-nitroquinoxaline-2,3-dione (CNQX), D-amino-phosphonovalerate (APV), bicuculline methiodide (bicuculline) and strychnine hydrochloride (strychnine) purchased from Tocris (Bristol, UK); $MgCl_2$ and H_2O_2 were from Sigma (Milan, Italy). Tetrodotoxin (TTX) was obtained from Latoxan (Valence, France) and thapsigargin from Calbiochem (Merck Chemicals, Darmstadt, Germany). Drugs were applied by superfusion. Because the focus of the present study was on the toxic activity of free oxygen radicals, as a routine, H_2O_2 was applied at 1 mM concentration because this dose was previously shown to produce neurotoxicity of *in vitro* spinal neurons (Taccola *et al.*, 2008). Similar effects were seen in preliminary experiments with 0.5 mM H_2O_2. We checked that 1 mM H_2O_2 did not vary the pH of the superfusing solution (observed pH change switching from control Krebs to H_2O_2 containing solution was from 7.38 to 7.40).

Data analysis

In voltage-clamp experiments, cell input resistance (R_{in}) was calculated by measuring the current response to 10 mV hyperpolarizing steps from V_h. In current-clamp experiments, R_{in} was calculated by measuring the voltage response to −50 pA current injections (Pagnotta *et al.*, 2005; Quitadamo *et al.*, 2005). Spontaneous and miniature, excitatory and inhibitory, postsynaptic currents (sPSCs, mIPSCs and mEPSCs) were detected using the template search software Clampfit 10.0 (Axon Instruments). Cumulative probability plots of synaptic events were constructed with SigmaPlot 9.01 software (Jandel Scientific, San Rafael, CA, USA). In accordance with the standard protocols used by Ptak *et al.* (2005), Enomoto *et al.* (2006), Aracri *et al.* (2006) and Magistretti *et al.* (2006), persistent inward currents (PICs) were evoked by injecting triangular voltage commands at the rate of 21 mV/s. The voltage-activated inward current was obtained after subtracting the passive leak current (Cramer *et al.*, 2007; Theiss *et al.*, 2007), extrapolated from linear regression fits to the *I–V* curve at membrane voltages between −80 and −60 mV. The inward current area was also measured as the area below the trace baseline after leak correction. SIGMAPLOT 9.01 software was used for linear regression analysis including the quantification of the time dependence of firing frequency. Gradual changes in spike firing following a long current pulse injection were investigated by Sawczuk *et al.* (1995), who used HMs of rat brainstem slices in control solution to show multiphasic decay in the firing frequency after the initial high rate. In analogy with these studies we examined changes in spike firing rate before and after application of H_2O_2 by fitting a cubic polynomial function to the plot of the interspike intervals vs. the spike sequence in the train (see Fig. 5D), as shown by the following equations:

$$\text{Control}: y_1 = 0.0148 + 0.0189x - 0.0029x^2 + 0.0001x^3 \quad \text{with } r = 0.8528, \quad \text{and}$$

$$H_2O_2: y_2 = 0.0084 + 0.0035x - 0.0002x^2 + 3.92 \times 10^{-6}x^3 \quad \text{with } r = 0.8999$$

We then calculated the difference integral for the first 13 spikes in the plot and normalized the result with respect to control to give the % change. It is noteworthy that this analysis was performed with data obtained under non-steady-state conditions because of the developing

toxic action of H_2O_2 on HMs. Because H_2O_2 application was transient to mimic a temporary oxidative stress and it induced ongoing changes in baseline membrane potential and neuronal properties under non-steady-state conditions, it was not feasible to perform standard tests of HM firing responses to varying amplitudes of injected current. CorelDraw (Vector Capital, San Francisco, CA, USA) was used for graphical data presentation.

Intracellular measurement of reactive oxygen species (ROS) generation

Generation of intracellular free oxygen radicals was evaluated with dihydrorhodamine 123 (DHR 123; Molecular Probes, Invitrogen, Milan, Italy; Sánchez-Carbente *et al.*, 2005; Jiang *et al.*, 2006). At room temperature, continuously oxygenated, thin slices (250 μm thick) were first incubated in Krebs solution or 1 mM H_2O_2 for 30 min, then treated with 5 μM DHR 123 and Hoechst 33342 (10 mg/mL stock from Molecular Probes, Invitrogen; final dilution was 1 : 1000) in Krebs solution for 20 min. Slices were finally washed, transferred to a glass chamber containing Krebs solution (without fixation) and examined with a TCS SP2 Leica confocal microscope (× 40). Hoechst 33342, used to counterstain slices, is a cell-permeable dye that, once bound to double-strand DNA, emits blue fluorescence. For fluorescence imaging of rhodamine 123 (Rho 123, the oxidized form of DHR 123), slices were visualized by excitation at 514 nm and emission at 530–610 nm. For each slice side and for both hypoglossal nuclei, a 40-μm z-stack (corresponding to one HMs plane) was acquired (5-μm step size); ImageJ software was used to create a 3D reconstruction of every hypoglossal nucleus in order to detect Hoechst 33342 and Rho 123 signal-positive voxels. To avoid background noise, an automatic threshold was set for both Rho 123 signal and Hoechst 33342 signal. Data are expressed as ratio of Rho 123 signal-positive voxels vs. Hoechst 33342 signal-positive voxels.

Viability assay

At room temperature, continuously oxygenated, thin slices (250 μm thick) were first incubated in Krebs solution or 1 mM H_2O_2 for 30 min or 1 h, then treated with propidium iodide (PI; 1 mg/mL stock from Sigma, Milan, Italy; final dilution was 1 : 3000) and Hoechst 33342 (10 mg/mL stock; final dilution was 1 : 1000) in Krebs solution for 45 min. Slices were finally washed, transferred to a glass chamber containing Krebs solution (without fixation) and examined with a TCS SP2 Leica confocal microscope (× 40). Hoechst 33342 provided the global number of cells (surviving plus damaged) in each tissue section. PI was used to investigate the number of cells killed by H_2O_2 treatment as it is a cell-impermeable DNA dye that can bind DNA and emits red fluorescence when cell and nuclear membranes have been damaged (Jones & Senft, 1985). For each slice side and for both hypoglossal nuclei, a 40-μm z-stack was acquired (5-μm step size); Leica confocal software was used to create a 2D average projection of each images series along the z-axis. An in-house-written ImageJ software macro was used to count PI- and Hoechst-positive cells. Images were first converted into binary images with the nuclei coloured in black over a white background. Thereafter, only nuclei of specified size and circularity were analysed, and measurements relative to particles count were displayed. Data are expressed as ratio of PI-positive cells vs. Hoechst-positive cells.

Immunocytochemistry

Brainstems removed from P3–P5 rats were cut in two thick (500 μm) slices comprising the nucleus hypoglossus in ice-cold, oxygenated Krebs solution; slices were incubated (under continuous oxygenation) either in Krebs solution or in 1 mM H_2O_2 for 30 min at room temperature, and rinsed. Treated and untreated slices were always processed in parallel to minimize bias. Slices were fixed either immediately for SMI 32 at the end of H_2O_2 application, or rinsed and kept for 1 h in Krebs solution for ATF-3 staining. The fixative medium was phosphate-buffered saline (PBS) containing 4% paraformaldehyde (24 h at 4°C) followed by 30% sucrose PBS for cryoprotection (24 h at 4°C). Cryostat tissue sections (30 μm) were collected sequentially and treated with blocking solution (1% foetal calf serum, 5% bovine serum albumin, 0.3% Triton X-100 in PBS) for 1 h at room temperature. Slices were then incubated overnight at 4°C with primary antibodies against SMI 32 (mouse monoclonal, 1 : 200 dilution; Covance Research Products, Berkeley, CA, USA) and/or ATF-3 (rabbit polyclonal, 1 : 500 dilution; Santa Cruz Biotechnology, Santa Cruz, CA, USA). AlexaFluor 488 and 594 were used as secondary antibodies (1 : 500 dilution; Molecular Probes, Invitrogen, Milan, Italy) for 2 h at room temperature. Omission of the primary antibodies did not produce any signal. Western blot analysis of lysates obtained from neonatal rat spinal cord tissue incubated with SMI 32 antibody showed bands with the expected molecular weight (Anujaianthi Kuzhandaivel, unpublished observation). Slices were mounted with Vectashield (Vector Laboratories Burlingame, CA, USA) to avoid photobleaching, and visualized with the confocal microscope (× 40). CellCounter software (Glance Vision Technologies s.r.l., Trieste, Italy) was used to count SMI 32-immunopositive HMs. CellCounter is a tool for automatic classification and counting of cells; the parameters like cell diameter and signal intensity threshold can be automatically estimated in the sample. Concerning SMI 32-stained images, average parameters setting was: cell diameter, 19.07 μm; intensity threshold, 0.371. The number of SMI 32-positive neurons was similar in untreated and treated brainstem slices (see Results). Because the confocal settings used for image acquisition were the same for treated and untreated slices, the average SMI 32 staining intensity was assumed to be identical for treated and untreated slices. Co-staining of ATF-3 and SMI 32 was analysed on the basis of their covariance. In probability theory and statistics, covariance is a measure of how much two variables change together. Covariance can assume any value between $-\infty$ and $+\infty$. If covariance is positive, the two variables change concordantly; if covariance is negative, the two variables change in an opposite way; finally, two variables whose covariance is zero are called uncorrelated. In our samples, for each images pair of ATF-3 and SMI 32 staining, a function converted red green blue images (I) to graded grey levels (I_g). Thereafter, the average intensity value of every image was subtracted from each pixel intensity ('I_g − average I_g'). The covariance (C) value was the scalar product of the two images ('I_{1g} − average I_{1g}' for ATF-3 and 'I_{2g} − average I_{2g}' for SMI 32) divided by the image pixel number according to the equation:

$$C = <(I_{1g} - \text{average}\, I_{1g}), (I_{2g} - \text{average}\, I_{2g})>/\text{image pixel number}$$

When the covariance value was significantly higher than control, this indicated stronger ATF-3 staining intensity because the SMI 32 fluorescence remained similar.

Covariance between ATF-3 staining and SMI 32 staining was analysed by means of a MATLAB 7.1 software macro kindly provided by Dr Walter Vanzella (Glance Vision Technologies).

Statistics

Results were expressed as means ± SEM; *n* refers to the number of cells or animals, as indicated. For statistical calculations, we used SIGMASTAT 3.11 (Systat Software, Chicago, IL, USA): in particular, data distribution was first processed with a normality test and, then, with the Student's *t*-test (power of performed test with alpha = 0.050) or the Mann–Whitney test used for parametric or non-parametric data (for the latter, *T* represents the Mann–Whitney *T*-statistic value, which is the sum of the ranks in the smaller sample group or from the first selected group when both groups are of the same size. This value was compared with the population of all possible rankings in order to determine the occurrence of *T*). For paired comparison of non-parametric data, Wilcoxon Sign Rank test was applied; the Wilcoxon test statistic *W* was computed by ranking all the differences before and after the treatment based on their absolute value, then attaching the signs of the difference to the corresponding ranks. The signed ranks were then summed and compared. Concerning association analysis, statistical significance was assessed with the Pearson Product Moment Correlation Coefficient. The Kolmogorov–Smirnov test was used to assess statistical significance for probability distribution. Two groups of data were considered statistically different if $P \leq 0.05$.

Results

Application of H_2O_2 induced changes in HM electrophysiological characteristics

Bath-applied H_2O_2 (1 mM; 30 min) increased HM input resistance that, on average, rose from 383 ± 32 MΩ to 408 ± 37 MΩ when measured on the same neurons before and after application (Student's *t*-test, $t_5 = 3.922$, $P = 0.011$, $n = 6$). Figure 1A shows, for each cell, normalized data for such an input resistance change that on average was 6 ± 1% (Wilcoxon Signed Rank Test, $W = -21.00$, $P = 0.031$, $n = 6$). This effect could not be reversed even after prolonged (30 min) washout in four cells, while it was reversible in two of them.

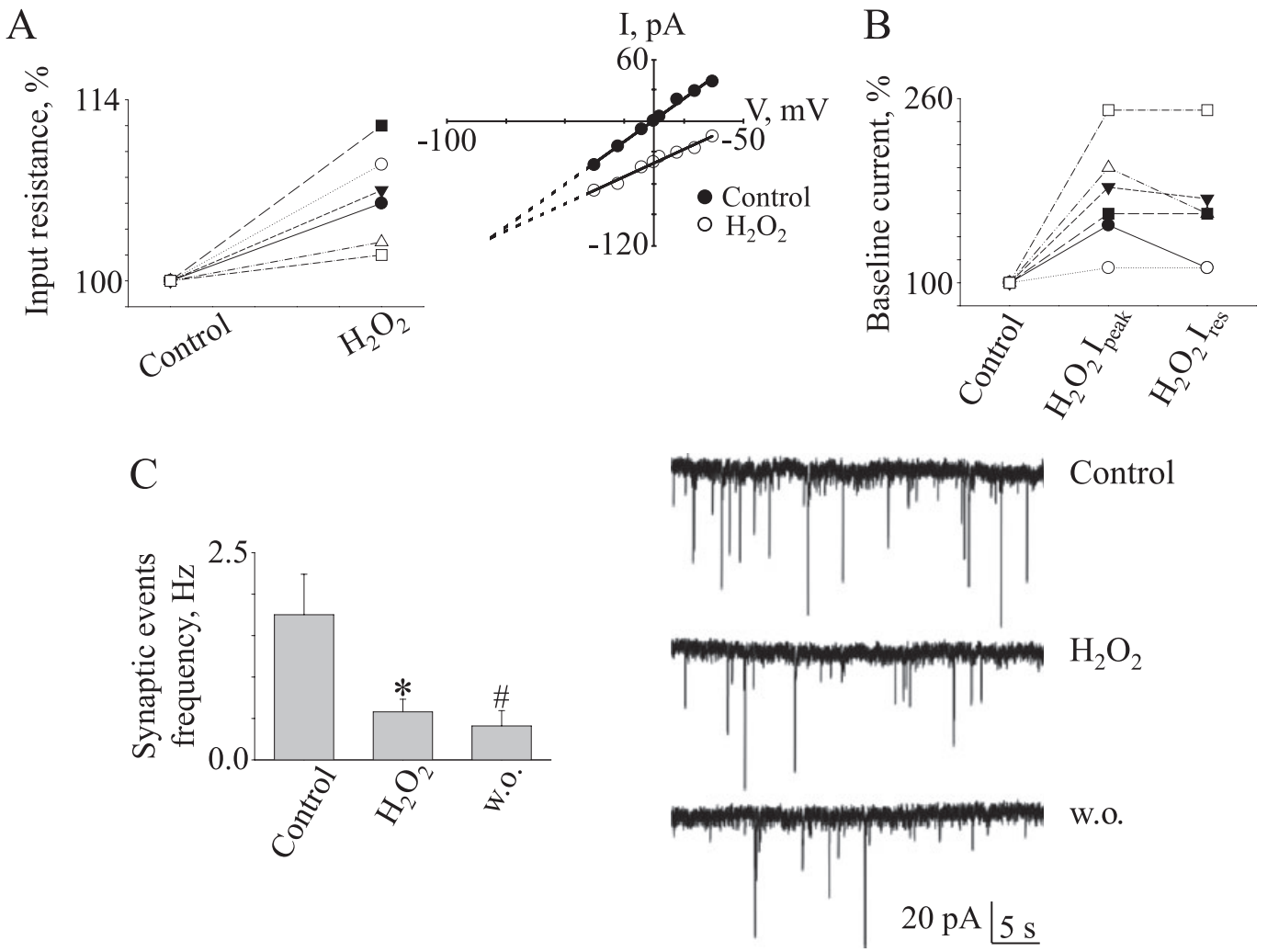

FIG. 1. HM electrophysiological characteristics after application of 1 mM H_2O_2. (A) Increased input resistance observed in voltage-clamp configuration after H_2O_2 application (Student's *t*-test, $t_5 = 3.922$, $P = 0.011$, $n = 6$; 6 ± 1%, Wilcoxon Signed Rank Test, $W = -21.00$, $P = 0.031$, $n = 6$). Each line represents an individual neuron. Inset shows example of current/voltage plot in control (filled circles) or during application of H_2O_2 (open circles). Note decreased slope of the linear portion of the plot with extrapolated crossover at −93 mV. (B) H_2O_2 caused an inward current reaching its maximum value at ≥ 15 min (H_2O_2 I_{peak}, 76 ± 19%, $n = 6$), the effect was maintained for the length of H_2O_2 bath application (residual current following H_2O_2, I_{res}, 61 ± 21%, $n = 6$). Each line represents an individual neuron. (C) Fall in spontaneous synaptic events frequency after application of H_2O_2 (Student's *t*-test, $t_5 = -3.403$, $^*P = 0.019$, $n = 6$). This effect was not reversible even after prolonged washout (Student's *t*-test, $t_5 = -3.784$, $^{\#}P = 0.013$, $n = 6$). Inset (right) shows example of depression of synaptic event frequency by H_2O_2 with poor recovery on washout. w.o., washout.

Comparable tests run for an analogous length of time did not indicate a gradual rise in input resistance under control conditions. The example of Fig. 1A (inset) indicates that the slope of the linear plot of the current/voltage relation is decreased with extrapolated crossover at −93 mV. The rise in input resistance was accompanied by the onset of an inward current reaching its maximum at ≥ 15 min (−98.3 ± 25.5 pA I_{peak} vs. −53.3 ± 10.2 pA baseline, Student's *t*-test, $t_5 = -2.773$, $\#P = 0.039$, $n = 6$; Fig. 1B) corresponding to a 76 ± 19% change. Even if the current increase tended to fade towards the end of H_2O_2 application, the inward current amplitude (residual current; I_{res}) was still significantly augmented (61 ± 21%) when compared with control condition (−88.7 ± 21.7 I_{res} vs. −53.3 ± 10.2 pA, Student's *t*-test, $t_5 = -2.576$, $P = 0.050$, $n = 6$; Fig. 1B), with poor recovery on washout (−85.0 ± 22.6 pA). Furthermore, 1 mM H_2O_2 induced global depression of sPSC frequency (0.58 ± 0.15 Hz vs. 1.75 ± 0.49 Hz control, Student's *t*-test, $t_5 = -3.403$, $*P = 0.019$, $n = 6$), that persisted even after washout (0.41 ± 0.19 Hz, Student's *t*-test, $t_5 = -3.784$, $\#P = 0.013$, $n = 6$; see histograms and sample traces in Fig. 1C). Conversely, there was no significant change in event amplitude caused by H_2O_2 (−48.5 ± 5.3 control vs. −33.8 ± 5.9 pA in H_2O_2 solution; Student's *t*-test, $t_5 = 2.192$, $P = 0.080$, $n = 6$).

Relative contribution by excitatory and inhibitory synaptic transmission to the effects of H_2O_2

Synaptic depression evoked by H_2O_2 might have had a complex origin, which we attempted to investigate by studying whether H_2O_2 modulated release of the excitatory transmitter glutamate (O'Brien *et al.*, 1997; Essin *et al.*, 2002) or of the inhibitory transmitters γ-aminobutyric acid (GABA) and glycine (Donato & Nistri, 2000). To explore any direct action, we blocked premotor interneuron activity with TTX, and looked at the effects of H_2O_2 on motoneuron intrinsic properties and release mechanisms. Table S1 shows that, although TTX per se did not change control input resistance (Student's *t*-test, $t_4 = 0.706$, $P = 0.519$, $n = 5$), it slightly reduced the baseline holding current (Student's *t*-test, $t_4 = 4.921$, $*P = 0.004$, $n = 5$) indicating a tonic contribution by synaptic transmitter release to the baseline current. Figure 2A and B illustrates the persistence of the effect of H_2O_2 on input resistance (293 ± 35 MΩ vs. 208 ± 20 MΩ TTX, Student's *t*-test, $t_5 = 3.176$, $*P = 0.025$, $n = 6$) and baseline holding current (−91.6 ± 15.3 pA I_{peak} vs. −56.6 ± 14.0 pA TTX, Student's *t*-test, $t_5 = -3.130$, $^{\#}P = 0.026$, $n = 6$; −77.5 ± 15.9 pA I_{res}, Student's *t*-test, $t_5 = -2.751$, $P = 0.040$, $n = 6$) after blocking ionotropic glutamate receptors with APV (50 μM) and CNQX (10 μM). Unexpectedly, H_2O_2 significantly enhanced mIPSC frequency (3.19 ± 0.59 Hz vs. 1.55 ± 0.26 Hz TTX, Student's *t*-test, $t_5 = 3.383$, $P = 0.015$, $n = 6$; Fig. 2C) without changing their amplitude (−34.3 ± 4.8 pA vs. −28.6 ± 2.4 pA TTX, Student's *t*-test, $t_5 = -1.200$, $P = 0.275$, $n = 6$; Fig. 2D).

Figure 2E and F exemplifies the time course of changes in holding current and miniature inhibitory postsynaptic potential frequency during H_2O_2 application: after the slight outward current and fall in event frequency observed with the administration of TTX, CNQX and APV (filled arrow), superfusion with H_2O_2 (red arrow) elicited a slow increase in holding current (peaking at 15 min, asterisk) together with a large rise in event frequency, thereafter the holding current faded, despite the persistently high event frequency that was attenuated on washout. Figure 2G shows that the action of H_2O_2 consisted of a broad increase in the probability of event detection without affecting threshold or maximum. These data, thus, suggest that H_2O_2 not only caused an inward (depolarizing) current, but also facilitated inhibitory transmitter release through apparently distinct mechanisms.

Parallel tests done after block of glycine and GABA receptors with 0.4 μM strychnine and 10 μM bicuculline (Donato & Nistri, 2000) indicated that H_2O_2 significantly increased input resistance (263 ± 40 MΩ vs. 227 ± 30 MΩ TTX, Student's *t*-test, $t_5 = 2.396$, $*P = 0.043$, $n = 6$; Fig. 3A). However, as exemplified in Fig. S1, under these conditions there was no significant change in baseline holding current (−51.7 ± 7.4 pA I_{peak} vs. −42.5 ± 6.9 pA TTX, Student's *t*-test, $t_5 = -2.015$, $P = 0.100$, $n = 6$; −50.8 ± 6.8 pA I_{res}, Student's *t*-test, $t_5 = -2.076$, $P = 0.093$, $n = 6$; Fig. 3B). While the frequency of mEPSCs is usually low (Quitadamo *et al.*, 2005; Lamanauskas & Nistri, 2008), H_2O_2 evoked a significant event frequency increase that, on average, was 0.93 ± 0.16 Hz (vs. 0.58 ± 0.08 Hz in control, Student's *t*-test, $t_5 = 3.130$, $\#P = 0.014$, $n = 6$; Fig. 3C) without altering their amplitude (−12.6 ± 0.9 pA vs. −15.0 ± 1.2 pA TTX, Student's *t*-test, $t_5 = 2.252$, $P = 0.054$, $n = 6$; Fig. 3D). Figure 3E and F shows that H_2O_2 induced a leftward parallel shift in the event probability plot, and that the largest number of events appeared in the amplitude region of −8 to −12 pA (without changes in holding current; Fig. S1).

These data suggest that miniature excitatory synaptic transmission was also facilitated by H_2O_2 even though the frequency of such events was smaller than the one of inhibitory events. The consistent facilitation of mIPSCs and mEPSCs by H_2O_2 might have been due to a large rise in intracellular free Ca^{2+} to promote transmitter release under resting conditions. Table 1 shows that H_2O_2 significantly enhanced global frequency of miniature events (Student's *t*-test, $t_4 = 3.706$, $*P = 0.021$, $n = 5$), an effect mimicked by thapsigargin (1 μM, Student's *t*-test, $t_4 = 2.932$, $*P = 0.043$, $n = 5$) that, by blocking Ca^{2+} store pumps, is known to increase intracellular Ca^{2+} (Kirby *et al.*, 1992; Reyes & Stanton, 1996; Takahashi *et al.*, 2007; Table 1).

H_2O_2 treatment modulated persistent Na^+ and Ca^{2+} currents

Our experiments indicated how H_2O_2 affected synaptic transmission and intrinsic properties of HMs, but they did not show if there were also changes in excitability within the membrane potential region of repeated HM firing. Previous studies have shown that PICs expressed by the soma of HMs (Moritz *et al.*, 2007) contribute to integration of motoneuron signals for patterned output (Brownstone, 2007), and are mediated by sustained influx of Na^+ and/or Ca^{2+} (Crill, 1996; Russo & Hounsgaard, 1999). Because PIC(Na) is reported to be increased in motoneurons of the presymptomatic ALS genetic mouse model (Kuo *et al.*, 2005; van Zundert *et al.*, 2008), we explored the possibility that H_2O_2 could affect PICs using a slow ramp protocol (see top schemes in Fig. 4A and B). In accordance with previous studies (Crill, 1996; Russo & Hounsgaard, 1999; Lamanauskas & Nistri, 2008), we assumed that the Mn^{2+}-sensitive component represented PIC(Ca), while the TTX-sensitive component represented PIC(Na). Figure 4A shows an example of global PIC observed in control conditions (Krebs). This response [attenuated by 1 μM TTX to pharmacologically isolate PIC(Ca)] was largely inhibited by H_2O_2 (1 mM; 30 min), as indicated by the superimposed traces of the current responses in the inset to Fig. 4A. Average data are given in Table 2.

In a separate set of experiments we applied 2 mM Mn^{2+} to measure PIC(Na) in isolation (Fig. 4B). Adding Mn^{2+} reduced the amplitude of the global PIC and disclosed PIC(Na) that, following H_2O_2 application, was decreased as depicted by the superimposed records in the inset to Fig. 4B. Summary data from these tests with Mn^{2+} are shown

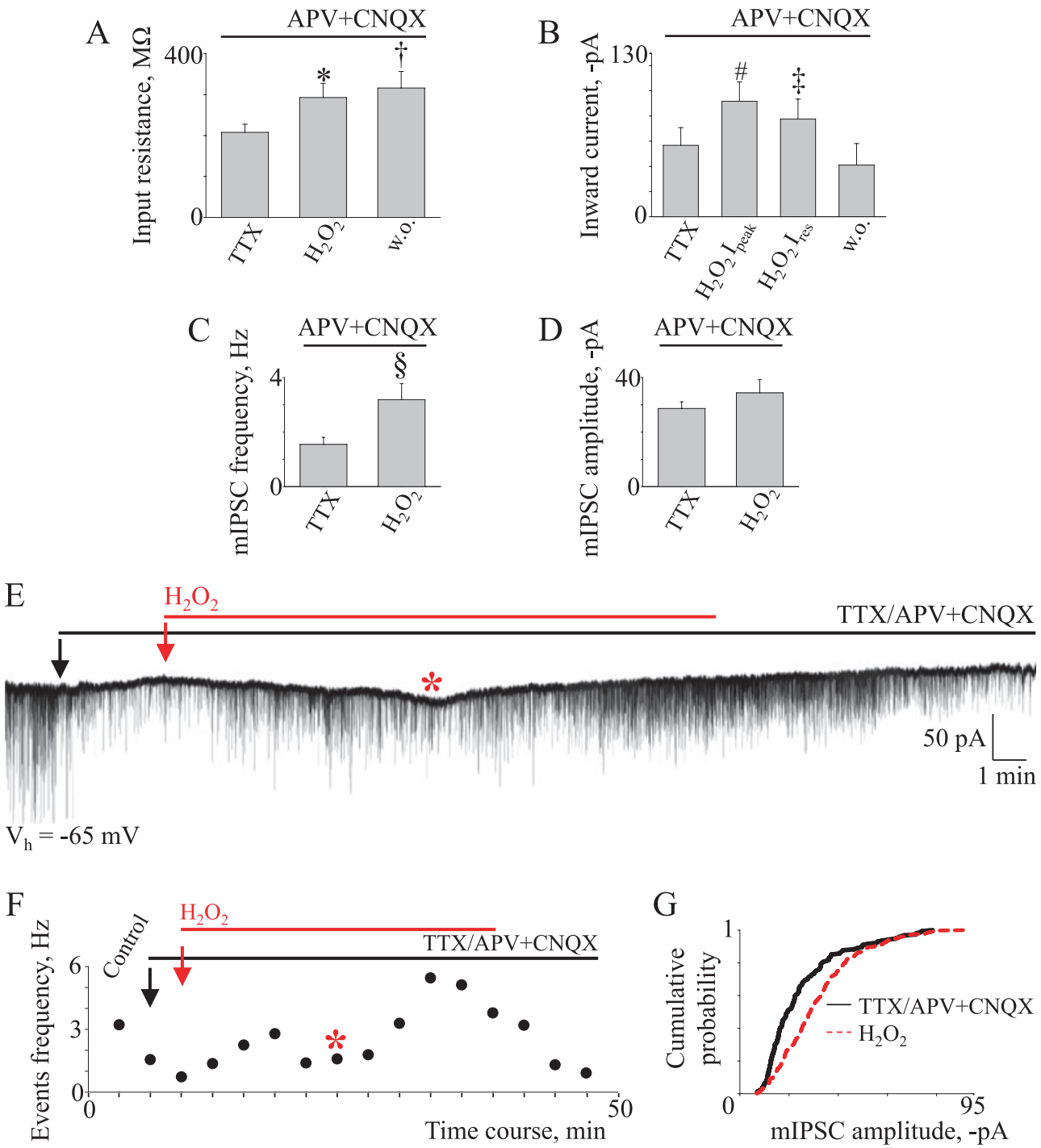

FIG. 2. H_2O_2-induced electrophysiological changes were insensitive to glutamatergic blockers. (A) In the presence of D-amino-phosphonovalerate (APV; 50 μM) and 6-cyano-7-nitroquinoxaline-2,3-dione (CNQX; 10 μM), H_2O_2 increased HM input resistance, an effect not reversible even after prolonged washout (Student's *t*-test, $t_5 = 3.176$, $^*P = 0.025$ for H_2O_2 vs. control; $t_5 = 2.664$, $^\dagger P = 0.045$ for w.o. vs. control, $n = 6$). (B) APV and CNQX did not alter the effect of H_2O_2 on inward current amplitude that rose during the application, reached a maximum value (H_2O_2 I_{peak}, Student's *t*-test, $t_5 = -3.130$, $^\# P = 0.026$, $n = 6$), and persisted for the duration of the treatment (H_2O_2 I_{res}; Student's *t*-test, $t_5 = -2.751$, $^\ddagger P = 0.040$, $n = 6$). (C) H_2O_2 significantly increased miniature inhibitory postsynaptic current (mIPSC) frequency (Student's *t*-test, $t_5 = 3.383$, $^\S P = 0.015$, $n = 6$). (D) mIPSC amplitude did not change following H_2O_2 (Student's *t*-test, $t_5 = -1.200$, $P = 0.275$, $n = 6$). (E) Time course of changes in HM holding current ($V_h = -65$ mV). Tetrodotoxin (TTX)/APV/CNQX application caused a slight outward current (filled arrow); note slowly developing inward current following H_2O_2 superfusion (red arrow) that reached its maximum after 15-min treatment (asterisk). The inward current persisted for the length of H_2O_2 application (30 min), although it slowly declined. (F) Time course of mIPSC frequency during TTX/APV/CNQX and H_2O_2 application shows biphasic rise with recovery on washout. Arrows and asterisks correspond to record sections indicated in (E). (G) Plot of cumulative probability distribution of mIPSC amplitude that was shifted to the right by 1 mM H_2O_2 (dashed line). In TTX/APV/CNQX condition, the cumulative probability plot comprised 154 events, while after H_2O_2 it included 365 events. w.o., washout.

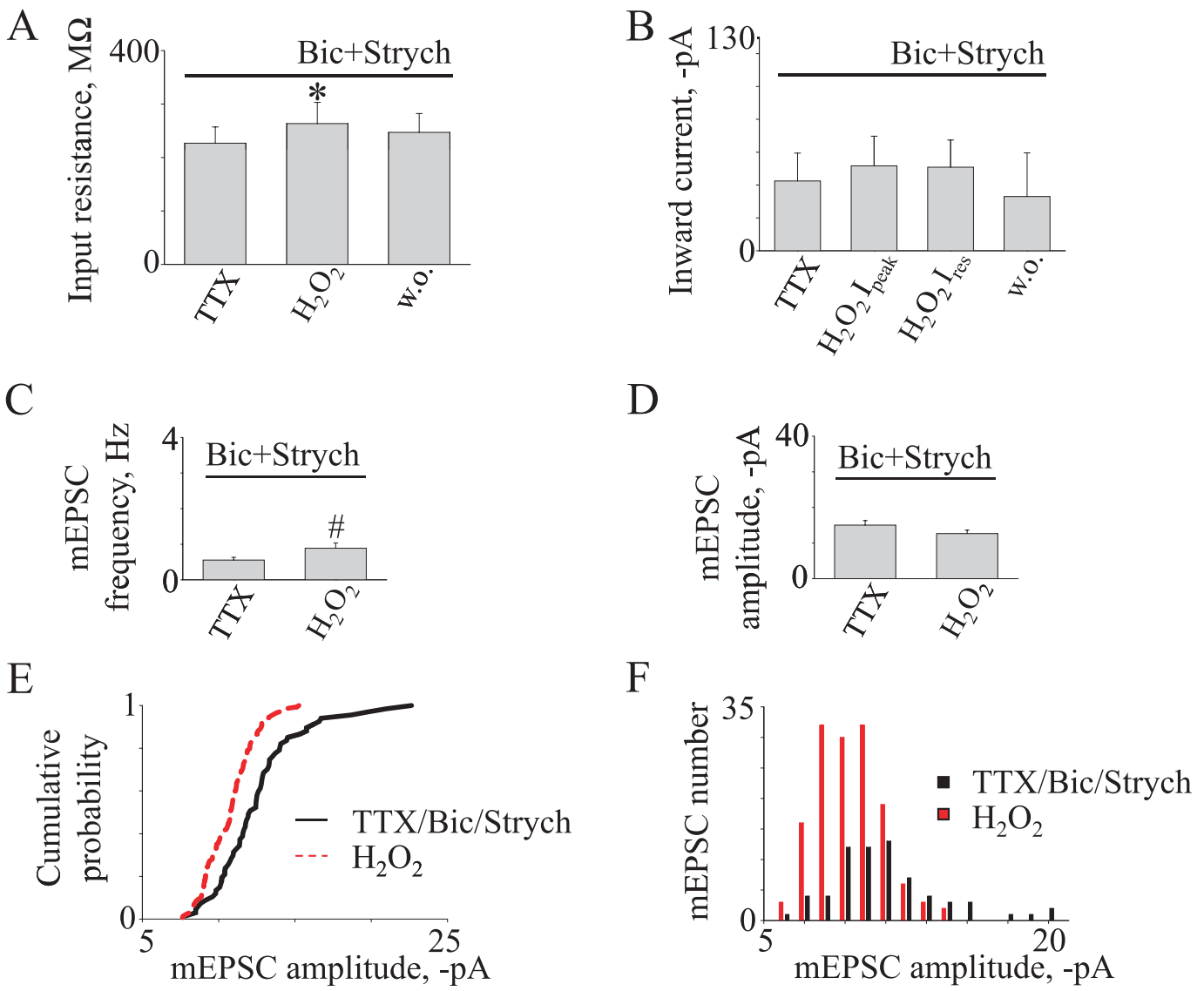

FIG. 3. Contribution of GABAergic and glycinergic transmission to H_2O_2 effects on HM electrophysiological properties. (A) In the presence of bicuculline (Bic; 10 μM) and strychnine (Strych; 0.4 μM), H_2O_2 could enhance HM input resistance (Student's *t*-test, $t_5 = 2.396$, $^*P = 0.043$, $n = 6$). (B) Blockers of $GABA_A$ and glycine receptors prevented the effect of H_2O_2 on baseline inward current (Student's *t*-test; H_2O_2 I_{peak}, $t_5 = -2.015$, $P = 0.100$; H_2O_2 I_{res}, $t_5 = -2.076$, $P = 0.093$; $n = 6$). (C) In the presence of tetrodotoxin (TTX), H_2O_2 enhanced miniature excitatory postsynaptic current (mEPSC) frequency (Student's *t*-test, $t_5 = 3.130$, $^{\#}P = 0.014$, $n = 6$) without changing mEPSC amplitude (D; Student's *t*-test, $t_5 = 2.252$, $P = 0.054$, $n = 6$). (E) Plot of cumulative probability distribution of mEPSC amplitude was shifted to the left by H_2O_2 application (dashed line). In TTX/bicuculline/strychnine solution, the cumulative probability plot comprised 67 events, while after H_2O_2 it included 143 events. (F) Histograms showing mEPSC amplitude distribution before and after H_2O_2 treatment; data are from the same cell shown in (E). w.o., washout.

in Table 2. On average, it appears that H_2O_2 decreased PIC(Ca) amplitude and area by 79%, while the corresponding falls in PIC(Na) amplitude and area were 38% and 50%, respectively, without any significant variation of activation thresholds. We did not observe recovery in the PIC(Na) or PIC(Ca) amplitude after washout.

Hyperexcitability of HMs treated with H_2O_2

The PIC-inhibiting ability of H_2O_2 was surprising in view of the reported hyperexcitability of motoneurons from presymptomatic ALS genetic models (Kuo *et al.*, 2005; van Zundert *et al.*, 2008). Hence, we investigated whether H_2O_2 might influence rat HM firing properties. Figure 5A shows an example of HM responses to bath-applied H_2O_2 at resting membrane potential (V_m) of −65 mV (on average, initial V_m was −63 ± 1 mV; $n = 26$). Following application of H_2O_2, there was gradual membrane depolarization (7 mV; on average, V_m after H_2O_2 was −59 ± 1, Student's *t*-test, $t_{25} = 5.186$, $P \leq 0.001$, $n = 26$) that persisted during washout. We used rectangular current pulses to induce repeated firing and to detect the sensitivity of spike activity to H_2O_2. Current steps (300 pA for 500 ms) injected into HMs evoked firing as exemplified in Fig. 5A and B. In control condition, this motoneuron fired 14 spikes (Fig. 5B, left trace) while, during H_2O_2 application, the HM (repolarized to the original V_m) responded with 26 spikes superimposed on the larger amplitude of the membrane voltage change (Fig. 5B, right trace). The example of Fig. 5C shows a plot of instantaneous firing frequency vs. time (during the 500 ms pulse) in control (filled circles) or in the presence of H_2O_2

TABLE 1. Similar effects of H_2O_2 and thapsigargin on miniature events frequency

	Miniature frequency (Hz)	Student's t_4-value	*P*-value	*n*
TTX	0.54 ± 0.08	3.706	0.021	5
TTX + H_2O_2	2.33 ± 0.54			
TTX	0.34 ± 0.05	2.932	0.043	5
TTX + thapsigargin	0.99 ± 0.27			

(open circles). There was an upward shift of the graph that was best fitted with double exponential (τ_1 and τ_2) decay (in accordance with the study by Sawczuk *et al.*, 1995) with values of 0.01 s τ_1 and 8.33 s τ_2 for control, and 0.02 s τ_1 and 11.11 s τ_2 for H_2O_2 treatment. The adequacy of the fit was confirmed by the correlation values $r = 0.9980$ and 0.9925 for control and H_2O_2, respectively.

Figure 5D demonstrates that, on six cells held at the same membrane potential (−65 mV), there was a relatively consistent interspike interval value throughout the firing phase when H_2O_2 was applied (open circles; see Lape & Nistri, 2000), unlike the complex changes detected prior to the treatment. Using the function described in the methods for fitting data of Fig. 5D, we observed a 55% area difference between controls and H_2O_2-treated responses.

Averaging out data for 26 HMs showed that H_2O_2 significantly enhanced the mean firing frequency (45 ± 2 Hz vs. 31 ± 2 Hz, Student's *t*-test, $t_{25} = 9.588$, $P \leq 0.001$, $n = 26$). This phenomenon was accompanied by a significant rise in input resistance (179 ± 15 MΩ vs. 128 ± 9 MΩ control; Student's *t*-test, $t_{25} = 4.986$, $P \leq 0.001$, $n = 26$). Table S2 shows that H_2O_2 increased input resistance, spike firing and evoked membrane depolarization even when applied in the presence of APV and CNQX, or bicuculline and strychnine, suggesting that these effects were, at least in part, due to a direct action on HMs.

Ca^{2+} -activated K^+ conductances responsible for the spike AHP are activated by PIC(Ca) in rat motoneurons (Li & Bennett, 2007) and powerfully modulate the cell excitability (Rekling *et al.*, 2000; Kuo *et al.*, 2005). Because our results demonstrated that H_2O_2 induced a preferential reduction of PIC(Ca) associated with hyperexcitability in rat HMs, we wondered if these effects could be explained by decreased AHP amplitude by H_2O_2. Thus, we measured the amplitude of the slow AHP at the end of the 300-pA depolarizing current pulse (at the same V_m before and during H_2O_2 application) and correlated it to the number of spikes (Fig. 5D; $n = 13$). In control condition (filled symbols), there was the expected linear relation between the AHP amplitude and the spikes number ($r = 0.895$, $P \leq 0.001$). In the presence of H_2O_2 (Fig. 5C, open symbols), not only this relation was lost ($r = 0.437$,

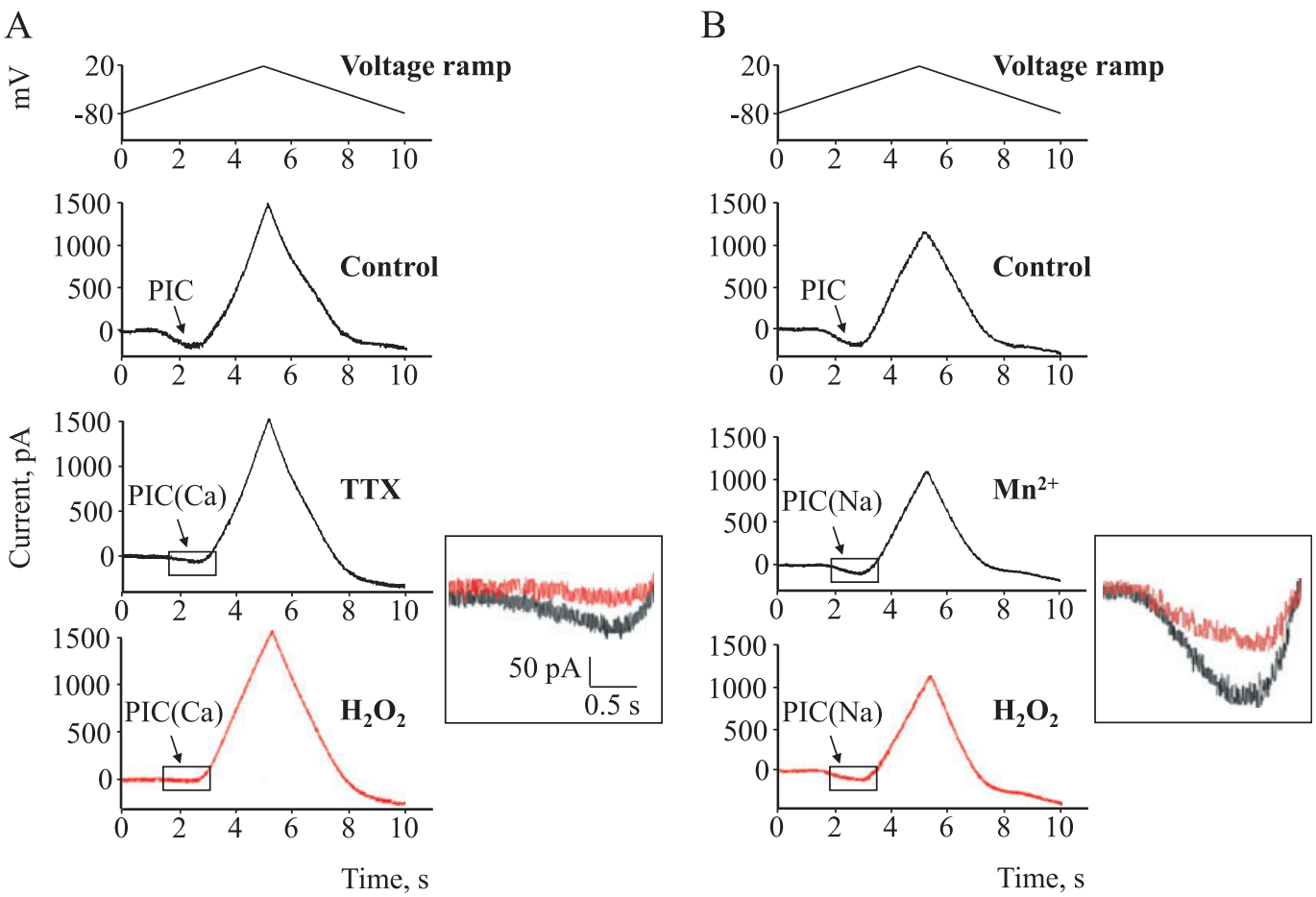

FIG. 4. Voltage-activated persistent inward currents (PICs) were modulated by H_2O_2. (A) On HMs, voltage ramps (from −80 to +20 mV; rate = 21 mV/s; see top scheme) induced PICs (mediated by Na^+ and Ca^{2+}; see arrow) followed by a large outward current in control solution (Krebs). Tetrodotoxin (TTX; 1 μM) was applied to pharmacologically isolate PIC(Ca) (Crill, 1996; Russo & Hounsgaard, 1999). After H_2O_2 application, PIC(Ca) was depressed as indicated by the superimposed traces of the current responses in the inset. (B) PIC(Na) current, isolated after PIC(Ca) block with 2 mM Mn^{2+}, was also reduced following application of H_2O_2. The superimposed records in the inset depict the reduction (larger current and time bars). Calibrations in inset to (A) apply also to inset to (B).

TABLE 2. Persistent inward currents in the presence of H_2O_2

	Amplitude (pA)	Area (pA/s)	Threshold (mV)
Mn^{2+}-sensitive component			
PIC (n = 7)	209 ± 26	231 ± 41	−60.9 ± 1.2
PIC(Ca) (n = 7)	97 ± 16	81 ± 16	−55.4 ± 3.2
t_6-value*	−3.395	−3.106	1.857
P-value*	0.015	0.021	0.122
PIC(Ca) after H_2O_2 (n = 7)	21 ± 5	17 ± 5	−56.5 ± 2.3
t_6-value†	−4.860	−3.969	−0.346
P-value†	0.003	0.007	0.743
TTX-sensitive component			
PIC (n = 7)	127 ± 22	133 ± 28	−60.4 ± 1.5
PIC(Na) (n = 7)	72 ± 15	74 ± 15	−56.8 ± 2.5
t_6-value‡	−6.835	−4.164	2.640
P-value‡	0.002	0.014	0.058
PIC(Na) after H_2O_2 (n = 7)	45 ± 15	37 ± 12	−57.4 ± 2.3
t_6-value¶	−3.056	−5.421	−0.535
P-value¶	0.038	0.006	0.621

Student's t-test was used for comparison of data pairs. *PIC(Ca) vs. PIC and †PIC(Ca) after H_2O_2 vs. PIC(Ca) for the Mn^{2+}-sensitive component PIC(Ca). ‡PIC(Na) vs. PIC and ¶PIC(Na) after H_2O_2 vs. PIC(Na) for the TTX-sensitive component PIC(Na). PIC, persistent inward current.

P = 0.135), but the AHP amplitude was reduced in spite of augmented firing (1.39 ± 0.24 mV vs. 1.96 ± 0.18 mV control, Student's t-test, t_{12} = 2.335, P = 0.038, n = 13). The inset to Fig. 5E shows that, at −65 mV, superimposed AHPs (evoked by 20 spikes) were markedly different in amplitude between control (1.70 mV; black trace) and H_2O_2 solution (0.45 mV; red trace).

H_2O_2 was effective in inducing oxidative stress damage to HMs

To demonstrate the HM redox stress induced by 1 mM H_2O_2, we used dihydrorhodamine 123, a non-fluorescent and lipophilic molecule that, by oxidation, yields the fluorescent probe Rho 123 (Sánchez-Carbente *et al.*, 2005; Jiang *et al.*, 2006). Figure 6A compares confocal images of intracellular generation of ROS (red pseudocolour) following incubation (for 30 min) in Krebs solution (top, left) or H_2O_2 (bottom, left). Hoechst 33342 was used as a cell counterstain (blue pseudocolour). Note that, despite the analogous number of Hoechst-positive cells in either condition, the number of Rho 123-positive cells (with > 25 μm soma) was higher following H_2O_2. These observations are quantified in the histograms of Fig. 6B in which the confocal images throughout the slices were reconstructed in 3D and the rhodamine signal expressed as a fraction of the Hoechst 33342 one (0.26 ± 0.04 vs. 0.13 ± 0.05, Mann–Whitney Rank Sum Test, T = 489.00, *P = 0.002, n = 5 rats).

H_2O_2 did not alter short-term cell survival

Because H_2O_2 application was accompanied by increased intracellular oxidative processes, we next addressed the question whether this phenomenon actually affected HM survival. First, we investigated the consequence of H_2O_2 application on the global hypoglossal nucleus cell population (Kitamura *et al.*, 1983; Boone & Aldes, 1984; Viana *et al.*, 1990) in unfixed specimens using the nuclear dye PI, which penetrates into cells only after membrane disruption (Kristensen *et al.*, 2001; Bonde *et al.*, 2003; Babot *et al.*, 2005; Bösel *et al.*, 2005). The total number of cells (intact as well as damaged) within each hypoglossal nucleus section was estimated with Hoechst 33342. Figure 7A shows staining with PI and Hoechst 33342 within the nucleus hypoglossus after incubation in Krebs solution (left) or after applying H_2O_2 for 30 min (top right) or 1 h (bottom right). In each example there was presence of co-staining, indicating a degree of cell damage in control or after treatment. Quantification of these observations (Fig. 7B) demonstrates that after either 30 min or 1 h application of H_2O_2 there was no significant increase in cell death (Mann–Whitney Rank Sum Test, T = 1283.00 or 919.00, P = 0.240 or 0.202 for 30 min or 1 h, respectively, n = 8 rats). Likewise, analysis of HM numbers with the motoneuron marker SMI 32 (Fig. 7C), a monoclonal antibody against the non-phosphorylated form of neurofilament H (Jacob *et al.*, 2005; Raoul *et al.*, 2005), confirmed similar presence in control (Krebs, left) or after H_2O_2 application (right). The histograms of Fig. 7D related to the sampled area (see inset to Fig. 7D) indicate that, on average, H_2O_2 did not change the number of HMs within the nucleus hypoglossus (53 ± 1 vs. 50 ± 4, Mann–Whitney Rank Sum Test, T = 25.00, P = 0.690, n = 5 rats).

ATF-3 expression by HMs treated with H_2O_2

The dissociation between intracellular redox stress and unchanged survival of HMs after H_2O_2 application led us to look for a biomarker that could signal motoneuron damage. For this purpose, we used ATF-3, a member of the ATF/CREB family of transcription factors, whose expression has been shown to rise after injurious stimuli (Tsujino *et al.*, 2000; Hai & Hartman, 2001; Vlug *et al.*, 2005). Figure 8A shows staining by ATF-3 (bottom) or SMI 32 (top) of hypoglossal nuclei fixed 1 h after washout of 1 mM H_2O_2 (right) or control solution (left). While the total number of HMs (SMI 32-immunopositive cells) was comparable between control (Krebs) and after H_2O_2, HMs expressing ATF-3 were more frequently detected in slices treated with H_2O_2. We next quantified the simultaneous occurrence of SMI 32 and ATF-3 within the same HMs. For this purpose we expressed co-staining for these markers as covariance values (see Materials and methods). Figure 8B summarizes these observations: whereas in Krebs solution the covariance value between ATF-3 and SMI 32 fluorescence was 139 ± 50, this value significantly increased to 434 ± 128 in the presence of H_2O_2 (Mann–Whitney Rank Sum Test, T = 46.00, *P = 0.021, n = 8 rats).

Discussion

The principal finding of the present report is the characterization of the early changes of rat HMs exposed to H_2O_2. It was interesting to observe a complex chain of events that included reduced premotor interneuron activity and enhanced HM firing. These effects were not accompanied by early cell death, but were associated with activation of the stress factor ATF-3. Our data suggest that acute oxidative stress induced a series of functional changes hitherto unreported and potentially relevant to the theory of oxidative damage in ALS (Turner *et al.*, 2009; Vucic & Kiernan, 2009).

H_2O_2 application as a model to investigate oxidative stress of HMs

Although the neuropathological results obtained from human ALS autopsy cases are valuable and important, almost all such cases represent only the terminal stage of the disease. This makes it difficult to clarify how and why ALS motoneurons are impaired at each clinical stage from disease onset to death and, as a consequence, human

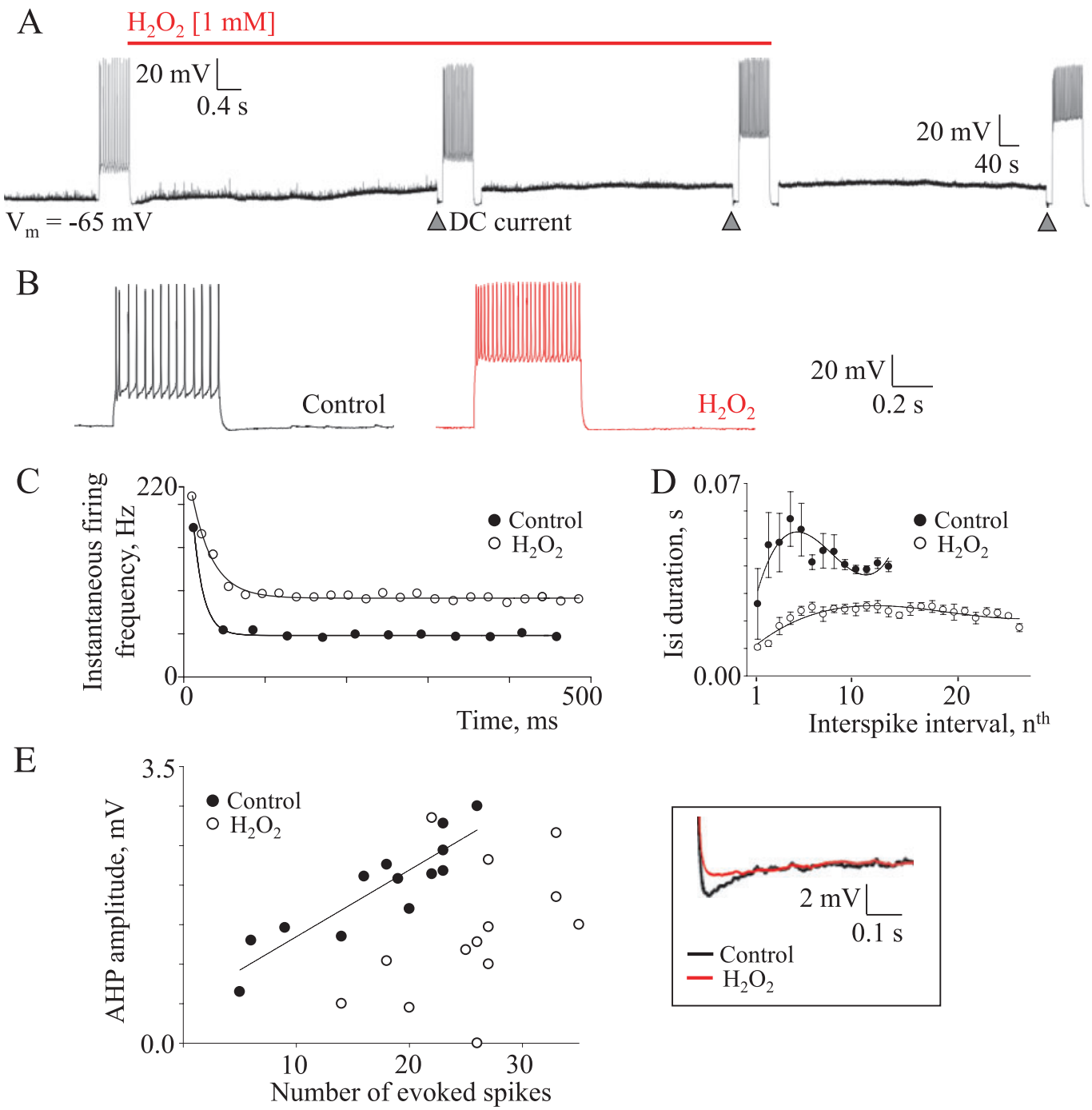

FIG. 5. Changes in HM excitability induced by H_2O_2. (A) Examples of responses of HM to bath-applied H_2O_2. Trace is a continuous, slow record of a cell with initial V_m of −65 mV. Segments of this trace are also shown on a faster time base to depict spike firing evoked by intracellular injection of 300 pA (500 ms). Note that, following application of H_2O_2, there is gradual membrane depolarization (7 mV) associated with enhanced spike activity (when the V_m is repolarized back to rest). Prolonged washout was not able to reverse the observed effects. (B) Fast time base example of evoked firing (300 pA; 500 ms) in control and after H_2O_2 application. Note the higher number of spikes and the larger amplitude of the membrane voltage response to the same current injection pulse following H_2O_2. (C) Example of instantaneous firing frequency in control (filled symbols) and following H_2O_2 application (open symbol). Data are fitted with double exponential function in accordance with Sawczuk *et al.* (1995). (D) Plot of average (n = 6 cells) interspike interval (isi) vs. spike interval in the 500-ms train. Data were fitted with a cubic polynomial function (see Materials and methods) and the curves difference integral for the first 13 spikes calculated. Subtraction of the treated area (open circles) from control (filled circles) gave $\int_1^{13}(y_1-y_2) = 0.6141$, indicating the change evoked by H_2O_2. Control area was $\int_1^{13} y_1 = 1.1206$. After normalization, the H_2O_2-mediated decrease in area was equal to 0.6141/1.1206 * 100 = 55%. (E) Scatter plot of the afterhyperpolarization (AHP) amplitude vs. the number of evoked spikes in control condition (filled symbols) and following H_2O_2 bath application (open symbols). AHP amplitude was measured at the end of a 300-pA depolarizing current pulse, applied at the same V_m before and after H_2O_2 treatment (n = 13). In control condition, the AHP amplitude increased with the number of evoked spikes (regression equation: $y = 0.08\ x + 0.50$; $r = 0.895$; $P \leq 0.001$). In the presence of H_2O_2 the linear relation was lost ($r = 0.437$; $P = 0.135$) and, despite the larger number of action potentials, the AHP amplitude was decreased (Student's t-test, $t_{12} = 2.335$, $P = 0.038$, n = 13). The inset shows that, at −65 mV, superimposed AHPs (evoked by 20 spikes) were markedly different between control (1.70 mV; black trace) and H_2O_2 solution (0.45 mV; red trace).

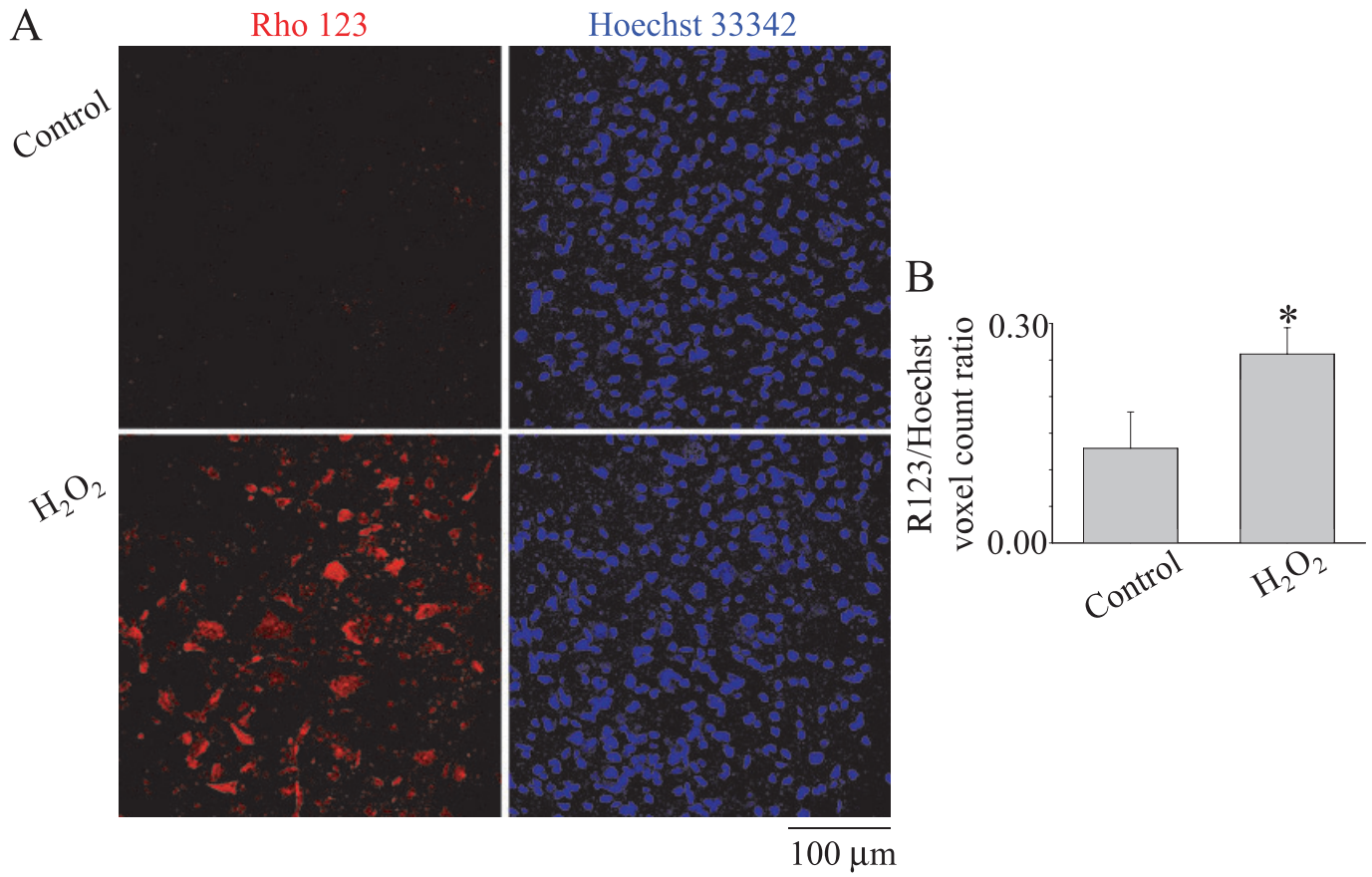

FIG. 6. Oxidative stress of HMs caused by H_2O_2. (A) Histological example of rhodamine 123 (Rho 123) staining of cells in hypoglossal slices incubated for 30 min in Krebs solution or in the presence of H_2O_2 (1 mM). After rinsing, cells were stained with dihydrorhodamine 123 (red pseudocolour) to reveal intracellular oxidative processes (Sánchez-Carbente *et al.*, 2005; Jiang *et al.*, 2006) and Hoechst 33342 (blue pseudocolour) to show cell nuclei. Note that, notwithstanding the analogous number of Hoechst-positive cells, there was a larger number of rhodamine 123-positive, large soma cells following H_2O_2. (B) Histograms show the ratio of rhodamine-positive cells over Hoechst-positive cells, indicating a significant rise after H_2O_2. Data are from five animals and were quantified with ImageJ software (Mann–Whitney Rank Sum Test, $T = 489.00$, $^*P = 0.002$).

autopsy cases alone yield little insight into potential therapies for ALS (Kato, 2008). Clinical electrophysiology data suggest that the ALS disease is widespread at the time of diagnosis, implying that it has been active and disseminated through the motor system for some time prior to presentation with weakness and atrophy (Swash & Ingram, 1988). This realization calls for experimental models that can yield important information for clarifying the early pathogenesis of ALS in humans (Kato, 2008).

Current theories of ALS propose that motoneuron damage may result from oxidative stress, as indicated by the host (> 130) of SOD-1 mutations implicated in the genetic forms of ALS that, however, are only 10% of all clinical cases and have generated a large number of mouse genetic models (Vucic & Kiernan, 2009). Such experimental studies have not provided a uniform theory to account for motoneuron damage and have been primarily conducted with mouse motoneurons. Because some experimental manipulations are difficult on mice because of their innate size, rat models of ALS have also been developed. Like its murine counterpart, the rat G93A model reproduces the major phenotype of motoneuron degeneration (Aoki *et al.*, 2005), although spinal rather than brainstem motoneurons are primarily affected (Lladó *et al.*, 2006).

Because the vast majority of ALS cases are sporadic and presumably imply an environmental toxic agent (Cleveland & Rothstein, 2001), we wished to understand how rat HMs could respond to strong oxidative stress to identify certain mechanisms that might lead to motoneuron degeneration. Of course, the present study suffers from certain intrinsic limitations like the use of neonatal motoneurons and the inability to follow up the long-term evolution of damage because brain slices have restricted survival *in vitro*. Nevertheless, the present results offer a novel insight into the early events of oxidative stress.

Early consequences of H_2O_2 application on synaptic transmission and HM excitability

H_2O_2 evoked a slowly developing inward current (depolarization) with input resistance rise and relatively poor recovery on washout. Regardless of the application of receptor or channel blockers, and of voltage- or current-clamp recording, we consistently found a significant rise in input resistance evoked by H_2O_2. This observation implied depression of a leak background current that was not inhibited by intracellular Cs^+ contained in the patch pipette. Previous studies indicated that rat motoneurons possess a background K^+ current rather resistant to Cs^+ (Fisher & Nistri, 1993) subsequently identified as a member of the TWIK-related acid-sensitive K^+ channel (TASK) family of K^+ channels, whose main constituent, namely TASK-1, is expressed chiefly by motoneurons (Talley *et al.*, 2000; Bayliss *et al.*, 2001). In accordance with this notion, in the presence of H_2O_2, the current response had a very negative extrapolated reversal potential with linear *I/V* plot, consistent with the properties of TASK-1. It is

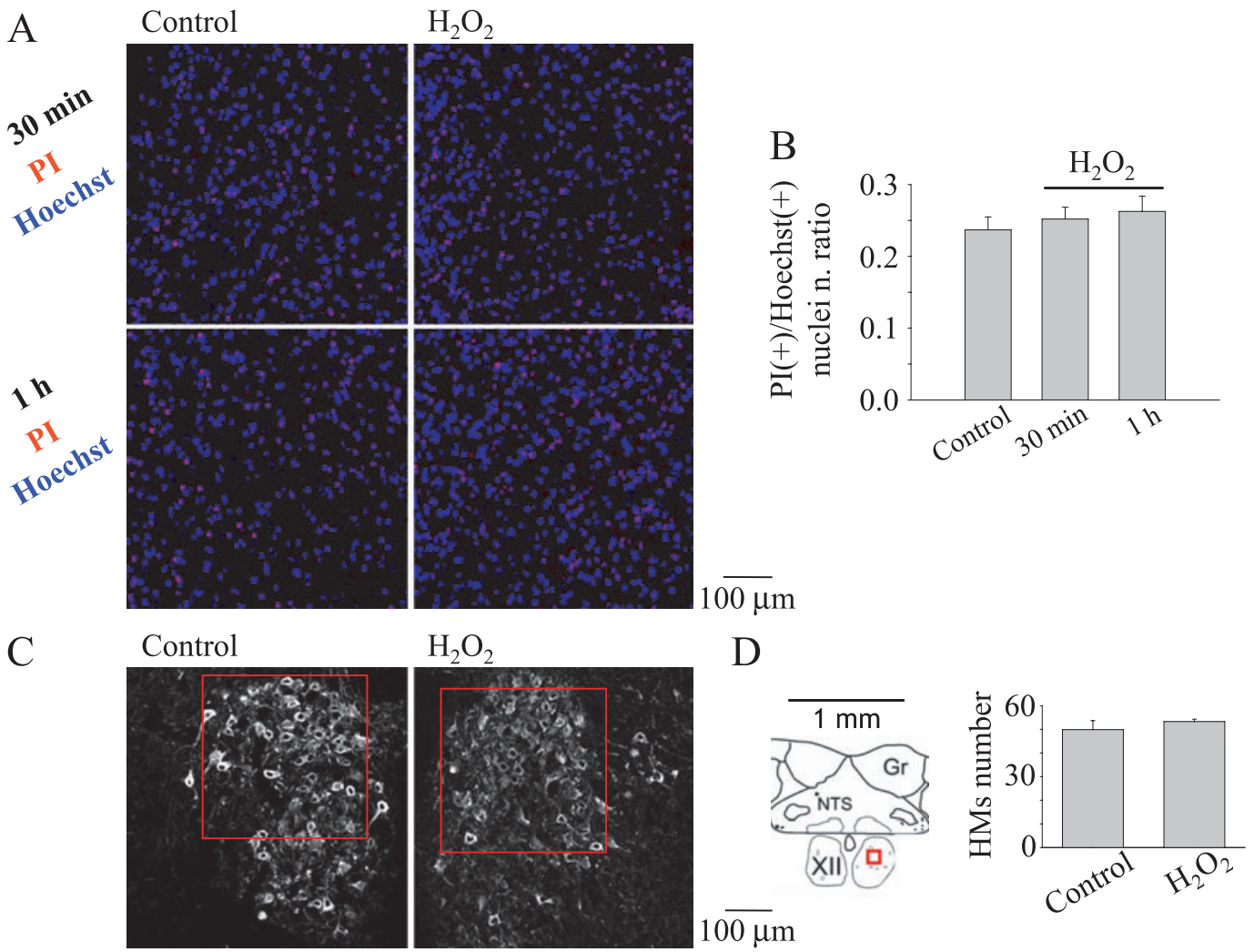

FIG. 7. H_2O_2 did not alter short-term cell survival. (A) Examples of fluorescence cell counts after staining with propidium iodide (PI), a DNA dye that labels membrane-damaged cells (red pseudocolour), and Hoechst 33342 (blue pseudocolour) in two experimental protocols: Krebs vs. either 30 min H_2O_2 (top row) or 1 h H_2O_2 (bottom row). In each panel, PI-positive cells are indicative of dead cells. (B) Histograms showing no increase in cell death after exposure to either 30 min H_2O_2 or 1 h H_2O_2 (control value comprises cells damaged by the brain-slicing preparation). Data (collected from eight rats) were quantified with ImageJ software and expressed as ratio of PI-positive cells over Hoechst-positive cells. Mann–Whitney Rank Sum Test gave $T = 1283.00$, $P = 0.240$ for the difference between Krebs and 30 min H_2O_2; $T = 919.00$, $P = 0.202$ for the difference between Krebs and 1 h H_2O_2. (C) Example of confocal images of HMs labeled with the motoneuron marker SMI 32 (Jacob *et al.*, 2005; Raoul *et al.*, 2005) in control condition and after 30 min H_2O_2 (the red box is the sample area used to count HMs). (D) Left, scheme of sampled area used for confocal images, shown in red within one nucleus hypoglossus. Right, histograms quantifying the number of HMs (SMI 32-positive) with no significant difference between control and H_2O_2 treatment. Data were quantified with CellCounter (Mann–Whitney Rank Sum Test, $T = 25.00$, $P = 0.690$, $n = 5$ rats).

likely that the larger input resistance of motoneurons contributed to their higher excitability.

This phenomenon, accompanied by a significant reduction in the frequency of sPSCs, suggested a complex origin that might have comprised changes in the release of various transmitters. To examine this issue more directly, we used TTX to investigate how miniature synaptic events responded to H_2O_2. Blocking fast glutamatergic transmission with APV and CNQX did not prevent the effects by H_2O_2 on baseline current or input resistance, and revealed a paradoxical rise in the frequency of inhibitory synaptic events that are known to be mediated by glycine and GABA (Donato & Nistri, 2000). Because H_2O_2 is known to raise intracellular free Ca^{2+} (Zheng & Shen, 2005; Takahashi *et al.*, 2007; Gerich *et al.*, 2009) and its action was mimicked by thapsigargin, our data accord with the potentiation by H_2O_2 of GABAergic miniature event frequency via increased intracellular free Ca^{2+} (Takahashi *et al.*, 2007). Neurochemical experiments on rat hippocampal slices also demonstrate that H_2O_2 markedly potentiates GABA release (Saransaari & Oja, 2008). Blocking inhibitory synaptic transmission with strychnine and bicuculline eliminated the effects by H_2O_2 on motoneuron baseline current, yet enabled us to observe a significant increase in glutamatergic miniature events as well as in input resistance. Thus, H_2O_2 seemingly facilitated release of glutamate, GABA and glycine, indicating a presynaptic origin for this process at the level of network-independent release. Extracellular GABA and glycine had an impact on baseline HM current presumably because of their positive reversal potential at this stage of development (Marchetti *et al.*, 2002).

While our data indicate enhancement of miniature event frequency, they contrast with the observed fall in premotor interneuron-mediated synaptic events. The latter finding has been reported on hippocampal pyramidal neurons on which H_2O_2 depresses electrically evoked excitatory and inhibitory synaptic

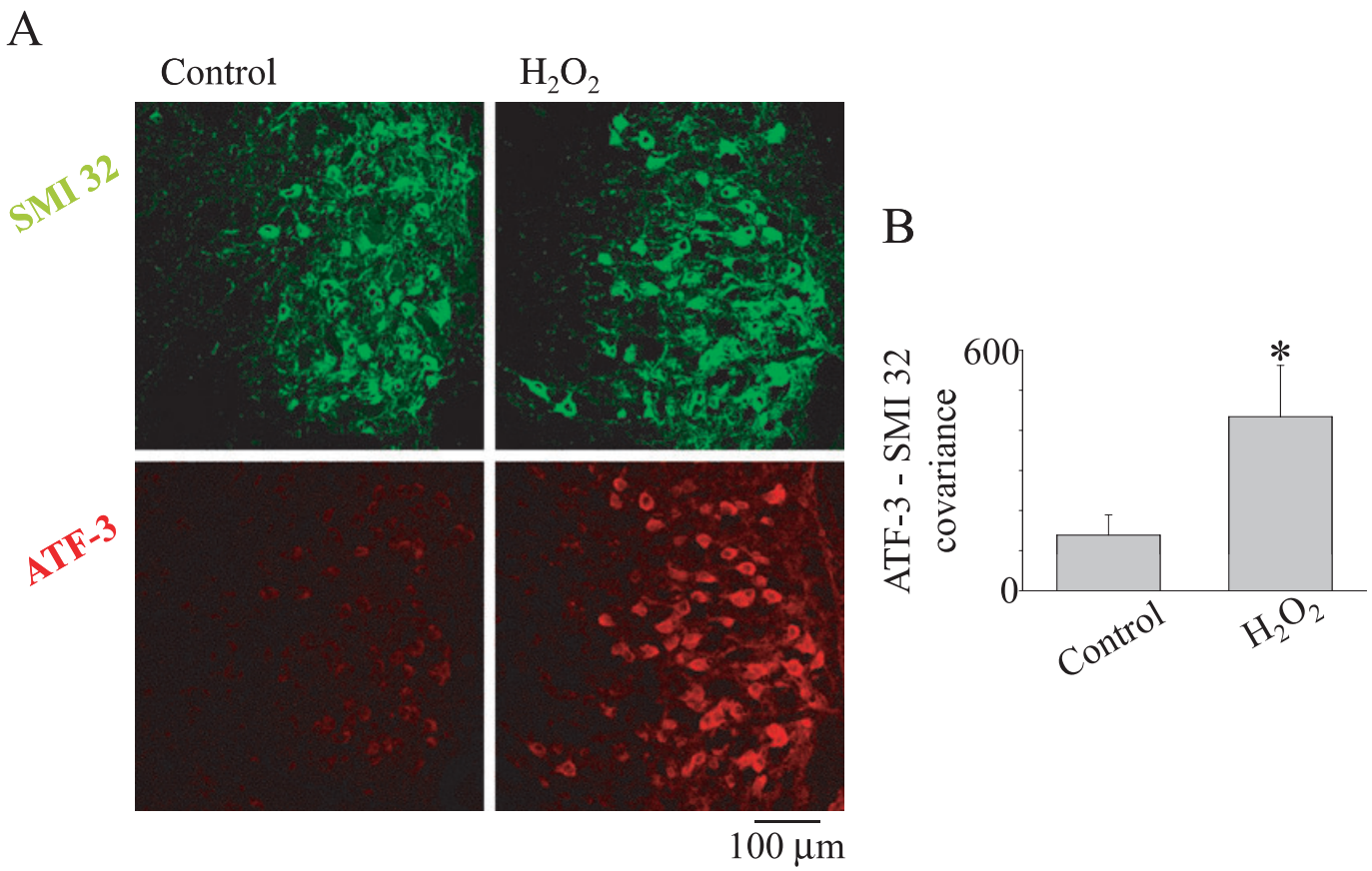

FIG. 8. Activating transcription factor 3 (ATF-3) expression by HMs treated with H_2O_2. (A) Examples of SMI 32 (top) and ATF-3 (bottom) immunoreactivity of nucleus hypoglossus in control (left) and after H_2O_2 (right). Note that, despite a similar number of HMs (SMI 32-positive), ATF-3 staining was highly enhanced following H_2O_2. ATF-3, a member of the ATF/CREB family of transcription factors, is proposed to be a marker of neuronal injury (Tsujino *et al.*, 2000; Hai & Hartman, 2001; Vlug *et al.*, 2005). (B) Histograms show the covariance between ATF-3 staining and SMI 32 staining, indicating a significant rise after H_2O_2. Data are from eight animals and were quantified with MATLAB 7.1 software (Mann–Whitney Rank Sum Test, $T = 46.00$, $*P = 0.021$).

potentials (Pellmar, 1987). This discrepancy led us to investigate changes in voltage-dependent currents that may be responsible for neuronal excitability.

Raised HM firing despite PIC suppression by H_2O_2

Previous studies have shown that mammalian spinal neuron excitability is largely mediated by PICs that comprised PIC(Na) (Darbon *et al.*, 2004; Harvey *et al.*, 2006; Zhong *et al.*, 2007) and PIC(Ca) (Li & Bennett, 2007). These currents are also expressed by neonatal rat HMs (Lamanauskas & Nistri, 2008) and are found to be potentiated in the mouse $SOD1^{G93A}$ model (van Zundert *et al.*, 2008), in analogy with $SOD1^{G93A}$ spinal motoneurons in culture (Kuo *et al.*, 2005). It is, however, interesting that spinal motoneurons of the $SOD1^{G85R}$ model display less excitability than wild-type cells (Bories *et al.*, 2007), even if their repeated firing is proposed to be regulated by PIC(Na) (Amendola *et al.*, 2007).

In the present study we observed that H_2O_2 induced a larger reduction of PIC(Ca) (79%) than of PIC(Na) (38%) without threshold alteration. Notwithstanding the impaired amplitude of PICs by H_2O_2, we detected accelerated firing rates of HMs with strong inhibition of the AHP. Because H_2O_2 only partly depressed PIC(Na), this effect would not be sufficient to change excitability because nearly complete block PIC(Na) is necessary for strong depression of HM firing (Lamanauskas & Nistri, 2008).

Blocking Ca^{2+} channels often prolongs the action potential and raises neuronal excitability, an effect opposite to the one expected from blocking the entry of positively charged ions (Bean, 2007). This reflects powerful and rapid coupling of Ca^{2+} entry to the activation of Ca^{2+}-activated K^+ channels, so that the net effect of blocking Ca^{2+} influx is to inhibit a net outward current and, therefore, to increase excitability (Bean, 2007). In accordance with this notion, we suggest that H_2O_2 enhanced firing because it largely depressed Ca^{2+} influx, as shown by the decrease in PIC(Ca), important for the activation of the Ca^{2+}-dependent K^+ conductances underlying the AHP (Umemiya & Berger, 1994; Lape & Nistri, 1999; Li & Bennett, 2007). These effects were apparently distinct from the facilitation by H_2O_2 of Ca^{2+} release from presynaptic intracellular stores (as discussed above), a phenomenon that developed in the absence of firing following TTX application.

Early motoneuron damage by H_2O_2

We next explored whether, as a result of exposure to H_2O_2, HMs were damaged. We first ascertained that this treatment was actually accompanied by a significant rise in intracellular oxidative processes. It is interesting that advanced oxidation protein products are higher in the cerebrospinal fluid of patients with ALS, with concurrent decrease in antioxidant capacity, compared with controls with other neurological diseases (Siciliano *et al.*, 2007). Furthermore, we counted the number of PI-positive cells or SMI 32-positive HMs to find out if there

had been a rapid and extensive cell death. Our results indicated that there was no change in the number of motoneurons in the slices, suggesting that oxidative stress, albeit of strong intensity, did not produce early motoneuronal death. It was, however, apparent that the H_2O_2 application had evoked an important reaction in HMs because of the large increase in their immunocytochemical expression of ATF-3.

ATF-3 is a transcription factor induced by harmful extracellular stimuli that trigger intracellular kinase activity responsible for neosynthesis of ATF-3 and its translocation to the cell nucleus where it can be observed after neuronal lesion (Tsujino *et al.*, 2000; Nakagomi *et al.*, 2003; Lindwall *et al.*, 2004). ATF-3 has a Janus-like function subserving either damage repair or degeneration depending on the nature of the insult (Tsujino *et al.*, 2000; Nakagomi *et al.*, 2003; Vlug *et al.*, 2005). In SOD^{G93A} mouse motoneurons ATF-3 is strongly expressed prior to neurodegeneration (Vlug *et al.*, 2005). We suggest that the ATF-3 signal observed in the present study was an index of initial distress of motoneuron subsequent to H_2O_2 treatment. Its cytoplasmic location was probably due to the fact that the DNA transcriptional effects of ATF-3 require its *de novo* protein synthesis in the cytosol (Lindwall *et al.*, 2004).

In conclusion, most research into neurophysiological biomarkers of ALS has focussed on the development of surrogate markers of motor unit loss (Turner *et al.*, 2009). Electrophysiological studies of early stage ALS have shown increased motoneuron excitability attributed to dysfunction of motor cortex (Turner *et al.*, 2009). However, lower motoneuron hyperexcitability is also an important feature of the disease presentation. If we assume that oxidative stress may be a significant contributor to ALS pathology (Turner *et al.*, 2009; Vucic & Kiernan, 2009), our current results suggest that even a transient oxidative stress can render brainstem motoneuron hyperexcitable through a combination of enhanced input resistance and firing rate, a condition accompanied by ATF-3 activation.

Supporting Information

Additional supporting information may be found in the online version of this article:

Fig. S1. Example of baseline current (under voltage clamp) from HM in the continuous presence of TTX, bicuculline and strychnine.

Table S1. Average change in input resistance and baseline current induced by application of TTX.

Table S2. Changes in input resistance, average firing frequency and membrane potential evoked by H_2O_2 in standard solution or in the presence of blockers of glutamatergic transmission (CNQX and APV) or inhibitory synaptic transmission (bicuculline and strychnine).

Please note: As a service to our authors and readers, this journal provides supporting information supplied by the authors. Such materials are peer-reviewed and may be re-organized for online delivery, but are not copy-edited or typeset by Wiley-Blackwell. Technical support issues arising from supporting information (other than missing files) should be addressed to the authors.

Acknowledgements

This work was supported by a grant from Ministero dell'Università e Ricerca (Progetti di Ricerca di Interesse Nazionale) and grants from the Friuli Venezia Giulia Region. We thank Dr Micaela Grandolfo, Dr Miranda Mladinic, and Dr Walter Vanzella for their support with histological data acquisition and analysis. We thank Giacomo Bisson for his mathematical advice on data analysis.

Abbreviations

AHP, afterhyperpolarization; ALS, amyotrophic lateral sclerosis; APV, D-amino-phosphonovalerate; ATF-3, activating transcription factor 3; CNQX, 6-cyano-7-nitroquinoxaline-2,3-dione; DHR 123, dihydrorhodamine 123; GABA, γ-aminobutyric acid; HM, hypoglossal motoneuron; I_{res}, residual current; mEPSC, miniature excitatory postsynaptic current; mIPSC, miniature inhibitory postsynaptic current; PBS, phosphate-buffered saline; PI, propidium iodide; PIC, persistent inward current; Rho 123, rhodamine 123; ROS, reactive oxygen species; SOD-1, superoxide dismutase 1; sPSC, spontaneous postsynaptic current; TASK, TWIK-related acid-sensitive K^+ channel; TTX, tetrodotoxin.

References

Amendola, J., Gueritaud, J.P., d'Incamps, B.L., Bories, C., Liabeuf, S., Allene, C., Pambo-Pambo, A. & Durand, J. (2007) Postnatal electrical and morphological abnormalities in lumbar motoneurons from transgenic mouse models of amyotrophic lateral sclerosis. *Arch. Ital. Biol.*, **145**, 311–323.

Aoki, M., Kato, S., Nagai, M. & Itoyama, Y. (2005) Development of a rat model of amyotrophic lateral sclerosis expressing a human SOD1 transgene. *Neuropathology*, **25**, 365–370.

Aracri, P., Colombo, E., Mantegazza, M., Scalmani, P., Curia, G., Avanzini, G. & Franceschetti, S. (2006) Layer-specific properties of the persistent sodium current in sensorimotor cortex. *J. Neurophysiol.*, **95**, 3460–3468.

Babot, Z., Cristofol, R. & Sunol, C. (2005) Excitotoxic death induced by released glutamate in depolarized primary cultures of mouse cerebellar granule cells is dependent on $GABA_A$ receptors and niflumic acid-sensitive chloride channels. *Eur. J. Neurosci.*, **21**, 103–112.

Bayliss, D.A., Talley, E.M., Sirois, J.E. & Lei, Q. (2001) TASK-1 is a highly modulated pH-sensitive 'leak' K^+ channel expressed in brainstem respiratory neurons. *Respir. Physiol.*, **129**, 159–174.

Beal, M.F., Ferrante, R.J., Browne, S.E., Matthews, R.T., Kowall, N.W. & Brown, R.H., Jr (1997) Increased 3-nitrotyrosine in both sporadic and familial amyotrophic lateral sclerosis. *Ann. Neurol.*, **42**, 644–654.

Bean, B.P. (2007) The action potential in mammalian central neurons. *Nat Rev Neurosci.*, **8**, 451–465.

Bogdanov, M., Brown, R.H., Matson, W., Smart, R., Hayden, D., O'Donnell, H., Flint Beal, M. & Cudkowicz, M. (2000) Increased oxidative damage to DNA in ALS patients. *Free Radical Biol Med.*, **29**, 652–658.

Bonde, C., Sarup, A., Schousboe, A., Gegelashvili, G., Zimmer, J. & Noraberg, J. (2003) Neurotoxic and neuroprotective effects of the glutamate transporter inhibitor dl-threo-betabenzyloxyaspartate (DL-TBOA) during physiological and ischemia-like conditions. *Neurochem. Int.*, **43**, 371–380.

Boone, T.B. & Aldes, L.D. (1984) The ultrastructure of two distinct neuron populations in the hypoglossal nucleus of the rat. *Exp. Brain Res.*, **54**, 321–326.

Bories, C., Amendola, J., Lamotte d'Incamps, B. & Durand, J. (2007) Early electrophysiological abnormalities in lumbar motoneurons in a transgenic mouse model of amyotrophic lateral sclerosis. *Eur. J. Neurosci.*, **25**, 451–459.

Bösel, J., Gandor, F., Harms, C., Synowitz, M., Harms, U., Djoufack, P.C., Megow, D., Dirnagl, U., Hörtnagl, H., Fink, K.B. & Endres, M. (2005) Neuroprotective effects of atorvastatin against glutamate-induced excitotoxicity in primary cortical neurones. *J. Neurochem.*, **92**, 1386–1398.

Brown, R.H., Jr & Robberecht, W. (2001) Amyotrophic lateral sclerosis: pathogenesis. *Semin. Neurol.*, **21**, 131–139.

Brownstone, R.M. (2007) Take your PIC: motoneuronal persistent inward currents may be somatic as well as dendritic. *J. Neurophysiol.*, **98**, 579–580.

Cleveland, D.W. & Rothstein, J.D. (2001) From Charcot to Lou Gehrig: deciphering selective motor neuron death in ALS. *Nat Rev Neurosci.*, **2**, 806–819.

Cramer, N.P., Li, Y. & Keller, A. (2007) The whisking rhythm generator: a novel mammalian network for the generation of movement. *J. Neurophysiol.*, **97**, 2148–2158.

Crill, W.E. (1996) Persistent sodium current in mammalian central neurons. *Annu. Rev. Physiol.*, **58**, 349–362.

Darbon, P., Yvon, C., Legrand, J.C. & Streit, J. (2004) I_{NaP} underlies intrinsic spiking and rhythm generation in networks of cultured rat spinal cord neurons. *Eur. J. Neurosci.*, **20**, 976–988.

Donato, R. & Nistri, A. (2000) Relative contribution by GABA or glycine to Cl^--mediated synaptic transmission on rat hypoglossal motoneurons in vitro. *J. Neurophysiol.*, **84**, 2715–2724.

Enomoto, A., Han, J.M., Hsiao, C.F., Wu, N. & Chandler, S.H. (2006) Participation of sodium currents in burst generation and control of membrane

excitability in mesencephalic trigeminal neurons. *J. Neurosci.*, **26**, 3412–3422.
Essin, K., Nistri, A. & Magazanik, L. (2002) Evaluation of GluR2 subunit involvement in AMPA receptor function of neonatal rat hypoglossal motoneurons. *Eur. J. Neurosci.*, **15**, 1899–1906.
Ferrante, R.J., Browne, S.E., Shinobu, L.A., Bowling, A.C., Baik, M.J., MacGarvey, U., Kowall, N.W., Brown, R.H., Jr & Beal, M.F. (1997) Evidence of increased oxidative damage in both sporadic and familial amyotrophic lateral sclerosis. *J. Neurochem.*, **69**, 2064–2074.
Fisher, N.D. & Nistri, A. (1993) A study of the barium-sensitive and insensitive components of the action of thyrotropin-releasing hormone on lumbar motoneurons of the rat isolated spinal cord. *Eur. J. Neurosci.*, **5**, 1360–1369.
Gerich, F.J., Funke, F., Hildebrandt, B., Fasshauer, M. & Müller, M. (2009) H_2O_2-mediated modulation of cytosolic signaling and organelle function in rat hippocampus. *Pflugers Arch.*, **458**, 937–952.
Gurney, M.E., Pu, H., Chiu, A.Y., Dal Canto, M.C., Polchow, C.Y., Alexander, D.D., Caliendo, J., Hentati, A., Kwon, Y.W., Deng, H.X., Chen, W., Zhai, P., Sufit, R.L. & Siddique, T. (1994) Motorneuron degeneration in mice that express a human Cu,Zn superoxide dismutase mutation. *Science*, **264**, 1772–1774.
Hai, T. & Hartman, M.G. (2001) The molecular biology and nomenclature of the activating transcription factor/cAMP responsive element binding family of transcription factors: activating transcription factor proteins and homeostasis. *Gene*, **273**, 1–11.
Halliwell, B. (1992) Reactive oxygen species in the central nervous system. *J. Neurochem.*, **59**, 1609–1623.
Harvey, P.J., Li, Y., Li, X. & Bennett, D.J. (2006) Persistent sodium currents and repetitive firing in motoneurons of the sacrocaudal spinal cord of adult rats. *J. Neurophysiol.*, **96**, 1141–1157.
Ihara, Y., Nobukuni, K., Takata, H. & Hayabara, T. (2005) Oxidative stress and metal content in blood and cerebrospinal fluid of amyotrophic lateral sclerosis patients with and without a Cu,Zn-superoxide dismutase mutation. *Neurol. Res.*, **27**, 105–108.
Jacob, D.A., Bengston, C.L. & Forger, N.G. (2005) Effects of *Bax* gene deletion on muscle and motoneuron degeneration in a sexually dimorphic neuromuscular system. *J. Neurosci.*, **25**, 5638–5644.
Jiang, Z.G., Lu, X.C., Nelson, V., Yang, X., Pan, W., Chen, R.W., Lebowitz, M.S., Almassian, B., Tortella, F.C., Brady, R.O. & Ghanbari, H.A. (2006) A multifunctional cytoprotective agent that reduces neurodegeneration after ischemia. *Proc Nat Acad Sci USA*, **103**, 1581–1586.
Jones, K.H. & Senft, J.A. (1985) An improved method to determine cell viability by simultaneous staining with fluorescein diacetate-propidium iodide. *J. Histochem. Cytochem.*, **33**, 77–79.
Kato, S. (2008) Amyotrophic lateral sclerosis models and human neuropathology: similarities and differences. *Acta Neuropathol.*, **115**, 97–114.
Kirby, M.S., Sagara, Y., Gaa, S., Inesi, G., Lederer, W.J. & Rogers, T.B. (1992) Thapsigargin inhibits contraction and Ca^{2+} transient in cardiac cells by specific inhibition of the sarcoplasmic reticulum Ca^{2+} pump. *J. Biol. Chem.*, **267**, 12545–12551.
Kitamura, S., Nishiguchi, T. & Sakai, A. (1983) Location of cell somata and the peripheral course of axons of the geniohyoid and thyrohyoid motoneurons: a horseradish peroxidase study in the rat. *Exp. Neurol.*, **79**, 87–96.
Kristensen, B.W., Noraberg, J. & Zimmer, J. (2001) Comparison of excitotoxic profiles of ATPA, AMPA, KA and NMDA in organotypic hippocampal slice cultures. *Brain Res.*, **917**, 21–44.
Kühnlein, P., Gdynia, H.J., Sperfeld, A.D., Lindner-Pfleghar, B., Ludolph, A.C., Prosiegel, M. & Riecker, A. (2008) Diagnosis and treatment of bulbar symptoms in amyotrophic lateral sclerosis. *Nat Clin Pract Neurol.*, **4**, 366–374.
Kuo, J.J., Siddique, T., Fu, R. & Heckman, C.J. (2005) Increased persistent Na^+ current and its effect on excitability in motoneurones cultured from mutant SOD1 mice. *J. Physiol.*, **563**, 843–854.
Lamanauskas, N. & Nistri, A. (2006) Persistent rhythmic oscillations induced by nicotine on neonatal rat hypoglossal motoneurons in vitro. *Eur. J. Neurosci.*, **24**, 2543–2556.
Lamanauskas, N. & Nistri, A. (2008) Riluzole blocks persistent Na^+ and Ca^{2+} currents and modulates release of glutamate via presynaptic NMDA receptors on neonatal rat hypoglossal motoneurons in vitro. *Eur. J. Neurosci.*, **27**, 2501–2514.
Lape, R. & Nistri, A. (1999) Voltage-activated K^+ currents of hypoglossal motoneurons in a brain stem slice preparation from the neonatal rat. *J. Neurophysiol.*, **81**, 140–148.
Lape, R. & Nistri, A. (2000) Current and voltage clamp studies of the spike medium afterhyperpolarization of hypoglossal motoneurons in a rat brain stem slice preparation. *J. Neurophysiol.*, **83**, 2987–2995.
Laslo, P., Lipski, J. & Funk, G.D. (2001a) Differential expression of Group I metabotropic glutamate receptors in motoneurons at low and high risk for degeneration in ALS. *Neuroreport*, **12**, 1903–1908.
Laslo, P., Lipski, J., Nicholson, L.F., Miles, G.B. & Funk, G.D. (2001b) GluR2 AMPA receptor subunit expression in motoneurons at low and high risk for degeneration in amyotrophic lateral sclerosis. *Exp. Neurol.*, **169**, 461–471.
von Lewinski, F. & Keller, B.U. (2005) Ca^{2+}, mitochondria and selective motoneuron vulnerability: implications for ALS. *Trends Neurosci.*, **28**, 494–500.
Li, X. & Bennett, D.J. (2007) Apamin-sensitive calcium-activated potassium currents (SK) are activated by persistent calcium currents in rat motoneurons. *J. Neurophysiol.*, **97**, 3314–3330.
Lindwall, C., Dahlin, L., Lundborg, G. & Kanje, M. (2004) Inhibition of c-Jun phosphorylation reduces axonal outgrowth of adult rat nodose ganglia and dorsal root ganglia sensory neurons. *Mol. Cell. Neurosci.*, **27**, 267–279.
Lladó, J., Haenggeli, C., Pardo, A., Wong, V., Benson, L., Coccia, C., Rothstein, J.D., Shefner, J.M. & Maragakis, N.J. (2006) Degeneration of respiratory motor neurons in the SOD1 G93A transgenic rat model of ALS. *Neurobiol Dis.*, **21**, 110–118.
Magistretti, J., Castelli, L., Forti, L. & D'Angelo, E. (2006) Kinetic and functional analysis of transient, persistent and resurgent sodium currents in rat cerebellar granule cells in situ: an electrophysiological and modeling study. *J. Physiol.*, **573**, 83–106.
Marchetti, C., Pagnotta, S., Donato, R. & Nistri, A. (2002) Inhibition of spinal or hypoglossal motoneurons of the newborn rat by glycine or GABA. *Eur. J. Neurosci.*, **15**, 975–983.
Medina, L., Figueredo, C.G., Rothstein, J.D. & Reiner, A. (1996) Differential abundance of glutamate transporter subtypes in amyotrophic lateral scleroses (ALS)-vulnerable versus ALS-resistant brain stem motor cell groups. *Exp. Neurol.*, **142**, 287–295.
Moritz, A.T., Newkirk, G., Powers, R.K. & Binder, M.D. (2007) Facilitation of somatic calcium channels can evoke prolonged tail currents in rat hypoglossal motoneurons. *J. Neurophysiol.*, **98**, 1042–1047.
Nakagomi, S., Suzuki, Y., Namikawa, K., Kiryu-Seo, S. & Kiyama, H. (2003) Expression of the activating transcription factor 3 prevents c-Jun N-terminal kinase-induced neuronal death by promoting heat shock protein 27 expression and Akt activation. *J. Neurosci.*, **23**, 5187–5196.
O'Brien, J.A., Isaacson, J.S. & Berger, A.J. (1997) NMDA and non-NMDA receptors are co-localized at excitatory synapses of rat hypoglossal motoneurons. *Neurosci. Lett.*, **227**, 5–8.
Pagnotta, S.E., Lape, R., Quitadamo, C. & Nistri, A. (2005) Pre- and postsynaptic modulation of glycinergic and GABAergic transmission by muscarinic receptors on rat hypoglossal motoneurons in vitro. *Neuroscience*, **130**, 783–795.
Pasinelli, P. & Brown, R.H. (2006) Molecular biology of amyotrophic lateral sclerosis: insights from genetics. *Nat Rev Neurosci.*, **7**, 710–723.
Pellmar, T.C. (1987) Peroxide alters neuronal excitability in the CA1 region of guinea-pig hippocampus in vitro. *Neuroscience*, **23**, 447–456.
Ptak, K., Zummo, G.G., Alheid, G.F., Tkatch, T., Surmeier, D.J. & McCrimmon, D.R. (2005) Sodium currents in medullary neurons isolated from the pre-Botzinger complex region. *J. Neurosci.*, **25**, 5159–5170.
Quitadamo, C., Fabbretti, E., Lamanauskas, N. & Nistri, A. (2005) Activation and desensitization of neuronal nicotinic receptors modulate glutamatergic transmission on neonatal rat hypoglossal motoneurons. *Eur. J. Neurosci.*, **22**, 2723–2734.
Raoul, C., Abbas-Terki, T., Bensadoun, J.C., Guillot, S., Haase, G., Szulc, J., Henderson, C.E. & Aebischer, P. (2005) Lentiviral-mediated silencing of SOD1 through RNA interference retards disease onset and progression in a mouse model of ALS. *Nat. Med.*, **11**, 423–428.
Rekling, J.C., Funk, G.D., Bayliss, D.A., Dong, X.W. & Feldman, J.L. (2000) Synaptic control of motoneuronal excitability. *Physiol. Rev.*, **80**, 767–852.
Reyes, M. & Stanton, P.K. (1996) Induction of hippocampal long-term depression requires release of Ca^{2+} from separate presynaptic and postsynaptic intracellular stores. *J. Neurosci.*, **16**, 5951–5960.
Rosen, D.R., Siddique, T., Patterson, D., Figlewicz, D.A., Sapp, P. *et al.* (1993) Mutations in Cd/Zn superoxide dismutase gene are associated with familial amyotrophic lateral sclerosis. *Nature*, **362**, 59–62.
Russo, R.E. & Hounsgaard, J. (1999) Dynamics of intrinsic electrophysiological properties in spinal cord neurones. *Prog. Biophys. Mol. Biol.*, **72**, 329–365.
Sánchez-Carbente, M.R., Castro-Obregón, S., Covarrubias, L. & Narváez, V. (2005) Motoneuronal death during spinal cord development is mediated by oxidative stress. *Cell Death Differ.*, **12**, 279–291.
Saransaari, P. & Oja, S.S. (2008) Characteristics of GABA release induced by free radicals in mouse hippocampal slices. *Neurochem. Res.*, **33**, 384–393.

Sawczuk, A., Powers, R.K. & Binder, M.D. (1995) Spike frequency adaptation studied in hypoglossal motoneurons of the rat. *J. Neurophysiol.*, **73**, 1799–1810.

Schwindt, P.C. & Crill, W.E. (1980) Properties of a persistent inward current in normal and TEA-injected motoneurons. *J. Neurophysiol.*, **43**, 1700–1724.

Shaw, P.J. & Ince, P.G. (1997) Glutamate, excitotoxicity and amyotrophic lateral sclerosis. *J. Neurol.*, **244**, 3–14.

Shaw, P.J., Ince, P.G., Falkous, G. & Mantle, D. (1995) Oxidative damage to protein in sporadic motor neuron disease spinal cord. *Ann. Neurol.*, **38**, 691–695.

Siciliano, G., Piazza, S., Carlesi, C. *et al.* (2007) Antioxidant capacity and protein oxidation in cerebrospinal fluid of amyotrophic lateral sclerosis. *J. Neurol.*, **254**, 575–580.

Swash, M. & Ingram, D. (1988) Preclinical and subclinical events in motor neuron disease. *J. Neurol. Neurosurg. Psychiatry*, **51**, 165–168.

Taccola, G., Margaryan, G., Mladinic, M. & Nistri, A. (2008) Kainate and metabolic perturbation mimicking spinal injury differentially contribute to early damage of locomotor networks in the in vitro neonatal rat spinal cord. *Neuroscience*, **155**, 538–555.

Takahashi, A., Mikami, M. & Yang, J. (2007) Hydrogen peroxide increases GABAergic mIPSC through presynaptic release of calcium from IP3 receptor-sensitive stores in spinal cord substantia gelatinosa neurons. *Eur. J. Neurosci.*, **25**, 705–716.

Talley, E.M., Lei, Q., Sirois, J.E. & Bayliss, D.A. (2000) TASK-1, a two-pore domain K^+ channel, is modulated by multiple neurotransmitters in motoneurons. *Neuron*, **25**, 399–410.

Theiss, R.D., Kuo, J.J. & Heckman, C.J. (2007) Persistent inward currents in rat ventral horn neurones. *J. Physiol.*, **580**, 507–522.

Tsujino, H., Kondo, E., Fukuoka, T., Dai, Y., Tokunaga, A., Miki, K., Yonenobu, K., Ochi, T. & Noguchi, K. (2000) Activating transcription factor 3 (ATF3) induction by axotomy in sensory and motoneurons: a novel neuronal marker of nerve injury. *Mol. Cell. Neurosci.*, **15**, 170–182.

Turner, M.R., Kiernan, M.C., Leigh, P.N. & Talbot, K. (2009) Biomarkers in amyotrophic lateral sclerosis. *Lancet Neurol.*, **8**, 94–109.

Umemiya, M. & Berger, A.J. (1994) Properties and function of low- and high-voltage activated Ca^{2+} channels in hypoglossal motoneurons. *J. Neurosci.*, **14**, 5652–5660.

Viana, F., Gibbs, L. & Berger, A.J. (1990) Double- and triple-labeling of functionally characterized central neurons projecting to peripheral targets studied *in vitro*. *Neuroscience*, **38**, 829–841.

Vlug, A.S., Teuling, E., Haasdijk, E.D., French, P., Hoogenraad, C.C. & Jaarsma, D. (2005) ATF3 expression precedes death of spinal motoneurons in amyotrophic lateral sclerosis-SOD1 transgenic mice and correlates with c-Jun phosphorylation, CHOP expression, somato dendritic ubiquitination and Golgi fragmentation. *Eur. J. Neurosci.*, **22**, 1881–1894.

Vucic, S. & Kiernan, M.C. (2009) Pathophysiology of neurodegeneration in familial amyotrophic lateral sclerosis. *Curr Mol Med.*, **9**, 255–272.

Zheng, Y. & Shen, X. (2005) H_2O_2 directly activates inositol 1,4,5-trisphosphate receptors in endothelial cells. *Redox Rep.*, **10**, 29–36.

Zhong, G., Masino, M.A. & Harris-Warrick, M.R. (2007) Persistent sodium currents participate in fictive locomotion generation in neonatal mouse spinal cord. *J. Neurosci.*, **27**, 4507–4518.

van Zundert, B., Peuscher, M.H., Hynynen, M., Chen, A., Neve, R.L., Brown, R.H., Jr, Constantine-Paton, M. & Bellingham, M.C. (2008) Neonatal neuronal circuitry shows hyperexcitable disturbance in a mouse model of the adult-onset neurodegenerative disease amyotrophic lateral sclerosis. *J. Neurosci.*, **28**, 10864–10874.

EJN fens EUROPEAN JOURNAL OF NEUROSCIENCE

European Journal of Neuroscience, pp. 1–15, 2011 doi:10.1111/j.1460-9568.2010.07579.x

Riluzole is a potent drug to protect neonatal rat hypoglossal motoneurons *in vitro* from excitotoxicity due to glutamate uptake block

Alessandra Cifra,[1] Francesca Nani[1] and Andrea Nistri[1,2]
[1]Neurobiology Sector, International School for Advanced Studies (SISSA), Via Bonomea 265, 34136 Trieste, Italy
[2]SPINAL (Spinal Person Injury Neurorehabilitation Applied Laboratory), Istituto di Medicina Fisica e Riabilitazione, Udine, Italy

Keywords: amyotrophic lateral sclerosis, astrocyte, ATF3, brain stem, motoneuron disease, neuroprotection

Abstract

Excitotoxic damage to motoneurons is thought to be an important contribution to the pathogenesis of amyotrophic lateral sclerosis (ALS), a slowly developing degeneration of motoneurons that, in most cases of sporadic occurrence, is associated with impaired glial glutamate uptake. Riluzole is the only drug licensed for symptomatic ALS treatment and is proposed to delay disease progression. As riluzole is administered only after full ALS manifestation, it is unclear if its early use might actually prevent motoneuron damage. We explored this issue by using, as a simple *in vitro* model, hypoglossal motoneurons (a primary target of ALS) of the neonatal rat brainstem slice preparation exposed to excitotoxic stress due to glutamate uptake block by DL-threo-β-benzyloxyaspartate (TBOA). TBOA evoked sustained network bursting, early (1 h) enhancement of the S100B immunostaining of gray matter astrocytes, and activated the motoneuronal stress ATF-3 transcription factor; 4 h later, loss (30%) of motoneuron staining ensued and pyknosis appeared. Riluzole (5 μM; applied 15 min after TBOA) inhibited bursting, decreased the frequency of spontaneous glutamatergic events, reversed changes in S100B immunostaining and prevented late loss of motoneuron staining. These results show that excitotoxicity induced by glutamate uptake block developed slowly, and was sensed by glia and motoneurons with delayed cell death. Our data provide novel evidence for the neuroprotective action of riluzole on motoneurons and glia when applied early after an excitotoxic stimulus.

Introduction

Amyotrophic lateral sclerosis (ALS) is a fatal neurodegenerative disease affecting brain and spinal motoneurons. No cure is known despite recent progress in the understanding of certain pathophysiological mechanisms contributing to the disease onset and development (Bruijn *et al.*, 2004). Although a minority of cases has a genetic origin linked to mutation of the enzyme superoxide dismutase 1 (Rosen *et al.*, 1993), the very large majority (90%) has sporadic origin (Gonzalez de Aguilar *et al.*, 2007) for which various environmental causes have been suggested (Mitchell & Borasio, 2007). About half of the sporadic cases are associated with large increases in glutamate levels in the cerebrospinal fluid of ALS patients (Spreux-Varoquaux *et al.*, 2002) and with impaired glial transport of the excitatory transmitter glutamate (Rothstein *et al.*, 1992; Cleveland & Rothstein, 2001), with potential excitotoxic damage to motoneurons. Riluzole is the only drug currently licensed for the symptomatic treatment of ALS (Lacomblez *et al.*, 1996; Meininger *et al.*, 2000) as it can delay, at least for a few months, its progression (Van Den Bosch *et al.*, 2006). The mechanism of action of riluzole is complex as it includes inhibition of glutamate release at low concentrations (Chéramy *et al.*, 1992) and of the persistent sodium current of motoneurons at higher concentrations (Del Negro *et al.*, 2005; Miles *et al.*, 2005; Theiss *et al.*, 2007; Lamanauskas & Nistri, 2008). It is, however, unclear whether riluzole might protect motoneurons if administered at a much earlier stage of the disease.

We have recently developed a simple *in vitro* model of excitotoxic stress to motoneurons of the nucleus hypoglossus (an early target of ALS especially in its bulbar form), by applying the glutamate uptake inhibitor DL-threo-β-benzyloxyaspartate (TBOA) (Sharifullina & Nistri, 2006). This compound preferentially blocks the glutamate transport system of glial cells and is experimentally advantageous because it is devoid of effects on glutamate receptors and is not transported by the glutamate carrier (Anderson *et al.*, 2001), thus avoiding amino acid hetero-exchange. The usefulness of this model, which relies on the use of neonatal brain tissue, is, of course, limited to clarifying the basic mechanisms preceding the onset of motoneuron damage induced by excitotoxicity. Recent reviews have highlighted the importance of *in vitro* rodent tissue models and even cultures to analyze the motoneuron degeneration process in detail and to test preclinical therapeutic attempts (Boillée *et al.*, 2006; Kato, 2008).

In the present study we investigated the ability of riluzole to change the excitotoxicity consequent to TBOA application in terms of

Correspondence: Andrea Nistri, [1]Neurobiology Sector, as above.
E-mail: nistri@sissa.it

Received 23 June 2010, revised 30 November 2010, accepted 1 December 2010

network bursting and survival of motoneurons. We enquired if riluzole, given at a concentration (5 μM) similar to the plasma therapeutic concentration in human (Wokke, 1996; Cheah *et al.*, 2010), could suppress the deadly bursting of motoneurons and protect their numbers. We also explored if TBOA could affect glia and if riluzole could change this action as previous studies have indicated a contribution by non-neuronal cells to the disease pathogenesis (Anneser *et al.*, 2004; Barbeito *et al.*, 2004; Neusch *et al.*, 2007; Van Den Bosch & Robberecht, 2008).

Materials and methods

Slice preparation

All experiments were carried out in accordance with the regulations of the Italian Animal Welfare act (DL 27/1/92 no.116) following the European Community directives no. 86/609 93/88 (D 69/98-B, Italian Ministry of Health authorization for the local animal care facility, SISSA animal house, managed by personnel from the Department of Life Sciences of the University of Trieste), and approved by the local authority veterinary service (Prof. Giuseppe Stradaioli, University of Udine). In accordance with recent reports (Quitadamo *et al.*, 2005; Lamanauskas & Nistri, 2006, 2008; Nani *et al.*, 2010), brainstem slices (250–300 μm thick) from urethane anaesthetized neonatal (post-natal day 1–5; P1–P5) Wistar rats were cut after decapitation with a vibracut (FTB, Bensheim, Germany) in ice-cold, oxygenated (95% O_2/5% CO_2) Krebs solution, containing (in mM): 130 NaCl, 3 KCl, 1.5 NaH_2PO_4, 1 $CaCl_2$, 5 $MgCl_2$, 25 $NaHCO_3$ and 100 glucose (pH 7.4; 300–320 mOsm). After 20 min recovery at 32°C and 10 min at room temperature (22–24°C), they were used for recording.

Electrophysiological recordings

Hypoglossal motoneurons (HMs) were identified within the nucleus hypoglossus with an infrared video-camera. All cell recordings were obtained, at ambient temperature, under whole-cell patch-clamp conditions. For voltage-clamp experiments, patch electrodes had 3–4 MΩ resistance, whereas for current-clamp experiments they had 8–10 MΩ resistance. Cells were clamped at values between −60 and −70 mV holding potential (V_h), as close as possible to the initial resting potential. Cells were used for voltage-clamp analysis when series resistance increases did not exceed 10% with respect to the initial value (in the range of 7–10 MΩ). In current-clamp mode, neurons were kept at their initial resting level of membrane potential (V_m), and the bridge was routinely balanced throughout the experiment.

Voltage and current pulse generation and data acquisition were performed using pCLAMP 9.2 software (Axon Instruments, Molecular Devices, Sunnyvale, CA, USA). Patch pipettes were filled with an intracellular solution containing (in mM): 130 CsCl, 5 NaCl, 2 $MgCl_2$, 1 $CaCl_2$, 10 HEPES, 10 EGTA, 2 ATP-Mg and 2 sucrose (pH 7.2 with CsOH; 280–300 mOsm) for voltage-clamp experiments. Intracellular CsCl, which minimized the leak current of the recorded cell, was used to enable larger changes in V_h. In some voltage-clamp experiments, N-2,6-dimethylphenylcarbamoylmethyl triethylammonium bromide (QX–314, 5–10 mM) was added to the patch solution to block voltage-activated Na^+ currents and the hyperpolarization-activated current (Perkins & Wong, 1995; Marchetti *et al.*, 2002). This drug preserved recording stability that allowed TBOA-induced bursting to be observed for at least 35 min (Sharifullina & Nistri, 2006). For current-clamp experiments, 130 mM KCl always replaced CsCl.

A liquid junction potential of 3.5 mV in current-clamp configuration and of 4 mV in voltage-clamp experiments was corrected offline after an experiment. Records were filtered at 3–10 kHz and sampled at 5–10 kHz.

Solutions and drugs

Slices were superfused (2–3 mL/min) with a gassed solution containing (in mM): 130 NaCl, 3 KCl, 1.5 NaH_2PO_4, 1.5 $CaCl_2$, 1 $MgCl_2$, 25 $NaHCO_3$ and 10 glucose (pH 7.4; 300–320 mOsm). The following drugs were used: bicuculline methiodide (bicuculline), strychnine hydrochloride (strychnine), TBOA, QX-314 and riluzole, all purchased from Tocris (Bristol, UK). Drugs were applied by superfusion by switching to an appropriate extracellular solution.

Electrophysiological data analysis

In voltage-clamp experiments, the cell input resistance (R_{in}) was calculated by measuring the current response to 10 mV hyperpolarizing steps from V_h. In current-clamp experiments, R_{in} was calculated by measuring the voltage response to −50 pA current injections (Pagnotta *et al.*, 2005; Quitadamo *et al.*, 2005). Spontaneous post-synaptic currents were detected using the template search software CLAMPFIT 9.2 (Axon Instruments). The occurrence of synaptic events was expressed as the interevent interval (IEI). CORELDRAW (Vector Capital, San Francisco, CA, USA) was used for graphical data presentation.

Immunohistochemistry

Parallel experiments were run to examine the effects of TBOA and TBOA + riluzole on HM survival in slice preparations of the nucleus hypoglossus. To this end, brainstems removed from P2–P4 rats were cut with the vibracut in two thick (500 μm) slices in ice-cold, oxygenated Krebs solution. Slices were incubated (under continuous oxygenation) in either Krebs solution, TBOA (50 μM) or TBOA + riluzole (riluzole, 5 μM, added 15 min after TBOA) for 1 or 4 h at room temperature, then rinsed and fixed. Treated and untreated slices were always processed in parallel to minimize bias.

We next investigated how much the slicing procedure might affect HMs (and glia) not only at the level of the cutting plane where cells are inevitably destroyed, but also in terms of long-term maintenance of such cells under *in vitro* control conditions. For this purpose, we evaluated the numbers of HMs (stained with SMI 32; see below) and astrocytes (stained with S100B; see below) as well as the expression level of the motoneuron distress marker activating transcription factor-3 (ATF-3) (see below) in sections taken from *en-bloc* brainstems fixed histologically prior to cryostat sectioning (time: −1), fixed immediately after slice cutting with the vibratome (time: 0), or followed-up for 1–4 h in an *in vitro* chamber containing oxygenated Krebs solution.

The fixative medium was phosphate-buffered saline containing 4% paraformaldehyde (24 h at 4 °C) followed by 30% sucrose phosphate-buffered saline for cryoprotection (24 h at 4 °C). Usually, from each 500 μm slice, 16 cryostat tissue sections (30 μm) were collected sequentially on histology slides. For quantitative measurements, we normally analyzed 8–10 sections that corresponded to the largest coronal area (on average 111 359 ± 2439 μm^2, n = 72) of the nucleus.

Sections were treated with blocking solution (1% fetal calf serum, 5% bovine serum albumin, 0.3% Triton X-100 in phosphate-buffered saline) for 1 h at room temperature and then incubated overnight at

4 °C with the following primary antibodies: anti-SMI 32 (mouse monoclonal, 1 : 200 dilution; Covance Research Products Inc., Berkeley, CA, USA), anti-S100 (rabbit polyclonal, 1 : 100 dilution; Dako, Glostrup, Denmark) and anti-ATF-3 (rabbit polyclonal, 1 : 500 dilution; Santa Cruz Biotechnology, Santa Cruz, CA, USA). AlexaFluor 488 and 594 were used as secondary antibodies (1 : 500 dilution; Molecular Probes, Invitrogen, Milan, Italy) for 2 h at room temperature. Omission of the primary antibodies did not produce any signal. The use of the anti-ATF-3 antibody to assess motoneuronal distress has recently been validated in our laboratory (Nani *et al.*, 2010). The use and specificity of the anti-SMI 32 (which targets a motoneuronal cytoskeletal protein) and anti-S100 (which targets the S100B calcium-binding protein in the cytoplasm and nuclei of astrocytes and ependymal cells; Cocchia, 1981; Donato, 2003) antibodies are detailed in recent reports from our laboratory (Taccola *et al.*, 2008; Kuzhandaivel *et al.*, 2010a; Mazzone *et al.*, 2010; Nani *et al.*, 2010). In the adult rat brain, both fibrous and protoplasmic astrocytes express S100B (Cocchia, 1981; Didier *et al.*, 1986), but only the former express a large amount of glial fibrillary acidic protein (GFAP), an intermediate filament protein characteristic of white matter astrocytes (Eng, 1985; Didier *et al.*, 1986). According to Miller & Raff (1984), fibrous and protoplasmic astrocytes represent distinct classes of glial cells; the former are located primarily in the white matter, whereas the latter are found mainly in the gray matter and appear at least 1 week before fibrous astrocytes. In accordance with this notion, in the P4 rat nucleus hypoglossus, we could observe only very few GFAP-positive (tested with mouse monoclonal anti-GFAP, 1 : 400; Sigma, Milan, Italy) astrocytes in the gray matter (Supporting Information Fig. S1A). To confirm that this observation was a typical characteristic of motor nuclei, we also investigated the presence of GFAP- and S100B-positive cells in the ventral horn area of the P4 rat spinal cord (Supporting Information Fig. S1B and C), demonstrating a distribution of such cells analogous to that in the nucleus hypoglossus. On the basis of the aforementioned considerations, in this report we considered S100B-positive cells as protoplasmic astrocytes.

After the incubation with the secondary antibody, slices were rinsed and stained with the cell-permeable DNA dye Hoechst 33342 (10 mg/mL stock from Molecular Probes, Invitrogen; final dilution was 1 : 1000). Slices were finally mounted with Vectashield (Vector Laboratories, Burlingame, CA, USA) to avoid photobleaching, and visualized with a TCS SP2 Leica confocal microscope (10–20–40×). A 100 000 μm^2 region of interest (see examples of box sections in Supporting Information Fig. S2B and C) was selected for each nucleus section (Supporting Information Fig. S2A) in which SMI 32-immunopositive HMs as well as S100B-immunopositive astrocytes were counted using ImageJ (version 1.41 c, Wayne Rasband, National Institutes of Health, USA) software. Only cells showing SMI 32/Hoechst 33342 or S100B/Hoechst 33342 co-staining were considered for the analysis. We also estimated that the number of motoneurons in untreated slices was 25% of the total number of Hoechst 33342-positive cells in the region of interest.

Co-staining of ATF-3 and SMI 32 was analyzed on the basis of the co-variance of these markers as detailed by Nani *et al.* (2010) because we were interested in assessing how much these two variables could change together. Thus, if co-variance is positive, the two variables change concordantly; if co-variance is negative, the two variables change in an opposite way; finally, two variables whose co-variance is zero are uncorrelated. The mathematical analysis of the co-variance for the fluorescence pixel signal of the two antibodies is fully reported in our former study (Nani *et al.*, 2010). As the confocal settings used for image acquisition were the same for treated and untreated slices, the average SMI 32 staining intensity was assumed to be identical for treated and untreated sections. Thus, when the co-variance value was significantly higher than control, this indicated stronger ATF-3 staining intensity because the SMI 32 fluorescence remained similar. Co-variance values between ATF-3 and SMI 32 stainings were analyzed with a MATLAB 7.1 software macro kindly provided by Dr Walter Vanzella (Glance Vision Technologies, Trieste, Italy).

Statistics

Results were expressed as means ± SEM; *n* refers to the number of cells or animals, as indicated. For statistical calculations, we used SigmaStat 3.11 (Systat Software, Chicago, IL, USA); when comparing two groups, the Student's *t*-test for parametric data (power of performed test with alpha = 0.050) was applied. For multiple comparisons, the one-way ANOVA for parametric data, and the Kruskal–Wallis one-way ANOVA on ranks for non-parametric data were applied. The Dunn's method was used for *post-hoc* pair-wise comparisons. For the analysis of synaptic event frequency and amplitude before and after treatments, the paired *t*-test for parametric data and the Wilcoxon Signed Rank test for non-parametric data were applied. Two groups of data were considered statistically different if $P \leq 0.05$. The Kolmogorov–Smirnov test was employed to assess the cumulative probability distribution of synaptic event amplitude and frequency.

Results

Bursting induced by TBOA was abolished by riluzole application

As previously reported by Sharifullina & Nistri (2006), bath application of TBOA (50 μM) elicited, in a percentage of HMs (50%, 25/50), strong bursting activity. As shown by the example of the current-clamp records in Fig. 1A, bursts were characterized by large depolarizing waves with superimposed spikes and interposed spontaneous synaptic events. On average, current-clamp-recorded TBOA-evoked bursts had an amplitude from resting potential (−65 ± 1 mV) of 22.2 ± 3.0 mV, period of 84 ± 12 s (26 ± 5% coefficient of variation, CV) and burst duration of 34 ± 4 s (n = 12). When the application of TBOA lasted <20 min (about 10 min in the example of Fig. 1A), bursts disappeared on washout, whereas longer exposures are known to produce irreversible damage to HMs (Sharifullina & Nistri, 2006).

Because of its network origin (Sharifullina & Nistri, 2006), bursting activity could not be blocked by direct hyperpolarization via DC current injection (−85 mV in Fig. 1B). After the onset of bursting activity, subsequent application of riluzole (5 μM) abolished TBOA-evoked bursts even when the membrane potential was kept at the initial resting level (−72 mV; Fig. 1B). The insets to Fig. 1B show, on a faster timescale, the transient inactivation of Na^+ channels in the presence of TBOA, which conferred a 'butterfly-like' shape to the burst events, and its attenuation by riluzole.

Even when synaptic inhibition was pharmacologically suppressed with strychnine (0.4 μM) and bicuculline (10 μM) (see Donato & Nistri, 2000; Marchetti *et al.*, 2002), riluzole abolished TBOA-evoked bursts (n = 10), an effect observed under both current-clamp and voltage-clamp conditions (Fig. 1C and D). Of a total of 18 cells (nine recorded under current-clamp and nine under voltage-clamp configuration), riluzole (started, on average, 15 min after TBOA application) fully blocked bursting activity within 379 ± 64 s in 83% of the cells (15/18 cells). In the remaining three cells, bursts were attenuated (−394 ± 70 pA amplitude, 29 ± 2 s duration and 56 ± 10 s period in

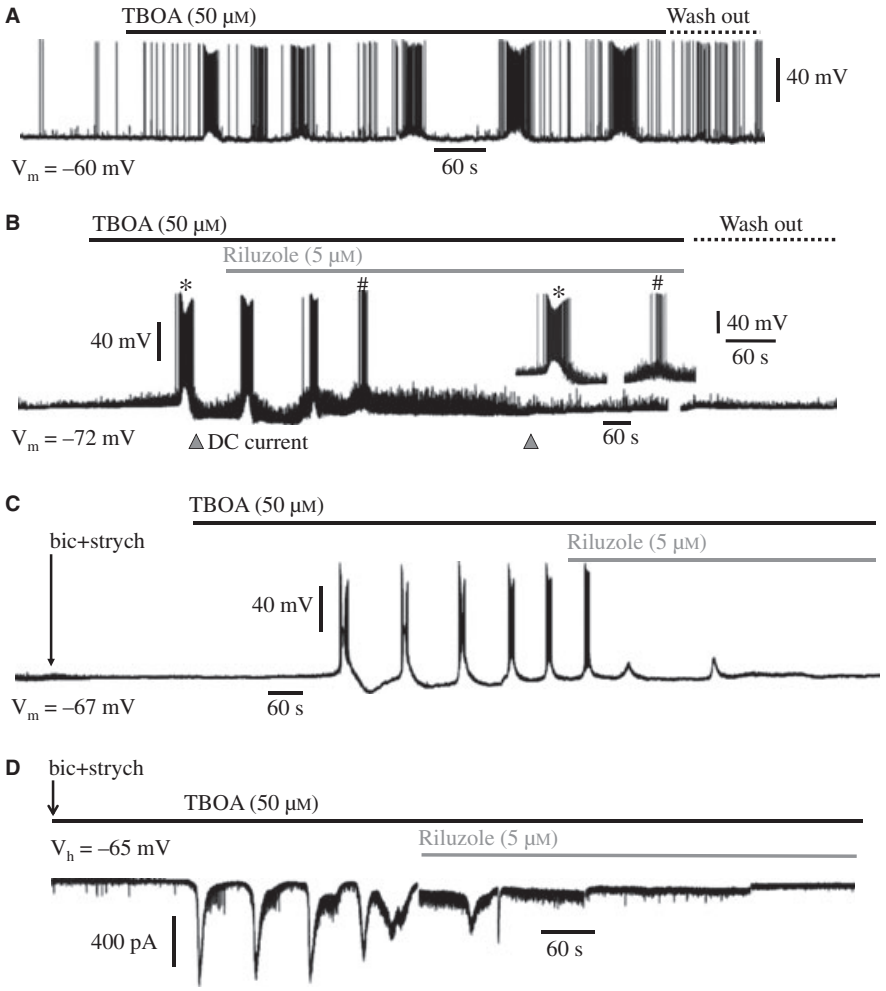

FIG. 1. Bursting induced by TBOA was abolished by riluzole application. (A) Sample record under current-clamp configuration (V_m = −60 mV) showing bursting activity elicited by application of 50 μM TBOA. Bursts were characterized by large depolarizing waves with superimposed spikes and interposed spontaneous synaptic events. In this example, the application of TBOA lasted <10 min and bursts disappeared on washout. (B) Direct HM hyperpolarization via DC current injection (triangle) from −72 mV resting potential could not suppress bursting activity. Subsequent application of 5 μM riluzole abolished TBOA-evoked bursts, even when the membrane potential was repolarized to the initial resting level (triangle). (Different cell from that in A.) The insets show, on a faster timescale, that the transient inactivation of Na^+ channels in the presence of TBOA, which conferred a 'butterfly-like' shape to the burst events, was attenuated by riluzole. (C and D) Even in the presence of strychnine (strych, 0.4 μM) and bicuculline (bic, 10 μM), riluzole could abolish TBOA-evoked bursts, an effect observed under both current-clamp (C; V_m = −67 mV) and voltage-clamp (D; different HM clamped at −65 mV holding potential) configurations. In D, the last trace was obtained ∼ 50 min from the start of the record.

TABLE 1. Average HM input resistance values during control [bicuculline (10 μM) + strychnine (0.4 μM)], TBOA (50 μM), TBOA + riluzole [riluzole started at 15 min after TBOA application (5 μM)] and washout (bicuculline + strychnine) in voltage-clamp experiments

Input resistance (MΩ)	
Bicuculline + strychnine	161 ± 25
TBOA	178 ± 27
TBOA + riluzole	177 ± 26
Washout	172 ± 27
Statistics	One-way repeated-measures ANOVA $F_{7,3}$ = 1.937, P = 0.155, n = 8

TBOA values were collected in the interburst intervals, whereas the TBOA + riluzole data were collected after bursting was inhibited.

TBOA vs. −105 ± 22 pA amplitude, 36 ± 5 s duration and 182 ± 106 s period after 20 min of riluzole application) although never completely suppressed. As previously reported (Sharifullina & Nistri, 2006; Lamanauskas & Nistri, 2008), bursting activity was not related to changes in HM R_{in} (Table 1).

Riluzole effects on glutamatergic currents

On HMs, riluzole can block not only voltage-activated sodium and calcium currents but also glycine and glutamate synaptic events (Hubert *et al.*, 1994; Umemiya & Berger, 1995; Del Negro *et al.*, 2005; Miles *et al.*, 2005; Theiss *et al.*, 2007; Lamanauskas & Nistri, 2008). As TBOA-induced bursting is associated with strong facilitation of endogenous glutamate release (Sharifullina & Nistri, 2006), we used inhibitors of γ-aminobutyric acid (GABA) and glycine receptors (bicuculline, 10 μM, and strychnine, 0.4 μM, respectively) to test whether the effect of riluzole was related to changes in network-dependent glutamatergic synaptic events. Previous studies have indicated that riluzole inhibits miniature glutamatergic currents recorded in the presence of tetrodotoxin (Lamanauskas & Nistri, 2008), which, being a powerful blocker of TBOA-evoked bursts

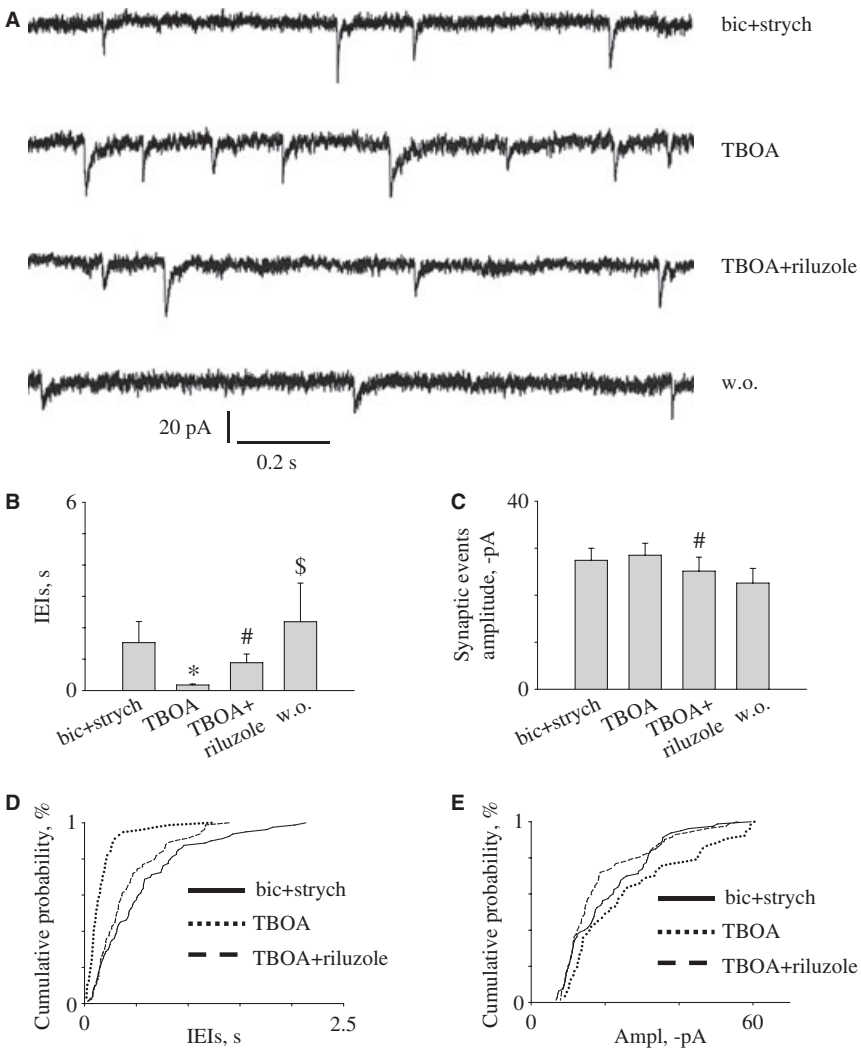

FIG. 2. Riluzole reduced the occurrence of spontaneous post-synaptic glutamatergic currents. (A) Voltage-clamp traces (V_h = −65 mV) showing examples of spontaneous glutamatergic currents under control [bicuculline (bic) + strychnine (strych)], TBOA (recorded during interburst interval), TBOA + riluzole (recorded after bursting inhibition) and washout (w.o.) conditions. (B) Average data showing that, in the presence of strychnine (0.4 μM) and bicuculline (10 μM), TBOA (50 μM) significantly enhanced the spontaneous glutamatergic event frequency, an effect fully reversed by riluzole (5 μM; applied at 15 min after TBOA administration). Wilcoxon Signed Rank test: P = 0.004 for bicuculline + strychnine vs. TBOA (*) and TBOA vs. TBOA + riluzole (#) comparisons; P = 0.047 vs. TBOA + riluzole ($); n = 9. (C) Event amplitude did not change during TBOA application as compared with control condition, but it was decreased by riluzole. Paired t-test: P = 0.649 for bicuculline + strychnine vs. TBOA comparison and P = 0.042 for TBOA vs. TBOA + riluzole (#) comparison; n = 9. (D and E) Cumulative probability plots from a representative HM to show the effect of TBOA and TBOA + riluzole on synaptic interevent intervals (IEIs) (D) or amplitude (E). Whereas TBOA (dotted line) shifted the IEI graph to the left (D = 0.5466, P = 0.0001), it was returned to control values (solid line) by TBOA + riluzole (dashed line; D = 0.4701, P = 0.0001). No change in the amplitude probability plot was observed (D = 0.1838, P = 0.126 for bicuculline + strychnine vs. TBOA; D = 0.1945, P = 0.082 for bicuculline + strychnine vs. TBOA + riluzole) with the exception of TBOA vs. TBOA + riluzole (D = 0.2658, P = 0.006). In control conditions (bicuculline + strychnine), the cumulative probability plot was made from 80 events, whereas after TBOA and TBOA + riluzole application it was made from 77 and 82 events, respectively.

(Sharifullina & Nistri, 2006), could not be used for the present investigation.

Under voltage-clamp configuration, the frequency and amplitude of glutamatergic spontaneous post-synaptic currents (sPSCs) were measured in the interburst intervals during TBOA application and after the addition of riluzole. The sample traces in Fig. 2A exemplify the enhanced glutamatergic event occurrence with similar event amplitude. On average, TBOA significantly enhanced glutamatergic sPSC occurrence (expressed as IEI), which fell from 1.5 ± 0.7 s in control (bicuculline + strychnine) to 0.2 ± 0.01 s (Wilcoxon Signed Rank test, W = −45.000, P = 0.004, n = 9, Fig. 2B), an effect fully reversed by riluzole (0.9 ± 0.3 s, Wilcoxon Signed Rank test, W = 45.000, P = 0.004, n = 9), with subsequent recovery on washout (Fig. 2B). However, although the event amplitude did not change during TBOA application as compared to the control condition (−28.5 ± 2.5 vs. −27.4 ± 2.6 pA, paired t-test, t_8 = 0.473, P = 0.649), it was slightly decreased by riluzole (−25.1 ± 3.0 pA, paired t-test, t_8 = −2.412, P = 0.042, Fig. 2C). Figure 2D and E shows the probability distribution (Kolmogorov–Smirnov plot) of event frequency and amplitude obtained from a representative HM before and after application of TBOA and TBOA + riluzole. TBOA shifted the frequency graph to the left (Kolmogorov–Smirnov test, D = 0.5466, P = 0.0001) without changing the event amplitude. The application of riluzole not only reversed this effect of TBOA (Kolmogorov–Smirnov test, D = 0.4701, P = 0.0001), but it also caused the appearance of smaller synaptic events as compared to TBOA alone (Kolmogorov–

Smirnov test, $D = 0.2658$, $P = 0.006$). Globally, these data suggested that 5 μM riluzole (a concentration below the threshold for suppressing voltage-gated currents of HMs; Lamanauskas & Nistri, 2008) blocked bursting probably because of the decreased glutamatergic synaptic transmission at network level.

Cell viability in vitro

Previous experiments with patch-clamp recording and Ca^{2+} imaging indicated discrete deleterious effects produced by TBOA on HMs at relatively short intervals (1 h) (Sharifullina & Nistri, 2006). In the present study we decided to extend the observation time following TBOA application to better detect the potential neuroprotective action of riluzole in relation to HMs and astroglia.

Because the survival of cells after brain slicing is inherently limited, we first examined the immediate consequences of this procedure on HMs and astrocytes, and their viability *in vitro*. We tested the following conditions: *en-bloc* brainstem histologically fixed prior to sectioning (time: −1), slices fixed immediately after vibratome cutting (time: 0), and slices fixed 1 or 4 h after cutting and subsequent *in vitro* incubation. The analysis of HM numbers was carried out with the motoneuron marker SMI 32, tested with a monoclonal antibody against the non-phosphorylated form of neurofilament H (Jacob *et al.*, 2005; Raoul *et al.*, 2005) in a region of interest of the nucleus hypoglossus (see also Supporting Information Fig. S2). To label protoplasmic astrocytes we

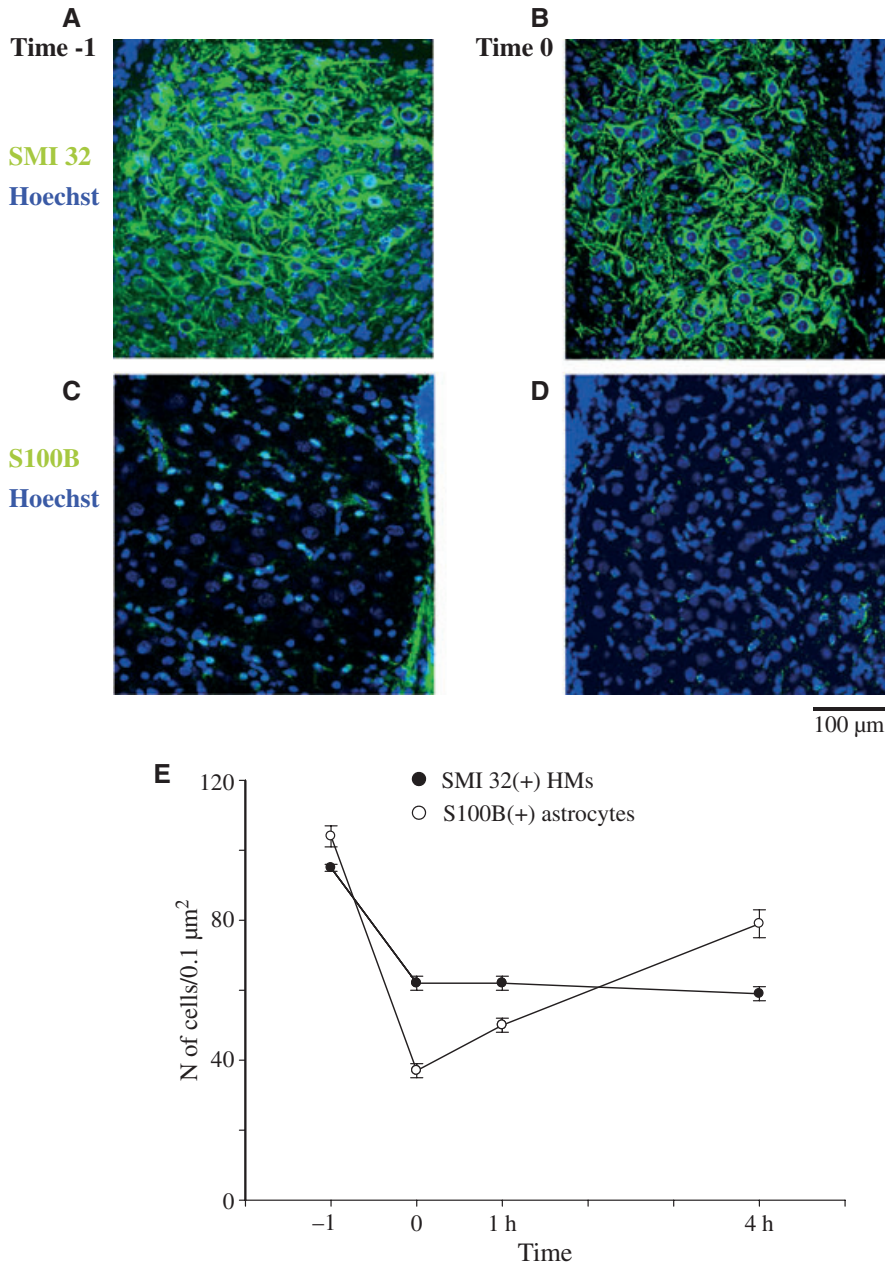

FIG. 3. Motoneuron and astrocyte viability after the slicing procedure and *in vitro* incubation. (A) Example of confocal images of nucleus hypoglossus taken from a brainstem preparation fixed immediately after dissection (time: −1). Green signal is immunolabeling for the HM marker SMI 32, whereas blue indicates Hoechst 33342 staining. (B) Similar image taken from a brainstem slice cut with a vibratome and fixed immediately (time: 0). (C and D) S100B staining of astrocytes (green) in histological sections fixed immediately after dissection or after vibratome slicing (time: −1 and 0, respectively). (E) Plots of SMI 32-positive HMs (filled circles) and S100B-positive astrocytes (open circles) counted in histological sections taken from dissected brainstem (time: −1), brain-sliced brainstem (time: 0) and 1 or 4 h brain slice incubation in Krebs solution. Data are from three rats.

used the anti-S100 polyclonal antibody that targets the S100B calcium-binding protein found in the cytoplasm and nucleus of such cells, and whose level of expression depends on environmental factors (Donato, 2003) and pathological conditions (Migheli *et al.*, 1999; Rothermundt *et al.*, 2003; Stroick *et al.*, 2006; Blackburn *et al.*, 2009).

Figure 3 exemplifies the effects of brain slicing on HMs (Fig. 3B) and astrocytes (Fig. 3D) in comparison with histological preparations fixed prior to cryostat sectioning (Fig. 3A and C for HMs and glia, respectively). Average data indicate that cutting produced a rapid loss of HMs and astrocytes (35 and 65%, respectively; Fig. 3E). Nevertheless, the average number of HMs remained stable *in vitro* for up to 4 h, whereas there were time-dependent changes in S100B immunoreactivity (which labels a Ca^{2+}-binding protein) as the early fall was replaced by gradual recovery (Fig. 3E).

Effects of TBOA on hypoglossal motoneurons

Figure 4A shows similar HM immunoreactivity after 1 h treatment in control (Krebs; left) or TBOA (50 μM; right) solutions. These results are quantified in the histogram of Fig. 4B indicating that, on average, TBOA did not change the number of HMs within the nucleus hypoglossus after 1 h treatment (63 ± 2 vs. 62 ± 2 control, Student's *t*-test, $t_{1,28} = -0.391$, $P = 0.699$, $n = 3$ rats). Our previous experiments (Cifra *et al.*, 2009), however, indicated that, after 1 h TBOA treatment, there is an increased number of hypoglossal cells stained by the membrane-impermeable propidium iodide, suggesting damage to their cell membrane even though their identity had not been fully characterized. The issue of early motoneuron damage despite preserved numbers was therefore further investigated by examining their immunoreactivity to the transcription factor ATF-3, a widely used marker of initial motoneuron distress (Tsujino *et al.*, 2000; Hai & Hartman, 2001; Vlug *et al.*, 2005; Nani *et al.*, 2010). In *en-bloc* brainstem preparations, the ATF-3 signal was undetectable; nevertheless, after vibratome cutting, a weak ATF-3 immunofluorescence appeared (Fig. 5A) that increased after 1 h *in vitro* and, as indicated by the co-variance values in Fig. 5B, was associated with SMI 32-positive HMs. After application of TBOA (1 h), the ATF-3 signal was strongly enhanced, a phenomenon reversed with TBOA + riluzole (Fig. 5A and B; co-variance value = 153 ± 29, 0 h Krebs; 235 ± 36, 1 h Krebs; 427 ± 46, 1 h TBOA; 81 ± 9, 1 h TBOA + riluzole; Kruskal–Wallis one-way ANOVA on ranks, $H_3 = 44.217$, $P < 0.001$; *post-hoc* Dunn's method, $P < 0.05$ for 0 h Krebs vs. 1 h TBOA, 1 h Krebs vs. 1 h TBOA + riluzole, 1 h Krebs vs. 1 h TBOA, and 1 h TBOA vs.1 h TBOA + riluzole comparisons; $n = 3$ rats).

Globally, these data suggested that, despite preserved HM numbers after 1 h TBOA, signs of HM distress were intensified by exposure to this agent and were reversed by riluzole.

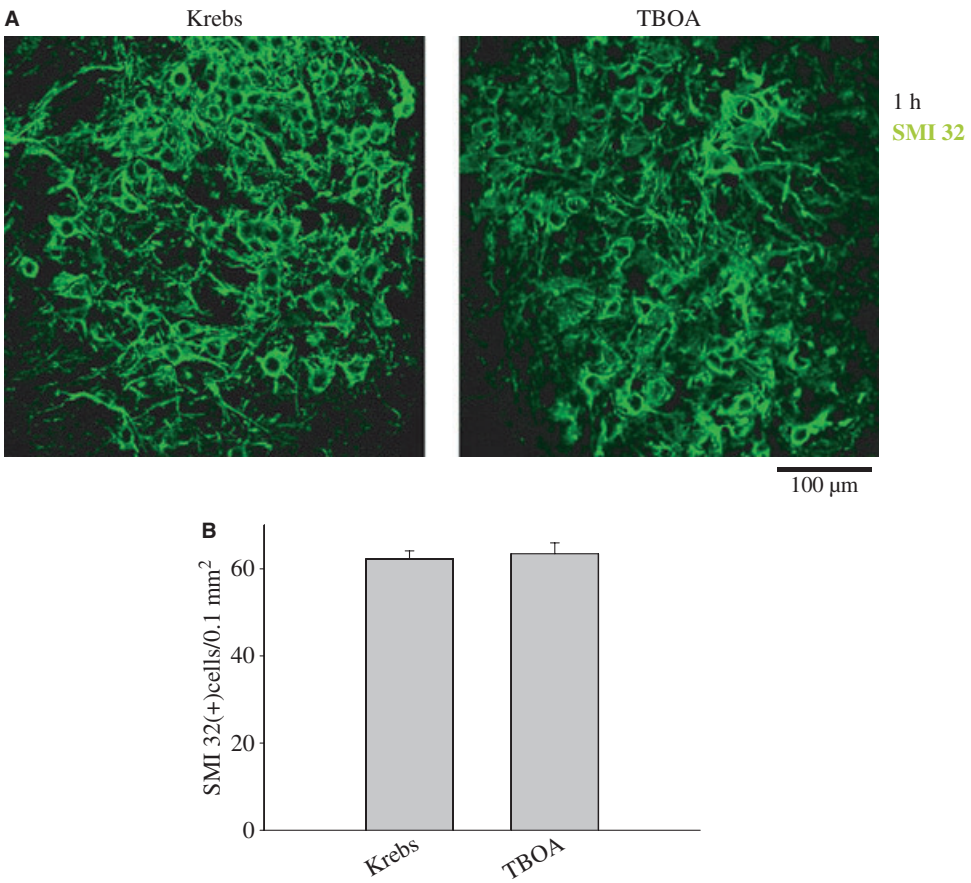

FIG. 4. TBOA did not alter short-term HM survival. (A) Example of confocal fluorescence microscopy images (40×) of HMs labeled with the motoneuron marker SMI 32 (green) after 1 h incubation in control condition (Krebs) or TBOA solution (50 μM). (B) Histogram quantifying the number of HMs with no significant difference between control and TBOA treatment. Data were analyzed with IMAGEJ software (Student's *t*-test, $t_{1,28} = -0.391$, $P = 0.699$, $n = 3$ rats).

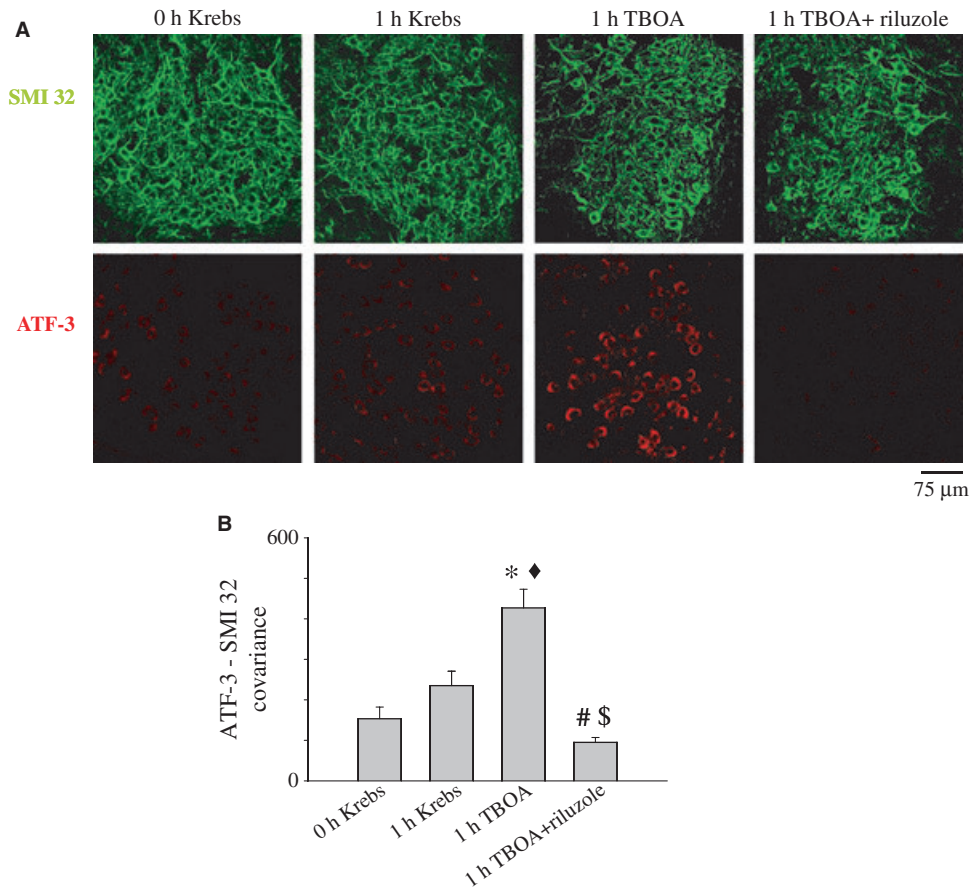

FIG. 5. ATF-3 immunoreactivity of HMs after 1 h application of TBOA and TBOA + riluzole. (A) From left to right (top row), examples of confocal images of HMs stained with SMI 32 (green) immediately after brain slicing, 1 h incubation in Krebs solution, 1 h TBOA, or TBOA + riluzole application. Bottom row shows corresponding confocal images with ATF-3 staining. Images are at 40× magnification. (B) Analysis of co-variance of ATF-3 and SMI 32 signals taken at the time of slicing, 1 h Krebs incubation, 1 h TBOA or TBOA + riluzole application. Data were quantified with a MATLAB 7.1 software macro [Kruskal–Wallis one-way ANOVA on ranks gave $H_3 = 44.217$, $P < 0.001$ for the difference among treatment groups, whereas *post-hoc* Dunn's method gave $P < 0.05$ for 0 h Krebs vs. 1 h TBOA (*), 1 h Krebs vs. 1 h TBOA + riluzole (#), 1 h Krebs vs. 1 h TBOA (◆) and 1 h TBOA vs.1 h TBOA + riluzole ($) comparisons: $n = 3$].

Riluzole protected against TBOA-induced hypoglossal motoneuron delayed loss

In the rat spinal cord motor networks, excitotoxicity evoked by kainate produces motoneuron disappearance 4 h later (Taccola *et al.*, 2008; Mazzone *et al.*, 2010). Thus, we investigated whether rat brainstem slices showed loss of motoneurons when TBOA application lasted 4 h. Confocal analysis of HM numbers at such a time (Fig. 6A) revealed loss of HM staining after TBOA treatment (50 µM; Fig. 6A, middle) vs. controls kept for the same time *in vitro* (Fig. 6A, left). Interestingly, riluzole (5 µM, started 15 min after TBOA and continuously applied with the latter up to 4 h) protected HMs, the numbers of which did not differ from the controls (Fig. 6A, right). Quantification of these effects is shown in Fig. 6B (numbers of SMI 32-positive cells: 59 ± 2, Krebs; 42 ± 3, TBOA; 57 ± 3, TBOA + riluzole; one-way ANOVA, $F_{2,45} = 11.361$, $P < 0.001$; *post-hoc* Holm–Sidak method $P < 0.05$ for Krebs vs. TBOA, and for TBOA vs. TBOA + riluzole comparisons; $n = 3$ rats).

We further investigated if loss of HM staining was actually associated with the typical sign of cell death, namely pyknosis, which in the case of motoneuron excitotoxicity is manifested as condensed chromatin in the nucleus (Taccola *et al.*, 2008; Kuzhandaivel *et al.*, 2010a,b; Mazzone *et al.*, 2010). Using Hoechst 33342 as a marker of nuclear staining (Sharifullina & Nistri, 2006; Cifra *et al.*, 2009), we could detect a significant increase in the number of pyknotic nuclei after 4 h TBOA application (see example in Fig. 6C, middle), an effect fully prevented by riluzole (Fig. 6C, right). On average, the percentage of pyknotic nuclei was 2.0 ± 0.3%, Krebs; 9.1 ± 1.1%, TBOA; and 2.4 ± 0.3%, TBOA + riluzole (Kruskal–Wallis one-way ANOVA on ranks, $H_2 = 35.982$, $P < 0.001$; *post-hoc* Dunn's method, $P < 0.05$ for Krebs vs. TBOA, and TBOA vs. TBOA + riluzole comparisons, $n = 4$ rats; Fig. 6D). The middle panels of Fig. 6A and C show, on the same histological section, that when a pyknotic nucleus was detected, it corresponded to loss of SMI 32 staining (see yellow arrows). In view of the fact that HMs are only 25% of the cell population within the nucleus section (see Materials and methods), whereas pyknosis is a process affecting all cell types, it is not surprising that the increased occurrence of pyknosis after TBOA application, although significant, was still a limited phenomenon within the global cell population. These data are similar to those observed in the rat spinal cord after kainate-evoked excitotoxicity (Margaryan *et al.*, 2010).

It is noteworthy that, at a shorter (1 h) incubation time in Krebs or TBOA solution, the percentage of pyknosis was very low, namely 0.9 ± 0.2 and 1.1 ± 0.2% (data not shown; Mann–Whitney Rank Sum Test, $T_1 = 381.000$, $P = 0.438$, $n = 4$ rats).

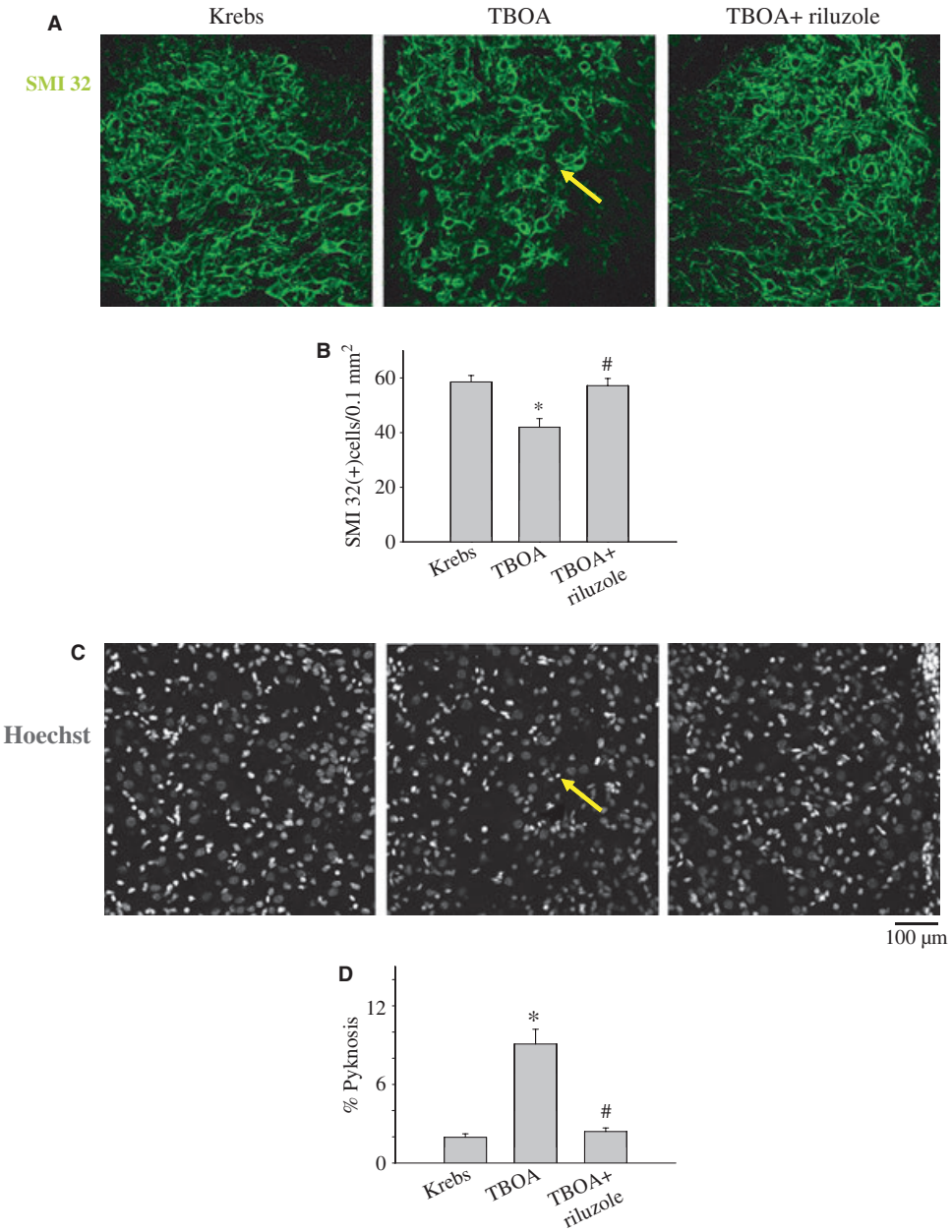

FIG. 6. Riluzole protected HMs against TBOA-induced delayed loss. (A) From left to right, examples of confocal images (40×) of HMs labeled with the motoneuron marker SMI 32 (green) after 4 h treatment in control (Krebs), TBOA (50 μM) or TBOA + riluzole [riluzole (5 μM) started at 15 min after TBOA and continuously co-applied up to 4 h]. Middle panels (A and C) show, on the same histological section, that when a pyknotic nucleus was detected with Hoechst 33342 (gray; C), it corresponded to loss of SMI 32 staining (A; see yellow arrows). (B) Histogram quantifying the number of HMs (SMI 32-positive cells) in the three different conditions show significant loss of cell staining after TBOA treatment as compared with controls, an effect fully prevented by riluzole. Data were analyzed with IMAGEJ software; one-way ANOVA: $F_2 = 11.361$, $P < 0.001$; *post-hoc* Holm–Sidak method: $P < 0.05$ for Krebs vs. TBOA (*) and TBOA vs. TBOA + riluzole (#) comparisons; $n = 3$ rats. (C) Examples of confocal images of nucleus hypoglossus stained (from left to right) with the nuclear dye Hoechst 33342 (gray) after 4 h incubation in Krebs solution, TBOA solution or TBOA + riluzole. (D) Histogram shows the percentage of pyknotic nuclei, detected with the nuclear dye Hoechst 33342. Pyknosis significantly increased after 4 h TBOA application, but was decreased by riluzole [Kruskal–Wallis one-way ANOVA on ranks: $H_2 = 35.982$, $P < 0.001$; *post-hoc* Dunn's method: $P < 0.05$ for Krebs vs. TBOA (*) and TBOA vs. TBOA + riluzole (#) comparisons; $n = 4$ rats].

The next issue was to study whether HMs remaining at 4 h showed high immunoreactivity to ATF-3. Figure 7A and B demonstrates that, after TBOA (4 h), the association between ATF-3 (red) and SMI 32 (green) co-staining remained significantly elevated as suggested by the high value of co-variance, which was subsequently normalized by riluzole (co-variance value: 144 ± 17, Krebs; 501 ± 40, TBOA; 90 ± 9, TBOA + riluzole; Kruskal–Wallis one-way ANOVA on ranks, $H_2 = 70.560$, $P < 0.001$; *post-hoc* Dunn's method, $P < 0.05$ for Krebs vs. TBOA, and TBOA vs. TBOA + riluzole comparisons; $n = 3$).

These results showed that the loss of HM staining and significant increment in pyknotic nuclei were evoked by continuous pharmacological block of glutamate uptake by TBOA for a few hours, and that this effect could be suppressed by riluzole. Surviving HMs showed sign of distress (ATF-3 immunoreactivity), which was reduced by riluzole.

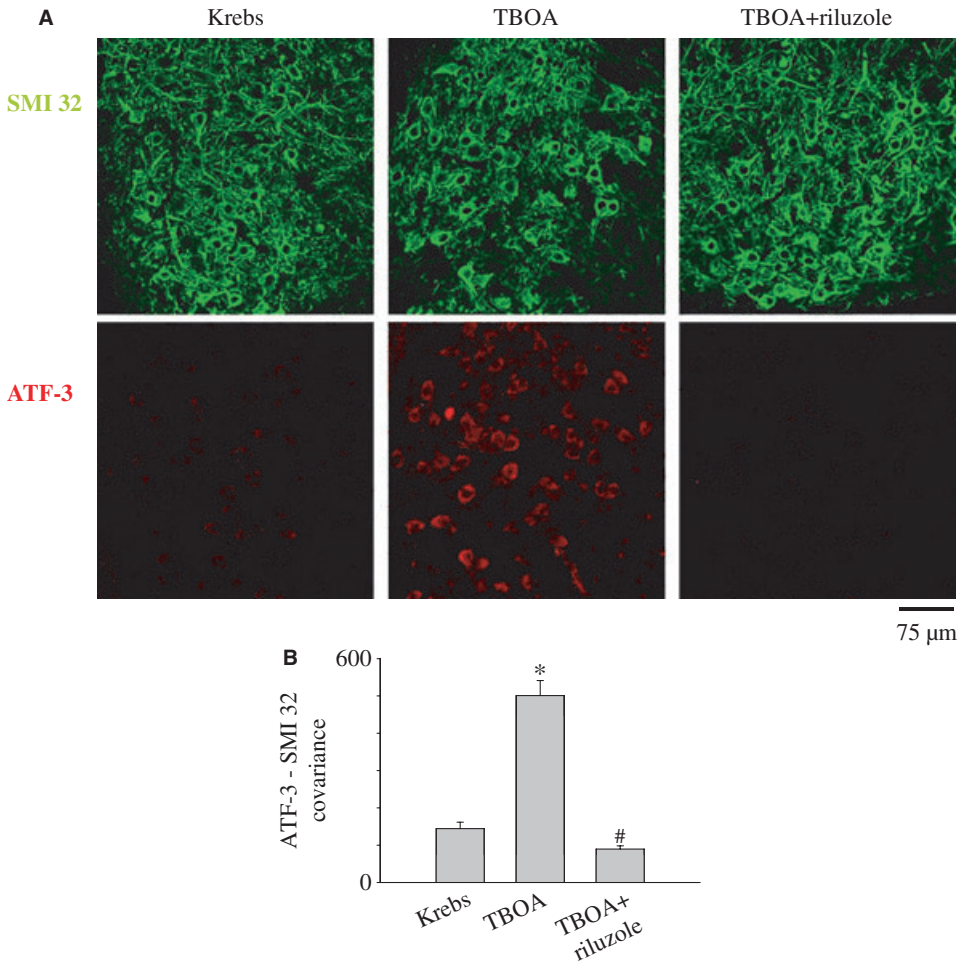

FIG. 7. ATF-3 immunoreactivity of HMs after 4 h application of TBOA and TBOA + riluzole. (A) From left to right (top row), examples of confocal images of HMs stained with SMI 32 (green) after 4 h treatment in control (Krebs), TBOA (50 μM) or TBOA + riluzole (5 μM, started 15 min after TBOA and continuously co-applied up to 4 h). Bottom row shows corresponding confocal images with ATF-3 staining. Images are at 40× magnification. (B) Analysis of co-variance of ATF-3 and SMI 32 signals taken at 4 h Krebs incubation, 4 h TBOA or TBOA + riluzole application. Data were quantified with a MATLAB 7.1 software macro [Kruskal–Wallis one-way ANOVA on ranks: $H_2 = 70.560$, $P < 0.001$; *post-hoc* Dunn's method: $P < 0.05$ for Krebs vs. TBOA (*) and TBOA vs. TBOA + riluzole (#) comparisons; $n = 3$].

Changes in S100B immunoreactivity of protoplasmic astrocytes after TBOA application

Our aim was to investigate whether astroglial cells (which primarily express the glutamate transporters) (Danbolt, 2001) were similarly affected by TBOA and protected by riluzole.

A 1 h application of TBOA enhanced the number of S100B-immunopositive cells (labeled green, whereas SMI 32-positive HMs are in red; Fig. 8A, middle) in the nucleus hypoglossus as compared to control slices (Fig. 8A, left), whereas riluzole (5 μM, started 15 min after TBOA and continuously co-applied up to 1 h) prevented this effect (Fig. 8A, right). Quantification of the number of S100B-immunoreactive cells in these three experimental conditions is shown in Fig. 8B (number of S100B-positive cells: 50 ± 2, Krebs; 63 ± 3, TBOA; 50 ± 2, TBOA + riluzole; one-way ANOVA, $F_{2,57} = 10.027$, $P < 0.001$; *post-hoc* Holm–Sidak method, $P < 0.05$ for Krebs vs. TBOA comparison; $n = 4$ rats).

We next investigated the evolution of such an effect (4 h after TBOA application). In this case, the number of S100B-positive cells (green; Fig. 8C, middle) fell after prolonged TBOA application to values actually close to those observed immediately after slicing (see Fig. 3E for comparison). Nevertheless, after application of riluzole, there was a rebound in the number of S100B-positive cells at 4 h (Fig. 8C, right). Figure 8D shows the average numbers of S100B-positive cells for the three experimental conditions (4 h) (79 ± 4, Krebs; 54 ± 2, TBOA; 69 ± 2, TBOA + riluzole; one-way ANOVA, $F_{2,45} = 21.805$, $P < 0.001$; *post-hoc* Holm–Sidak method, $P < 0.05$ for Krebs vs. TBOA and TBOA vs. TBOA + riluzole comparisons; $n = 3$ rats). Thus, regardless of the length of incubation time, TBOA always produced a change in S100B-positive cells opposite to that observed in Krebs solution and always antagonized by riluzole.

Discussion

The principal novel finding of the present study is that riluzole suppressed not only the excitotoxic bursting of HMs elicited by inhibition of glutamate uptake (Cifra *et al.*, 2009), but also protected their numbers and prevented their distress response (ATF-3 activation), despite prolonged application of the glutamate uptake blocker. Likewise, riluzole reversed the action of TBOA on astrocytes. These new data suggest that riluzole might be efficient to protect motoneurons and glia at the very early stage of excitotoxic damage.

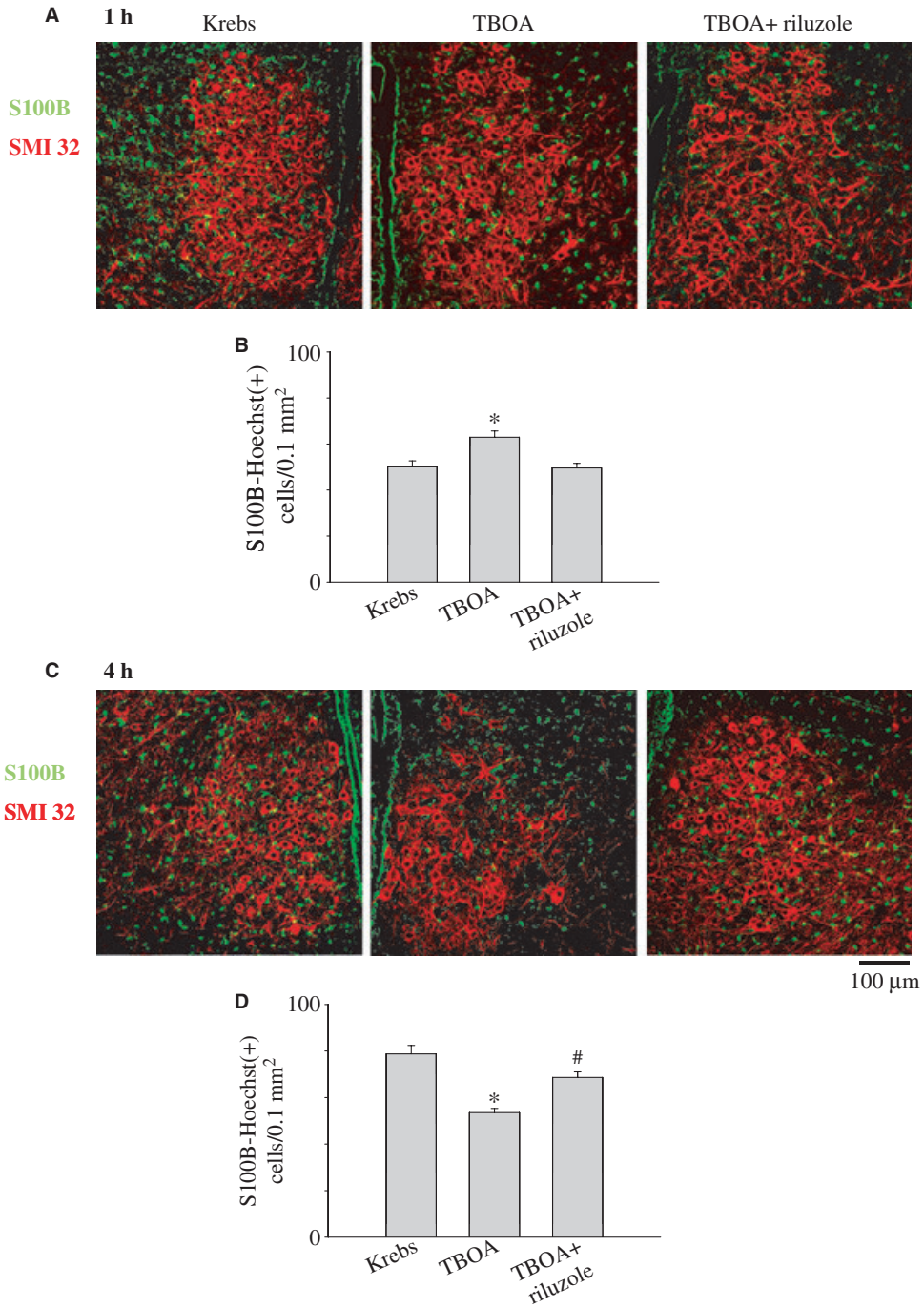

FIG. 8. S100B immunolabeling in the nucleus hypoglossus after TBOA or TBOA + riluzole treatment. (A) Examples of confocal images (40×) showing S100B + SMI 32 (green and red, respectively) immunoreactivity of nucleus hypoglossus after 1 h incubation in control (Krebs; left), TBOA (50 μM; middle) or TBOA + riluzole [riluzole (5 μM) started at 15 min after TBOA and continuously co-applied up to 1 h; right]. Note that S100B immunoreactivity is also present in ependymal cells (see Materials and methods). (B) Histogram quantifies the number of cells positive for both S100B and Hoechst 33342 staining (identified as protoplasmic astrocytes, see Materials and methods) in the three different conditions. Data were quantified with IMAGEJ software [one-way ANOVA: $F_{2,57} = 10.027$, $P < 0.001$; *post-hoc* Holm–Sidak method: $P < 0.05$ for Krebs vs. TBOA (*) comparison; $n = 4$ rats]. (C) S100B + SMI 32 (green and red, respectively) immunoreactivity after 4 h treatment in control (Krebs), TBOA or TBOA + riluzole (from left to right). (D) Histogram shows the average numbers of S100B/Hoechst 33342-positive cells for the three experimental conditions [4 h; one-way ANOVA: $F_{2,45} = 21.805$, $P < 0.001$; *post-hoc* Holm–Sidak method: $P < 0.05$ for Krebs vs. TBOA (*) and TBOA vs. TBOA + riluzole (#) comparisons; $n = 3$ rats].

Motoneurons in brain slices – are they a suitable in vitro *preparation to test excitotoxicity?*

Brain slices offer undeniable advantages in terms of access to the basic mechanisms of action of pathophysiological events and drugs. It is, however, interesting to assess how far the slicing procedure can change the normal operation of motoneurons and impair their extended survival *in vitro* because these factors may impact the evaluation of motoneuron degeneration in experimental protocols. In the present study, we observed that preparing brainstem slices led to an

unavoidable loss of motoneurons presumably because of the damage due to slicing. Nonetheless, those motoneurons surviving after this procedure retained good electrophysiological properties (resting potential, input resistance, action potential firing) and remained stable in their numbers for up to 4 h. It should also be noted that, even if not directly affected by slicing, certain motoneurons probably suffered a modest degree of metabolic distress as we could detect a weak ATF-3 signal that was completely absent in preparations not sliced before fixation. This observation should not, however, seriously hamper the interpretation of our data concerning the effect of TBOA because in this case the ATF-3 signal grew by orders of magnitude. Thus, any background stress in control condition was not accompanied by significant loss of function and it merely confirmed that brain slice experiments are normally time-constrained.

TBOA-evoked bursting – a model of excitotoxicity that evolves from hyperexcitability to delayed cell damage

The exact etiology of most cases of ALS remains unknown. It is clear that any reported deficit in the glial glutamate transporter mechanism is not due to insufficient synthesis of these proteins (Rao & Weiss, 2004), and that the potential offender should be sought in an environmentally-based stimulus (Bruijn *et al.*, 2004). This realization makes it advantageous to employ TBOA (a pharmacological blocker of the glutamate glial transporter) to try to mimic the very early events through which excitotoxicity (due to gradual build-up of extracellular glutamate) may trigger motoneuron degeneration. Previous pre-clinical studies of ALS pathogenesis have largely employed models of motoneurons from brain slices or culture preparations (Boillée *et al.*, 2006; Kato, 2008; Jaiswal & Keller, 2009) supplied from embryonic or neonatal tissues. Our present study has used neonatal rat motoneurons because the application of the patch-clamp technique to brainstem slices from adult rodents is exceptionally difficult (Jaiswal & Keller, 2009). Vucic & Kiernan (2009) have stated that, for the glutamate hypothesis to be plausible as a mechanism of motoneuron degeneration, it must explain how motoneurons are damaged by overactivity of the glutamatergic system. Our model has attempted to address this issue and has indicated that, in analogy to the human pathology (Swash & Ingram, 1988), the extent of motoneuron damage is patchy.

Strong electrical bursting of motoneurons induced by TBOA precedes their functional impairment in terms of poor electrical excitability and high intracellular Ca^{2+} levels (Sharifullina & Nistri, 2006). This phenomenon is accompanied by a significant increase in the occurrence of spontaneous glutamatergic currents up to the point of triggering bursts because of the rise in ambient glutamate that depolarizes network pre-motoneurons via activation of AMPA and metabotropic glutamate receptors type 1 (mGluR1) receptors (Sharifullina *et al.*, 2005; Sharifullina & Nistri, 2006).

Although the reason why some motoneurons are spared in the TBOA-toxicity model remains unclear, this phenomenon is reminiscent of the human pathology as clinical symptoms appear when the loss of motoneurons is still limited (Swash & Ingram, 1988).

Mechanisms of riluzole block of bursting

The mode of action of riluzole is composite and dependent on its actual concentration. In our model system, we used riluzole at 5 μM, because this concentration is close to the human plasma therapeutic concentration (0.1–6.7 μM range; Cheah *et al.*, 2010). The human pharmacokinetic properties of riluzole are complex; in fact, as at least 90% of riluzole is bound to plasma proteins, the free (active) serum fraction is much lower (Wokke, 1996). Because riluzole distribution is seemingly preferential to the brain with a fivefold increase over the plasma level (Cheah *et al.*, 2010), the highest concentration of free riluzole in the human brain tissue attainable with therapeutic doses is approximately 3.5 μM, a value therefore very close to the 5 μM concentration used for the present experiments. Previous studies have shown that 5 μM riluzole preferentially inhibits glutamatergic transmission (Chéramy *et al.*, 1992) rather than blocking the fast and persistent sodium (and calcium) currents (Hubert *et al.*, 1994; Del Negro *et al.*, 2005; Miles *et al.*, 2005; Theiss *et al.*, 2007; Lamanauskas & Nistri, 2008), which are believed to be important components of the pathological hyperexcitability of motoneurons (Elbasiouny *et al.*, 2010).

On the large majority of HMs showing TBOA-evoked bursting, riluzole switched off this phenomenon together with significant inhibition of the occurrence of spontaneous glutamatergic currents. These data pointed to a pre-synaptic, network-mediated depression of excitatory transmitter release (Lamanauskas & Nistri, 2008) developing even when synaptic inhibition was pharmacologically blocked. Changes in synaptic event amplitude were minimal, with the only significant alteration being the slight reduction in amplitude after riluzole application in accordance with the report by Lamanauskas & Nistri (2008).

Our former study of the action of 5 μM riluzole on persistent currents of motoneurons failed to observe a significant reduction in these responses elicited with standard electrophysiological protocols (Lamanauskas & Nistri, 2008). However, as, even at a concentration of 5 μM, riluzole could attenuate the inactivation of the spike mechanisms responsible for the 'butterfly' shape of bursts, it is likely that an effect by riluzole on voltage-activated conductances strongly activated by the very intense firing associated with TBOA-evoked bursts might have partly contributed to the overall suppression of bursting.

Hypoglossal motoneuron protection by riluzole

Even if TBOA did not lead to significant loss of HM staining after 1 h application, there were indications of early distress of motoneurons as shown by their very strong immunoreactivity to ATF-3 (tightly correlated with the HM marker SMI 32), and restored to low levels by riluzole. These observations suggest that riluzole could stop early HM distress and could therefore prevent their lapsing into full-blown excitotoxicity.

The present report shows that significant loss of motoneuron staining (approximately 30%) was detected at 4 h from the start of TBOA application. This was not a trivial loss inasmuch as only half of the HM population shows TBOA-evoked bursting (Sharifullina & Nistri, 2006). This observation accords with our recent study demonstrating that, even after a very large excitotoxic stimulus by kainate, loss of rat spinal motoneurons is a delayed process (Mazzone *et al.*, 2010). It is interesting that, after 4 h of TBOA application, even surviving HMs showed ATF-3 activation, suggesting that they were also affected (although to a lesser degree) by excitotoxicity. Riluzole (5 μM) applied after TBOA enabled preservation of the same number of HMs found in control conditions, and blocked the appearance of the high ATF-3 signal.

TBOA effects on astroglia were inhibited by riluzole

Astroglial cells are important to control the ionic environment, water transport and uptake of transmitters (Kettenmann & Verkhratsky,

2008), and play a major role in pathological processes whereby reactive astrogliosis is fundamental for limiting damage and for post-insult recovery (Giaume *et al.*, 2007; Heneka *et al.*, 2010). Injury-deranged glial activity may, however, exacerbate brain damage (Giaume *et al.*, 2007; Heneka *et al.*, 2010).

Astrocytes are the main cellular defense against glutamate excitotoxicity as they express a high density of glutamate transporters responsible for accumulating up to 80% of the total glutamate released in the brain (Danbolt, 2001; Chvátal *et al.*, 2008). These cells also express ionotropic and metabotropic glutamate receptors (Gallo & Ghiani, 2000), thus allowing a high degree of sophistication in deciphering signals carried by external glutamate (Verkhratsky & Kirchhoff, 2007).

In the post-natal rat central nervous system, the main astrocyte type is the protoplasmic one (Miller & Raff, 1984), which is readily immunolabeled via the Ca^{2+}-binding protein S100B (Cocchia, 1981; Didier *et al.*, 1986). S100 proteins regulate the activity of many effectors, such as enzymes implicated in energy metabolism and signal transduction (Donato, 2003). However, although immunocytochemical and reverse transcription–polymerase chain (RT-PCR) chain reaction data suggest that individual S100 proteins are expressed in a cell-specific manner in mature normal tissues, the level of expression of an S100 protein also depends strongly on environmental factors (Donato, 2003). Depending on its concentration, S100B can exert beneficial (neurotrophic) or detrimental (neurotoxic) effects on surrounding glia and neurons (Rothermundt *et al.*, 2003). Changes in S100B immunoreactivity have, in fact, been associated with brain damage and degenerative brain diseases (Rothermundt *et al.*, 2003; Blackburn *et al.*, 2009) including ALS (Migheli *et al.*, 1999).

The present report observed that the number of S100B-positive cells changed dynamically at different time-points of our *in vitro* preparation. It fell drastically immediately after sectioning, suggesting sensitivity to the inevitable mechanical and metabolic disturbance due to the slicing procedure (Dugué *et al.*, 2005; Davie *et al.*, 2006). Thereafter, it gradually returned toward pre-sectioning levels, suggesting perhaps a slow recovery process. Within this framework, we found that TBOA always produced a change in S100B-positive cells opposite to that observed in Krebs solution and always antagonized by riluzole. Although we are unable to clarify the functional nature of the observed changes in S100B immunoreactivity, we can envisage that S100B is a crucial molecular sensor picking up a variety of stimuli including an excitotoxic insult. Further investigations are needed to elucidate the mechanisms and the significance of astrocytic changes and their consequences for HM survival.

Implications of early pathophysiology of amyotrophic lateral sclerosis

The use of an acute neonatal brain slice preparation cannot, of course, replicate the complex cell pathology affecting motoneurons of patients with ALS. Nevertheless, the present report is based on a model in which excitotoxicity was actually produced by raising endogenous glutamate rather than by giving a glutamate agonist; hence, this protocol might provide some helpful insights into the basic cellular mechanisms triggered by the gradual glutamate increase (due to uptake downregulation) observed in the cerebrospinal fluid of patients with ALS (Rothstein *et al.*, 1992).

The present study showed how deadly rhythmic bursting of motoneurons, produced by blocking glutamate uptake (Sharifullina & Nistri, 2006), and delayed motoneuron loss could be suppressed by riluzole, an agent usually given to patients as a symptomatic treatment at the full-blown disease stage. Should a range of reliable biomarkers (Süssmuth *et al.*, 2008; Turner *et al.*, 2009) be available to diagnose the likelihood of ALS development at pre-symptomatic stage, then pharmacological inhibition of motor network hyperactivation elicited by stressful challenges like excitotoxicity might become a useful strategy to delay disease progression.

Supporting Information

Additional supporting information may be found in the online version of this article:

Fig. S1. Astrocyte population in the P4 rat nucleus hypoglossus and spinal cord. (A) Example of a confocal image (20×) of hypoglossal nuclei labeled with GFAP (fibrous astrocyte marker; green) and Hoechst 33342 (blue). The inset (higher magnification) shows how GFAP labeling is limited to the central canal profile. (B) Example of GFAP (green) and S100B (protoplasmic astrocytic marker; red) immunoreactivity of the spinal cord ventral horn (fluorescence microscopy image, l0×). (C) Histological example of GFAP (green) and DAPI (blue) staining of cell in the rat spinal cord (fluorescence microscopy image, 5×).

Fig. S2. Immunostaining of motoneurons and astrocytes in the nucleus hypoglossus of P4 rat. (A) Example of a confocal images (l0×) of hypoglossal nuclei labeled with SMI 32 (motoneuron marker; green) and Hoechst 33342 (blue). Inset shows schematic location of nuclei in brainstem section. (B) Higher magnification (20×) of the example in A, showing the region of interest (ROI: white box; 100 000 μm^2) used for cell counting. (C) Histological example of S100B (green; astrocytes) and Hoechst 33342 (blue) staining.

Please note: As a service to our authors and readers, this journal provides supporting information supplied by the authors. Such materials are peer-reviewed and may be re-organized for online delivery, but are not copy-edited or typeset by Wiley-Blackwell. Technical support issues arising from supporting information (other than missing files) should be addressed to the authors.

Acknowledgements

This work was supported by a grant from Ministero dell'Università e Ricerca (Progetti di Ricerca di Interesse Nazionale) and grants from the government of the Friuli Venezia Giulia Region. We thank Dr Miranda Mladinic for spinal cord images and advice on immunohistochemistry experiments, and Dr Micaela Grandolfo and Dr Walter Vanzella for their support with histological data acquisition and analysis.

Abbreviations

ALS, amyotrophic lateral sclerosis; ATF-3, activating transcription factor-3; CV, coefficient of variation; DAPI, 4′,6-diamidino-2-phenylindole; GABA, γ-aminobutyric acid; GFAP, glial fibrillary acidic protein; HM, hypoglossal motoneuron; IEI, inter-event interval; I_h, hyperpolarization-activated current; P1-P5, postnatal day 0–5; QX-314, *N*-2,6-dimethylphenylcarbamoylmethyl triethylammonium bromide; R_{in}, cell input resistance; sPSC, spontaneous postsynaptic current; TBOA, DL-threo-β-benzyloxyaspartate; V_h, holding potential under voltage clamp mode; V_m, membrane potential under current clamp mode; w.o., washout.

References

Anderson, C.M., Bridges, R.J., Chamberlin, A.R., Shimamoto, K., Yasuda-Kamatani, Y. & Swanson, R.A. (2001) Differing effects of substrate and non-

substrate transport inhibitors on glutamate uptake reversal. *J. Neurochem.*, **79**, 1207–1216.
Anneser, J.M.H., Chahli, C., Ince, P.G., Borasio, G.D. & Shaw, P.J. (2004) Glial proliferation and metabotropic glutamate receptor expression in amyotrophic lateral sclerosis. *J. Neuropathol. Exp. Neurol.*, **63**, 831–840.
Barbeito, L.H., Pehar, M., Cassina, P., Vargas, M.R., Peluffo, H., Viera, L., Estévez, A.G. & Beckman, J.S. (2004) A role for astrocytes in motor neuron loss in amyotrophic lateral sclerosis. *Brain Res. Brain Res. Rev.*, **47**, 263–274.
Blackburn, D., Sargsyan, S., Monk, P.N. & Shaw, P.J. (2009) Astrocyte function and role in motor neuron disease: a future therapeutic target? *Glia*, **57**, 1251–1264.
Boillée, S., Vande Velde, C. & Cleveland, D.W. (2006) ALS: a disease of motor neurons and their nonneuronal neighbors. *Neuron*, **52**, 39–59.
Bruijn, L.I., Miller, T.M. & Cleveland, D.W. (2004) Unraveling the mechanisms involved in motor neuron degeneration in ALS. *Annu. Rev. Neurosci.*, **27**, 723–749.
Cheah, B.C., Vucic, S., Krishnan, A.V. & Kiernan, M.C. (2010) Riluzole, neuroprotection and amyotrophic lateral sclerosis. *Curr. Med. Chem.*, **17**, 1942–1959.
Chéramy, A., Barbeito, L., Godeheu, G. & Glowinski, J. (1992) Riluzole inhibits the release of glutamate in the caudate nucleus of the cat in vivo. *Neurosci. Lett.*, **147**, 209–212.
Chvátal, A., Anderová, M., Neprasová, H., Prajerová, I., Benesová, J., Butenko, O. & Verkhratsky, A. (2008) Pathological potential of astroglia. *Physiol. Res.*, **57**, 101–110.
Cifra, A., Nani, F., Sharifullina, E. & Nistri, A. (2009) A repertoire of rhythmic bursting produced by hypoglossal motoneurons in physiological and pathological conditions. *Philos. Trans. R. Soc. Lond. B Biol. Sci.*, **364**, 2493–2500.
Cleveland, D.W. & Rothstein, J.D. (2001) From Charcot to Lou Gehrig: deciphering selective motor neuron death in ALS. *Nat. Rev. Neurosci.*, **2**, 806–819.
Cocchia, D. (1981) Immunocytochemical localization of S-100 protein in the brain of adult rat. An ultrastructural study. *Cell Tissue Res.*, **214**, 529–540.
Danbolt, N.C. (2001) Glutamate uptake. *Prog. Neurobiol.*, **65**, 1–105.
Davie, J.T., Kole, M.H., Letzkus, J.J., Rancz, E.A., Spruston, N., Stuart, G.J. & Häusser, M. (2006) Dendritic patch-clamp recording. *Nat. Protoc.*, **1**, 1235–1247.
Del Negro, C.A., Morgado-Valle, C., Hayes, J.A., Mackay, D.D., Pace, R.W., Crowder, E.A. & Feldman, J.L. (2005) Sodium and calcium current-mediated pacemaker neurons and respiratory rhythm generation. *J. Neurosci.*, **25**, 446–453.
Didier, M., Harandi, M., Aguera, M., Bancel, B., Tardy, M., Fages, C., Calas, A., Stagaard, M., Møllgård, K. & Belin, M.F. (1986) Differential immunocytochemical staining for glial fibrillary acidic (GFA) protein, S-100 protein and glutamine synthetase in the rat subcommissural organ, nonspecialized ventricular ependyma and adjacent neuropil. *Cell Tissue Res.*, **245**, 343–351.
Donato, R. (2003) Intracellular and extracellular roles of S100 proteins. *Microsc. Res. Tech.*, **60**, 540–551.
Donato, R. & Nistri, A. (2000) Relative contribution by GABA or glycine to Cl^--mediated synaptic transmission on rat hypoglossal motoneurons in vitro. *J. Neurophysiol.*, **84**, 2715–2724.
Dugué, G.P., Dumoulin, A., Triller, A. & Dieudonné, S. (2005) Target-dependent use of co-released inhibitory transmitters at central synapses. *J. Neurosci.*, **25**, 6490–6498.
Elbasiouny, S.M., Schuster, J.E. & Heckman, C.J. (2010) Persistent inward currents in spinal motoneurons: Important for normal function but potentially harmful after spinal cord injury and in amyotrophic lateral sclerosis. *Clin. Neurophysiol.*, **121**, 1669–1679.
Eng, L.F. (1985) Glial fibrillary acidic protein (GFAP): the major protein of glial intermediate filaments in differentiated astrocytes. *J. Neuroimmunol.*, **8**, 203–214.
Gallo, V. & Ghiani, C.A. (2000) Glutamate receptors in glia: new cells, new inputs and new functions. *Trends Pharmacol. Sci.*, **21**, 252–258.
Giaume, C., Kirchhoff, F., Matute, C., Reichenbach, A. & Verkhratsky, A. (2007) Glia: the fulcrum of brain diseases. *Cell Death Differ.*, **14**, 1324–1335.
Gonzalez de Aguilar, J., Echaniz-Laguna, A., Fergani, A., René, F., Meininger, V., Loeffler, J. & Dupuis, L. (2007) Amyotrophic lateral sclerosis: all roads lead to Rome. *J. Neurochem.*, **101**, 1153–1160.
Hai, T. & Hartman, M.G. (2001) The molecular biology and nomenclature of the activating transcription factor/cAMP responsive element binding family of transcription factors: activating transcription factor proteins and homeostasis. *Gene*, **273**, 1–11.
Heneka, M.T., Rodríguez, J.J. & Verkhratsky, A. (2010) Neuroglia in neurodegeneration. *Brain Res. Rev.*, **63**, 189–211.
Hubert, J.P., Delumeau, J.C., Glowinski, J., Prémont, J. & Doble, A. (1994) Antagonism by riluzole of entry of calcium evoked by NMDA and veratridine in rat cultured granule cells: evidence for a dual mechanism of action. *Br. J. Pharmacol.*, **113**, 261–267.
Jacob, D.A., Bengston, C.L. & Forger, N.G. (2005) Effects of *Bax* gene deletion on muscle and motoneuron degeneration in a sexually dimorphic neuromuscular system. *J. Neurosci.*, **25**, 5638–5644.
Jaiswal, M.K. & Keller, B.U. (2009) Cu/Zn superoxide dismutase typical for familial amyotrophic lateral sclerosis increases the vulnerability of mitochondria and perturbs Ca^{2+} homeostasis in SOD1G93A mice. *Mol. Pharmacol.*, **75**, 478–489.
Kato, S. (2008) Amyotrophic lateral sclerosis models and human neuropathology: similarities and differences. *Acta Neuropathol.*, **115**, 97–114.
Kettenmann, H. & Verkhratsky, A. (2008) Neuroglia: the 150 years after. *Trends Neurosci.*, **31**, 653–659.
Kuzhandaivel, A., Margaryan, G., Nistri, A. & Mladinic, M. (2010a) Extensive glial apoptosis develops early after hypoxic-dysmetabolic insult to the neonatal rat spinal cord in vitro. *Neuroscience*, **169**, 325–338.
Kuzhandaivel, A., Nistri, A. & Mladinic, M. (2010b) Kainate-mediated excitotoxicity induces neuronal death in the rat spinal cord in vitro via a PARP-1 dependent cell death pathway (parthanatos). *Cell. Mol. Neurobiol.*, **30**, 1001–1012.
Lacomblez, L., Bensimon, G., Leigh, P.N., Guillet, P. & Meininger, V. (1996) Dose-ranging study of riluzole in amyotrophic lateral sclerosis. Amyotrophic Lateral Sclerosis/Riluzole Study Group II. *Lancet*, **347**, 1425–1431.
Lamanauskas, N. & Nistri, A. (2006) Persistent rhythmic oscillations induced by nicotine on neonatal rat hypoglossal motoneurons in vitro. *Eur. J. Neurosci.*, **24**, 2543–2556.
Lamanauskas, N. & Nistri, A. (2008) Riluzole blocks persistent Na^+ and Ca^{2+} currents and modulates release of glutamate via presynaptic NMDA receptors on neonatal rat hypoglossal motoneurons in vitro. *Eur. J. Neurosci.*, **27**, 2501–2514.
Marchetti, C., Pagnotta, S., Donato, R. & Nistri, A. (2002) Inhibition of spinal or hypoglossal motoneurons of the newborn rat by glycine or GABA. *Eur. J. Neurosci.*, **15**, 975–983.
Margaryan, G., Mattioli, C., Mladinic, M. & Nistri, A. (2010) Neuroprotection of locomotor networks after experimental injury to the neonatal rat spinal cord in vitro. *Neuroscience*, **165**, 996–1010.
Mazzone, G.L., Margaryan, G., Kuzhandaivel, A., Nasrabady, S.E., Mladinic, M. & Nistri, A. (2010) Kainate-induced delayed onset of excitotoxicity with functional loss unrelated to the extent of neuronal damage in the in vitro spinal cord. *Neuroscience*, **168**, 451–462.
Meininger, V., Lacomblez, L. & Salachas, F. (2000) What has changed with riluzole? *J. Neurol.*, **247**, 19–22.
Migheli, A., Cordera, S., Bendotti, C., Atzori, C., Piva, R. & Schiffer, D. (1999) S-100beta protein is upregulated in astrocytes and motor neurons in the spinal cord of patients with amyotrophic lateral sclerosis. *Neurosci. Lett.*, **261**, 25–28.
Miles, G.B., Dai, Y. & Brownstone, R.M. (2005) Mechanisms underlying the early phase of spike frequency adaptation in mouse spinal motoneurones. *J Physiol.*, **566**, 519–532.
Miller, R.H. & Raff, M.C. (1984) Fibrous and protoplasmic astrocytes are biochemically and developmentally distinct. *J. Neurosci.*, **4**, 585–592.
Mitchell, J.D. & Borasio, G.D. (2007) Amyotrophic lateral sclerosis. *Lancet*, **369**, 2031–2041.
Nani, F., Cifra, A. & Nistri, A. (2010) Transient oxidative stress evokes early changes in the functional properties of neonatal rat hypoglossal motoneurons in vitro. *Eur. J. Neurosci.*, **31**, 951–966.
Neusch, C., Bähr, M. & Schneider-Gold, C. (2007) Glia cells in amyotrophic lateral sclerosis: new clues to understanding an old disease? *Muscle Nerve*, **35**, 712–724.
Pagnotta, S.E., Lape, R., Quitadamo, C. & Nistri, A. (2005) Pre- and postsynaptic modulation of glycinergic and GABAergic transmission by muscarinic receptors on rat hypoglossal motoneurons in vitro. *Neuroscience*, **130**, 783–795.
Perkins, K.L. & Wong, R.K. (1995) Intracellular QX-314 blocks the hyperpolarization-activated inward current Iq in hippocampal CA1 pyramidal cells. *J. Neurophysiol.*, **73**, 911–915.

Quitadamo, C., Fabbretti, E., Lamanauskas, N. & Nistri, A. (2005) Activation and desensitization of neuronal nicotinic receptors modulate glutamatergic transmission on neonatal rat hypoglossal motoneurons. *Eur. J. Neurosci.*, **22**, 2723–2734.

Rao, S.D. & Weiss, J.H. (2004) Excitotoxic and oxidative cross-talk between motor neurons and glia in ALS pathogenesis. *Trends Neurosci.*, **27**, 17–23.

Raoul, C., Abbas-Terki, T., Bensadoun, J.C., Guillot, S., Haase, G., Szulc, J., Henderson, C.E. & Aebischer, P. (2005) Lentiviral-mediated silencing of SOD1 through RNA interference retards disease onset and progression in a mouse model of ALS. *Nat. Med.*, **11**, 423–428.

Rosen, D.R., Siddique, T., Patterson, D., Figlewicz, D.A., Sapp, P., Rahmani, Z., Krizus, A., McKenna-Yasek, D., Cayabyab, A., Gaston, S.M., Berger, R., Tanzi, R.E., Halperin, J.J., Herzfeldt, B., Van den Bergh, R., Hung, W.Y., Bird, T., Deng, G., Mulder, D.W., Smyth, C., Laing, N.G., Soriano, E., Pericak-Vance, M.A., Haines, J., Rouleau, G.A., Gusella, J.S., Horvitz, H.R., Brown, Jr R.H. (1993) Mutations in Cd/Zn superoxide dismutase gene are associated with familial amyotrophic lateral sclerosis. *Nature*, **362**, 59–62.

Rothermundt, M., Peters, M., Prehn, J.H.M. & Arolt, V. (2003) S100B in brain damage and neurodegeneration. *Microsc. Res. Tech.*, **60**, 614–632.

Rothstein, J.D., Martin, L.J. & Kuncl, R.W. (1992) Decreased glutamate transport by the brain and spinal cord in amyotrophic lateral sclerosis. *N. Engl. J. Med.*, **326**, 1464–1468.

Sharifullina, E. & Nistri, A. (2006) Glutamate uptake block triggers deadly rhythmic bursting of neonatal rat hypoglossal motoneurons. *J. Physiol.*, **572**, 407–423.

Sharifullina, E., Ostroumov, K. & Nistri, A. (2005) Metabotropic glutamate receptor activity induces a novel oscillatory pattern in neonatal rat hypoglossal motoneurones. *J. Physiol.*, **563**, 139–159.

Spreux-Varoquaux, O., Bensimon, G., Lacomblez, L., Salachas, F., Pradat, P.F., Le Forestier, N., Marouan, A., Dib, M. & Meininger, V. (2002) Glutamate levels in cerebrospinal fluid in amyotrophic lateral sclerosis: a reappraisal using a new HPLC method with coulometric detection in a large cohort of patients. *J. Neurol. Sci.*, **193**, 73–78.

Stroick, M., Fatar, M., Ragoshke-Schumm, A., Fassbender, K., Bertsch, T. & Hennerici, M.G. (2006) Protein S-100B–a prognostic marker for cerebral damage. *Curr. Med. Chem.*, **13**, 3053–3060.

Süssmuth, S.D., Brettschneider, J., Ludolph, A.C. & Tumani, H. (2008) Biochemical markers in CSF of ALS patients. *Curr. Med. Chem.*, **15**, 1788–1801.

Swash, M. & Ingram, D. (1988) Preclinical and subclinical events in motor neuron disease. *J. Neurol. Neurosurg. Psychiatry*, **51**, 165–168.

Taccola, G., Margaryan, G., Mladinic, M. & Nistri, A. (2008) Kainate and metabolic perturbation mimicking spinal injury differentially contribute to early damage of locomotor networks in the in vitro neonatal rat spinal cord. *Neuroscience*, **155**, 538–555.

Theiss, R.D., Kuo, J.J. & Heckman, C.J. (2007) Persistent inward currents in rat ventral horn neurones. *J. Physiol.*, **580**, 507–522.

Tsujino, H., Kondo, E., Fukuoka, T., Dai, Y., Tokunaga, A., Miki, K., Yonenobu, K., Ochi, T. & Noguchi, K. (2000) Activating transcription factor 3 (ATF3) induction by axotomy in sensory and motoneurons: a novel neuronal marker of nerve injury. *Mol. Cell. Neurosci.*, **15**, 170–182.

Turner, M.R., Kiernan, M.C., Leigh, P.N. & Talbot, K. (2009) Biomarkers in amyotrophic lateral sclerosis. *Lancet Neurol.*, **8**, 94–109.

Umemiya, M. & Berger, A.J. (1995) Inhibition by riluzole of glycinergic postsynaptic currents in rat hypoglossal motoneurones. *Br. J. Pharmacol.*, **116**, 3227–3230.

Van Den Bosch, L. & Robberecht, W. (2008) Crosstalk between astrocytes and motor neurons: what is the message? *Exp. Neurol.*, **211**, 1–6.

Van Den Bosch, L., Van Damme, P., Bogaert, E. & Robberecht, W. (2006) The role of excitotoxicity in the pathogenesis of amyotrophic lateral sclerosis. *Biochim. Biophys. Acta*, **1762**, 1068–1082.

Verkhratsky, A. & Kirchhoff, F. (2007) Glutamate-mediated neuronal-glial transmission. *J. Anat.*, **210**, 651–660.

Vucic, S. & Kiernan, M.C. (2009) Pathophysiology of neurodegeneration in familial amyotrophic lateral sclerosis. *Curr. Mol. Med.*, **9**, 255–272.

Vlug, A.S., Teuling, E., Haasdijk, E.D., French, P., Hoogenraad, C.C. & Jaarsma, D. (2005) ATF3 expression precedes death of spinal motoneurons in amyotrophic lateral sclerosis-SOD1 transgenic mice and correlates with c-Jun phosphorylation, CHOP expression, somato dendritic ubiquitination and Golgi fragmentation. *Eur. J. Neurosci.*, **22**, 1881–1894.

Wokke, J.H. (1996) Riluzole. *Lancet*, **348**, 795–799.

Respiratory Physiology & Neurobiology 179 (2011) 89–96

Contents lists available at ScienceDirect

Respiratory Physiology & Neurobiology

journal homepage: www.elsevier.com/locate/resphysiol

Review

Respiratory motoneurons and pathological conditions: Lessons from hypoglossal motoneurons challenged by excitotoxic or oxidative stress☆

Alessandra Cifra[a], Francesca Nani[a], Andrea Nistri[a,b,*]

[a] Neurobiology Sector, International School for Advanced Studies (SISSA), Via Bonomea 265, 34136 Trieste, Italy
[b] SPINAL (Spinal Person Injury Neurorehabilitation Applied Laboratory), Istituto di Medicina Fisica e Riabilitazione, 33100 Udine, Italy

ARTICLE INFO

Article history:
Accepted 19 March 2011

Keywords:
Lou Gehrig disease
Amyotrophic lateral sclerosis
Burst
Motoneuron disease
Nucleus hypoglossus
Glutamate uptake

ABSTRACT

Hypoglossal motoneurons (HMs) are respiration-related brainstem neurons that command rhythmic contraction of the tongue muscles in concert with the respiratory drive. In experimental conditions, HMs can exhibit a range of rhythmic patterns that may subserve different motor outputs and functions. Neurodegenerative diseases like amyotrophic lateral sclerosis (ALS; Lou-Gehrig disease) often damage HMs with distressing symptoms like dysarthria, dysphagia and breathing difficulty related to degeneration of respiratory motoneurons. While the cause of ALS remains unclear, early diagnosis remains an important goal for potential treatment because fully blown clinical symptoms appear with degeneration of about 30% motoneurons. Using a simple in vitro model of the rat brainstem to study the consequences of excitotoxicity or oxidative stress (believed to occur during the onset of ALS) on HMs, it is possible to observe distinct electrophysiological effects associated with HM experimental pathology. In fact, excitotoxicity caused by glutamate uptake block triggers sustained bursting and enhanced synaptic transmission, whereas oxidative stress generates slow depolarization, augmented repeated firing, and decreased synaptic transmission. In either case, only a subpopulation of HMs shows abnormal functional changes. Although these two insults induce separate functional signatures, the consequences on HMs after a few hours are similar and are preceded by activation of the stress transcription factor ATF-3. The deleterious action of excitotoxicity is inhibited by early administration of riluzole, a drug currently employed for the symptomatic treatment of ALS, demonstrating that this in vitro model can be useful for testing potential neuroprotective agents.

1. Introduction

The respiratory function relies on neuronal (rhythm and pattern generators) and anatomical (motor output) substrates. A complex network of medullary neurons, composed by different types of pacemaker cells, and inspiratory and expiratory neurons with excitatory and inhibitory connections, is responsible for the three-phasic respiratory rhythm of mammals (Ramirez et al., 2004; Ramirez and Viemari, 2005; Richter et al., 1992). The motor output, instead, involves muscles (like the diaphragm) that mainly express an air pump function, and those that subserve valve or airway stability functions (Berger, 2000; Feldman and Del Negro, 2006). The valve muscles, including the laryngeal, pharyngeal and the tongue muscles, form together with soft tissues the upper airways. In particular, tongue muscles, subdivided into intrinsic (longitudinal, transversal and vertical) and extrinsic (hypoglossus, styloglossus, geniohyloid and genioglossus) ones, are exclusively innervated by the axons originating from the hypoglossal nucleus (XII cranial nucleus located in the medulla oblongata). In the rat, HMs are somatotopically organized (Aldes, 1995; McClung and Goldberg, 1999; Sokoloff, 2000): such organization allows the fine control of tongue movements (Lowe, 1980) during breathing as well as a variety of non-respiratory functions such as vocalization, suckling and swallowing. All these behaviours require rhythmic contractions with appropriate muscle coordination to allow dynamic changes in airway size (Horner, 2008) without obstruction of upper airways by

Abbreviations: AHP, afterhyperpolarization; ALS, amyotrophic lateral sclerosis; AMPA, α-amino-3-hydroxy-5-methyl-4-isoxazolepropionic acid; ATF-3, activating transcription factor-3; ChAT, choline acetyltransferase; GABA, γ-aminobutyric acid; GluR2, glutamate receptor subunit 2; HM, hypoglossal motoneuron; H_2O_2, hydrogen peroxide; I_{CaP}, persistent calcium current; I_h, hyperpolarization-activated current; I_{NaP}, persistent sodium current; mPSC, miniature postsynaptic current; MTT, 3-(4,5-dimethylthiazol-2-yl)-2,5-diphenyl tetrazolium bromide; NMDA, N-methyl-D-aspartate; ROS, reactive oxygen species; SOD1, superoxide dismutase 1; sPSC, spontaneous postsynaptic current; TBOA, threo-β-benzyloxyaspartate; TTX, tetrodotoxin; TEA, tetraethylammonium chloride; V_m, membrane potential under current clamp mode; w.o., washout.

☆ This paper is part of a special issue entitled "Recruitment of Respiratory Motoneurons", guest-edited by Drs. F. Fregosi, E. Fiona Bailey, David D. Fuller.

* Corresponding author at: SISSA, Via Bonomea 265, 34136 Trieste, Italy. Tel.: +39 040 3787718; fax: +39 040 3787702.
E-mail address: nistri@sissa.it (A. Nistri).

1569-9048/$ – see front matter © 2011 Elsevier B.V. All rights reserved.
doi:10.1016/j.resp.2011.03.017

the tongue. Axons of the HMs exit the hypoglossal nucleus and coalesce to form the hypoglossal nerve (XII cranial nerve) which runs to the floor of the mouth where it distributes its finer branches to tongue muscles.

The brainstem slice preparation comprising an intact pre-Bötzinger Complex is canonically used to study respiratory network mechanisms (see recent review by Greer et al., 2006). Thus, XII nerve recording has been widely used to monitor the motor output of the respiratory centres to examine functional changes in respiratory rhythm generation and its modulation (Funk et al., 1993; Ramirez et al., 1997; Telgkamp and Ramirez, 1999; Shao and Feldman, 2005).

Certain neurodegenerative diseases affecting motoneurons produce severe dysfunction of brainstem motoneurons, especially the HMs: these pathophysiological changes are often manifested with dysarthria, dysphagia and tongue biting, indicating a high vulnerability of these motoneurons to ALS-like diseases (Mitchell and Borasio, 2007; Kühnlein et al., 2008). Thus, it is interesting to investigate how the basic mechanisms used by HMs for physiological rhythmic bursting in control conditions can be transformed into dysfunctional discharges in pathological states.

The aim of the present review is to discuss the relation between electrophysiological changes of hypoglossal motoneurons and cell damage following excitotoxicity or oxidative stress as a model to unveil early pathophysiological alterations of brainstem motoneurons.

2. Basic properties of HM bursts: role of glutamate receptor activity

Despite their rhythmic discharges during respiration (and other functions), hypoglossal motoneurons are not endowed with spontaneous rhythmicity even after membrane depolarization by intracellular current injection or application of high K^+ solution (Sharifullina et al., 2005, 2008). Furthermore, unlike spinal motoneurons, HMs do not express spontaneous rhythmic bursting when synaptic inhibition is blocked (Bracci et al., 1996). These observations indicate that HM bursting, necessary to induce rhythmic contraction of tongue muscles, has predominantly a network origin so that periodic synaptic inputs produced by premotoneurons (see Berger, this issue) are integrated by the intrinsic properties of HMs to generate an oscillatory motor output. HMs can express a range of bursting patterns with different mechanisms of action, yet with two fundamental requirements, namely the presence of gap junctions (particularly important in neonatal HMs) and discrete distribution of bursters, since about half of the HM population does not express rhythmicity when challenged with various protocols (as reviewed by Nistri et al., 2006). In neonatal and adult rat brainstem, electrical coupling depends on carbenoxolone-sensitive gap junctions composed by different types of connexins (Solomon et al., 2001; Solomon, 2003), indicating that neurons probably synchronize their bursting activity through these membrane proteins specialized in interneuronal communication (Cifra et al., 2009). The present review will examine the characteristics that allow HMs to burst in control or in pathological conditions.

As discussed elsewhere in this (issue see Berger, this issue), glutamate is the main excitatory neurotransmitter acting on HMs via both NMDA and non-NMDA receptors at synaptic sites (O'Brien et al., 1997). Conversely, even at early postnatal age, GABA and glycine are both inhibitory neurotransmitters via Cl^- mediated increase in membrane permeability (Donato and Nistri, 2000). In certain cases, these neutral amino acids may be present in the same presynaptic vesicles to be co-released from the same presynaptic terminal (O'Brien and Berger, 1999).

One example of HM rhythmic bursting with a strong intrinsic component is the one driven by sustained activation of NMDA receptors (Sharifullina et al., 2008). This rhythm, usually observed in about 75% of HMs in vitro, has low frequency (0.43 ± 0.07 Hz), is unaffected by blockers of excitatory or inhibitory synaptic transmission, and is preserved despite fluctuations in extracellular Mg^{2+}. It is interesting that NMDA receptor-dependent bursting can be potently modulated by intracellular current injection that, through spreading via gap junctions, can synchronize the activity of HMs (Sharifullina et al., 2008) which become "conditional group bursters" (Feldman and Del Negro, 2006). On the other hand, activation of AMPA receptors cannot trigger repeated bursting probably because of the rapid desensitization of these receptors (Sharifullina et al., 2008).

Pharmacological activation by 3,5-dihydroxyphenylglycine (DHPG) of subtype 1 receptors of group I metabotropic glutamate receptors (mGluR; widely expressed in the brainstem; Del Negro and Chandler, 1998) can also evoke in 40% HMs a characteristic pattern of bursting that falls within the range of the so-called theta oscillations (Sharifullina et al., 2005). These bursts are caused by patterned discharges of excitatory signals by premotoneurons mainly located in the dorsal medullary reticular column (DMRC), require gap junctions and are apparently paced by the cyclic activation of K_{ATP} conductances, thus linking such electrical discharges to the cell energy metabolism. The input resistance increase induced by DHPG via inhibition of a background leak conductance, presumably similar to one mediated by TWIK-related K^+ channels (Enyedi and Czirják, 2010), is also a contributor to the rhythm expression (Sharifullina et al., 2005).

Theta frequency bursts are also generated by presynaptic facilitation of glutamate release through nicotinic cholinergic receptors (Quitadamo et al., 2005) when persistently stimulated by nicotine (Lamanauskas and Nistri, 2006). Unexpectedly, despite the relatively fast process of desensitization of neuronal nicotinic receptors (Giniatullin et al., 2005), this effect of nicotine is relatively long-lasting and is associated with a large increase in the frequency of glutamatergic synaptic events. Nicotine-evoked bursting is suppressed by AMPA receptor blockers or by group I mGluR antagonists, but it is insensitive to NMDA receptor antagonism (Lamanauskas and Nistri, 2006). These observations suggest that nicotine-induced bursting also requires a robust release of endogenous glutamate acting concurrently via AMPA as well as metabotropic receptors.

These results indicate that pharmacological agents can trigger diverse, yet always reversible rhythmic activity suggestive of complex motor control over tongue muscles via multiple membrane receptor mechanisms.

3. Firing of HMs in vitro: conductance mechanisms

The firing behaviour of HMs is determined primarily by the interplay between their intrinsic membrane properties and their synaptic inputs (Berger, 2000). HMs express the classic tetrodotoxin (TTX)-sensitive voltage-dependent transient sodium channels, responsible for the rapid depolarizing phase of the action potential, and the delayed rectifier K^+ channels (sensitive to tetraethylammonium chloride; TEA) which are responsible in part for the repolarizing phase of the action potential (Mosfeldt Laursen and Rekling, 1989; Viana et al., 1993b). HMs also possess both low-threshold (T-type) and high-threshold (N-, P/Q- and L-types) calcium channels important for certain sub- and supra-threshold behaviours of such motoneurons (Umemiya and Berger, 1994; Viana et al., 1993a). Integrative and firing properties of HMs are also related to different types of K^+ conductances responsible for two types of afterhyperpolarization (AHP) following the action potential (Viana et al., 1993b) as well as for the hyperpolarization-activated current I_h (Bayliss et al.,

1994). Finally, HMs express persistent inward currents mediated by Na^+ and/or Ca^{2+} (I_{NaP} and I_{CaP}; Del Negro et al., 2005; Lamanauskas and Nistri, 2008; Powers and Binder, 2003) important for integrating synaptic inputs and for prolonged rhythmic discharges.

In summary, dysfunction of HMs underlying severe pathophysiological conditions can arise from a variety of network and membrane mechanisms.

4. HM neurodegeneration: ALS

While HM control of tongue muscles is crucial for modulation of the upper airway flow (Horner, 2008), amyotrophic lateral sclerosis (ALS), a fatal neurodegenerative disease of motoneurons, strongly alters such functions (especially in the bulbar form; Rowland and Shneider, 2001) with distressing symptoms like slurred speech, difficulty in mastication and swallowing, and, eventually, breathing failure (Walling, 1999).

This motoneuron degeneration affects only a limit number of cells despite the severity of symptoms and the terminal nature of the disease. In fact, clear clinical symptoms appear when 30% motoneurons have degenerated (Turner et al., 2009), while pathological examination of post-mortem tissue shows that at least 30% motoneurons survive at the time of ALS death (Swash and Ingram, 1988).

HMs appear to be particularly vulnerable to ALS because they express AMPA receptors lacking the GluR2 subunits, a property that confers them high Ca^{2+} permeability (Del Cano et al., 1999; Essin et al., 2002; Shaw and Ince, 1997; Van Den Bosch et al., 2006). In addition, HMs possess an intrinsically low intracellular Ca^{2+} buffering capacity (Van Den Bosch et al., 2006), that limit their Ca^{2+} homeostasis.

ALS is a primarily sporadic disease whose exact etiology remains unknown. A small minority (about 5–10%) of ALS patients has a genetic form of the disease, classified as the familial type (FALS). In 10–20% FALS cases, mutations of the enzyme superoxide dismutase 1 (SOD1; Rosen et al., 1993), which normally scavenges toxic reactive oxygen species (ROS), are reputed to produce motoneuron degeneration because of inability to prevent oxidative stress. Conversely, about half of the sporadic cases are associated with increases in the cerebrospinal fluid levels of the excitatory neurotransmitter glutamate (Spreux-Varoquaux et al., 2002), whose excessive concentration is thought to induce motoneuron excitotoxicity. Several studies combine these two notions to support the idea of a cross-link between oxidative stress and excitotoxicity in ALS pathogenesis (Bruijn et al., 2004; Cleveland and Rothstein, 2001; Rao and Weiss, 2004). Despite the different pathogenetic theories, it is clear that understanding how HMs are damaged and the dynamics of this process might provide useful biomarkers for early diagnosis. This approach is rarely feasible not only in man but also with in vivo animal models. Thus, to address the issue of motoneuron toxicity, at least in the short term, and to unveil changes occurring perhaps at the presymptomatic stage, we focused on simple in vitro models based on brainstem slices in which we tested the consequences of mimicking the micro-environmental changes thought to occur within the nucleus hypoglossus at the ALS onset.

With this aim, we enquired about the role of excitotoxicity and oxidative stress for HM degeneration with certain specific objectives: (1) Is it possible to demonstrate that raised extracellular levels of endogenous glutamate are sufficient to produce excitotoxicity? (2) What are the electrophysiological hallmarks of this type of excitotoxicity? (3) What is the time course of HM damage? (4) Is drug neuroprotection feasible? (5) How does this process compare with the effect of a strong oxidative stress?

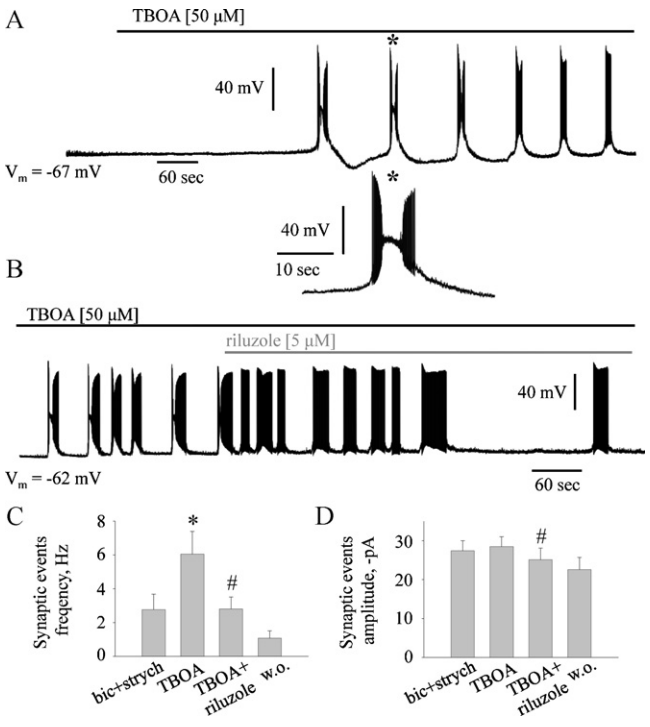

Fig. 1. Riluzole effects on TBOA-evoked bursts and spontaneous postsynaptic glutamatergic currents. (A) Sample record under current clamp configuration ($V_m = -67$ mV) showing bursting activity elicited by 50 μM application of TBOA. Bursts are characterized by large depolarizing waves with superimposed spike activity. The inset shows, on a faster timescale, the transient inactivation of Na^+ channels in the presence of TBOA, which conferred a 'butterfly' shape to the burst event. Adapted from Cifra et al. (2011). (B) Riluzole (5 μM; applied 15 min after TBOA administration) attenuates TBOA-evoked bursts as well as the 'butterfly' shape of each burst event, before fully switching off burst activity (not shown here, see Cifra et al., 2011). Different cell from (A); adapted from Cifra et al. (2009). (C) In the presence of strychnine (strych; 0.4 μM) and bicuculline (bic; 10 μM), TBOA (50 μM) significantly enhances spontaneous glutamatergic event frequency, an effect fully reversed by riluzole (5 μM; applied 15 min after TBOA administration; paired *t*-test: $^{*,\#}P \leq 0.05$; $n = 9$). (D) On the other hand, while event amplitude is unchanged during TBOA application, it becomes slightly smaller following riluzole (paired *t*-test: $^{\#}P \leq 0.05$; $n = 9$). Histograms summarize event amplitude and frequency data, collected under voltage clamp experiments (traces not shown; see Cifra et al., 2011). Unless otherwise stated, data are unpublished results by A.C.

5. Excitotoxic rhythmicity: a type of deadly motoneuron bursting evoked by block of glutamate uptake systems

The extracellular concentration of glutamate is kept at low (or sub) micromolar levels by the concerted operation of glutamate uptake carriers predominantly present in astroglia and, partly, in neurons (Danbolt, 2001). Previous studies have shown that glutamate uptake block is excitotoxic to the retina (Izumi et al., 2002) and evokes epileptic activity (Campbell and Hablitz, 2005). However, a range of glutamate uptake blockers possess a complex action that may involve direct activation of glutamate receptors and/or transport by glutamate carriers which then reverse their normal mode of operation (Anderson et al., 2001). Threo-β-benzyloxyaspartate (TBOA) is a potent and selective uptake blocker devoid of such effects (Anderson et al., 2001) and, thus, useful to investigate the consequences of excitotoxicity. Fig. 1A shows an example of TBOA evoked bursting on a single HM patch-clamped in the slice preparation (Sharifullina and Nistri, 2006): this pattern starts with a latency of few min and is manifested with very large membrane depolarizations that, due to voltage-dependent sodium current inactivation, confer a "butterfly" shape to bursts (see inset to Fig. 1A). This bursting process concerns only approximately half of the HM population (Sharifullina and Nistri, 2006; Cifra et al., 2009, 2011).

Population studies based on intracellular free Ca^{2+} imaging confirm heterogeneity in the HM response to TBOA (applied at an uptake saturating concentration) as only a subset of HMs distributed throughout the nucleus hypoglossus displays irreversible rise of their Ca^{2+} levels. Likewise, an irreversible loss of membrane resistance (together with a large inward current) emerges for certain HMs only (Sharifullina and Nistri, 2006). Pharmacological block of inhibitory neurotransmission does not alter burst characteristics as it simply increases the probability of detecting bursting motoneurons (Sharifullina and Nistri, 2006). Although there are no systematic clinical studies showing that ALS patients express rhythmic activity of their brainstem motoneurons, involuntary contractions of tongue muscles are frequently detected in these patients (Kühnlein et al., 2008). The origin of such symptoms is probably due to muscle denervation, but it does not exclude a central component caused by motoneuron rhythmic discharges.

The question then arises whether these functional data may be a prodromic index of impending cell death. Recent experiments have indicated that, within the nucleus hypoglossus, cell loss is chiefly preceded by glial alteration, while motoneurons disappear later, after at least 4 h (Cifra et al., 2011). The first sign of HM distress is activation of ATF-3, a CREB-dependent transcription factor that migrates to the nucleus after cell damage (Lindwall et al., 2004; Nakagomi et al., 2003; Tsujino et al., 2000). These data indicate that strong functional impairment of such motoneurons observed early after glutamate uptake block is not due to rapid death via a mechanism like necrosis. In fact, the number of HMs remains similar to control after 1 h of TBOA administration (Cifra et al., 2011). After 4 h, however, the number of surviving HMs is decreased (Fig. 2A and C) and those left show strong positivity for ATF-3 activation (Fig. 2A and B), as ATF-3 and the motoneuron marker SMI 32 (Jacob et al., 2005) are co-expressed (Fig. 2B). This deleterious evolution can be arrested by early administration of riluzole (Fig. 2; Cifra et al., 2011), the only drug currently licensed for the symptomatic treatment of ALS (Lacomblez et al., 1996).

The ability of riluzole, applied at a low concentration (5 μM) similar to the plasma therapeutic concentration in man (Wokke, 1996; Cheah et al., 2010), to arrest HM distress and death is paralleled by the suppression of deadly bursting induced by TBOA (Cifra et al., 2011). This action of riluzole is manifested with a gradual decrease in burst intensity (with loss of the "butterfly" shape and emergence of smaller underlying depolarization; Fig. 1B). Bursting frequency is slowed down prior to full block (Cifra et al., 2011). Concomitantly with these effects, riluzole reverses the rise in synaptic event frequency due to TBOA and it only slightly decreases the event amplitude (Fig. 1C and D; Cifra et al., 2011). Previous investigations have shown that in primary cultures (Estevez et al., 1995) or organotypic spinal cultures (Rothstein and Kuncl, 1995), co-application of riluzole with an excitotoxic agent can limit the neuronal damage assessed in terms of 3-(4,5-dimethylthiazol-2-yl)-2,5-diphenyl tetrazolium bromide (MTT) metabolism or of choline acetyltransferase (ChAT) activity, respectively. These studies, however, have not examined the functional timecourse of neuronal degeneration.

In summary, a number of interesting issues emerge from these reports. First, it is possible to produce motoneuron excitotoxicity by simply increasing extracellular endogenous glutamate in a brainstem slice preparation. The idealized diagram of Fig. 3 summarizes our current view on the action of TBOA leading to deadly motoneuron bursting. Second, excitotoxicity is not synonymous of necrosis as HM can strongly and repeatedly burst without cell death in the short term, suggesting an early dissociation between loss of electrophysiological function and cell survival. Third, activation of distress elements like ATF-3 is an advantageous index to assess HM viability, and may represent an index to test neuroprotective agents. Fourth, very low concentrations of riluzole (5 μM), when applied early after the onset of the excitotoxic insult, can protect motoneurons in terms of electrophysiological function as well as survival. It seems, therefore, useful to consider this simple in vitro model as a convenient system for screening of neuroprotective agents with the important caveat that the model relies on neonatal HMs of an in vitro condition.

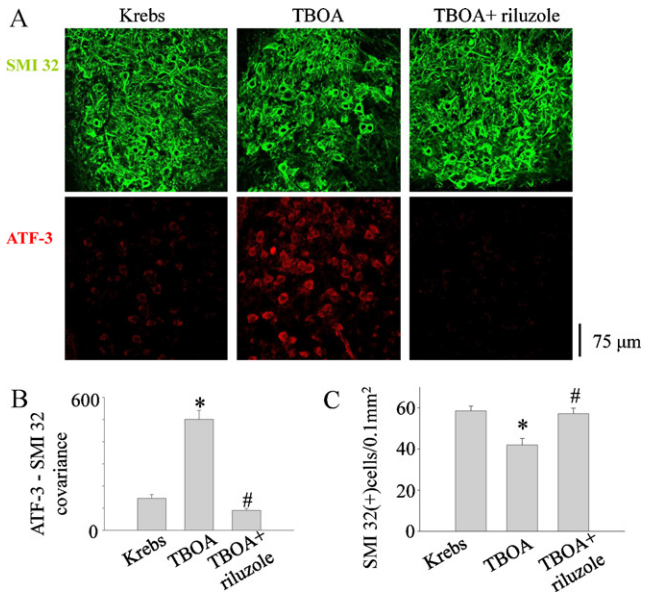

Fig. 2. Riluzole protects HMs against TBOA-induced ATF-3 enhancement and delayed loss. (A) From left to right (top row), examples of confocal images of HMs stained with the motoneuron marker SMI 32 (shown in green) targeting the non-phosphorylated form of neurofilament H (Jacob et al., 2005) after 4 h in control Krebs solution, TBOA (50 μM) or TBOA + riluzole (riluzole 5 μM, started 15 min after TBOA and continuously co-applied up to 4 h). Bottom row shows corresponding confocal images with ATF-3 (activating transcription factor 3, member of the ATF/CREB family of transcription factors typical of neuronal distress; Tsujino et al., 2000) staining. Images are at 40× magnification. (B) Analysis of covariance of ATF-3 and SMI 32 signals taken after 4 h Krebs incubation, 4 h TBOA application, or 4 h TBOA + riluzole. $P < 0.05$ for Krebs vs. TBOA (*) and TBOA vs. TBOA + riluzole (#) comparisons; $n = 3$ rats. (C) Histograms quantifying the number of HMs (SMI 32 positive-cells) in the abovementioned three different experimental conditions, show significant loss of cell staining after TBOA treatment compared to control, an effect fully prevented by riluzole. $P < 0.05$ for Krebs vs. TBOA (*) and TBOA vs. TBOA + riluzole (#) comparisons; $n = 3$ rats.
Adapted from Cifra et al. (2011).

6. Oxidative stress: transient motoneuron hyperexcitability induced by hydrogen peroxide

Oxidative stress arises from an imbalance between the production of reactive oxygen species (ROS, which are a by-product of aerobic metabolism; Coyle and Puttfarcken, 1993; Halliwell and Gutteridge, 1999; Lenaz, 1998) and the ability of cells to metabolize them. The SOD1 enzyme normally catalyzes dismutation of superoxide radicals to hydrogen peroxide (H_2O_2) and oxygen in a two-step redox reaction (Barber et al., 2006), protecting cells from the potential toxic damage of oxidizing agents to proteins, lipids and DNA (including changes in protein conformation, oxidation of unsaturated fatty acids and DNA/RNA alterations; Barber et al., 2006). Since more than 140 mutations in the SOD1 gene have been associated to FALS (Bergemalm et al., 2006; Boillée et al., 2006), this realization has lead to the generation of a variety of murine genetic models expressing the ALS mutated human SOD-1 protein (Cleveland and Rothstein, 2001; Gurney et al., 1994). Such transgenic animals develop late neuromuscular symptoms similar to ALS (probably because of the mutated SOD1 gain-of-function leading to motoneuron degeneration; Ferrante et al., 1997). However,

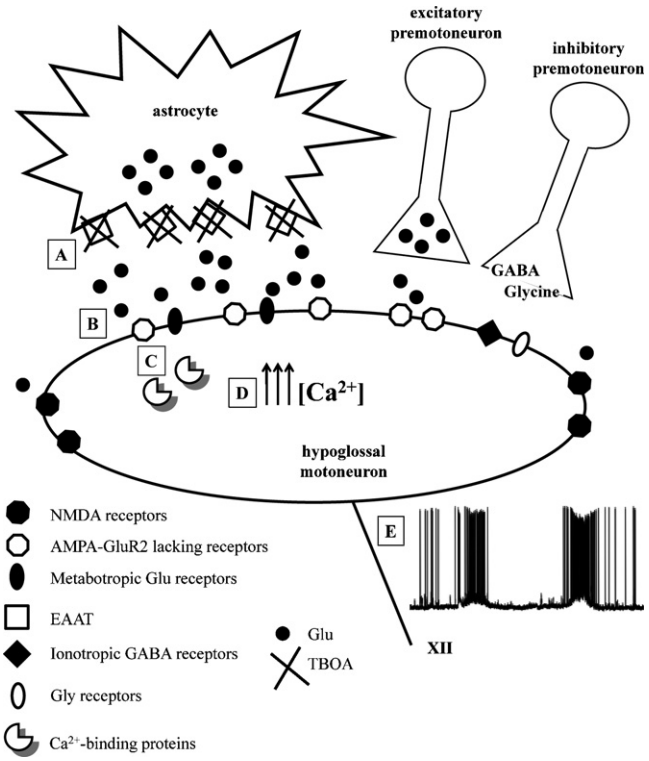

Fig. 3. Idealized scheme to account for TBOA effects on HMs. TBOA blocks glutamate uptake by inhibiting preferentially glutamate transporters (here indicated with the general term EAAT, Excitatory-Amino-Acid-Transporter) expressed by astrocytes (A). As a consequence, endogenous glutamate levels rise in the extracellular space, leading to a persistent, excessive activation (excitotoxicity) of glutamate receptors on motoneurons (B). Motoneurons are particularly vulnerable to an excitotoxic insult because they express GluR2-lacking (Ca^{2+}-permeable) AMPA receptors together with low levels of intracellular Ca^{2+} binding proteins (C), thus limiting their Ca^{2+} homeostasis. Therefore, persistent activation of glutamate receptors (NMDA, AMPA and metabotropic ones), results in a large HM depolarization which spreads through gap junctions and synchronizes HM excitation: these phenomena are accompanied by a strong increase in intracellular Ca^{2+} concentration ($[Ca^{2+}]$; D) due to Ca^{2+} influx through Ca^{2+}-permeable AMPA receptors as well as rhythmic intracellular Ca^{2+} release from internal stores (not shown). All these mechanisms are important contributors to bursting activity (E). The irreversible, large increase in intracellular Ca^{2+} is thought to represent a crucial step in the cell death pathways leading to HM excitotoxic damage.

their electrophysiological phenotype is very complex: for example, while SOD^{G93A} motoneurons show hyperexcitability because of enhanced I_{NaP} (Kuo et al., 2005; van Zundert et al., 2008), SOD^{G85R} motoneurons display, instead, decreased excitability (Bories et al., 2007). These results, together with the observation that oxidative stress has been implicated as a major player for ALS etiopathogenesis even in the absence of mutated SOD-1 (Bogdanov et al., 2000; Ferrante et al., 1997; Ihara et al., 2005; Shaw et al., 1995), make it interesting to investigate the consequences of an acute oxidative stress to wildtype motoneurons. This seems to be an important issue to find out whether apparently healthy motoneurons react to acute oxidative challenge in a way comparable to the SOD1-mutated HMs as a test for the general applicability of this theory to motoneuron disease.

To this aim, we have used the neonatal rat brainstem in vitro model to explore the very early HM response to oxidative stress by bath-applying 1 mM H_2O_2 (Nani et al., 2010) that exerts its toxic effects through the ferrous-iron-dependent (Fenton reaction) and superoxide-driven (Haber–Weiss reaction) generation of the highly reactive hydroxyl radical (Halliwell, 1992; Nani et al., 2010). Fig. 4A shows how bath-applied H_2O_2 (30 min) slowly induces an inward (depolarizing) current reaching its maximum at about 15 min (Nani et al., 2010) and accompanied by an increase in

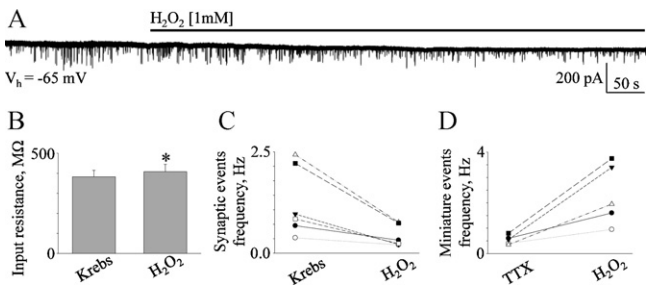

Fig. 4. HM electrophysiological characteristics after application of H_2O_2. (A) Sample of current clamp trace showing the inward current elicited by H_2O_2 application (1 mM; 30 min), reaching its maximum value after about 15 min. (B) Histograms summarizing the effect of H_2O_2 application on HM input resistance measured in voltage-clamp configuration ($P = 0.011$, $n = 6$ cells). (C) Fall in spontaneous synaptic events frequency after application of H_2O_2 ($^{*}P = 0.019$, $n = 6$). This effect is not reversible even after prolonged washout (not shown). Each line represents an individual neuron. (D) In the presence of TTX, H_2O_2 enhances mPSC frequency ($^{\#}P = 0.014$, $n = 6$) without changing mPSC amplitude (not shown). Each line represents an individual neuron.
Adapted from Nani et al. (2010).

motoneuron input resistance (Fig. 4B). Despite these effects that suggest an H_2O_2-induced increase in HMs excitability, global spontaneous post-synaptic currents (sPSCc) frequency is depressed after H_2O_2 application (Fig. 4C), without changing event amplitude (Nani et al., 2010). However, when network activity is blocked with TTX, miniature excitatory and inhibitory synaptic event frequency is increased by H_2O_2 (Fig. 4D) with no effect on event amplitude (Nani et al., 2010): these data may suggest facilitation of miniature synaptic transmission probably due to a H_2O_2-related rise in intracellular free Ca^{2+} at presynaptic level to promote transmitter release (Nani et al., 2010).

Several studies have implicated a gain of function of the I_{NaP} as an important change to enhance motoneuron excitability after oxidative distress of the genetic models of ALS (Kuo et al., 2005; van Zundert et al., 2008). On neonatal rat HMs, H_2O_2 elicits limited depression of the I_{NaP} and stronger reduction of the persistent I_{CaP}, suggesting that an actual decrease in the influx of Ca^{2+} might be responsible for the diminished spike AHP and the large increment in HM firing (Nani et al., 2010). The molecular mechanisms responsible for impairment in Ca^{2+} and Na^{+} influx are presently unclear and might consist of a direct action of reactive oxygen species on such channels or of an effect mediated via intracellular second messengers. Furthermore, H_2O_2 significantly increases HM input resistance, making these cells more sensitive to network synaptic inputs. We hypothesize that this action of H_2O_2 is mediated by blocking TASK-1 conductance mechanisms that belong to a category of leak channels responsible for neuronal membrane potential and rather sensitive to oxidative stress (Enyedi and Czirják, 2010). The combined result of these effects can account for the large facilitation of HM firing. It is noteworthy that, unlike TBOA, H_2O_2 does not produce HM bursting even if the observed changes in HM excitability are persistent and not apparently reversible. Fig. 5 shows an idealized scheme proposing how H_2O_2 may increment HM excitability through the block of TASK-1 channels and I_{AHP} conductances.

The next question is how the effects of acute oxidative stress are translated into motoneuron survival. There is no doubt that this protocol does produce oxidative distress to HMs as shown by the enhanced oxidation of membrane permeable biomarker dihydrorhodamine 123 (Cifra et al., 2009; Nani et al., 2010). This effect is not accompanied by early death of HMs (Nani et al., 2010). A clear increase in immunoreactivity to ATF-3 is, however, observed already 1 h after H_2O_2 treatment as shown by Fig. 6A (an effect clearly associated with the SMI 32 biomarker; Fig. 6B), indicating early distress to HMs induced by H_2O_2 application.

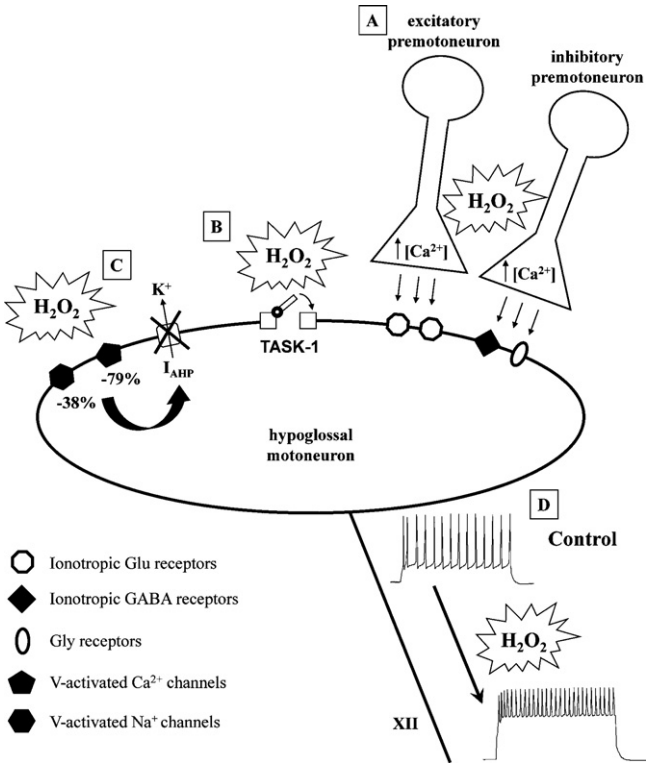

Fig. 5. Idealized scheme summarizing H_2O_2 effects on HM electrophysiological properties. (A) H_2O_2 enhances the frequency of both excitatory and inhibitory miniature events presumably via increased intracellular free Ca^{2+} in premotoneuron synaptic terminals. (B) H_2O_2 augments HM input resistance presumably by depressing a leak background current mediated by TASK-1, a member of the TASK family of K^+ channels, chiefly expressed by motoneurons. (C) H_2O_2 induces a reduction of I_{CaP} (mediated by V-activated Ca^{2+} channels) larger than that of I_{NaP} (mediated by V-activated Na^+ channels). The molecular mechanism responsible for impairment in Ca^{2+} and Na^+ influx might consist of a direct action on such channels or of an effect mediated via intracellular second messengers. Thus, the lessened Ca^{2+} influx has a negative effect on the activation of Ca^{2+} dependent K^+ conductances underlying the AHP. Inhibition of such a outward current, together with the HM larger input resistance (see B), is likely to contribute to HM higher excitability (D) whereby for the same depolarizing current step a greater number of spikes is generated on top of an enhanced amplitude of the voltage response. Further details are available in Nani et al. (2010).

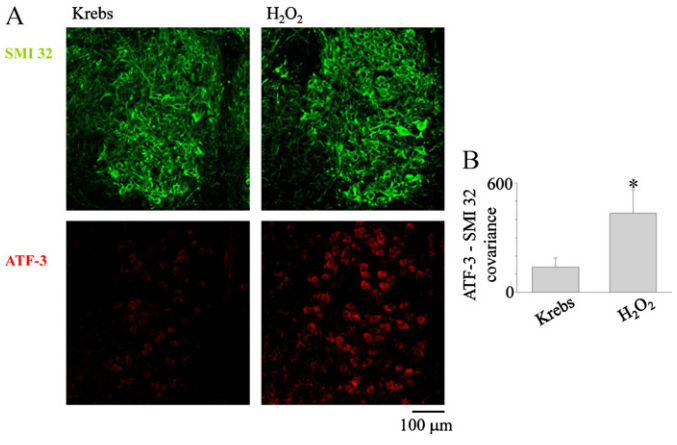

Fig. 6. ATF-3 activation by HMs treated with H_2O_2. (A) Examples of the motoneuron marker SMI 32 (top row) and of the distress-related ATF-3 (bottom row) immunoreactivity of nucleus hypoglossus after 90 min in Krebs solution (left) or 30 min of 1 mM H_2O_2 followed by 60 min washout (right). Note that, despite a similar number of HMs (SMI 32-positive cells), ATF-3 staining is manifested following H_2O_2. (B) Histograms show the covariance between ATF-3 and SMI 32 staining, indicating a significant rise after H_2O_2. Data are from 8 animals (*$P = 0.021$).
Adapted from Nani et al. (2010).

7. More than one way to die: comparison between excitotoxicity and oxidative stress

The present observations suggest that either excitotoxicity or oxidative stress does not kill motoneurons very rapidly. Furthermore, HM loss is patchy indicating yet-unidentified cell populations more resistant to stress than others. These data, albeit obtained with in vitro neonatal motoneurons, raise the possibility that neuroprotective drugs might be employed to arrest disease progression. Riluzole is an interesting example to show that functional loss and activation of intracellular cell death pathways may be inhibited by this agent when applied in vitro.

On the basis of the results discussed above it seems clear that, at least at an early stage, excitotoxicity and oxidative distress show very distinct electrophysiological hallmarks: long-lasting bursting and strong facilitation of network synaptic transmission versus slow depolarization and inhibition of network synaptic transmission, respectively. These diverging effects are all followed by ATF-3 activation, suggesting a common final biochemical pathway. Nonetheless, the precise process responsible for motoneuron death remains elusive: in the rat spinal cord excitotoxicity kills motoneurons via a non-apoptotic mode of cell death termed parthanatos (Kuzhandaivel et al., 2010a), while oxidative stress (plus hypoxia) predominantly activates apoptosis. These mechanisms will have to be investigated also for HMs and compared to the mechanisms responsible for the motoneuron death of SOD1 mutants. Thus, these data allude to the possibility of expanding the range of cellular and biochemical targets to be considered for protecting motoneurons from neurodegeneration. It is worth noting that neither excitotoxicity nor oxidative stress induces electrophysiological changes of HM activity similar to acute anoxia applied to neonatal rat brainstem slices. In the latter case, a short lasting (1–2 min) augmentation of motoneuronal activity is soon replaced by a strong depression, that is not associated with full suppression for a considerable length of time (Ramirez et al., 1997) in accordance with the known resistance of neonatal preparation to anoxia.

8. Conclusions

A simple preparation of the neonatal rat brainstem offers the opportunity to study the mechanisms responsible for early damage to HMs and approaches to contrast it. Of course, the use of neonatal tissue in vitro has limitations for the applicability of these results to adult tissue, but provides an unimpeded insight into a scenario of cell pathology and dysfunction that is difficult to obtain with other experimental conditions. Future work should be aimed at clarifying the precise timecourse and the signal transduction cascades triggered by excitotoxicity or oxidative stress to devise preclinical tests for neuroprotective strategies. These might have to be tailored to the initial etiopathological insult.

Acknowledgments

This work was supported by a grant from Ministero dell'Università e Ricerca (Progetti di Ricerca di Interesse Nazionale) and grants from the Friuli Venezia Giulia Region. We thank Dr. Miranda Mladinic for advice in implementing immunohistochemistry experiments, and Dr. Micaela Grandolfo, and Dr. Walter Vanzella for their support with histological data acquisition and analysis.

References

Aldes, L.D., 1995. Subcompartmental organization of the ventral (protrusor) compartment in the hypoglossal nucleus of the rat. J. Comp. Neurol. 353, 89–108.

Anderson, C.M., Bridges, R.J., Chamberlin, A.R., Shimamoto, K., Yasuda-Kamatani, Y., Swanson, R.A., 2001. Differing effects of substrate and non-substrate transport inhibitors on glutamate uptake reversal. J. Neurochem. 79, 1207–1216.
Barber, S.C., Mead, R.J., Shaw, P.J., 2006. Oxidative stress in ALS: a mechanism of neurodegeneration and a therapeutic target. Biochim. Biophys. Acta 1762, 1051–1067.
Bayliss, D.A., Viana, F., Bellingham, M.C., Berger, A.J., 1994. Characteristics and postnatal development of a hyperpolarization-activated inward current in rat hypoglossal motoneurons in vitro. J. Neurophysiol. 71, 119–128.
Bergemalm, D., Jonsson, P.A., Graffmo, K.S., Andersen, P.M., Brännström, T., Rehnmark, A., Marklund, S.L., 2006. Overloading of stable and exclusion of unstable human superoxide dismutase-1 variants in mitochondria of murine amyotrophic lateral sclerosis models. J. Neurosci. 26, 4147–4154.
Berger, A.J., 2000. Determinants of respiratory motoneuron output. Respir. Physiol. 122, 259–269.
Bogdanov, M., Brown, R.H., Matson, W., Smart, R., Hayden, D., O'Donnell, H., Flint Beal, M., Cudkowicz, M., 2000. Increased oxidative damage to DNA in ALS patients. Free Radic. Biol. Med. 29, 652–658.
Boillée, S., Yamanaka, K., Lobsiger, C.S., Copeland, N.G., Jenkins, N.A., Kassiotis, G., Kollias, G., Cleveland, D.W., 2006. Onset and progression in inherited ALS determined by motor neurons and microglia. Science 312, 1389–1392.
Bories, C., Amendola, J., Lamotte d'Incamps, B., Durand, J., 2007. Early electrophysiological abnormalities in lumbar motoneurons in a transgenic mouse model of amyotrophic lateral sclerosis. Eur. J. Neurosci. 25, 451–459.
Bracci, E., Ballerini, L., Nistri, A., 1996. Spontaneous rhythmic bursts induced by pharmacological block of inhibition in lumbar motoneurons of the neonatal rat spinal cord. J. Neurophysiol. 75, 640–647.
Bruijn, L.I., Miller, T.M., Cleveland, D.W., 2004. Unraveling the mechanisms involved in motor neuron degeneration in ALS. Annu. Rev. Neurosci. 27, 723–749.
Campbell, S., Hablitz, J.J., 2005. Modification of epileptiform discharges in neocortical neurons following glutamate uptake inhibition. Epilepsia 46, 129–133.
Cheah, B.C., Vucic, S., Krishnan, A.V., Kiernan, M.C., 2010. Riluzole, neuroprotection and amyotrophic lateral sclerosis. Curr. Med. Chem. 17, 1942–1959.
Cifra, A., Nani, F., Sharifullina, E., Nistri, A., 2009. A repertoire of rhythmic bursting produced by hypoglossal motoneurons in physiological and pathological conditions. Philos. Trans. R. Soc. Lond. B: Biol. Sci. 364, 2493–2500.
Cifra, A., Nani, F., Nistri, A., 2011. Riluzole is a potent drug to protect neonatal rat hypoglossal motoneurons in vitro from excitotoxicity due to glutamate uptake block. Eur. J. Neurosci. 33, 899–913.
Cleveland, D.W., Rothstein, J.D., 2001. From Charcot to Lou Gehrig: deciphering selective motor neuron death in ALS. Nat. Rev. Neurosci. 2, 806–819.
Coyle, J.T., Puttfarcken, P., 1993. Oxidative stress, glutamate, and neurodegenerative disorders. Science 262, 689–695.
Danbolt, N.C., 2001. Glutamate uptake. Prog. Neurobiol. 65, 1–105.
Del Cano, G.G., Millan, L.M., Gerrikagoitia, I., Sarasa, M., Matute, C., 1999. Ionotropic glutamate receptor subunit distribution on hypoglossal motoneuronal pools in the rat. J. Neurocytol. 28, 455–468.
Del Negro, C.A., Chandler, S.H., 1998. Regulation of intrinsic and synaptic properties of neonatal rat trigeminal motoneurons by metabotropic glutamate receptors. J. Neurosci. 18, 9216–9226.
Del Negro, C.A., Morgado-Valle, C., Hayes, J.A., Mackay, D.D., Pace, R.W., Crowder, E.A., Feldman, J.L., 2005. Sodium and calcium current-mediated pacemaker neurons and respiratory rhythm generation. J. Neurosci. 25, 446–453.
Donato, R., Nistri, A., 2000. Relative contribution by GABA or glycine to Cl^--mediated synaptic transmission on rat hypoglossal motoneurons in vitro. J. Neurophysiol. 84, 2715–2724.
Enyedi, P., Czirják, G., 2010. Molecular background of leak K^+ currents: two-pore domain potassium channels. Physiol. Rev. 90, 559–605.
Essin, K., Nistri, A., Magazanik, L., 2002. Evaluation of GluR2 subunit involvement in AMPA receptor function of neonatal rat hypoglossal motoneurons. Eur. J. Neurosci. 15, 1899–1906.
Estevez, A.G., Stutzmann, J.M., Barbeito, L., 1995. Protective effect of riluzole on excitatory amino acid-mediated neurotoxicity in motoneuron-enriched cultures. Eur. J. Pharmacol. 280, 47–53.
Feldman, J.L., Del Negro, C.A., 2006. Looking for inspiration: new perspectives on respiratory rhythm. Nat. Rev. Neurosci. 7, 232–242.
Ferrante, R.J., Browne, S.E., Shinobu, L.A., Bowling, A.C., Baik, M.J., MacGarvey, U., Kowall, N.W., Brown Jr., R.H., Beal, M.F., 1997. Evidence of increased oxidative damage in both sporadic and familial amyotrophic lateral sclerosis. J. Neurochem. 69, 2064–2074.
Funk, G.D., Smith, J.C., Feldman, J.L., 1993. Generation and transmission of respiratory oscillations in medullary slices: role of excitatory amino acids. J. Neurophysiol. 70, 1497–1515.
Giniatullin, R., Nistri, A., Yakel, J.L., 2005. Desensitization of nicotinic ACh receptors: shaping cholinergic signaling. Trends Neurosci. 28, 371–378.
Greer, J.J., Funk, G.D., Ballanyi, K., 2006. Preparing for the first breath: prenatal maturation of respiratory neural control. J. Physiol. 570, 437–444.
Gurney, M.E., Pu, H., Chiu, A.Y., Dal Canto, M.C., Polchow, C.Y., Alexander, D.D., Caliendo, J., Hentati, A., Kwon, Y.W., Deng, H.X., Chen, W.J., Zhai, P., Sufit, R.L., Siddique, T., 1994. Motor neuron degeneration in mice that express a human Cu,Zn superoxide dismutase mutation. Science 264, 1772–1775.
Halliwell, B., 1992. Reactive oxygen species in the central nervous system. J. Neurochem. 59, 1609–1623.
Halliwell, B., Gutteridge, J.M.C., 1999. Free Radicals in Biology and Medicine, 3rd ed. Oxford Univ. Press, Oxford.
Horner, R.L., 2008. Neuromodulation of hypoglossal motoneurons during sleep. Respir. Physiol. Neurobiol. 164, 179–196.
Jacob, D.A., Bengston, C.L., Forger, N.G., 2005. Effects of *Bax* gene deletion on muscle and motoneuron degeneration in a sexually dimorphic neuromuscular system. J. Neurosci. 25, 5638–5644.
Kühnlein, P., Gdynia, H.J., Sperfeld, A.D., Lindner-Pfleghar, B., Ludolph, A.C., Prosiegel, M., Riecker, A., 2008. Diagnosis and treatment of bulbar symptoms in amyotrophic lateral sclerosis. Nat. Clin. Pract. Neurol. 4, 366–374.
Kuo, J.J., Siddique, T., Fu, R., Heckman, C.J., 2005. Increased persistent Na^+ current and its effect on excitability in motoneurones cultured from mutant SOD1 mice. J. Physiol. 563, 843–854.
Kuzhandaivel, A., Margaryan, G., Nistri, A., Mladinic, M., 2010a. Extensive glial apoptosis develops early after hypoxic-dysmetabolic insult to the neonatal rat spinal cord in vitro. Neuroscience 169, 325–338.
Ihara, Y., Nobukuni, K., Takata, H., Hayabara, T., 2005. Oxidative stress and metal content in blood and cerebrospinal fluid of amyotrophic lateral sclerosis patients with and without a Cu,Zn-superoxide dismutase mutation. Neurol. Res. 27, 105–108.
Izumi, Y., Shimamoto, K., Benz, A.M., Hammerman, S.B., Olney, J.W., Zorumski, C.F., 2002. Glutamate transporters and retinal excitotoxicity. Glia 39, 58–68.
Lacomblez, L., Bensimon, G., Leigh, P.N., Guillet, P., Meininger, V., 1996. Doseranging study of riluzole in amyotrophic lateral sclerosis. Amyotrophic Lateral Sclerosis/Riluzole Study Group II. Lancet 347, 1425–1431.
Lamanauskas, N., Nistri, A., 2006. Persistent rhythmic oscillations induced by nicotine on neonatal rat hypoglossal motoneurons in vitro. Eur. J. Neurosci. 24, 2543–2556.
Lamanauskas, N., Nistri, A., 2008. Riluzole blocks persistent Na^+ and Ca^{2+} currents and modulates release of glutamate via presynaptic NMDA receptors on neonatal rat hypoglossal motoneurons in vitro. Eur. J. Neurosci. 27, 2501–2514.
Lenaz, G., 1998. Role of mitochondria in oxidative stress and ageing. Biochim. Biophys. Acta 1366, 53–67.
Lindwall, C., Dahlin, L., Lundborg, G., Kanje, M., 2004. Inhibition of c-Jun phosphorylation reduces axonal outgrowth of adult rat nodose ganglia and dorsal root ganglia sensory neurons. Mol. Cell. Neurosci. 27, 267–279.
Lowe, A.A., 1980. The neural regulation of tongue movements. Prog. Neurobiol. 15, 295–344.
Mitchell, J.D., Borasio, G.D., 2007. Amyotrophic lateral sclerosis. Lancet 369, 2031–2041.
McClung, J.R., Goldberg, S.J., 1999. Organization of motoneurons in the dorsal hypoglossal nucleus that innervate the retrusor muscles of the tongue in the rat. Anat. Rec. 254, 222–230.
Mosfeldt Laursen, A., Rekling, J.C., 1989. Electrophysiological properties of hypoglossal motoneurons of guinea-pigs studied in vitro. Neuroscience 30, 619–637.
Nakagomi, S., Suzuki, Y., Namikawa, K., Kiryu-Seo, S., Kiyama, H., 2003. Expression of the activating transcription factor 3 prevents c-Jun N-terminal kinase-induced neuronal death by promoting heat shock protein 27 expression and Akt activation. J. Neurosci. 23, 5187–5196.
Nani, F., Cifra, A., Nistri, A., 2010. Transient oxidative stress evokes early changes in the functional properties of neonatal rat hypoglossal motoneurons in vitro. Eur. J. Neurosci. 31, 951–966.
Nistri, A., Ostroumov, K., Sharifullina, E., Taccola, G., 2006. Tuning and playing a motor rhythm: how metabotropic glutamate receptors orchestrate generation of motor patterns in the mammalian central nervous system. J. Physiol. 572, 323–334.
O'Brien, J.A., Isaacson, J.S., Berger, A.J., 1997. NMDA and non-NMDA receptors are co-localized at excitatory synapses of rat hypoglossal motoneurons. Neurosci. Lett. 227, 5–8.
O'Brien, J.A., Berger, A.J., 1999. Cotransmission of GABA and glycine to brain stem motoneurons. J. Neurophysiol. 82, 1638–1641.
Powers, R.K., Binder, M.D., 2003. Persistent sodium and calcium currents in rat hypoglossal motoneurons. J. Neurophysiol. 89, 615–624.
Quitadamo, C., Fabbretti, E., Lamanauskas, N., Nistri, A., 2005. Activation and desensitization of neuronal nicotinic receptors modulate glutamatergic transmission on neonatal rat hypoglossal motoneurons. Eur. J. Neurosci. 22, 2723–2734.
Ramirez, J.M., Quellmalz, U.J., Wilken, B., 1997. Developmental changes in the hypoxic response of the hypoglossus respiratory motor output in vitro. J. Neurophysiol. 78, 383–392.
Ramirez, J.M., Tryba, A.K., Peña, F., 2004. Pacemaker neurons and neuronal networks: an integrative view. Curr. Opin. Neurobiol. 14, 665–674.
Ramirez, J.M., Viemari, J.C., 2005. Determinants of inspiratory activity. Respir. Physiol. Neurobiol. 147, 145–157.
Rao, S.D., Weiss, J.H., 2004. Excitotoxic and oxidative cross-talk between motor neurons and glia in ALS pathogenesis. Trends Neurosci. 27, 17–23.
Richter, D.W., Ballanyi, K., Schwarzacher, S., 1992. Mechanisms of respiratory rhythm generation. Curr. Opin. Neurobiol. 2, 788–793.
Rosen, D.R., Siddique, T., Patterson, D., Figlewicz, D.A., Sapp, P., et al., 1993. Mutations in Cd/Zn superoxide dismutase gene are associated with familial amyotrophic lateral sclerosis. Nature 362, 59–62.
Rothstein, J.D., Kuncl, R.W., 1995. Neuroprotective strategies in a model of chronic glutamate-mediated motor neuron toxicity. J. Neurochem. 65, 643–651.
Rowland, L.P., Shneider, N.A., 2001. Amyotrophic lateral sclerosis. N. Engl. J. Med. 344, 1688–1700.
Shao, X.M., Feldman, J.L., 2005. Cholinergic neurotransmission in the preBötzinger Complex modulates excitability of inspiratory neurons and regulates respiratory rhythm. Neuroscience 130, 1069–1081.

Sharifullina, E., Ostroumov, K., Nistri, A., 2005. Metabotropic glutamate receptor activity induces a novel oscillatory pattern in neonatal rat hypoglossal motoneurones. J. Physiol. 563, 139–159.
Sharifullina, E., Nistri, A., 2006. Glutamate uptake block triggers deadly rhythmic bursting of neonatal rat hypoglossal motoneurons. J. Physiol. 572, 407–423.
Sharifullina, E., Ostroumov, K., Grandolfo, M., Nistri, A., 2008. N-methyl-D-aspartate triggers neonatal rat hypoglossal motoneurons in vitro to express rhythmic bursting with unusual Mg^{2+} sensitivity. Neuroscience 154, 804–820.
Shaw, P.J., Ince, P.G., Falkous, G., Mantle, D., 1995. Oxidative damage to protein in sporadic motor neuron disease spinal cord. Ann. Neurol. 38, 691–695.
Shaw, P.J., Ince, P.G., 1997. Glutamate, excitotoxicity and amyotrophic lateral sclerosis. J. Neurol. 2, S3–14.
Solomon, I.C., Halat, T.J., El-Maghrabi, M.R., O'Neal, M.H., 2001. Localization of connexin26 and connexin32 in putative CO_2-chemosensitive brainstem regions in rat. Respir. Physiol. 129, 101–121.
Solomon, I.C., 2003. Connexin36 distribution in putative CO_2-chemosensitive brainstem regions in rat. Respir. Physiol. Neurobiol. 139, 1–20.
Sokoloff, A.J., 2000. Localization and contractile properties of intrinsic longitudinal motor units of the rat tongue. J. Neurophysiol. 84, 827–835.
Spreux-Varoquaux, O., Bensimon, G., Lacomblez, L., Salachas, F., Pradat, P.F., Le Forestier, N., Marouan, A., Dib, M., Meininger, V., 2002. Glutamate levels in cerebrospinal fluid in amyotrophic lateral sclerosis: a reappraisal using a new HPLC method with coulometric detection in a large cohort of patients. J. Neurol. Sci. 193, 73–78.
Swash, M., Ingram, D., 1988. Preclinical and subclinical events in motor neuron disease. J. Neurol. Neurosurg. Psychiatry 51, 165–168.
Telgkamp, P., Ramirez, J.M., 1999. Differential responses of respiratory nuclei to anoxia in rhythmic brain stem slices of mice. J. Neurophysiol. 82, 2163–2170.
Tsujino, H., Kondo, E., Fukuoka, T., Dai, Y., Tokunaga, A., Miki, K., Yonenobu, K., Ochi, T., Noguchi, K., 2000. Activating transcription factor 3 (ATF3) induction by axotomy in sensory and motoneurons: a novel neuronal marker of nerve injury. Mol. Cell. Neurosci. 15, 170–182.
Turner, M.R., Kiernan, M.C., Leigh, P.N., Talbot, K., 2009. Biomarkers in amyotrophic lateral sclerosis. Lancet Neurol. 8, 94–109.
Umemiya, M., Berger, A.J., 1994. Properties and function of low- and high-voltage-activated Ca^{2+} channels in hypoglossal motoneurons. J. Neurosci. 14, 5652–5660.
Van Den Bosch, L., Van Damme, P., Bogaert, E., Robberecht, W., 2006. The role of excitotoxicity in the pathogenesis of amyotrophic lateral sclerosis. Biochim. Biophys. Acta 1762, 1068–1082.
Viana, F., Bayliss, D.A., Berger, A.J., 1993a. Calcium conductances and their role in the firing behavior of neonatal rat hypoglossal motoneurons. J. Neurophysiol. 69, 2137–2149.
Viana, F., Bayliss, D.A., Berger, A.J., 1993b. Multiple potassium conductances and their role in action potential repolarization and repetitive firing behavior of neonatal rat hypoglossal motoneurons. J. Neurophysiol. 69, 2150–2163.
Walling, A.D., 1999. Amyotrophic lateral sclerosis: Lou Gehrig's disease. Am. Fam. Physician 59, 1489–1496.
Wokke, J.H., 1996. Riluzole. Lancet 348, 795–799.
van Zundert, B., Peuscher, M.H., Hynynen, M., Chen, A., Neve, R.L., Brown Jr., R.H., Constantine-Paton, M., Bellingham, M.C., 2008. Neonatal neuronal circuitry shows hyperexcitable disturbance in a mouse model of the adult-onset neurodegenerative disease amyotrophic lateral sclerosis. J. Neurosci. 28, 10864–10874.

Postnatal Developmental Profile of Neurons and Glia in Motor Nuclei of the Brainstem and Spinal Cord, and Its Comparison with Organotypic Slice Cultures

Alessandra Cifra,[1] Graciela L. Mazzone,[1] Francesca Nani,[1]* Andrea Nistri,[1,2] Miranda Mladinic[1,2]

[1] Neurobiology Sector and IIT Unit, International School for Advanced Studies (SISSA), Trieste, Italy

[2] SPINAL (Spinal Person Injury Neurorehabilitation Applied Laboratory), Istituto di Medicina Fisica e Riabilitazione, Udine, Italy

Received 8 September 2011; accepted 18 October 2011

ABSTRACT: ***In vitro*** **preparations of the neonatal rat spinal cord or brainstem are useful to investigate the organization of motor networks and their dysfunction in neurological disease models. Long-term spinal cord organotypic cultures can extend our understanding of such pathophysiological processes over longer times. It is, however, surprising that detailed descriptions of the type (and number) of neurons and glia in such preparations are currently unavailable to evaluate cell-selectivity of experimental damage. The focus of the present immunohistochemical study is the novel characterization of the cell population in the lumbar locomotor region of the rat spinal cord and in the brainstem motor nucleus hypoglossus at 0–4 postnatal days, and its comparison with spinal organotypic cultures at 2–22 days *in vitro*. In the nucleus hypoglossus, neurons were 40% of all cells and 80% of these were motoneurons. Astrocytes (35% of total cells) were the main glial cells, while microglia and oligodendrocytes were <10%. In the spinal gray matter, the highest neuronal density was in the dorsal horn (>80%) and the lowest in the ventral horn (≤57%) with inverse astroglia numbers and few microglia. The number of neurons (including motoneurons) and astrocytes was stable after birth. Like in the spinal cord, motoneurons in organotypic spinal culture were <10% of ventral horn cells, with neurons <40%, and the rest made up by glia. The present report indicates a comparable degree of neuronal and glial maturation in brainstem and spinal motor nuclei, and that this condition is also observed in 3-week-old organotypic cultures.** © 2011 Wiley Periodicals, Inc. Develop Neurobiol 00: 000–000, 2011

Keywords: **motoneuron; astrocyte; microglia; oligodendrocyte; nucleus hypoglossus**

INTRODUCTION

In vitro models of the neonatal rat spinal cord (Clarac et al., 2004b; Grillner, 2006; Kiehn, 2006; Vinay and Jean-Xavier, 2008) and brain stem (Suzue, 1984; Smith and Feldman, 1987; Ramirez et al., 1996; Greer et al., 2006) have been extensively used to study physiological properties of rhythmic network activity in relation to patterned motor output. To ensure prolonged survival *in vitro* with robust network function, it is usually necessary to employ tissue preparations taken from rodents shortly after birth

Additional Supporting Information may be found in the online version of this article.

Alessandra Cifra and Graciela L. Mazzone contributed equally to this work.

**Present address:* Department of Neuroscience, Physiology and Pharmacology, Division of Biosciences, University College London, London, UK.

Correspondence to: A. Nistri (nistri@sissa.it).

Contract grant sponsors: Government of the Friuli Venezia Giulia Region; Italian Institute of Technology (IIT).

Published online 00 Month 2011 in Wiley Online Library (wiley onlinelibrary.com).
DOI 10.1002/dneu.20991

(P0–P5). Although it is known that functional maturation of these networks occurs postnatally (Paton et al., 1994; Berger et al., 1995; Clarac et al., 2004a), the identification of cell populations during this period is incompletely understood. To study long-term changes associated with motor circuit development and consolidation, spinal cord organotypic cultures that preserve the basic tissue cytoarchitecture can also be successfully employed (Spenger et al., 1991; Streit et al., 1991; Sibilla and Ballerini, 2009); nevertheless, their histological composition in terms of neurons and glia might depend on the length and conditions of the culturing procedure (Munoz-Garcia and Ludwin, 1985, 1986), an issue that requires clarification.

Recently, the neonatal rat spinal cord preparation has been exploited as a model to investigate early pathophysiological mechanisms triggered by experimental damage mimicking spinal cord injury (SCI; Taccola et al., 2008, 2010; Margaryan et al., 2010; Mazzone et al., 2010). Equally useful can also be studies with spinal cord organotypic cultures that allow long-term observation of and full experimental access to networks retaining the basic cytoarchitecture of the spinal cord (Sibilla and Ballerini, 2009). After 3 weeks *in vitro*, such cultures develop mature functional properties like Ca^{2+} oscillations (Fabbro et al., 2007) and synaptic activity (Streit et al., 1991) analogous to those observed in the postnatal spinal cord (Jiang et al., 1999) and express neuronal circuits identified with standard markers for neurotransmitters and ion channels (Avossa et al., 2003). Thus, several features of the injury model investigated with the isolated spinal cord can be recapitulated in organotypic slice cultures of the spinal cord, with similar process of nonapoptotic cell death ("parthanatos"-type) of neurons and motoneurons, and preservation of glial cells (Mazzone et al., 2010; Mazzone and Nistri 2011a). Furthermore, neuroprotection by glutamate receptor antagonists and riluzole observed in organotypic slices resembles the effect observed with the isolated spinal cord (Rothstein and Kuncl, 1995; Guzman-Lenis et al 2009; Mazzone and Nistri 2011b). It should be emphasized that such lesion models have demonstrated differential, cell-selective damage of neurons or glia depending on the experimental injury protocol (Cifra et al., 2011; Kuzhandaivel et al., 2011).

Although studies with the neonatal rat spinal cord have enabled a first estimate of the minimal network size necessary for expressing the locomotor program (Margaryan et al., 2009, 2010; Nistri et al., 2010; Kuzhandaivel et al., 2011), the full description of neuronal types belonging to the central pattern generator (CPG) network of locomotion remains incomplete despite recent advances in mouse genetics identifying certain CPG interneurons in the low thoracic-upper lumbar region (Goulding, 2009; Kiehn, 2011). Furthermore, even if survival of glial cells may be important for any successful neuroprotection or repair after SCI (Brenneman et al., 1997; Schumacher et al., 2007; Richter and Roskams, 2008; Quincozes-Santos and Gottfried, 2011), the exact role of these cells in lesion models remains poorly understood.

Likewise, brainstem hypoglossal motoneurons (HMs) controlling tongue contraction represent an important motor output for CPGs expressing breathing, vocalization, suckling and swallowing (Lowe, 1980; Jean, 2001), and are early targets for bulbar ALS (DePaul and Abbs, 1987; DePaul et al., 1988; Haenggeli and Kato, 2002; Mitchell and Borasio, 2007). Models to mimic the initial dysfunction of these cells prior to the full ALS manifestation have related electrophysiological deficit to cell damage (Nistri et al 2006; van Zundert et al., 2008; Cifra et al., 2009; Nani et al., 2010; Cifra et al., 2011). Despite the functional role of glia in controlling HM output, for example by regulating glutamate uptake (Nistri et al., 2006), little is known about the type of glia at this developmental stage, and its relation to neuronal numbers.

The focus of the present study is a comparative description of various cell types in these motor networks, particularly at neonatal age or in organotypic culture, since previous investigations have not systematically taken into account distinct cell types when assessing experimental damage and drug-mediated neuroprotection.

MATERIALS AND METHODS

Brainstem or Spinal Cord Preparations

All experiments were carried out in accordance with the regulations of the Italian Animal Welfare act (DL 27/1/92 n.116) following the European Community directives no. 86/609 93/88 (Italian Ministry of Health authorization for the local animal care facility in Trieste D 69/98-B), and approved by the local authority veterinary service. Brainstems or spinal cords were removed from neonatal (P0 or P4 day old) Wistar rats killed by slowly raising levels of CO_2, and dissected in ice-cold, oxygenated (95 % O_2/5 % CO_2) Krebs solution containing (in mM): NaCl, 130; KCl, 3; NaH_2PO_4, 1.5; $CaCl_2$, 1; $MgCl_2$, 5; $NaHCO_3$, 25; glucose, 100 (pH 7.4; 300–320 mOsm). Tissue was immediately fixed in phosphate-buffered saline (PBS) containing 4% paraformaldehyde (24 h at 4°C) followed by 30% sucrose PBS for cryoprotection (24 h at 4°C).

J_ID: DNEU Wiley Ed. Ref. No.: 00149-2011.R1 Customer A_ID: DNEU20991 Date: 3-NOVEMBER-11 Stage: I Page: 3

Preparation and Maintenance of Organotypic Cultures

The experiments were conducted with embryonic organotypic slice cultures of spinal cord from pregnant Wistar rats (13 days of gestation) as previously reported (Mazzone et al., 2010; Mazzone and Nistri, 2011). The fetuses were delivered by caesarian section from timed-pregnant rats killed by slowly raising levels of CO_2. All efforts were made to reduce the number of animals used and to minimize animal suffering.

Slices were maintained in a medium containing 82% Dulbecco's Modified Eagle medium, 8% sterile water for tissue culture, 10% fetal bovine serum (FBS; Invitrogen, Milano, Italy), 5 ng mL^{-1} nerve growth factor (NGF) (osmolarity 300 mOsm, pH 7.35), and grown in culture for 2, 7, or 22 days *in vitro* (DIV) in accordance with standard procedures (Spenger et al., 1991; Streit et al., 1991; Streit, 1993; Avossa et al., 2003, 2006). Dulbecco's modified Eagles' medium high glucose (DME/HIGH), penicillin and streptomycin were purchased from Euroclone (Paignton,UK). Fetal calf serum was obtained from Invitrogen. NGF was from Alomone Laboratories (Jerusalem, Israel), while the other reagents were purchased from Sigma–Aldrich, Milan, Italy.

Selection of Antibodies for Immunohistochemistry

As indicated in Supporting Information Table 1, the following antibodies were used: NeuN (mouse monoclonal, 1:50 dilution; Chemicon, Millipore, Billerica, MA), SMI32 (mouse monoclonal, 1:200 dilution; Covance, Berkeley, CA), ChAT (goat polyclonal, 1:50 dilution; Chemicon, Millipore), S100 (rabbit polyclonal, 1:100 dilution; Dako, Glostrup, Denmark), GFAP (mouse monoclonal, 1:100; Sigma–Aldrich), Iba1 (rabbit polyclonal, 1:500 dilution; Wako, Osaka, Japan), O4 (mouse monoclonal, 1:200 dilution; R&D Systems, Minneapolis, MN), RIP (mouse monoclonal, 1:1000 dilution; Chemicon, Millipore), and NG2 (rabbit polyclonal, 1:100 dilution; Chemicon, Millipore).

The NeuN (neuronal nucleus) monoclonal antibody, whose neuronal target has recently been identified as Fox-3 (Kim et al., 2009), has been widely used in our lab (Taccola et al., 2008; Margaryan et al., 2009, Kuzhandaivel et al., 2010) as a reliable tool to detect differentiated neurons. SMI32, a marker of nonphosphorylated neurofilaments, stains motor neurons in spinal cord slices (Gotow and Tanaka, 1994; Carriedo et al., 1995, 1996), and as such, has been extensively validated in our lab (Taccola et al., 2008; Margaryan et al., 2009, Kuzhandaivel et al., 2010; Nani et al., 2010; Cifra et al., 2011). Identification of motoneurons has been further confirmed by immunostaining with ChAT antibody that labels cholineacetyltransferase, the synthetic enzyme of acetylcholine (Barber et al., 1984). It is noteworthy to point out that large diameter, ventral horn cells were always found to express NeuN and SMI32 (or ChaT), indicating that, even at an early developmental stage, such cells were clearly identifiable as motoneurons.

Anti-S100 recognizes the S100 protein that belongs to the family of Ca^{2+} binding proteins found in the cytoplasm and nuclei of astrocytes (Schmidt-Kastner and Szymas, 1990; Donato, 2003), while anti-GFAP recognizes glial fibrillary acidic protein (GFAP), an intermediate filament protein characteristic for white matter astrocytes (Eng, 1985). Iba1 (Ionized calcium binding adaptor molecule 1) antibody recognizes the carboxy-terminal sequence of Iba1, a calcium binding protein, specifically expressed in macrophages/microglia (Imai et al., 1996; Ito et al., 1998). NG2 is a chondroitin sulfate proteoglycan, membrane protein expressed mainly on the surface of oligodendrocyte precursor cells (Nishiyama et al., 1996), while the anti-O4 antibody is the earliest recognized marker specific for a sulfated glycolipid antigen of oligodendroglia (Sommer and Schachner, 1981). RIP monoclonal antibody selectively stains oligodendrocytes and their processes containing myelin basic protein (Friedman et al., 1989).

Primary antibodies were visualized using the corresponding secondary fluorescent antibody (Alexa Fluor 488, 544, or 594, at 1:500 dilution; Invitrogen). To visualize cell nuclei, slices were incubated in 1 μg mL^{-1} solution of 4′, 6-diamidino-2-phenylindole (DAPI) for 1 h or stained with Hoechst 33342 (10 mg mL^{-1} stock, final dilution 1:1000; Invitrogen) and mounted using Vectastain mounting medium (Vector Laboratories, Burlingame, CA).

Brainstem Immunostaining Procedure and Cell Counting

En bloc fixed brainstems were sectioned to obtain, on average, 30 cryostat tissue sections (30-μm thick) from each brainstem, which were collected sequentially on histology slides. To prevent duplication in the counting procedure, we normally analyzed six nonsequential sections that corresponded to the largest coronal area of the nucleus hypoglossus (on average 90,051 $\pm$ 1878 and 111,359 $\pm$ 2439 μm^2 for P0 and P4, respectively; $n = 72$ sections, $n = 3$ rats), as electrophysiological tests are typically performed on this area because of better preservation of motoneuron numbers. Immunohistochemistry experiments for P0 and P4 slices were performed in parallel. Sections were treated with blocking solution (1% fetal calf serum, 5% bovine serum albumin, 0.3% Triton X-100 in PBS) for 1 h at room temperature and then incubated overnight at 4°C with the aforementioned primary antibodies (see Material and Methods, previous sections). After the incubation with the secondary antibody slides were rinsed, stained with Hoechst and finally visualized with a TCS SP2 Leica confocal microscope (pinhole was airy 1 corresponding to 102 or 120 μm for 20× or 40× lens, respectively). Since the total area of the nucleus increased from P0 to P4 because of developmental brain growth, a 20,000 μm^2 region of interest [ROI, comprising the central part of the hypoglossal nucleus; see examples of Fig. 1(A) and Fig. 2(A–C)] was selected for each nucleus section in which immunopositive cells were counted using ImageJ (version 1.41 c, Wayne Rasband, National Institutes of Health, Bethesda, MD) software. F1 F2

ID: selvarajn Date: 3/11/11 Time: 17:28 Path: N:/3B2/DNEU/Vol00000/110159/APPfile/JW-DNEU110159

Only cells showing the biomarker together with Hoechst 33342 were considered for analysis. For both P0 and P4 developmental stages, the final number of counted cells was expressed as the average of all analyzed sections. NeuN and SMI32 could not be used in the same section in view of antibody cross-reactivity. Thus, to calculate the percentage of motoneurons (SMI32 positive cells) with respect to the observed neuronal population (NeuN positive cells), the average number of SMI32 positive cells (obtained from all examined sections) was expressed as percent over the average number of NeuN positive cells (obtained from an equivalent number of sections). The standard deviation (σ) of this percentage was calculated from the following equation:

$$z(x,y) = \frac{x}{y}; \qquad \sigma_z = \sqrt{\left(\frac{\partial z(x,y)}{\partial x}\right)^2 \sigma_x{}^2 \left(\frac{\partial z(x,y)}{\partial y}\right)^2 \sigma_y{}^2}$$

where x is the average number of motoneurons, y the average number of neurons, z the ratio between these variables, and σ_x, σ_y, σ_z the standard deviation of x, y, and z, respectively, and ∂_z/∂_x and ∂_z/∂_y are the partial derivatives of z with respect to x and y.

Spinal Cord Immunostaining Procedure and Cell Counting

Spinal cord preparations were sectioned as described for brainstem preparations. Toluidine blue staining and immunohistochemical labeling were performed with a free-floating method as reported previously (Taccola et al., 2008) using epifluorescence microscopy (Zeiss Axioskop2,

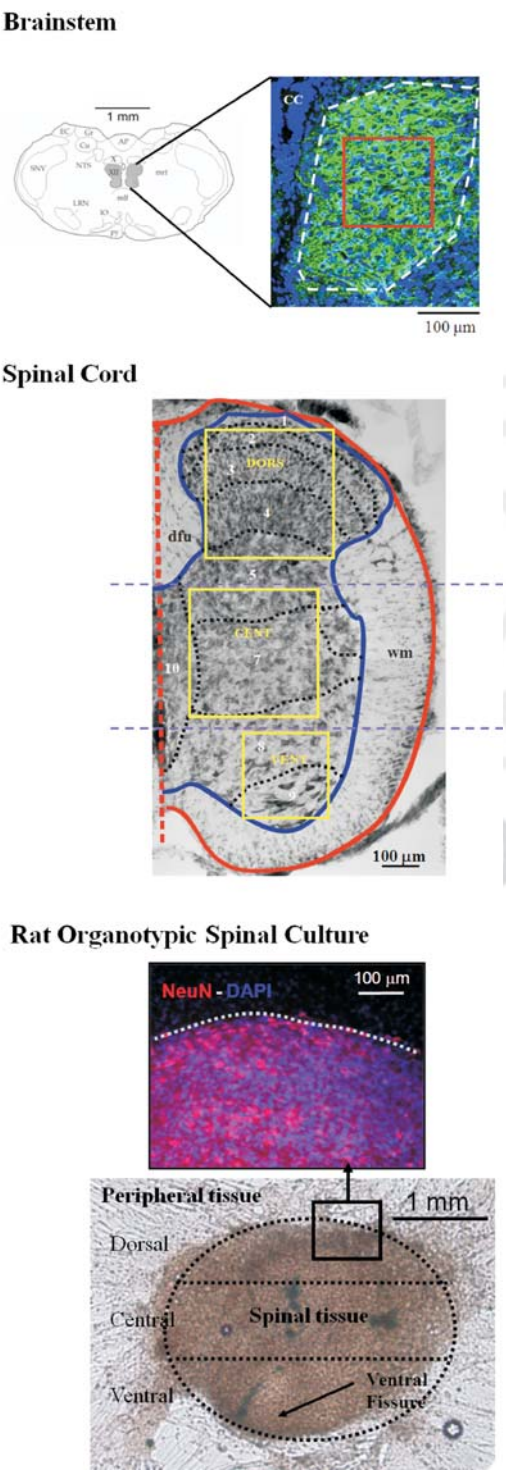

Figure 1 Schematic representation of ROIs in the brainstem, spinal cord and organotypic spinal culture preparations. (A) Brainstem: example of a confocal image of hypoglossal nucleus (dashed line) labeled with the motoneuron marker SMI32 (green) and cell marker Hoechst 33342 (blue). The red box indicates the 20,000 μm^2 ROI used for cell counting. Left scheme shows the localization of the nucleus in a brainstem section. CC = Central Canal. (B) Spinal cord: example of half section (30-μm thick) of lumbar 1 segment of the rat P0 spinal cord stained by Toluidine Blue. The gray matter has been outlined with blue line, while the contour of the spinal cord is shown in red. The Rexed layers have been outlined with dotted black lines and correspondently labeled with white Arabic numbers. Three different gray matter ROIs, namely dorsal, central and ventral, are shown with yellow boxes. The top horizontal dashed purple line indicates the lower edge of the dorsal funiculus (passing through the Rexed Layer 5) and is used to distinguish the dorsal ROI (comprising Rexed Layers 1–4 and the top part of Layer 5) from the central one (comprising Rexed Layers 5 (bottom)–7 and 10). A second horizontal purple line is drawn through the lower 1/3rd of the central gray area to distinguish the central ROI from the ventral one. Hence, the ventral ROI comprises Rexed Layers 8 and 9. The surface area of dorsal and central ROIs is 350 × 350 μm^2, while the ventral ROI is 235 × 235 μm^2. (C) Rat spinal cord organotypic culture. Example of 22 DIV slice with three ROIs, namely dorsal, central, and ventral (separated by the dotted lines). Inset shows typical neuronal staining (NeuN, in red) restricted to the spinal cord tissue region. DAPI (blue) is used for general cell staining.

COLOR

COLOR

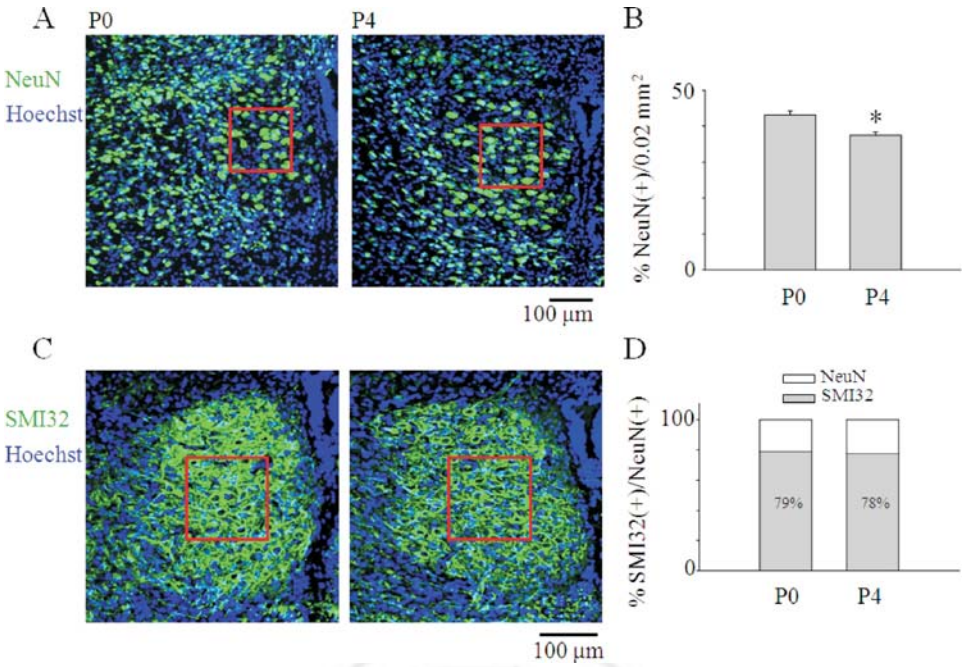

Figure 2 Neuronal (and motoneuronal) staining of rat hypoglossal nucleus. (A) Examples of confocal images showing NeunN positive cells (green) in the nucleus hypoglossus at P0 and P4 (left and right panel, respectively). Histogram (B) indicates the percentage of NeuN positive cells over the total Hoechst positive nuclei found in the ROI (red box) at P0 and P4 (Mann–Whitney Rank Sum test, $T = 434{,}000$, $p = 0.001$, $n = 3$ rats). (C) Motoneuronal SMI32 staining of nucleus hypoglossus ROI (red box) at P0 and P4 (left and right panel, respectively). Note that the NeuN antibody labels a nuclear epitope only, while the SMI32 antibody not only labels the motoneuron somatic filaments but also its processes, thus yielding a stronger immunopositive signal. Histogram (D) shows the percentage of SMI32 positive cells over the total NeuN positive neurons found at P0 and P4. σ values (omitted for clarity from the histogram) are 14 and 16% for P0 and P4, respectively (see Methods for the equation used for σ calculation; $n = 3$ rats).

Carl Zeiss MicroImaging, Thornwood, NY). In view of the very large number of histological sections provided by each rat spinal cord, we performed preliminary tests to assess if epifluorescence microscopy could supply numerical cell counts similar to the ones obtained with the more expensive and time-consuming confocal microscopy employed for the small number of brainstem sections. Hence, we used a standard ROI of 235 × 235 μm^2 [yellow boxes in Supporting Information Fig. 1(A)] to count and compare DAPI and NeuN positive nuclei under the two microscopy settings. First, with a Leica confocal microscope, we captured stack images from this ROI (using ten 30-μm-thick slices from three different spinal cords), and from each slice the confocal stack of 15 images [taken at 2 μm interval as exemplified by the insets to Supporting Information Fig. 1(A)] was averaged [Supporting Information Fig. 1(A)]. Second, the same region was analyzed with the fluorescence microscope [Supporting Information Fig. 1(B)]. The counting was performed with MetaVue software (Molecular Devices, Sunnyvale, CA). Supporting Information Fig. 1(C) shows that the results obtained with confocal and fluorescence microscopes were very similar. A very high correlation coefficient ($r = 0.989$) between observed cell numbers was calculated with either set of measures [Supporting Information Fig. 1(D)]. Thus, for routine counting of a large number of histological sections of the rat spinal cord, epifluorescence microscopy was used without appreciable loss of sensitivity for cell counting.

Figure 1(B) shows the three gray matter ROIs (dorsal, central, and ventral identified by corresponding yellow boxes) used for the present experiments with NeuN, SMI32, S100, and Iba1 markers. To construct these three ROIs reliably in each experiment, we identified regional borders by drawing a horizontal line [dashed purple in Fig. 1(B)] through the lower edge of the dorsal funiculus (dfu; passing through the Rexed Layer 5) to distinguish the dorsal ROI (comprising Rexed Layers 1–4 and the top part of Layer 5) from the central one (comprising Rexed Layers 5 (bottom)–7 and 10). A second dashed line passing through the lower 1/3rd of the central gray area was used to distinguish the central from the ventral ROI. Hence, the ventral ROI comprised Rexed Layers 8 and 9. The dimensions of dorsal and central ROIs were 350 × 350 μm^2, and 235 × 235 μm^2 for the ventral ROI [Fig. 1(B)]. At P0, T12 coronal hemisections showed that the average length of the gray matter from the tip of the dorsal horn to the tip of the ven-

tral horn was 1.22 ± 0.07 mm (halfwidth was 0.82 ± 0.08 mm; $n = 8$). These values became larger at P4 (1.48 ± 0.04 mm and 0.9 ± 0.09 mm; $n = 6$) because of tissue growth. Nonetheless, counting the total number of DAPI-positive cells in two random samples from P0 and P4 spinal cords yielded similar cell numbers (5443 at P0 and 5494 at P4) indicating that these cells were at postmitotic stage. Hence, the relative percentage of cells remained similar at these two ages: 19% (in the white matter) and 81% (in the gray matter) at P0, and 21% (in the white matter), and 79% (in the gray matter) at P4. These observations enabled comparing cell numbers at these two postnatal ages. For cell counting, we used either "eCELLence" (Glance Vision Tech, Trieste, Italy) or MetaVue software.

When biomarker staining was diffuse, like in the case of GFAP, NG2, O4, and RIP, data quantification was performed in terms of immunofluorescence intensity (expressed in arbitrary units, AU) with MetaVue imaging software using the densitometry function to calculate mean signal intensity in the white matter areas bordering the dorsal, central, and ventral gray matter. These regions were referred to with respect to the adjacent gray matter ROI. Data were averaged from at least three different sections from three different spinal cords.

Organotypic Slice Immunostaining and Cell Counting

Cultures were fixed in 4% paraformaldehyde for 30 min at room temperature and stored in PBS until use in accordance with previous reports (Mazzone et al., 2010; Mazzone and Nistri, 2011). Briefly, slices were blocked with 3% fetal calf serum (FCS), 3% bovine serum albumin (BSA), 0.3% Triton in PBS (blocking solution) for 1 h at room temperature, followed by overnight incubation at 4°C in a blocking solution containing the primary antibody, previously described, using the following dilutions: NeuN (1:250), SMI32 (1:1000), Iba1 (1:750), S100 (1:1000), O4 (1:200), GFAP (1:500), and NG2 (1:200). The selection of different antibody concentrations from those used for the brainstem or spinal cord was made to optimize immunostaining on the basis of tissue thickness and compactness. For each slice culture, the number of NeuN positive cells was obtained by counting stacks of 25–30 images (20× magnification) in an area of 0.56 mm^2 with a confocal microscope, and quantified with "eCELLence" software. NeuN positive cells were counted in three ROIs (namely, dorsal, central and ventral) as exemplified in Fig. 1(C). The relative size of ROI was arbitrarily chosen as 1/3rd of the total surface of the slice as previously described (Mazzone et al., 2010; Mazzone and Nistri, 2011). The number of motoneurons was counted using a Zeiss Axioskop2 microscope as previously described (Mazzone et al., 2010). Quantification of S100, NG2, and O4 at 2, 7, and 22 DIV was obtained, with a confocal microscope, by measuring the mean fluorescence intensity, and was performed by always maintaining the same pinhole (airy 1, corresponding to 85 μm with 10× lens) and the same confocal settings for comparison purpose between different samples, within a stack profile in an area of 2.17 mm^2. The S100 or GFAP biomarker signals were collected as mean fluorescence intensity of the three ROIs (0.25 mm^2 in each slice) with densitometry analysis using a Zeiss Axioskop2 microscope and MetaVue software. It should be pointed out that the organotypic culture method involves starting with a comparatively thick embryonic spinal cord slice that is progressively flattened out during culturing with incubation in a rotating drum system to finally achieve the basic spinal cytoarchitecture after a few weeks (Spenger et al., 1991; Streit et al., 1991). Hence, this procedure produces, on the one hand, loss of labile cells gradually eliminated into the extracellular medium as well as production of new (nonneuronal) cells through mitotic division (Gähwiler et al., 1997; Gähwiler et al., 2001). For these reasons, when certain glial biomarkers (S100, GFAP, NG2, O4) that do not unequivocally label nuclei only are employed, it is difficult to obtain absolute numbers of glial cells in a defined area and is more convenient to express immunostaining in terms of fluorescence intensity. This approach, however, cannot reliably differentiate between fluorescence changes within the same cell population or acquisition of new fluorescence signal by previously insensitive cells. These experimental constraints imply that fluorescence intensity data should be merely taken as an index of glial expression at that particular time point in culture. The number of Iba1 positive cells was analyzed using confocal microscopy, whereby a stack of five images (40× magnification) were counted with "eCELLence." The total number of Iba1 positive cells was obtained for each experimental condition as the total number of positive cells in all stacks in an area of 0.15 mm^2. For each marker, values (related to cell number and mean fluorescence intensity) were normalized by the area (μm^2) to obtain cell density.

Statistics

Results were expressed as means ± SEM unless otherwise indicated; n refers to the number of animals (brainstem) or sections (spinal cord) or slices (organotypic cultures). For statistical calculations, we used SigmaStat 3.11 (Systat Software, Chicago, IL). When comparing two groups, the Student's t test for parametric data (power of performed test with alpha = 0.050) or the Mann–Whitney Rank Sum Test for nonparametric data were applied. For multiple comparisons the ANOVA test for parametric data followed by the Tukey–Kramer *post hoc* test was used. Nonparametric values were analyzed with the Kruskal–Wallis test. Two groups of data were considered statistically different if $p \leqslant 0.05$.

RESULTS

Neuronal Populations in the Neonatal Rat Nucleus Hypoglossus

To describe the relative neuronal composition in the nucleus hypoglossus during neonatal development,

we analyzed brainstem slices, comprising the nucleus hypoglossus, from P0 and P4 rats. At either age neurons represented about the 40% of the all Hoechst positive cells with a significant ($p = 0.001$) decrease in their number from P0 (43.1% ± 1.1%) to P4 [37.4% ± 0.9%; $n = 3$ rats; Fig. 2(B)]. We further investigated the number of SMI32 positive cells [with somatic diameter >25 μm; Fig. 2(C)] over the total NeuN positive cells to estimate the relative number of motoneurons, which according to the literature are the most abundant neuron type in the hypoglossal nucleus (Boone and Aldes, 1984; Viana et al., 1990). It is noteworthy that the NeuN antibody labels a nuclear epitope only, while the SMI32 antibody not only labels the motoneuron somatic filaments but also its processes, thus yielding a stronger immunopositive signal [Fig. 2(A–C)]. We found that motoneurons represented about the 30% of the all Hoechst positive cells in each ROI [30.2% ± 1.1% at P0 and 28.9% ± 0.9% at P4; $n = 3$ rats; Fig. 2(C,D)], corresponding to 79% ± 14% and 78% ± 16% (mean ± σ) of the neuronal population (see methods) at P0 and P4, respectively [Fig. 2(D)].

Thus, while these data confirm the preponderance of motoneurons in the rat nucleus hypoglossus, they provide for the first time their quantification (about 80%) over the total neuronal population. The remaining neurons likely belong to interneuron population of the rat nucleus hypoglossus (Boone and Aldes, 1984; Viana et al., 1990), mainly including inhibitory neurons (Takasu and Hashimoto, 1988; Tanaka et al., 2003).

Glia Populations in the Neonatal Rat Nucleus Hypoglossus

The hypoglossal nucleus is a compact motor network predominately made up of gray matter. Nonetheless, glial cells do exist within this structure and presumably contribute to the expression and function of the motor network (Grass et al., 2004). To characterize the different type of glial cells present in this nucleus, we first estimated the number of astrocytes using S100 and GFAP markers. In the adult rat brain, S100 is expressed by both fibrous and protoplasmic astrocytes in the gray matter (Cocchia, 1981; Didier et al., 1986), while GFAP, an intermediate filament protein, is characteristic for white matter astrocytes (Eng, 1985; Didier et al., 1986). Accordingly, in the P4 rat nucleus hypoglossus, there are very few GFAP positive astrocytes against the predominant occurrence of S100 positive cells (Cifra et al., 2011). Quantifying these cell populations indicated that the number of S100 positive astrocytes over the total Hoechst positive cells was 34.8% ± 1.5% and 33.7% ± 1.4% at P0 and P4, respectively [Fig. 3(A,B)]. GFAP staining, F3 instead, was detectable only in the pericanal zone at P4 [Fig. 3(C)] and along the slice outer edge at both P4 and P0 stages [Supporting Information Fig. 2(B), lower panels]. Consistent with this observation, NG2 and O4 staining, specific for distinct cells of the oligodendrocyte lineage, were detected only at the slice edge with no signal within the nucleus hypoglossus [Supporting Information Fig. 2(A,B)].

To estimate the percentage of microglia in the hypoglossal nucleus, we used Iba1 antibody staining that detected a low number of positive cells [10.2% ± 0.9% and 7.3% ± 0.5% at P0 and P4, respectively; Fig. 3(D,E)].

Thus, at P0 and P4 developmental stages, S100 positive astrocytes and Iba1 positive cells represented the main glia type in the rat nucleus hypoglossus: these two glial populations accounted for 45% of the total cell population within the nucleus hypoglossus ROI with S100 positive astrocytes being more abundant than any other glial cell type.

Neurons in the Neonatal Rat Spinal Cord

The relative proportion of neuronal and glial cells in the rat spinal cord at P0 and P4 was investigated in the T12-L2 segments that are believed to contain the principal neuronal elements of the rat locomotor CPG (Kiehn, 2006).

To reveal the percentage of neurons present in the P0 and P4 rat spinal cord, NeuN positive cells [Fig. 4(A), F4 upper panels] were compared with the total cell number of DAPI positive cell nuclei in three different ROIs (dorsal, central, and ventral) as shown in Figure 1(B). Thus, the neuronal content varied from ~50% in the ventral ROI to ~80% in the dorsal one [Fig. 4(B)]. Nevertheless, in dorsal and central ROIs the percentage of neurons did not significantly change from P0 to P4 [Fig. 4(B)], while it significantly fell (from 57% at P0 to 45% at P4) in the ventral ROI [Fig. 4(B)].

To ensure that the statistically significant drop in neurons located in the ventral horn from P0 to P4 was not due to the bias caused by the ROI placement, we repeated cell counting (on six different slices for each age) in a different ROI (200 × 300 μm^2) that still contained Rexed layer 9. As shown in Supporting Information Figure 3(A), comparison between the standard ventral ROI and the new ROI gave very similar results as % of NeuN positive cells. In fact, at P0 these values were 57 ± 2 and 58 ± 4, and at P4 45 ± 5 or 42 ± 5, respectively.

To examine the number of spinal motoneurons, we counted the large SMI32 positive cells in the ventral

J_ID: DNEU Wiley Ed. Ref. No.: 00149-2011.R1 Customer A_ID: DNEU20991 Date: 3-NOVEMBER-11 Stage: I Page: 8

COLOR

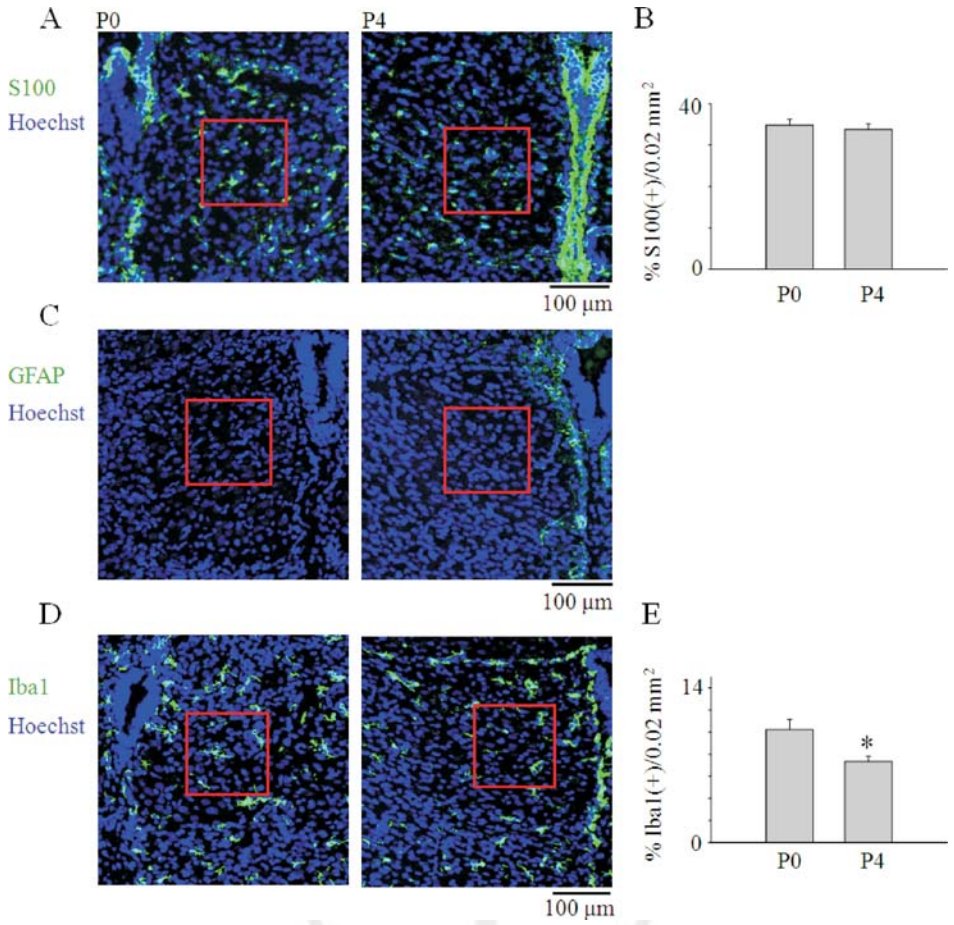

Figure 3 Glial staining of the nucleus hypoglossus. (A) Confocal images showing S100 positive astrocytes in the same ROI (red box) used for neuronal counting (see Fig. 2) at P0 and P4. Percentage of S100 positive cells over the total Hoechst positive nuclei is quantified in the histogram (B). As previously reported, S100 immunoreactivity is also present in ependymal cells (Cifra et al., 2011) outside the ROI. (C) Example of confocal images with no GFAP signal at P0 and P4. Note that, according to previous observations (Cifra et al., 2011), GFAP staining (green) is detectable along the borders of the central canal at P4 (right panel). (D) Examples of microglia staining (Iba1 positive cells; green) in the nucleus hypoglossus ROI (red box) at P0 and P4. Histogram (E) shows the percentage of Iba1 positive cells over the total Hoechst positive nuclei at P0 and P4 (Mann–Whitney Rank Sum Test, $T = 406{,}500$, $p = 0.021$, $n = 3$ rats).

gray matter [Fig. 4(A), lower panels, and Fig. 4(D), left], that correspond to ChaT positive cells [Fig. 4(D), middle] as indicated by their co-staining [Fig. 4(D), right]. Those cells had nuclear diameter >15 μm and a star-like soma with diameter >25 μm [Fig. 4(A), lower panels, Fig. 4(D)]. Approximately 18 such cells were detected from an average of ventral ROIs ($n = 18$) at P0 and P4 [Fig. 4(C)]. At P0, motoneurons represented 8% $\pm$ 4% of all cells in the ventral ROI (SMI32 over DAPI counting; $n = 10$ slices from three different spinal cords). At P4 this percentage did not significantly change (10% $\pm$ 2%; $n = 10$ slices from three different spinal cords).

S100 or GFAP Positive Glia in the Neonatal Rat Spinal Cord

The mean number of astrocytes was deduced by counting S100 positive cells [Fig. 5(A)] in the same ROI used for neuronal counts [Fig. 1(B)], and found to range from $\sim$15% in the dorsal region to 40% in the ventral one [Fig. 5(B)], where astrocyte numbers significantly increased from P0 to P4 [Fig. 5(B)]. Using the same approach employed to validate the data from NeuN counts [see Supporting Information Fig. 3(A)], we repeated S100 positive cell counts in these two ROIs [Supporting Information Fig. 3(B)] and found that, at P0, the S100 % values were 37 $\pm$ 3

F5

ID: selvarajn Date: 3/11/11 Time: 17:28 Path: N:/3B2/DNEU/Vol00000/110159/APPfile/JW-DNEU110159

J_ID: DNEU Wiley Ed. Ref. No.: 00149-2011.R1 Customer A_ID: DNEU20991 Date: 3-NOVEMBER-11 Stage: I Page: 9

COLOR

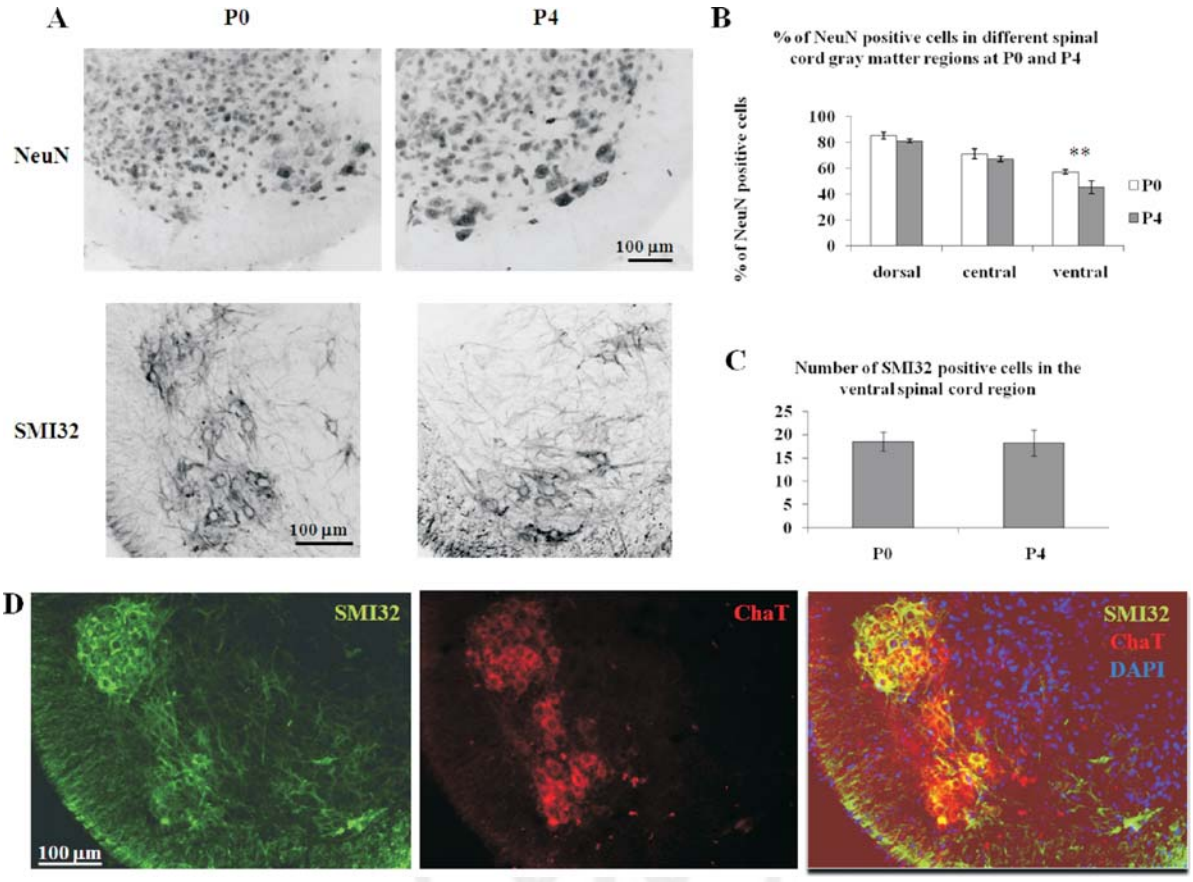

Figure 4 Quantification of neurons and motoneurons in sections of the P0 and P4 rat isolated spinal cord and co-staining of lumbar motoneurons in ventral ROI (P0) with the specific markers SMI32 and ChaT. (A) Examples of NeuN (upper panels) or SMI32 staining (lower panels) in the ventral ROI of the lumbar 1 segment from P0 (left panels) or P4 (right panels) rat spinal cord. (B) Percentage of NeuN positive cells over the total number of cells (DAPI positive nuclei) in dorsal, central and ventral ROIs at P0 (open bars) and P4 (gray bars). Data are from >12 sections from three rats. Ventral ROI data are significantly different ($p = 0.008$). (C) Similar number of motoneurons (SMI32 positive cells) in the ventral ROI at P0 and P4 (18 sections from three rats). (D) In 30 μm thick sections from the isolated spinal cord, complete signal overlap was observed confirming the equivalence of SMI32 and ChaT as motoneuron-specific markers. Scale bar (100 μm) applies to all panels.

or 38 ± 3, and, at P4, 47 ± 6 or 49 ± 6, respectively. All together, these results confirmed the slight, yet significant decrease in NeuN positive, and increase in S100 positive cells in the ventral horn between P0 and P4.

Unlike S100 immunoreactive cells, GFAP positive astrocytes had their cell body exclusively present in the white matter of both P0 and P4 spinal cords, from which their processes spread to the gray matter [Fig. 5(C)]. Because of the diffuse fibrillary GFAP staining, it was not possible to count the number of GFAP positive cells: their fluorescence signal intensity (measured in the regions adjacent the gray matter ROIs) did not change between P0 and P4 [Fig. 5(D)]. Nonetheless, GFAP staining suggested a topographical change from P0 to P4 in the orientation of cell processes, since the initial palisade-like arrangement [Fig. 5(C), left] was replaced by ample arborization at P4 [Fig. 5(C), right].

Iba1 Positive Cells in the Spinal Cord

Throughout a spinal hemisection, microglial cells, detected as Iba1 positive elements [Fig. 6(A), right panels], were found in low number compared with the total number of DAPI-stained cells [Fig. 6(A), left panels]. On average, these cells were about 4% at P0 and P4 [Fig. 6(B)]. The vast majority (95%) showed ramified morphology characteristic of resting microglia [Fig. 6(C)] with sporadic occurrence (5%) of ameboid microglia engulfing pyknotic cells, suggestive of their activated state [Fig. 6(D)].

ID: selvarajn Date: 3/11/11 Time: 17:29 Path: N:/3B2/DNEU/Vol00000/110159/APPfile/JW-DNEU110159

J_ID: DNEU Wiley Ed. Ref. No.: 00149-2011.R1 Customer A_ID: DNEU20991 Date: 3-NOVEMBER-11 Stage: I Page: 10

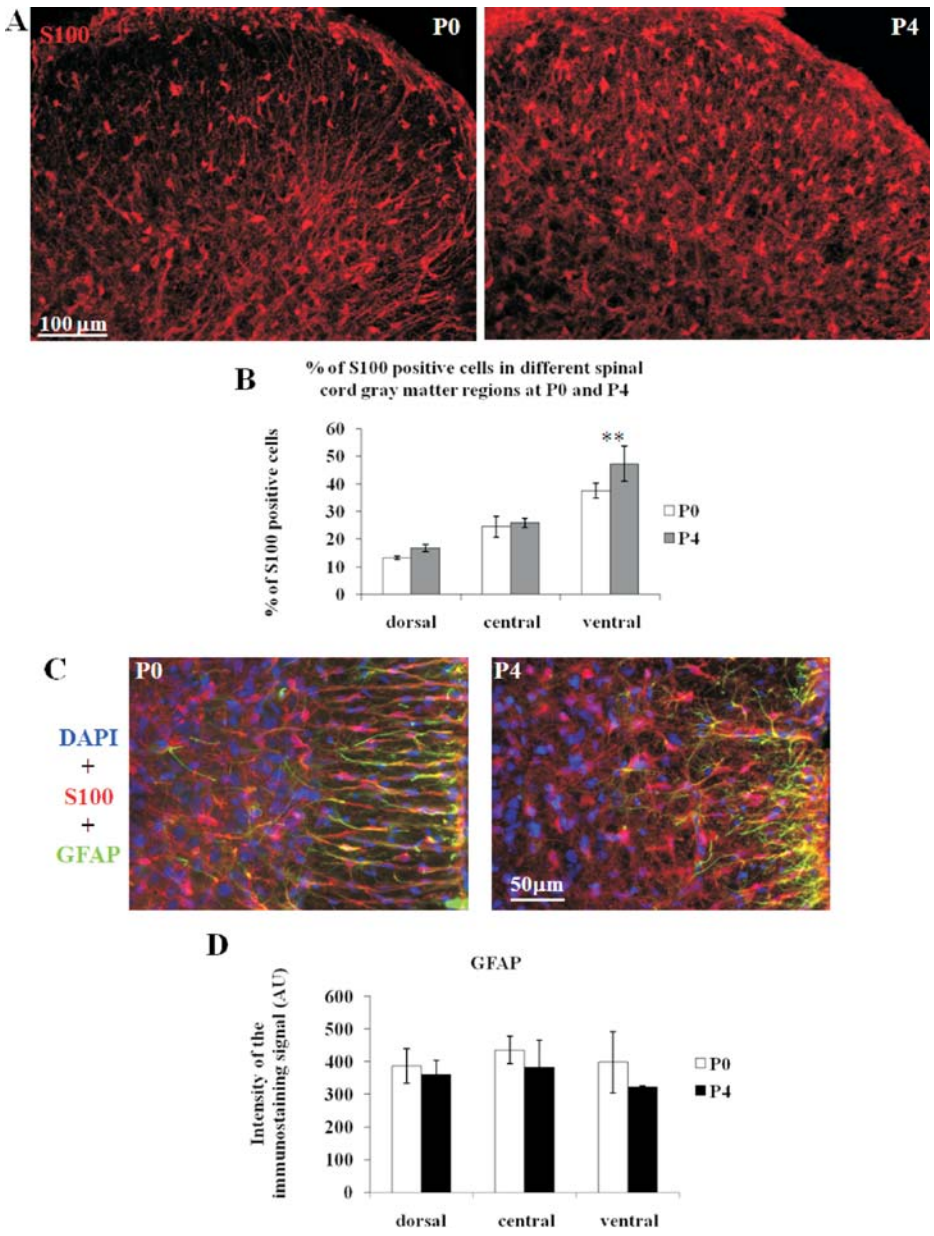

COLOR

Figure 5 Astrocyte labeling in sections of P0 and P4 rat L1 spinal cord. (A) S100 staining of the dorsal ROI at P0 (left) and P4 (right). (B) Percentage of S100 positive cells over total DAPI-stained cells in dorsal, central, and ventral ROIs (P0 white bars, P4 gray bars). Data are from >12 sections from three spinal cords: significant difference was found for the ventral ROI only ($p = 0.002$). (C) Examples of GFAP staining (green) at P0 (left) and P4 (right) restricted to the white matter of the central region, while S100 staining (red) was diffuse. (D) Histogram shows immunofluorescence intensity (expressed in arbitrary units, AU) with no significant difference between P0 and P4. Data were averaged from at least three white matter ROIs (>3 sections from three spinal cords).

NG2-O4 Positive Cells in the Spinal Cord

As detailed in methods, cells from oligodendrocyte lineage were detected using two different antibodies, namely NG2 that recognizes oligodendrocyte precursor cells, and O4 that is the earliest marker specific for the oligodendroglial maturation. In addition, the RIP antibody was used to detect myelin. Both NG2 [Fig. 7(A)] and O4 [Fig. 7(C)] immunoreactivity was limited to the white matter. Because NG2 and O4 do not clearly stain cell nuclei and the cells immuno-

F7

ID: selvarajn Date: 3/11/11 Time: 17:29 Path: N:/3B2/DNEU/Vol00000/110159/APPfile/JW-DNEU110159

J_ID: DNEU Wiley Ed. Ref. No.: 00149-2011.R1 Customer A_ID: DNEU20991 Date: 3-NOVEMBER-11 Stage: I Page: 11

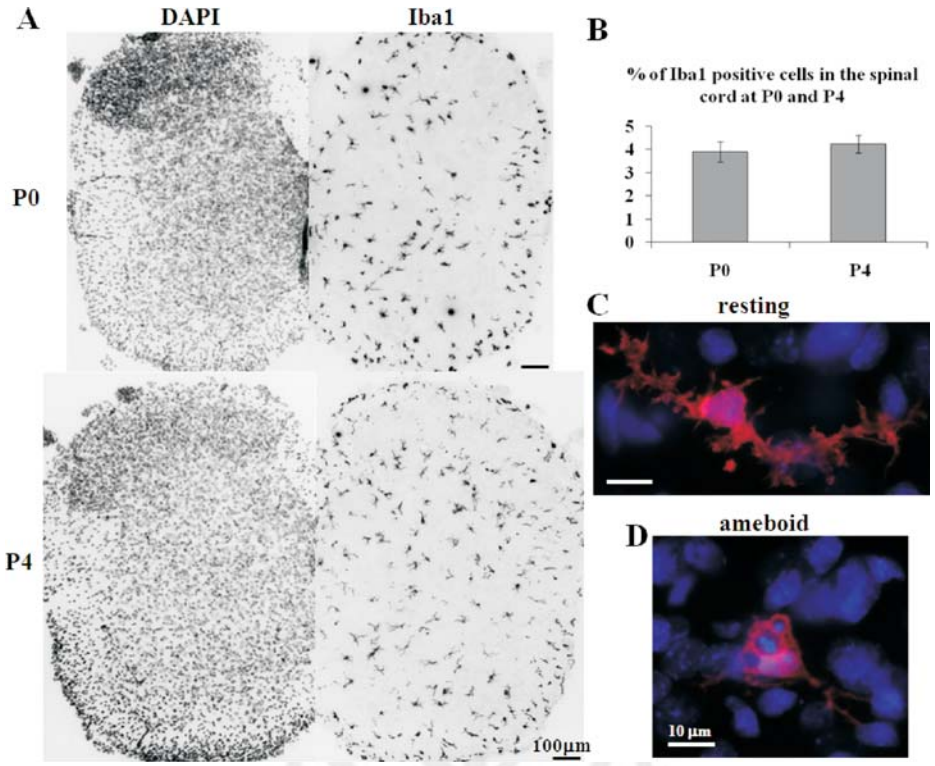

Figure 6 Quantification of microglial cells in lumbar sections of P0 and P4 spinal cords. (A) Left, DAPI staining at P0 (top panel) and P4 (bottom panel) is compared with Iba1 staining typical for microglia (right). (B) Histogram shows the percentage of Iba1 positive cells over total DAPI-positive cells. Data are from 30-μm-thick lumbar (L1) hemi-sections. No significant difference is apparent between P0 and P4 data (for each age $n = 7$ slices from 3 different spinal cords). (C) Example of resting microglia stained with Iba1 antibody (red; blue = DAPI staining) to show extensive arborization. (D) Example of ameboid microglia engulfing pyknotic nuclei stained with DAPI (blue). Scale bar in C and D = 10 μm.

positive to these markers have extensive processes, their staining pattern did not allow counting single cells. Thus, immunostaining intensity measured at P0 and P4 [Fig. 7(B–D)] suggested a significant decrease in NG2 staining from P0 to P4. Significant increase in O4 staining was found in the white matter bordering the ventral and central gray matter, while in the dorsal region the signal intensity remained similar [Fig. 7(D)]. Alongside such changes, at P4 we detected expression of mature oligodendrocytes producing myelin as indicated by the RIP signal apparent as a ring-like structure surrounding fibers [Fig. 7(E)].

Organotypic Spinal Cord Cultures

A prominent feature of the organotypic culture system is a time-dependent flattening and spreading of the tissue explants to remodel the networks in analogy to the original cytoarchitecture (Ballerini et al., 1999). Thus, we examined the topographical distribution of neuronal and non-neuronal cells in three ROI [indicated by the dotted lines in Fig. 1(C)], namely dorsal, central, and ventral. The relative size of each region was arbitrary chosen to represent circa 1/3rd of the total slice area as exemplified in Figure 1(C).

Neurons in the Organotypic Spinal Culture

Figure 8(A) exemplifies NeuN neuronal staining at 2, 7, and 22 DIV with data quantification in Figure 8(B), that demonstrates how NeuN positive elements were almost absent at 2 DIV, and rapidly grew after 7 DIV.

As exemplified in Figure 8(C), the number of NeuN positive cells at 22 DIV was very similar in the three ROIs and corresponded to 27% ± 3% of DAPI-positive cells. At the same time, NeuN staining was absent outside spinal tissue [see Fig. 1(C)].

Figure 8(D) (left panel) shows typical SMI32 staining in the ventral ROI (higher magnification in the right panel) where cells with typical motoneuron

ID: selvarajn Date: 3/11/11 Time: 17:29 Path: N:/3B2/DNEU/Vol00000/110159/APPfile/JW-DNEU110159

J_ID: DNEU Wiley Ed. Ref. No.: 00149-2011.R1 Customer A_ID: DNEU20991 Date: 3-NOVEMBER-11 Stage: I Page: 12

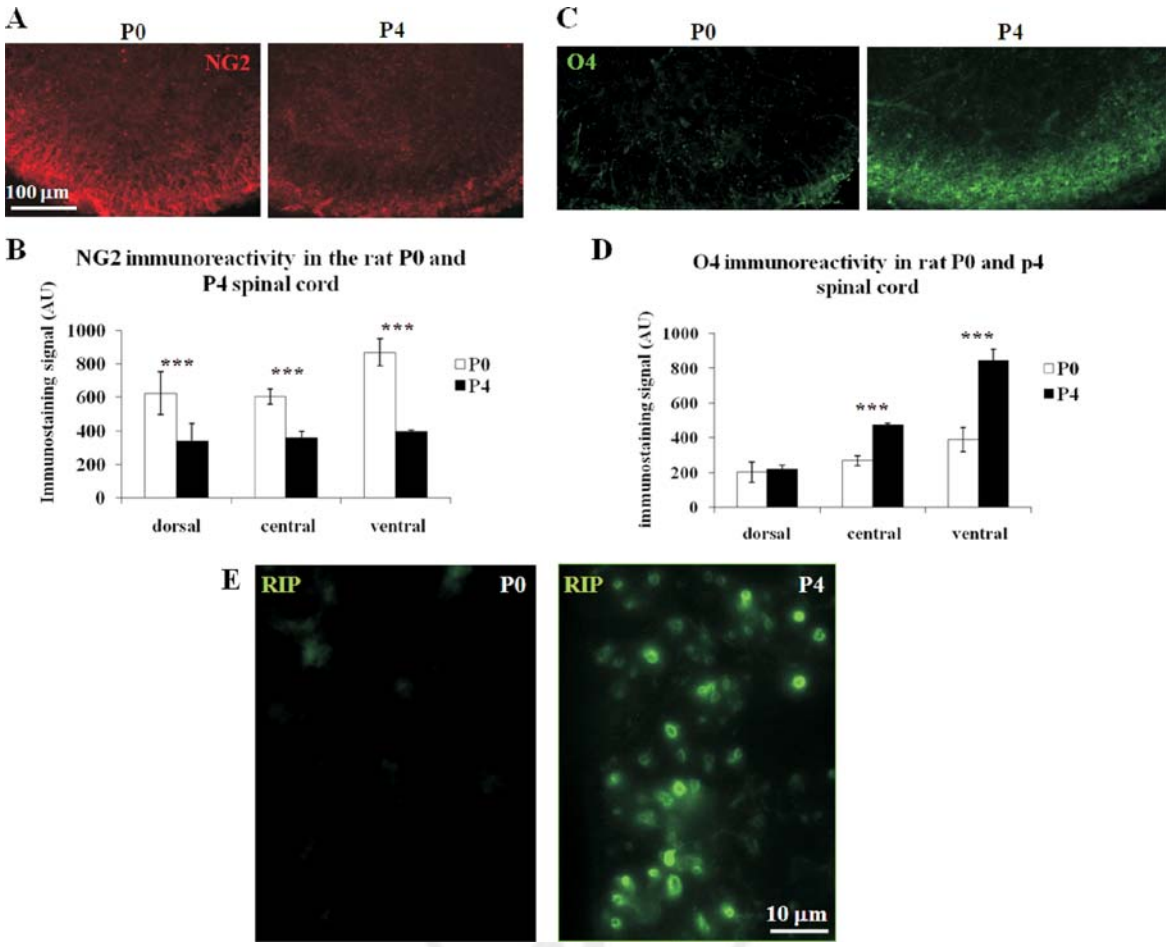

Figure 7 Quantification of oligodendrocyte staining in P0 and P4 rat spinal cords. (A) NG2 staining of oligodendrocyte precursor cells at P0 (left) and P4 (right) ventral lumbar (L1) ROI. Scale bar = 100 μm for A and C. (B) Histogram shows fall in immunofluorescence intensity (AU) from P0 to P4 for all white matter ROIs (>10 sections from three rats; $p < 0.001$). (C) Examples of O4 staining for mature oligodendrocytes at P0 (left) and P4 (right) in the same region as in (A). (D) Histogram shows increase in O4 immunofluorescence intensity (AU) from P0 to P4 for ventral and central white matter ROIs (>10 sections from three rats; $p < 0.001$). (E) Examples of myelin staining with RIP antibody in the central white matter at P0 (left) and P4 (right) spinal cords (30-μm-thick sections) showing very poor signal at P0, and substantial signal at P4 when ring-like staining is observed around axons.

size and morphology were seen (Spenger et al., 1991). In the ventral ROI at 22 DIV motoneurons were 11 ± 0.7 ($n = 18$), corresponding to ~6% of the local neurons. This result validates the delayed emergence of motoneurons in organotypic cultures of the mouse spinal cord (Avossa et al., 2003).

S100 or GFAP Positive Glia in Organotypic Slices

To characterize nonneuronal cells, we first analyzed the astrocyte maker S100 [Fig. 9(A)] that yielded differential immunopositivity at 2, 7, and 22 DIV, when considering the confocal mean fluorescence intensity within a stack profile of 2.17 mm^2 area. On average, mean fluorescence intensity values obtained with confocal whole slice analysis were different at the three time points in culture [Fig. 9(B)]. Once the cultures had reached the more advanced maturation stage (22 DIV), there was no significant difference in S100 immunopositivity in the three ROIs, in an area of 0.25 mm^2 [Fig. 9(C)].

At 22 DIV, GFAP immunopositivity confirmed widespread presence of astrocytes outside [Fig. 9(D), left] as well as inside [Fig. 9(D), middle] the spinal tissue where cells exhibited extensive arborization with a star-like soma [Fig. 9(D), right] and no regional difference in signal intensity [Fig. 9(E)].

ID: selvarajn Date: 3/11/11 Time: 17:29 Path: N:/3B2/DNEU/Vol00000/110159/APPfile/JW-DNEU110159

J_ID: DNEU Wiley Ed. Ref. No.: 00149-2011.R1 Customer A_ID: DNEU20991 Date: 3-NOVEMBER-11 Stage: I Page: 13

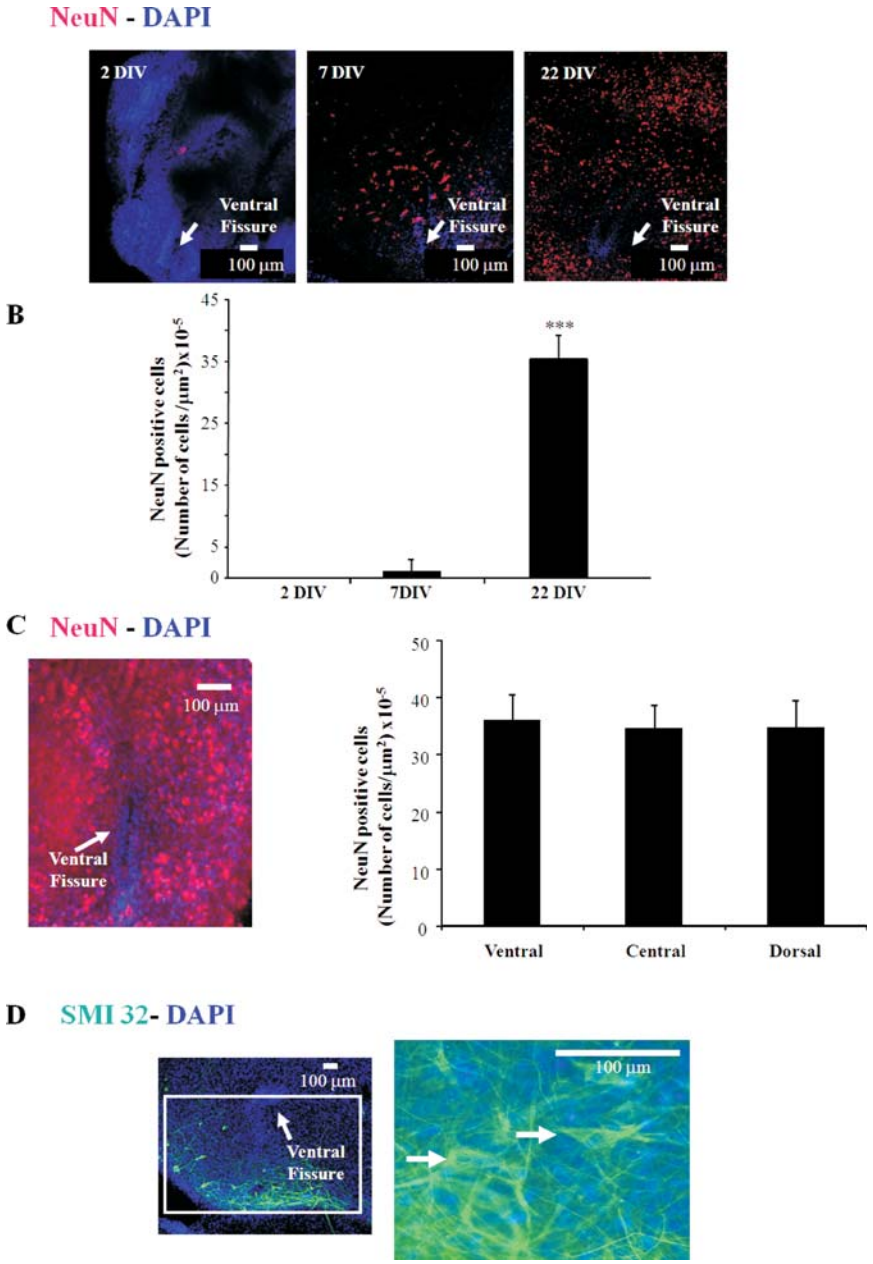

COLOR

Figure 8 Quantification of neuronal and motoneuronal staining in rat spinal cord organotypic cultures. (A) Examples of neuronal staining (red) at 2, 7, and 22 DIV. (B) Histogram showing the number of NeuN positive cells (4–14 different slices) over total number of DAPI-positive cells. Note that the average number of neurons was much larger at 22 DIV ($p = 0.0027$) vs. 7 DIV. (C) Histogram quantifies homogeneous distribution of NeuN staining (see example in red pseudo-color, left) at 22 DIV in three ROIs exemplified in Figure 1(C). (D) Motoneurons identified with SMI32 (green) after 22 DIV in the ventral ROI close to the ventral fissure (arrow; left panel). Higher magnification image (right panel) shows large soma of motoneurons.

Other Glial Cells in Organotypic Culture

The microglia marker Iba1 was evaluated at 2, 7, and 22 DIV as exemplified in Figure 10(A). At 2 DIV the immunoreactivity was restricted to spinal tissue with ameboid morphology [Fig. 10(A), top panels], while, at 7 DIV, the staining of ramified microglia was diffuse with similar distribution within and outside the slice [Fig. 10(A), middle panels]. At 22 DIV very few Iba1 positive cells were found confined to extraspinal spinal tissue [Fig. 10(A), lowermost panel]. Average

ID: selvarajn Date: 3/11/11 Time: 17:30 Path: N:/3B2/DNEU/Vol00000/110159/APPfile/JW-DNEU110159

J_ID: DNEU Wiley Ed. Ref. No.: 00149-2011.R1 Customer A_ID: DNEU20991 Date: 3-NOVEMBER-11 Stage: I Page: 14

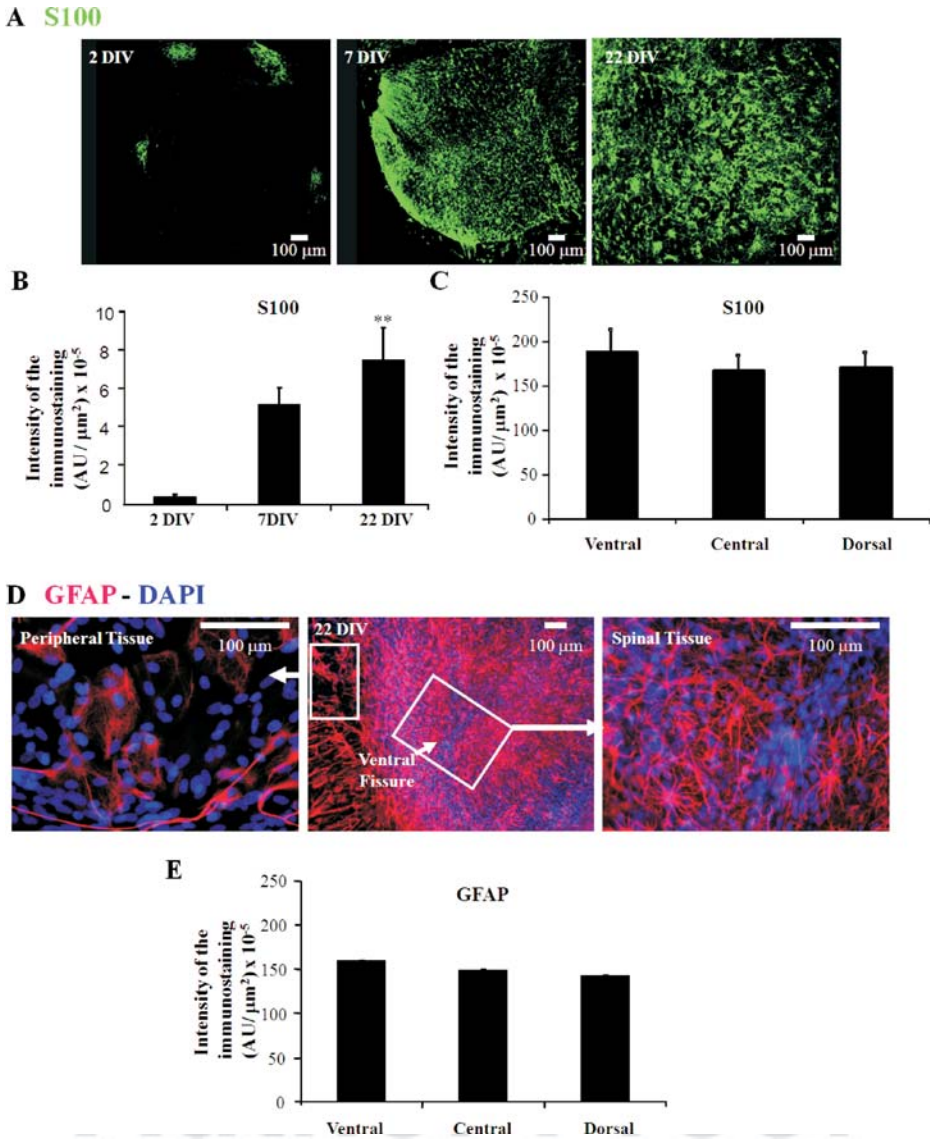

Figure 9 Quantification of glial staining in organotypic spinal cultures. (A) Representative S100 staining (green) at 2, 7, and 22 DIV. (B) Histogram showing strong increase in mean fluorescence intensity (AU) from 2 to 22 DIV ($n = 4$–5, $^{**}p < 0.01$ vs. 2 DIV). (C) Histogram shows equivalent staining of three ROIs with S100 at 22 DIV ($n = 12$). (D) Examples of GFAP staining (red) at 22 DIV within (middle, and right at higher magnification) or outside (left) the spinal tissue. (E) Histogram showing the GFAP fluoresce intensity quantify in the three ROIs of the spinal tissue ($n = 3$) with no significant difference.

data for Iba1 positive cells are provided in Fig. 10(B) showing time-dependent redistribution of microglia from the spinal tissue, where they represented 0.3% ± 0.1 % of total DAPI positive nuclei; $n = 4$ (compared to 2.5% ± 1.0% in extraspinal regions; $n = 4$). Oligodendrocytes were analyzed by using NG2 and O4 biomarkers as shown in Fig. 10(C) with representative immunostaining at 22 DIV. Low signal intensity was quantified with confocal analysis that demonstrated weak NG2 positivity without strong changes throughout the time in culture [Fig. 10(D)]. No RIP signal was detected at 2–22 DIV.

Comparative Summary of Neurons and Glia in the Three Preparations Under Study

To aid comparison across different preparations and experimental ages, Table 1 summarizes the occurrence of neurons and motoneurons in various areas of

ID: selvarajn Date: 3/11/11 Time: 17:30 Path: N:/3B2/DNEU/Vol00000/110159/APPfile/JW-DNEU110159

J_ID: DNEU Wiley Ed. Ref. No.: 00149-2011.R1 Customer A_ID: DNEU20991 Date: 3-NOVEMBER-11 Stage: I Page: 15

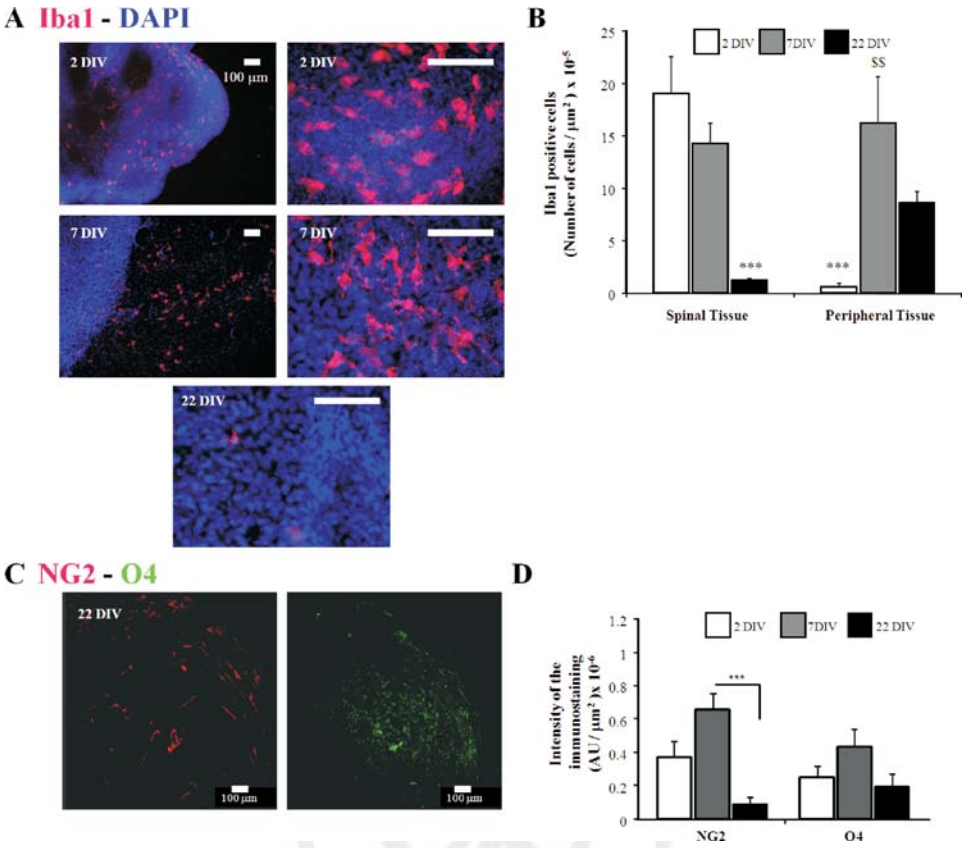

COLOR

Figure 10 Distribution of Iba1 positive cells and expression of immature and mature oligodendrocytes in organotypic spinal culture. (A) Representative staining (red) of Iba1 positive cells at 2 DIV (top panels), 7 DIV (middle panels), and 22 DIV (bottom panel). DAPI staining is shown in blue. Note, in spinal slice tissue, gradual disappearance of Iba1 positive cells from 2 to 22 DIV. (B) Histogram shows number of Iba1 positive cells in spinal tissue and outside it (peripheral tissue); *** = $p < 0.001$ vs. 2 DIV in spinal tissue. $$ = $p < 0.01$ vs. 2 DIV in peripheral tissue; $n = 4$–8 for all experiments. (C) Representative staining for NG2 (left panel; red) and O4 (right panel; green) at 22 DIV. (D) Histograms showing fluorescence intensity (AU) for both markers at 2, 7, and 22 DIV. Significant decrease in NG2 signal intensity was observed at 22 DIV vs. 7 DIV, ***$p < 0.001$, while no statistically difference was found for O4; $n = 5$–6.

the spinal cord or organotypic slice, and in the nucleus hypoglossus. Values collected from these ROIs are expressed as % of NeuN or SMI32 positive elements with respect to the total number of DAPI-positive elements. Table 1 also reports data pertaining to the largest glial cell population, namely the one immunoreactive to S100, and thought to correspond to protoplasmic astrocytes.

DISCUSSION

The principal finding of the present study is the novel quantification of neurons and glial cells in motor nuclei of the rat spinal cord and brainstem during the early postnatal period, and their comparison with organotypic slice cultures. These data help to clarify the basic cellular composition of these networks and their changes following experimental manipulations mimicking pathophysiological processes.

Nucleus Hypoglossus

The nucleus hypoglossus contains all motoneurons that contract tongue muscles and, therefore, plays an essential role in preserving airway patency (Friedland et al., 1995; Horner, 2008). The mature neuronal innervation of the tongue muscles is reached during antenatal development through the mechanism of motoneuron cell death (Friedland et al., 1995). The present report validates this notion since no significant difference in HM numbers between P0 and P4 emerged, while a slight decrease in interneuron numbers was found. A previous report by Sturrock (1991)

ID: selvarajn Date: 3/11/11 Time: 17:30 Path: N:/3B2/DNEU/Vol00000/110159/APPfile/JW-DNEU110159

Table 1 Summary of Neurons, Motoneurons and Protoplasmic Astrocytes (S100 Positive Cells) in Spinal Cord and Nucleus Hypoglossus at P0 and P4 Ages and in Organotypic Spinal Cultures After 2 or 22 Days In Vitro (DIV)

		Spinal Cord		Organotypic Spinal Culture		Nucleus Hypoglossus	
		P0	P4	2DIV	22DIV	P0	P4
Neurons as % of total cell population	Dorsal area	85	81	ND	36	43	37
	Central area	71	67		37		
	Ventral area	57	45		35		
Motoneurons as % of total cell population	Ventral area	8	10	ND	2	30	29
S100 positive cells as % of total cell population[a]	Dorsal area	13	17	0.3 ± 0.1	7.5 ± 1.6	35	34
	Central area	25	26				
	Ventral area	38	47				

ND = not detected.

[a]For organotypic cultures, values refer to S100 immunostaining intensity (expressed in AU/μm^2) throughout a slice. Data are expressed as shown in Figure 9(B).

on the mouse nucleus hypoglossus indicates that the number of motoneurons and interneurons remains stable from adulthood to old age and proposes that this result is due to the continuous tongue movements which are present throughout life time and help to preserve cell numbers. Our current data also confirmed the very large preponderance of HMs over other neurons as formerly described (Boone and Aldes, 1984; Takasu and Hashimoto, 1988; Viana et al., 1990; Friedland et al., 1995) and suggest that neuronal development within the nucleus hypoglossus occurs rather early in postnatal life.

In addition, the present study has shown, for the first time, the relative composition of neurons and glia in the nucleus hypoglossus, a result of crucial importance for studies concerning cell loss and survival in disease-related models, as well as for the identification of potential therapeutic targets. In view of the emerging role of glia in neurodegenerative diseases like ALS (Rao and Weiss, 2004; Neusch et al., 2007; Van Den Bosch and Robberecht, 2008), these new data should help to set up the background conditions of disease models.

To sum up, as neurons (of which circa 80% were motoneurons) represented about 40 % of cells in the developing rat nucleus hypoglossus, the prevailing cell population was made up by glia, the vast majority of which consisted of S100 positive astrocytes (plus a small presence of Iba1 positive cells). These percentages did not different significantly between P0 and P4 developmental stages. GFAP positive astrocytes and oligodendrocytes (either as NG2-positive precursors or O4-positive mature cells) were detected at low density outside the motor nucleus only. Thus, the present data suggest that, in the rat nucleus hypoglossus, maturation of neurons and glia was already present postnatally, although myelination largely lagged behind. Furthermore, the present results, by showing an extensive population of S100 positive astrocytes, emphasize the important role of these cells in the response to disease-related pathophysiological insults affecting this nucleus (Chung et al., 2004; Cifra et al., 2011). Hence, in this nucleus, as pointed out by Greer and Funk (2005), postnatal developmental maturation appears to concern the neurotransmitter receptor structure and function (for example, see Talley et al., 1997 for serotonin; see Singer et al., 1998 for glycine) and electrical properties (Viana et al., 1994; Berger et al., 1995) rather than the cell identity and number.

Spinal Cord

The global number of cells between P0 and P4 did not change despite the spinal cord postnatal growth. Interestingly, the neuronal population was the largest in the dorsal horn area, while the lowest value was in the ventral horn where motoneurons were 8–10% of the local cell population. Such a low number of motoneurons was in accordance with previous studies that also indicated that, after birth, naturally occurring motoneuron death is virtually nil (Hardman and Brown, 1985; Oppenheim, 1986; Lowrie and Lawson, 2000), since the peak period for rat motoneuron elimination takes place at embryonic Days 15–17 (Harris and McCaig, 1984). Conversely, a small fall in the number of ventral horn neurons was detected in keeping with the observation by Lawson et al. (1997), and with the current result for the rat brainstem slice.

Friese et al (2009) have reported that γ-motoneurons of the mouse spinal cord are selectively labeled by the transcription factor Err3 and that this genetic marker is typically associated with such cells after 2 weeks of age. In the present study we did not distin-

guish between α- and γ-motoneurons that are a clear minority of all motoneurons (Friese et al., 2009) and are usually expressed in low number at early postnatal stage (Hui et al., 2008; Shneider et al., 2009). Thus, while our motoneuron counts (obtained with SMI32 and ChAT markers) provided reliable absolute values, on the assumption that mouse motoneuron data can be applicable to the rat spinal cord, we cannot rule out that we slightly overestimated motoneuron proportion with respect to the global number of NeuN sensitive cells.

The present study also provided new data concerning the glial population of the rat lumbar spinal cord. In fact, S100 cells were the most abundant cell type in the ventral horn area, and their number rose in conjunction with the small fall in neuronal number. In central and dorsal regions, S100 positive astrocytes were still the commonest type of glial cell, although in a relatively low number in the dorsal horn when compared with the neuronal count. It is tempting to hypothesize that the limited number of astrocytes in the dorsal horn is an important factor to confer very high vulnerability of neurons to excitotoxicity (Taccola et al., 2008; Mazzone et al., 2010) probably because of the restricted capacity by fewer astrocytes to buffer large rises in extracellular glutamate.

Like in the nucleus hypoglossus, GFAP positive astrocytes were observed only in the white matter without overall change in their number from P0 to P4. Interestingly though, astrocyte morphology did change as these cells acquired a star-like shape with radial processes. It is currently unclear if this developmental alteration might reflect a different physiological function of such cells. Our previous report demonstrated how metabolic perturbation mimicking anoxia with redox stress *in vitro* evoked damage mainly to astroglia (Taccola et al., 2008).

Between P0 and P4, microglia was a clear minority member of the glial population with a relatively even distribution throughout spinal cord. Ameboid morphology of microglia was rarely observed, and, whenever present, found to be in close juxtaposition with pyknotic nuclei, suggesting that microglia had been activated to dispose of dead cells (Kettenmann et al., 2011). Nevertheless, the predominant presence of microglia in its resting (ramified) state (Kettenmann et al., 2011) indicated that these spinal preparations were in standard control conditions.

Scant myelination seemed to emerge at P4 as indicated by the appearance of oligodendrocytes immunopositive for RIP in the white matter. Earlier, labeling with the NG2 marker for oligodendrocyte precursors was observed in all white matter areas and fell significantly at P4. This reduction was mirrored by an increase in ventral and lateral white matter labeling for the O4 marker, which is regarded as an index of oligodendrocyte maturation (Sommer and Schachner, 1981; Noll and Miller, 1994).

Organotypic Spinal Slice Culture

In organotypic cultures, it was not surprising to find out a low number of neurons and glia without large regional differences possibly because of the culture rolling protocol required to flatten the network structure. Despite these experimental manipulations, the relative proportions of neurons, motoneurons and glia remained comparatively similar to those observed *in situ*, supporting the use of such cultures for *in vitro* studies. This information had not been available before. One notable exception to the similarity between *in situ* and *in vitro* systems was the presence of GFAP positive astrocytes abundantly detected in the organotypic spinal slice and in peripheral tissue. The reason for the preferential expression of GFAP positive astrocytes (with star-like shape) remains a subject for future investigation. On mouse spinal organotypic cultures, Avossa et al. (2003) have described GFAP only within the spinal cord, indicating a difference in the developmental maturation between these species.

The organotypic cultures prepared with embryonic spinal tissue produced very low immunoreactivity for neurons up to 7 DIV. Lack of NeuN immunoreactivity at 2 DIV was probably due to the insufficient expression of this protein by the embryonic tissue (Chung et al., 2010) rather than axotomy-induced loss of NeuN signal which is a functional response of damaged neurons in the adult spinal cord (McPhail et al., 2004).

Indeed, at a rather early stage in culture, functional network activity is very immature (Ballerini et al., 1999; Fabbro et al., 2007) and justifies the routine use of 22 DIV cultures (Mazzone et al., 2010) when circuits are strongly developed (Sibilla and Ballerini, 2009), and, in our conditions, neuronal numbers (NeuN positive cells) were found to be 30% of the total cell population. Like spinal motoneurons *in situ*, motoneuron numbers in the organotypic culture were low (6% of neurons) and restricted to the ventral area. Former studies have indicated that motoneuron numbers (though not quantified) substantially grow after at least 1 week *in vitro* and are topographically located at 14 DIV (Avossa et al., 2003).

The variability in overall motoneuron number reported by former studies might be due to differing culturing conditions : it is, therefore, reassuring that, with the present protocol, relative motoneuron num-

J_ID: DNEU Wiley Ed. Ref. No.: 00149-2011.R1 Customer A_ID: DNEU20991 Date: 3-NOVEMBER-11 Stage: I Page: 18

bers were very similar in culture and *in situ*. Together with the *in vitro* neuronal maturation, S100 positive cells largely grew from 2 to 22 DIV. Microglia was strongly observed at 2 and 7 DIV with a dramatic fall at 22 DIV with corresponding rise in such labeled cells outside the spinal slice tissue, perhaps suggesting their migration toward nonneuronal structures. Limited occurrence and maturation of oligodendrocytes was shown even at 22 DIV. Conversely, on mouse organotypic cultures, expression of myelin basic protein was reported after the first week *in vitro* (Avossa et al., 2003).

Implications for Studies of Motor Nuclei

The nucleus hypoglossus contained a very large number of motoneurons that vastly outnumbered other neurons, while the opposite was found in the spinal ventral horn. Interestingly, motoneuron density was not a predictor of their rhythmogenic properties. In fact, tightly packed HMs usually requires inputs from other brainstem nuclei to express motor patterns (Feldman and Del Negro, 2006). Conversely, the spinal ventral horn fully expresses intrinsic rhythmicity (Bracci et al., 1996) to which the low number of motoneurons can contribute with their voltage-dependent conductances (Hochman et al., 1994): an analogous property is observed in the spinal organotypic slice (Ballerini et al., 1999), where motoneurons possess intrinsic spiking ability (Magloire and Streit, 2009).

In brainstem and spinal motor nuclei, S100 positive astrocytes were the main glial population and represented $\sim$34% in the brainstem and 40% in the ventral horn of all DAPI-positive cells. It is widely accepted that astrocytic uptake of glutamate is the major process to remove the extracellular level of this excitatory transmitter (Danbolt, 2001) and that this mechanism protects neurons (Schousboe and Waagepetersen, 2005) including motoneurons (Cifra et al., 2009; Kuzhandaivel et al., 2011), and glia (Matute et al., 2007) from excitotoxic damage. Nonetheless, in the ventral horn (Taccola et al., 2008; Mazzone et al., 2010) as well as in organotypic cultures (Mazzone and Nistri, 2011), S100 positive astrocytes are essentially spared by excitotoxicity, while they do suffer the same fate as HMs in the nucleus hypoglossus (Cifra et al., 2011). These results suggest that neuroprotective mechanisms against motoneuronal excitotoxicity are perhaps different in the two motor nuclei, despite similar number of astrocytes whose contribution to neuroprotection is apparently region-specific. These observations suggest that conclusions concerning pathophysiological processes in a certain motor nucleus should not be readily extrapolated to another one.

In conclusion, the present report supplies novel information that can be a useful platform for further analysis of the cellular mechanisms causing motor deficits via selective cell loss affecting distinct cell groups of neurons and glia (Kuzhandaivel et al., 2011). Future studies are necessary to identify the excitatory or inhibitory function of such neurons and the transmitters released by them (Dallas et al., 2005) to provide a fully integrated map of motor nuclei.

M.M. is a research biologist of the Local Health Authority (ASS4 MedioFriuli).

REFERENCES

Avossa D, Grandolfo M, Mazzarol F, Zatta M, Ballerini L. 2006. Early signs of motoneuron vulnerability in a disease model system: Characterization of transverse slice cultures of spinal cord isolated from embryonic ALS mice. Neuroscience 138:1179–1194.

Avossa D, Rosato-Siri MD, Mazzarol F, Ballerini L. 2003. Spinal circuits formation: A study of developmentally regulated markers in organotypic cultures of embryonic mouse spinal cord. Neuroscience 122:391–405.

Ballerini L, Galante M, Grandolfo M, Nistri A. 1999. Generation of rhythmic patterns of activity by ventral interneurones in rat organotypic spinal slice culture. J Physiol 517:459–475.

Barber RP, Phelps PE, Houser CR, Crawford GD, Salvaterra PM, Vaughn JE. 1984. The morphology and distribution of neurons containing choline acetyltransferase in the adult rat spinal cord: an immunocytochemical study. J Comp Neurol 229:329–346.

Berger AJ, Bayliss DA, Bellingham MC, Umemiya M, Viana F. 1995. Postnatal development of hypoglossal motoneuron intrinsic properties. Adv Exp Med Biol 381: 63–71.

Boone TB, Aldes LD. 1984. The ultrastructure of two distinct neuron populations in the hypoglossal nucleus of the rat. Exp Brain Res 54:321–326.

Bracci E, Ballerini L, Nistri A. 1996. Spontaneous rhythmic bursts induced by pharmacological block of inhibition in lumbar motoneurons of the neonatal rat spinal cord. J Neurophysiol 75:640–647.

Brenneman DE, Phillips TM, Festoff BW, Gozes I. 1997. Identity of neurotrophic molecules released from astroglia by vasoactive intestinal peptide. Ann N Y Acad Sci 814:167–173.

Carriedo SG, Yin HZ, Lamberta R, Weiss JH. 1995. In vitro kainate injury to large, SMI-32(+) spinal neurons is Ca2+ dependent. Neuroreport 6:945–948.

Carriedo SG, Yin HZ, Weiss JH. 1996. Motor neurons are selectively vulnerable to AMPA/kainate receptor-mediated injury in vitro. J Neurosci 16:4069–4079.

ID: selvarajn Date: 3/11/11 Time: 17:30 Path: N:/3B2/DNEU/Vol00000/110159/APPfile/JW-DNEU110159

Chung SH, Kim CT, Jung YH, Lee NS, Jeong YG. 2010. Early cerebellar granule cell migration in the mouse embryonic development. Anat Cell Biol 43:86–95.

Chung YH, Joo KM, Lee YJ, Shin DH, Cha CI. 2004. Reactive astrocytes express PARP in the central nervous system of SOD(G93A) transgenic mice. Brain Res 1003: 199–204.

Cifra A, Nani F, Nistri A. 2011. Riluzole is a potent drug to protect neonatal rat hypoglossal motoneurons in vitro from excitotoxicity due to glutamate uptake block. Eur J Neurosci 33:899–913.

Cifra A, Nani F, Sharifullina E, Nistri A. 2009. A repertoire of rhythmic bursting produced by hypoglossal motoneurons in physiological and pathological conditions. Philos Trans R Soc Lond B Biol Sci 364:2493–2500.

Clarac F, Brocard F, Vinay L. 2004a. The maturation of locomotor networks. Prog Brain Res 143:57–66.

Clarac F, Pearlstein E, Pflieger JF, Vinay L. 2004b. The in vitro neonatal rat spinal cord preparation: a new insight into mammalian locomotor mechanisms. J Comp Physiol A Neuroethol Sens Neural Behav Physiol 190:343–357.

Cocchia D. 1981. Immunocytochemical localization of S-100 protein in the brain of adult rat. An ultrastructural study. Cell Tissue Res 214:529–540.

Dallas M, Deuchars SA, Deuchars J. 2005. Immunopharmacology—Antibodies for specific modulation of proteins involved in neuronal function. J Neurosci Methods 146: 133–148.

Danbolt NC. 2001. Glutamate uptake. Prog Neurobiol 65: 1–105.

DePaul R, Abbs JH. 1987. Manifestations of ALS in the cranial motor nerves: Dynametric, neuropathologic, and speech motor data. Neurol Clin 5:231–250.

DePaul R, Abbs JH, Caligiuri M, Gracco VL, Brooks BR. 1988. Hypoglossal, trigeminal, and facial motoneuron involvement in amyotrophic lateral sclerosis. Neurology 38:281–283.

Didier M, Harandi M, Aguera M, Bancel B, Tardy M, Fages C, Calas A, et al. 1986. Differential immunocytochemical staining for glial fibrillary acidic (GFA) protein, S-100 protein and glutamine synthetase in the rat subcommissural organ, nonspecialized ventricular ependyma and adjacent neuropil. Cell Tissue Res 245: 343–351.

Donato R. 2003. Intracellular and extracellular roles of S100 proteins. Microsc Res Tech 60:540–551.

Eng LF. 1985. Glial fibrillary acidic protein (GFAP): The major protein of glial intermediate filaments in differentiated astrocytes. J Neuroimmunol 8:203–214.

Fabbro A, Pastore B, Nistri A, Ballerini L. 2007. Activity-independent intracellular Ca2+ oscillations are spontaneously generated by ventral spinal neurons during development in vitro. Cell Calcium 41:317–329.

Feldman JL, Del Negro CA. 2006. Looking for inspiration: new perspectives on respiratory rhythm. Nat Rev Neurosci 7:232–242.

Friedland DR, Eden AR, Laitman JT. 1995. Naturally occurring motoneuron cell death in rat upper respiratory tract motor nuclei: A histological, fast DiI and immunocytochemical study in the hypoglossal nucleus. J Neurobiol 27:520–534.

Friedman B, Hockfield S, Black JA, Woodruff KA, Waxman SG. 1989. In situ demonstration of mature oligodendrocytes and their processes: An immunocytochemical study with a new monoclonal antibody rip. Glia 2: 380–390.

Friese A, Kaltschmidt JA, Ladle DR, Sigrist M, Jessell TM, Arber S. 2009. Gamma and alpha motor neurons distinguished by expression of transcription factor Err3. Proc Natl Acad Sci USA 106:13588–13593.

Gähwiler BH, Capogna M, Debanne D, McKinney RA, Thompson SM. 1997. Organotypic slice cultures: A technique has come of age. Trends Neurosci 20:471–477.

Gähwiler BH, Thompson SM, Muller D. 2001. Preparation and maintenance of organotypic slice cultures of CNS tissue. Curr Protoc Neurosci 6:1–11.

Gotow T, Tanaka J. 1994. Phosphorylation of neurofilament H subunit as related to arrangement of neurofilaments. J Neurosci Res 37:691–713.

Goulding M. 2009. Circuits controlling vertebrate locomotion: Moving in a new direction. Nat Rev Neurosci 10: 507–518.

Grass D, Pawlowski PG, Hirrlinger J, Papadopoulos N, Richter DW, Kirchhoff F, Hülsmann S. 2004. Diversity of functional astroglial properties in the respiratory network. J Neurosci 24:1358–1365.

Greer JJ, Funk GD. 2005. Perinatal development of respiratory motoneurons. Respir Physiol Neurobiol 149:43–61.

Greer JJ, Funk GD, Ballanyi K. 2006. Preparing for the first breath: prenatal maturation of respiratory neural control. J Physiol 570:437–444.

Grillner S. 2006. Biological pattern generation: The cellular and computational logic of networks in motion. Neuron 52:751–766.

Guzman-Lenis MS, Navarro X, Casas C. 2009. Drug screening of neuroprotective agents on an organotypic-based model of spinal cord excitotoxic damage. Restor Neurol Neurosci 27:335–349.

Haenggeli C, Kato AC. 2002. Differential vulnerability of cranial motoneurons in mouse models with motor neuron degeneration. Neurosci Lett 335:39–43.

Hardman VJ, Brown MC. 1985. Absence of postnatal death among motoneurones supplying the inferior gluteal nerve of the rat. Brain Res 351:1–9.

Harris AJ, McCaig CD. 1984. Motoneuron death and motor unit size during embryonic development of the rat. J Neurosci 4:13–24.

Hochman S, Jordan LM, Schmidt BJ. 1994. TTX-resistant NMDA receptor-mediated voltage oscillations in mammalian lumbar motoneurons. J Neurophysiol 72: 2559–2562.

Horner RL. 2008. Neuromodulation of hypoglossal motoneurons during sleep. Respir Physiol Neurobiol 164: 179–196.

Hui K, Kucera J, Henderson JT. 2008. Differential sensitivity of skeletal and fusimotor neurons to Bcl-2-mediated apoptosis during neuromuscular development. Cell Death Differ 15:691–699.

Imai Y, Ibata I, Ito D, Ohsawa K, Kohsaka S. 1996. A novel gene iba1 in the major histocompatibility complex class III region encoding an EF hand protein expressed in a monocytic lineage. Biochem Biophys Res Commun 224:855–862.

Ito D, Imai Y, Ohsawa K, Nakajima K, Fukuuchi Y, Kohsaka S. 1998. Microglia-specific localization of a novel calcium binding protein, Iba1. Brain Res Mol Brain Res 57:1–9.

Jean A. 2001. Brain stem control of swallowing: neuronal network and cellular mechanisms. Physiol Rev 81: 929–969.

Jiang Z, Rempel J, Li J, Sawchuk MA, Carlin KP, Brownstone RM. 1999. Development of L-type calcium channels and a nifedipine-sensitive motor activity in the postnatal mouse spinal cord. Eur J Neurosci 11:3481–3487.

Kettenmann H, Hanisch UK, Noda M, Verkhratsky A. 2011. Physiology of microglia. Physiol Rev 91:461–553.

Kiehn O. 2006. Locomotor circuits in the mammalian spinal cord. Annu Rev Neurosci 29:279–306.

Kiehn O. 2011. Development and functional organization of spinal locomotor circuits. Curr Opin Neurobiol 21: 100–109.

Kim KK, Adelstein RS, Kawamoto S. 2009. Identification of neuronal nuclei (NeuN) as Fox-3, a new member of the Fox-1 gene family of splicing factors. J Biol Chem 284:31052–31061.

Kuzhandaivel A, Nistri A, Mazzone GL, Mladinic M. 2011. Molecular mechanisms underlying cell death in spinal networks in relation to locomotor activity after acute injury in vitro. Front Cell Neurosci 5:9.

Kuzhandaivel A, Nistri A, Mladinic M. 2010. Kainate-mediated excitotoxicity induces neuronal death in the rat spinal cord in vitro via a PARP-1 dependent cell death pathway (Parthanatos). Cell Mol Neurobiol 30: 1001–1012.

Lawson SJ, Davies HJ, Bennett JP, Lowrie MB. 1997. Evidence that spinal interneurons undergo programmed cell death postnatally in the rat. Eur J Neurosci 9:794–799.

Liu XY, Li CY, Bu H, Li Z, Li B, Sun MM, Guo YS, et al. 2008. The neuroprotective potential of phase II enzyme inducer on motor neuron survival in traumatic spinal cord injury in vitro. Cell Mol Neurobiol 28:769–779.

Lowe AA. 1980. The neural regulation of tongue movements. Prog Neurobiol 15:295–344.

Lowrie MB, Lawson SJ. 2000. Cell death of spinal interneurones. Prog Neurobiol 61:543–555.

Magloire V, Streit J. 2009. Intrinsic activity and positive feedback in motor circuits in organotypic spinal cord slice cultures. Eur J Neurosci 30:1487–1497.

Margaryan G, Mattioli C, Mladinic M, Nistri A. 2010. Neuroprotection of locomotor networks after experimental injury to the neonatal rat spinal cord in vitro. Neuroscience 165:996–1010.

Margaryan G, Mladinic M, Mattioli C, Nistri A. 2009. Extracellular magnesium enhances the damage to locomotor networks produced by metabolic perturbation mimicking spinal injury in the neonatal rat spinal cord in vitro. Neuroscience 163:669–682.

Matute C, Alberdi E, Domercq M, Sánchez-Gómez MV, Pérez-Samartín A, Rodríguez-Antigüedad A, Pérez-Cerdá F. 2007. Excitotoxic damage to white matter. J Anat 210:693–702.

Mazzone GL, Margaryan G, Kuzhandaivel A, Nasrabady SE, Mladinic M, Nistri A. 2010. Kainate-induced delayed onset of excitotoxicity with functional loss unrelated to the extent of neuronal damage in the in vitro spinal cord. Neuroscience 168:451–462.

Mazzone GL, Nistri A. 2011a. Effect of the PARP-1 inhibitor PJ 34 on excitotoxic damage evoked by kainate on rat spinal cord organotypic slices. Cell Mol Neurobiol 31:469–478.

Mazzone GL, Nistri A. 2011b. Delayed neuroprotection by riluzole against excitotoxic damage evoked by kainate on rat organotypic spinal cord cultures. Neuroscience 190: 318–327.

McPhail LT, McBride CB, McGraw J, Steeves JD, Tetzlaff W. 2004. Axotomy abolishes NeuN expression in facial but not rubrospinal neurons. Exp Neurol 185:182–190.

Mitchell JD, Borasio GD. 2007. Amyotrophic lateral sclerosis. Lancet 369:2031–2041.

Munoz-Garcia D, Ludwin SK. 1985. Intermediate glial cells and reactive astrocytes revisited. A study in organotypic tissue culture. J Neuroimmunol 8:237–254.

Munoz-Garcia D, Ludwin SK. 1986. Gliogenesis in organotypic tissue culture of the spinal cord of the embryonic mouse. I. Immunocytochemical and ultrastructural studies. J Neurocytol 15:273–290.

Nani F, Cifra A, Nistri A. 2010. Transient oxidative stress evokes early changes in the functional properties of neonatal rat hypoglossal motoneurons in vitro. Eur J Neurosci 31:951–966.

Neusch C, Bähr M, Schneider-Gold C. 2007. Glia cells in amyotrophic lateral sclerosis: New clues to understanding an old disease? Muscle Nerve 35:712–724.

Nishiyama A, Lin XH, Giese N, Heldin CH, Stallcup WB. 1996. Colocalization of NG2 proteoglycan and PDGFa receptor on 02A progenitor cells in the developing rat brain. J Neurosci Res 43:299–314.

Nistri A, Ostroumov K, Sharifullina E, Taccola G. 2006. Tuning and playing a motor rhythm: How metabotropic glutamate receptors orchestrate generation of motor patterns in the mammalian central nervous system. J Physiol 572 (Part 2):323–334.

Nistri A, Taccola G, Mladinic M, Margaryan G, Kuzhandaivel A. 2010. Deconstructing locomotor networks with experimental injury to define their membership. Ann N Y Acad Sci 1198:242–251.

Noll E, Miller RH. 1994. Regulation of oligodendrocyte differentiation: A role for retinoic acid in the spinal cord. Development 120:649–660.

Paton JF, Ramirez JM, Richter DW. 1994. Mechanisms of respiratory rhythm generation change profoundly during early life in mice and rats. Neurosci Lett 170:167–170.

Oppenheim RW. 1986. The absence of significant postnatal motoneuron death in the brachial and lumbar spinal cord of the rat. J Comp Neurol 246:281–286.

Quincozes-Santos A, Gottfried C. 2011. Resveratrol modulates astroglial functions: Neuroprotective hypothesis. Ann N Y Acad Sci 1215:72–78.

Ramirez JM, Quellmalz UJ, Richter DW. 1996. Postnatal changes in the mammalian respiratory network as revealed by the transverse brainstem slice of mice. J Physiol 491:799–812.

Rao SD, Weiss JH. 2004. Excitotoxic and oxidative cross-talk between motor neurons and glia in ALS pathogenesis. Trends Neurosci 27:17–23.

Richter MW, Roskams AJ. 2008. Olfactory ensheathing cell transplantation following spinal cord injury: Hype or hope? Exp Neurol 209:353–367.

Rothstein JD, Kuncl RW. 1995. Neuroprotective strategies in a model of chronic glutamate-mediated motor neuron toxicity. J. Neurochem 65:643–651.

Schmidt-Kastner R, Szymas J. 1990. Immunohistochemistry of glial fibrillary acidic protein, vimentin and S-100 protein for study of astrocytes in hippocampus of rat. J Chem Neuroanat 3:179–192.

Schousboe A, Waagepetersen HS. 2005. Role of astrocytes in glutamate homeostasis: Implications for excitotoxicity. Neurotox Res 8:221–225.

Schumacher M, Guennoun R, Stein DG, De Nicola AF. 2007. Progesterone: Therapeutic opportunities for neuroprotection and myelin repair. Pharmacol Ther 116: 77–106.

Shneider NA, Brown MN, Smith CA, Pickel J, Alvarez FJ. 2009. Gamma motor neurons express distinct genetic markers at birth and require muscle spindle-derived GDNF for postnatal survival. Neural Dev 4:42.

Sibilla S, Ballerini L. 2009. GABAergic and glycinergic interneuron expression during spinal cord development: Dynamic interplay between inhibition and excitation in the control of ventral network outputs. Prog Neurobiol 89:46–60.

Singer JH, Talley EM, Bayliss DA, Berger AJ. 1998. Development of glycinergic synaptic transmission to rat brain stem motoneurons. J Neurophysiol 80:2608–2620.

Smith JC, Feldman JL. 1987. In vitro brainstem-spinal cord preparations for study of motor systems for mammalian respiration and locomotion. J Neurosci Methods 21: 321–333.

Sommer I, Schachner M. 1981. Monoclonal antibodies (O1 to O4) to oligodendrocyte cell surfaces: An immunocytological study in the central nervous system. Dev Biol 83:311–327.

Spenger C, Braschler UF, Streit J, Luscher HR. 1991. An organotypic spinal cord—Dorsal root ganglion—Skeletal muscle coculture of embryonic rat. I. The morphological correlates of the spinal reflex arc. Eur J Neurosci 3: 1037–1053.

Streit J. 1993. Regular oscillations of synaptic activity in spinal networks in vitro. J Neurophysiol 70:871–878.

Streit J, Spenger C, Luscher HR. 1991. An organotypic spinal cord—Dorsal root ganglion—Skeletal muscle coculture of embryonic rat. II. Functional evidence for the formation of spinal reflex arcs in vitro. Eur J Neurosci 3:1054–1068.

Sturrock RR. 1991. Stability of motor neuron and interneuron number in the hypoglossal nucleus of the ageing mouse brain. Anat Anz 173:113–116.

Suzue T. 1984. Respiratory rhythm generation in the in vitro brain stem-spinal cord preparation of the neonatal rat. J Physiol 354:173–183.

Taccola G, Margaryan G, Mladinic M, Nistri A. 2008. Kainate and metabolic perturbation mimicking spinal injury differentially contribute to early damage of locomotor networks in the in vitro neonatal rat spinal cord. Neuroscience 155:538–555.

Taccola G, Mladinic M, Nistri A. 2010. Dynamics of early locomotor network dysfunction following a focal lesion in an in vitro model of spinal injury. Eur J Neurosci 31: 60–78.

Takasu N, Hashimoto PH. 1988. Morphological identification of an interneuron in the hypoglossal nucleus of the rat: A combined Golgi-electron microscopic study. J Comp Neurol 271:461–471.

Talley EM, Sadr NN, Bayliss DA. 1997. Postnatal development of serotonergic innervation, 5-HT1A receptor expression, and 5-HT responses in rat motoneurons. J Neurosci 17:4473–4485.

Tanaka I, Ezure K, Kondo M. 2003. Distribution of glycine transporter 2 mRNA-containing neurons in relation to glutamic acid decarboxylase mRNA-containing neurons in rat medulla. Neurosci Res 47:139–151.

Van Den Bosch L, Robberecht W. 2008. Crosstalk between astrocytes and motor neurons: What is the message? Exp Neurol 211:1–6.

van Zundert B, Peuscher MH, Hynynen M, Chen A, Neve RL, Brown RH Jr, Constantine-Paton M, et al. 2008. Neonatal neuronal circuitry shows hyperexcitable disturbance in a mouse model of the adult-onset neurodegenerative disease amyotrophic lateral sclerosis. J Neurosci 28:10864–10874.

Viana F, Bayliss DA, Berger AJ. 1994. Postnatal changes in rat hypoglossal motoneuron membrane properties. Neuroscience 59:131–148.

Viana F, Gibbs L, Berger AJ. 1990. Double- and triple-labeling of functionally characterized central neurons projecting to peripheral targets studied in vitro. Neuroscience 38:829–841.

Vinay L, Jean-Xavier C. 2008. Plasticity of spinal cord locomotor networks and contribution of cation-chloride cotransporters. Brain Res Rev 57:103–110.

Discussion

The present study was able to address the scientific questions stated in the aims (see page 38), achieving the following publications and results:

1) In Cifra et al., 2011c, we provided the relative composition (numbers and types) of neurons and glia in the nucleus hypoglossus during postnatal development, a piece of information that was lacking in the literature, but that is of crucial importance for studies concerning cell loss and survival in disease-related models (often relying on neonatal rodents), as well as for the identification of potential therapeutic targets. Moreover, to better analyze and detect the effects of excitotoxicity on our *in vitro* model, in Cifra et al., 2011a we investigated the consequences of slicing and *in vitro* incubation on motoneuron and astrocyte viability, reporting that, despite the inevitable mechanical and metabolic disturbance associated to these procedures (Dugué et al., 2005; Davie et al., 2006), cell number and functionality were optimally preserved.

2) In Cifra et al., 2011a, we found that in the nucleus hypoglossus the block of glutamate up-take affected both motoneurons and astrocytes, triggering electrophysiological (bursting) and molecular (ATF-3 expression, SMI32 and S100 changes) responses which evolved in time. We demonstrated that riluzole, applied early after the onset of the excitotoxic insult at a concentration similar to the plasma therapeutic concentration in humans (Wokke, 1996; Cheah et al., 2010), not only suppressed TBOA-evoked bursting, but also protected HM numbers and prevented their distress response (ATF-3 activation); likewise, riluzole reversed the action of TBOA on astrocytes. These new data suggest that brainstem slices are a useful *in vitro* model to mimic some ALS-related pathological processes and that riluzole might be efficient to protect motoneurons and glia at the very early stage of excitotoxic damage.

3) In Cifra et al, 2009 and 2011b, we reviewed periodic electrical discharges expressed by HMs in physiological and pathological conditions, in particular providing a comparison between excitotoxicity and oxidative stress (believed to play a pivotal role in ALS pathogenesis) which triggered distinct electrophysiological effects on HMs: in fact, while excitotoxicity elicited sustained bursting and enhanced synaptic transmission,

oxidative stress generated slow depolarization, augmented repeated firing, and decreased synaptic transmission. However, despite their separate functional signatures, both insults induced early activation of the stress transcription factor ATF-3, suggesting an early common biochemical pathway of neuronal distress.

1. Neuronal and glial populations in the neonatal rat nucleus hypoglossus

The nucleus hypoglossus is a motor center containing all motoneurons that innervate tongue muscles, and, accordingly, previous qualitative observations in the literature have reported the very large preponderance of HMs over other neurons in this brain region (Boone and Aldes, 1984; Takasu and Hashimoto, 1988; Viana et al., 1990; Friedland et al., 1995). Even though our study was not concerned with the whole topography of the nucleus hypoglossus, we provided a first quantitative analysis of its relative neuronal and glial populations during postnatal development (P0, P4), using the brainstem slice preparation from neonatal rat, an extremely useful and widely employed experimental model (as reviewed in the introductory sections). We report that motoneurons represent about the 80 % of the total hypoglossal neuronal population. In relation to the type and number of glia, we found that up to the 45 % of the total hypoglossal cell population is made up of glia (with neurons representing another 40 %), the vast majority of which (35 %) consists of S100 positive astrocytes. Oligodendrocytes, instead, either as NG2-positive precursors or O4-positive mature cells, were detected at low density outside the motor nucleus only, suggesting that, in the rat nucleus hypoglossus, the maturation of neurons and glia is already present postnatally, while myelinization largely lags behind. Thus, despite this region represents a compact grey matter motor network in which motoneurons are the functional cellular core, its prevailing cell population is made up by glia (which presumably contributes to the expression and function of the motor network; Grass et al., 2004), with an extensive population of S100 positive astrocytes that may influence the response to disease-related pathophysiological insults affecting this nucleus (Chung et al., 2004; Cifra et al., 2011).

2. Brain slices – are they a suitable in vitro preparation to test excitotoxicity?

Brain slices offer undeniable advantages in terms of access to the basic mechanisms of action of pathophysiological events and drugs, approaches hardly achievable with other more preserved and complex preparations (such as *in vivo* and *in situ*). It is, however, interesting to assess how far the slicing procedure can change the normal operation of cells (motoneurons and glia) and impair their extended survival *in vitro* because these factors may impact the evaluation of cell-selective degeneration in experimental protocols. In the present study, we monitored the SMI32 motoneuronal marker together with the S100 astrocytic marker in en-bloc brainstem (histologically fixed prior to sectioning), slices fixed immediately after vibratome cutting, and slices fixed 1 or 4 h after cutting and subsequent *in vitro* incubation. We observed that preparing brainstem slices led to an unavoidable loss of motoneurons (35 %), suggesting significant sensitivity to the inevitable mechanical and metabolic disturbance due to the slicing procedure itself (Dugué et al., 2005; Davie et al., 2006). Nonetheless, despite surviving motoneurons probably suffered a modest degree of metabolic distress (as assessed by the presence of a weak ATF-3 signal that was completely absent in preparations not sliced before fixation), they retained good electrophysiological properties (resting potential, input resistance, action potential firing) and remained stable in their numbers for up to 4 h. Thus, any background stress in control condition was not accompanied by significant loss of function, with optimal preservation of motoneurons numbers. This realization allowed testing the effects of TBOA-evoked excitotoxic stress (Cifra et al., 2011a) which induced a further loss of motoneurons (~ 25 %) after 4 h of its administration.

As far as S100 positive astrocytes are concerned, we obtained different and intriguing results: in fact, while S100 immunoreactivity fell drastically (~ 65 %) immediately after sectioning, it then gradually returned to pre-sectioning levels, suggesting perhaps a slow recovery process. S100 proteins are Ca^{2+} binding proteins regulating the activity of many effectors, such as enzymes implicated in signal transduction and energy metabolism (Donato, 2003); their level of expression is strongly determined by environmental factors (Donato, 2003) and, depending on their concentration, S100 proteins can exert beneficial (neurotrophic) or detrimental (neurotoxic) effects on surrounding glia and neurons (Rothermundt et al., 2003). Therefore, it is possible that S100 may function as a sort of

'sensor', representing an adaptive response to physiological/metabolic alterations. Although we are unable to clarify the functional nature of the observed changes, it is noteworthy that, as compared to control Krebs, TBOA always exerted an opposite effect on the expression of S100 immunoreactivity (while riluzole always prevented TBOA action), suggesting that this protein may represent a crucial molecular sensor for astrocytes, picking up a variety of stimuli, including excitotoxicity.

3. TBOA – a model of excitotoxicity affecting motoneurons and glia

The exact etiology of most cases of ALS remains unknown. However, excitotoxicity due to disregulation of glutamate metabolism seems to play a pivotal role in ALS pathogenesis (Van Den Bosch et al., 2006) as indicated by the large increase in glutamate levels found in the cerebrospinal fluid of ALS patients (Rothstein et al., 1990; Shaw et al., 1995a; Spreux-Varoquaux et al., 2002) (probably caused by the impairment of the glial glutamate transport; Rothstein et al., 1992, 1995). It is suggested that any reported deficit in the glial glutamate transporter mechanism is not due to insufficient synthesis of these proteins (Rao & Weiss, 2004) and that the potential offender should be sought in an environmentally-based stimulus (Bruijn et al., 2004). This realization makes it advantageous to use blockers of the glutamate glial transporters (such as TBOA) to mimic the gradual build-up of extracellular endogenous glutamate rather than giving a direct-acting agonist (such as glutamate or kainate). Inhibitors of glutamate uptake have been already employed by other authors to model glutamate-related excitotoxicity on organotypic spinal cord cultures (Rothstein et al., 1993; Matyja et al., 2005) demonstrating slow degeneration of spinal motoneurons (and astroglial alterations; Matyja et al., 2006) over several weeks. Thus, in our laboratory, the same approach was used to model excitotocixity on slices from hypoglossal nucleus (Sharifullina and Nistri, 2006) being one of the most vulnerable motor nuclei to ALS (Medina et al., 1996; Laslo et al., 2000, 2001a,b). Although, acute slices are a time-constrained preparation which allow experimental observations only for a limited period (hours), they offer the undeniable possibility to follow up the development of a pathological insult in terms of both electrophysiological and molecular cell responses. Sharifullina and Nistri (2006) found that the bath application of TBOA triggers HM bursting which requires efficient network activity and is accompanied by strong enhancement in excitatory synaptic

transmission, neuronal recruitment, massive depolarization and increased intracellular Ca^{2+} concentration. Here we showed that excitotoxicity evolved in time from early (1 hour) signs of motoneuronal dysfunction to delayed (4 h) cell loss: in fact, bursting activity, irreversibly affecting HM physiological response after 40-60 min, was followed by the expression of the distress factor ATF-3 (increasing after 1 hour and persisting up to 4 hours in surviving motoneurons), with subsequent loss of the motoneuronal marker SMI32. These phenomena were accompanied by concomitant astrocytic alterations (as assessed by S100 immunoreactivity changes) suggesting a tight correlation between motoneuronal and glial reactions to the excitotoxic insult. Therefore, the current model, based on the block of glutamate uptake, allowed monitoring the response of the hypoglossal nucleus cell population (motoneurons and glia) challenged by excitotoxicity, disclosing electrophysiological and molecular pathological hallmarks useful for following up the evolution of excitotoxicity and for the identification of potential targets for neuroprotection.

4. Riluzole neuroprotection- targets and mechanisms

Riluzole is a complex drug with a multi-target mechanism of action and a powerful neuroprotective potential in experimental research. Documented cellular targets for this drug include: PICs (Miles et al., 2005; Harvey et al., 2006; Kuo et al., 2006; Lamanauskas and Nistri, 2008; Urbani and Belluzzi, 2000), calcium currents (Stefani et al., 1997; Huang et al., 1997; Wang et al., 2004), potassium channels (Zona et al., 1998; Duprat et al., 2000; Ahn et al., 2005), TTX-sensitive sodium channels (Song et al., 1997), glycinergic and GABAergic transmission (Umemiya and Berger, 1995a; He et al., 2002), protein kinases (Noh et al., 2000; Lamanauskas and Nistri, 2008), G-proteins (Doble et al., 1992; Hubert et al., 1994; Wang et al., 2004; Azbill et al., 2000) and glutamatergic transmission (Cheramy et al., 1992; Doble et al., 1992; Martin et al., 1993; Hubert et al., 1994; Coderre et al., 2007; Wang et al., 2004; Lamanauskas and Nistri, 2006). The selectivity of riluzole action depends on its concentration: in the present study we applied riluzole at 5 μM, a value at which it preferentially inhibits glutamate release (Chéramy et al., 1992) and which represents the therapeutic plasma concentration in humans (Wokke, 1996; Cheah et al., 2010). We found that riluzole, applied early (~ 15 min) after the starting of TBOA, was able to efficiently block TBOA-evoked bursting. As it also

reversed the effect of TBOA on the spontaneous glutamatergic current frequency (taking it back to control levels), it is likely that the inhibition of glutamate release (already powerfully demonstrated on HMs by Lamanauskas and Nistri, 2006) was a pivotal mechanism for riluzole to block bursting. However, since massive excitation (Sharifullina and Nistri, 2006) and PICs (Darbon et al., 2004; van Drongelen et al., 2006) are two important contributors to prolonged rhythmic discharges, we cannot exclude that inhibition of voltage-gated Na^+ channels and PICs were also involved. Similarly, it is difficult to disclose the exact mechanism(s) through which riluzole protected HM numbers and always prevented ATF-3 activation. One possibility (also in view of its early application) is that by reducing glutamategic release and global excitation (and thus bursting), riluzole acted at the very initial step of TBOA-induced insult, preventing the spreading of excitotoxicity and its evolution. Nevertheless, as loss of motoneuronal marker was delayed (4 h) and even in surviving motoneurons the expression of the distress factor ATF-3 remained elevated (suggesting that activation of distress pathways may take a certain time to trigger cell death), we can also envisage an interaction with intracellular targets downstream of glutamate release and receptor activation: this hypothesis was recently stated by Mazzone and Nistri (2011) who demonstrated delayed neuroprotection by riluzole against kainate-evoked damage on rat organotypic spinal cord cultures. Another possibility might lie behind riluzole-astrocytes interaction. It is known that glial cells play a major role in physiological and pathological processes, in the latter case limiting or exacerbating brain damage depending on the type and context of the insult, releasing proinflammatory or protective (growth) factors (Heneka et al., 2010). Peluffo et al. (1997) reported that, on motoneuron-enriched spinal cord cultures, astrocyte conditioned media treated with riluzole extended motoneuronal survival and stimulated motoneuron trophic activity as assessed by the level of neuritic growth and the expression of the p75 nerve growth factor (NGF) receptor. Moreover, riluzole was demonstrated to induce the synthesis of growth factors (such as the glial cell line-derived neurotrophic factor, GDNF) in cultured mouse astrocytes (Mizuta et al., 2001) and in rat C6 glioma cells (Tsuchioka et al., 2011). Although in the present study we did not investigate such potential effects of riluzole, we cannot exclude their occurrence; furthermore, since riluzole was always able to reverse TBOA-induced alterations in astrocytic immunoreactivity, we can speculate that protection of glia by this compound might have also included the restoration (or stimulation) of the astrocyte protective potential likely lost after TBOA application. All the mechanisms highlighted in this

section represent important potential targets for neuroprotection. Further detailed investigations would be of great impact as understanding the exact way of action of riluzole (together with the possibility of administering protective drugs at the onset of ALS in humans) might improve the efficacy of new compounds (with higher disease selectivity) for the treatment of ALS.

5. A comparison between excitotoxicity and oxidative stress

It is generally assumed that the disease classified as ALS is the result of defects in a variety of cellular mechanisms, which include oxidative stress and excitotoxicity (Cleveland and Rothstein, 2000; Shaw, 2005). Several authors have hypothesized a crosstalk between these two pathological processes as an integrative explanation for ALS pathogenesis (Trotti et al., 1998; Rao and Weiss, 2004). In fact, it has been reported that exposure to ROS is able to inhibit glutamate uptake on both glial and neuronal cells (Volterra et al., 1994; Trotti et al., 1996) and that glutamate induces ROS generation in cultured motoneurons which then pass across the plasma membrane to induce oxidation and disruption of glutamate uptake in neighboring astrocytes (Rao et al., 2003). Thus, Rao and Weiss (2004) have proposed that a feedforward cycle may contribute to ALS progression, as increases in extracellular glutamate concentration will result in higher motoneuron ROS generation and more severe damage to astrocytic glutamate transport, causing further rises in glutamate levels with selective motoneuron injury. In our laboratory, we have used brainstem slices to investigate the consequences of excitotoxicity (triggered by the block of glutamate uptake) and oxidative stress (elicited via application of H_2O_2) on the hypoglossal cell population physiology and survival. We found that these two factors triggered distinct effects in terms of HM electrophysiological responses (i.e., long-lasting bursting and strong facilitation of network synaptic transmission versus slow depolarization and inhibition of network synaptic transmission, respectively). Also cell specific alterations to motoneuron and glia were different, as loss of motoneuron staining plus S100 astrocytic immunoreactivity changes were reported after TBOA application. Conversely, no early change in HM numbers nor alterations in S100 immunoreactivity (this latter result is an unpublished observation by Francesca Nani) were associated to H_2O_2 treatment. Since we did not extend our observations up to 4 h, we cannot however exclude that the evolution of an oxidative challenge, in terms of cell-specific alterations, might be different later. However, both excitotoxicity and

oxidative stress induced early expression of ATF-3 distress factor in motoneurons. Despite the evidences supporting the interaction between excitotoxicity and oxidative stress in ALS pathogenesis, the initial pathological 'trigger' for these two processes remains distinct: in fact, while excitotoxicity is generally due to increased extracellular glutamate concentrations and subsequent excessive stimulation of glutamate receptors, an imbalance between the production of ROS (arising from oxidative phosphorylation in mitochondria, activity of oxidative enzymes and reduced metal ions in the cytosol; Barber et al., 2006) and the ability of the cells to remove them is, instead, the typical source of oxidative stress. Differences are also found in the cellular targets as massive ionic influx, activation of Ca^{2+}-dependent enzymatic pathways, energy consumption (due to overactivity of the cellular pumps acting to restore ionic balance) and mitochondria dysfunction are typical consequences of excitotoxicity (Doble, 1999; Van Den Bosch et al., 2006), while ROS usually damage DNA, proteins, membrane lipids and mitochondria (Barber et al., 2006). Therefore, it is not surprising that the electrophysiological signatures of an excitotoxic and oxidative insult to HMs are dissimilar. Recently, Nistri et al. (2010) have reported that also in the *in vitro* spinal cord (used as a model of spinal cord injury) excitotoxicity (kainate-induced) and metabolic disregulation (pathological medium, i.e. hypoxic / aglycemic solution containing toxic radicals) are characterized by distinct electrophysiological and molecular responses: in fact, while kainate always suppressed locomotor network activity, producing large gray matter damage mediated by PARP-1 dependent cell death pathway (Parthanatos; Kuzhandaivel et al., 2010a), exposure to the pathological medium only depressed locomotor network activity as damage mainly concerned white matter with activation of caspase-mediated death processes (Kuzhandaivel et al., 2010b). However, when kainate and pathological medium were combined together, they evoked extensive and irreversible lesion to the spinal cord (Taccola et al., 2008; Nistri et al., 2010). Although in the present study we did not investigate the effects of co-application of TBOA and H_2O_2, we can envisage a synergy of action if administered together. Since we found that both excitotoxic and oxidative challenges induced early expression of the distress factor ATF-3, the identification of the effector(s) downstream to its activation might disclose useful targets to stop ALS-related pathological processes at their very beginning. Depending on the specific case of the ALS (familial or sporadic), cell death might occur as the result of a single insult or through a combination of mechanisms, including excitotoxicity and oxidative stress. It is, therefore, not surprising that dissecting causes and effects is not a simple matter. Thus,

although our data show interesting and previously unreported changes in motoneuron and glia associated with excitotoxic and oxidative distress in an ALS-related model, new investigations and approaches are needed for an comprehensive understanding of the pathogenesis of this disease.

6. Final conclusions: implications of early pathophysiology of amyotrophic lateral sclerosis

ALS is a fatal and complex neurodegenerative disease whose diagnosis (in the absence of any established biological marker) is based on the presence of characteristic clinical findings in conjunction with investigations to exclude "ALS-mimic" syndromes (Silani et al., 2011b), with the final recognition based on postmortem tissue analysis. The neuropathological results obtained from human ALS autopsy cases provided fundamental observations for recognizing ALS-related histo-pathological hallmarks in humans. However, such cases represent only the terminal stage of the disease (which at the time of diagnosis has already been active and disseminated throughout the motor system). As a consequence, human autopsy cases alone yield little insight into potential therapies for ALS, calling for experimental models that can help in clarifying how and why ALS motoneurons are impaired at each clinical stage from disease onset to death (Kato, 2008). Recent reviews have highlighted the importance of *in vitro* rodent preparations to analyze the motoneuron degeneration process in detail and to test preclinical therapeutic attempts (Boillée et al., 2006; Kato, 2008). As the application of the patch-clamp technique to brainstem slices from adult rodents is exceptionally difficult (Jaiswal & Keller, 2009), in the present study we used neonatal rat motoneurons, a model which inevitably has certain limitations: first, it remains to be established whether mechanisms analogous to the ones reported here, might be applicable also to adult motoneurons (though, in the case of TBOA, it seems feasible as glutamate uptake is already expressed in the neonatal brain; Danbolt, 2001); second, we were unable to follow up the long term (days) evolution of damage because survival of *in vitro* brain slices is restricted to several hours. Nevertheless, our first attempt was to investigate how motoneurons are damaged by overactivity of the glutamatergic system mimicking the putative ALS-related raise in endogenous glutamate (which evoked patchy motoneuron damage) rather than producing

wide-spread excitotoxicity (using, for example, glutamate, AMPA or kainate). We were able to show how blocking glutamate uptake affected motoneurons and glia through a process which evolved from early signs of distress to delayed cell loss; this time-window, allowed testing the effects of riluzole applied early after the starting of the pathological insult, demonstrating effective protection against motoneurons and glia alterations. Moreover, we demonstrated that different pathological ALS-related factors (excitotoxicity and oxidative stress), despite bearing different electrophysiological signatures, may share a common pathway of distress: further investigations of such intracellular pathways might help in disclosing new important targets for potential neuroprotection.

References

Adachi T, Huxtable AG, Fang X and Funk GD (2010) Substance P modulation of hypoglossal motoneuron excitability during development: changing balance between conductances. J Neurophysiol. 104, 854-72.

Ahn HS, Choi JS, Choi BH, Kim MJ, Rhie DJ, Yoon SH, Jo YH, Kim MS, Sung KW and Hahn SJ (2005). Inhibition of the cloned delayed rectifier K+ channels, Kv1.5 and Kv3.1, by riluzole. Neurosci. 133, 1007-1019.

Altschuler SM, Bao X and Miselis RR (1994). Dendritic architecture of hypoglossal motoneurons projecting to extrinsic tongue musculature in the rat. J Comp Neurol. 342, 538-550.

Anderson CM, Bridges RJ, Chamberlin AR, Shimamoto K, Yasuda- Kamatani Y and Swanson RA (2001). Differing effects of substrate and non-substrate transport inhibitors on glutamate uptake reversal. J Neurochem. 79, 1207-1216.

Azbill RD, Mu X and Springer JE (2000). Riluzole increases high-affinity glutamate uptake in rat spinal cord synaptosomes. Brain Res. 871, 175-180.

Bakels R and Kernell D (1993). Matching between motoneurone and muscle unit properties in rat medial gastrocnemius. J Physiol. 463, 307-24.

Barber SC, Mead RJ and Shaw PJ (2006). Oxidative stress in ALS: A mechanism of neurodegeneration and a therapeutic target. Biochim Biophys Acta. 1762, 1051-1067.

Barnard EA, Sutherland M, Zaman S, Matsumoto M, Nayeem N, Green T, Darlison MG and Bateson AN (1993). Multiplicity, structure, and function in GABAA receptors. Ann N Y Acad Sci. 707, 116-125.

Bayliss DA, Viana F and Berger AJ(1992) Mechanisms underlying excitatory effects of thyrotropin-releasing hormone on rat hypoglossal motoneurons in vitro. J Neurophysiol. 68, 733-745.

Bayliss DA, Viana F, Kanter RK, Szymeczek-Seay CL, Berger AJ and Millhorn DE (1994a). Early postnatal development of thyrotropin-releasing hormone (TRH) expression, TRH receptor binding, and TRH responses in neurons of rat brainstem. J Neurosci. 14, 821-833.

Bayliss DA, Viana F, Bellingham MC and Berger AJ (1994b). Characteristics and postnatal development of a hyperpolarization-activated inward current in rat hypoglossal motoneurons in vitro. J Neurophysiol. 71, 119-128.

Bayliss DA, Umemiya M and Berger AJ (1995). Inhibition of N- and P-type calcium currents and the after-hyperpolarization in rat motoneurones by serotonin. J Physiol. 485, 635-647.

Bellingham MC and Berger AJ (1996). Presynaptic depression of excitatory synaptic inputs to rat hypoglossal motoneurons by muscarinic M2 receptors. J Neurophysiol. 76, 3758–3770.

Bellingham MC and Funk GD (2000). Cholinergic modulation of res- piratory brain-stem neurons and its function in sleep-wake state determination. Clin Exp Pharmacol Physiol. 27, 132–137.

Berger AJ, Bayliss DA and Viana F (1992). Modulation of neonatal rat hypoglossal motoneuron excitability by serotonin. Neurosci Lett. 143, 164-168.

Berger AJ, Bayliss DA, Bellingham MC, Umemiya M and Viana F (1995). Postnatal development of hypoglossal motoneuron intrinsic properties. Adv Exp Med Biol. 381, 63-71.

Berger AJ, Bayliss DA and Viana F (1996). Development of hypoglossal motoneurons. J Appl Physiol. 81, 1039-1048.

Berger AJ (2000). Determinants of respiratory motoneuron output. Respir Physiol. 122, 259-269.

Bogdanov M, Brown RH, Matson W, Smart R, Hayden D, O'Donnell H, Flint Beal M and Cudkowicz M (2000). Increased oxidative damage to DNA in ALS patients. Free Radic Biol Med. 29, 652-658.

Boillée S, Yamanaka K, Lobsiger CS, Copeland NG, Jenkins NA, Kassiotis G, Kollias G and Cleveland DW (2006). Onset and progression in inherited ALS determined by motor neurons and microglia. Science. 312, 1389-1392.

Boone TB and Aldes LD (1984). The ultrastructure of two distinct neuron populations in the hypoglossal nucleus of the rat. Exp Brain Res. 54, 321-326.

Borke RC, Nau, ME and Ringler RL (1983) Brain stem afferents of hypoglossal neurons in the rat. Brain Res. 269, 47-55.

Bruijn LI, Becher MW, Lee MK, Anderson KL, Jenkins NA, Copeland NG, Sisodia SS, Rothstein JD, Borchelt DR, Price DL and Cleveland DW (1997). ALS-linked SOD1 mutant G85R mediates damage to astrocytes and promotes rapidly progressive disease with SOD1-containing inclusions. Neuron. 18, 327-338.

Bruijn LI, Miller TM and Cleveland DW (2004). Unraveling the mechanisms involved in motor neuron degeneration in ALS. Annu Rev Neurosci. 27, 723-749.

Chang G, Guo Y, Jia Y, Duan W, Li B, Yu J and Li C (2010). Protective effect of combination of sulforaphane and riluzole on glutamate-mediated excitotoxicity. Biol Pharm Bull. 33, 1477, 1483.

Cheah BC, Vucic S, Krishnan AV and Kiernan MC (2010). Riluzole, neuroprotection and amyotrophic lateral sclerosis. Curr Med Chem. 17, 1942-1959.

Chen B P, Liang G, Whelan J and Hai T (1994). ATF3 and ATF3 delta Zip. Transcriptional repression versus activation by alterna- tively spliced isoforms. J. Biol Chem. 26915819-15826.

Cheramy A, Barbeito L, Godeheu G and Glowinski J (1992), Riluzole inhibits the release of glutamate in the caudate nucleus of the cat in vivo. Neurosci Len. 147, 209-212.

Chiò A, Benzi G, Dossena M, Mutani R and Mora G (2005). Severely increased risk of amyotrophic lateral sclerosis among Italian professional football players. Brain. 128, 472-476.

Chung YH, Joo KM, Lee YJ, Shin DH and Cha CI (2004). Reactive astrocytes express PARP in the central nervous system of SOD(G93A) transgenic mice. Brain Res. 1003:199-204.

Cifra A, Nani F, Sharifullina E and Nistri A (2009). A repertoire of rhythmic bursting produced by hypoglossal motoneurons in physiological and pathological conditions. Philos. Trans. R. Soc. Lond. B: Biol. Sci. 364, 2493–2500.

Cifra A, Nani F and Nistri A (2011a). Riluzole is a potent drug to protect neonatal rat hypoglossal motoneurons in vitro from excitotoxicity due to glutamate uptake block. Eur J Neurosci. 33, 899-913.

Cifra A, Nani F and Nistri A (2011b). Respiratory motoneurons and pathological conditions: Lessons from hypoglossal motoneurons challenged by excitotoxic or oxidative stress. Respir Physiol Neurobiol. 179, 89-96

Cifra A, Mazzone GL, Nani F, Nistri A and Mladinic M (2011c). Postnatal developmental profile of neurons and glia in motor nuclei of the brainstem and spinal cord, and its comparison with organotypic slice cultures. In press.

Clement AM, Nguyen MD, Roberts EA, Garcia ML, Boillée S, Rule M, McMahon AP, Doucette W, Siwek D, Ferrante RJ, Brown RH Jr, Julien JP, Goldstein LS and Cleveland DW (2003). Wild-type nonneuronal cells extend survival of SOD1 mutant motor neurons in ALS mice. Science. 302, 113-117.

Cleveland DW and Rothstein JD (2001). From Charcot to Lou Gehrig: deciphering selective motor neuron death in ALS. Nat Rev Neurosci. 2, 806-819.

Coderre TJ, Kumar N, Lefebvre CD and Yu JS (2007). A comparison of the glutamate release inhibition and anti-allodynic effects of gabapentin, lamotrigine, and riluzole in a model of neuropathic pain. J Neurochem. 100, 1289-1299.

Cooper MN (1981). The hypoglossal nucleus of the primate: a Golgi study. Neurosci Lett. 21, 249-254.

Cox PA, Banack SA and Murch SJ (2003). Biomagnification of cyanobacterial neurotoxins and neurodegenerative disease among the Chamorro people of Guam. Proc Natl Acad Sci USA. 100, 13380-13383.

Crill WE (1996). Persistent sodium current in mammalian central neurons. Annu Rev Physiol. 58, 349-362.

Cunningham ET and Jr. Sawchenko PE (2000). Dorsal medullary pathways subserving oromotor reflexes in the rat: implications for the central neural control of swallowing. J Comp Neurol. 417, 448-466.

Danbolt NC (2001). Glutamate uptake. Prog Neurobiol. 65, 1-105.

Darbon P, Yvon C, Legrand JC and Streit J (2004). INaP underlies intrinsic spiking and rhythm generation in networks of cultured rat spinal cord neurons. Eur J Neurosci. 20, 976-988.

Di Giorgio FP, Carrasco MA, Siao MC, Maniatis T and Eggan K (2007). Non-cell autonomous effect of glia on motor neurons in an embryonic stem cell-based ALS model. Nat Neurosci. 10, 608-614.

Dobbins EG and Feldman JL (1995). Differential innervation of protruder and retractor muscles of the tongue in rat. J Comp Neurol. 357, 376-394.

Doble A, Hubert JP and Blanchard JC (1992). Pertussis toxin pretreatment abolishes the inhibitory effect of riluzole and carbachol on aspartate art ate release from cerebellar granule cells. Neurosci Lett, 140, 251-254.

Doble A (1999) The role of excitotoxicity in neurodegenerative disease: implications for therapy. Pharmacol Ther. 81, 63-221.

Donato R and Nistri A (2000). Relative contribution by GABA or glycine to Cl-mediated synaptic transmission on rat hypoglossal motoneurons in vitro. J Neurophysiol. 84, 2715-2724.

Donato R, Lape R and Nistri A (2003). Pre and postsynaptic effects of metabotropic glutamate receptor activation on neonatal rat hypoglossal motoneurons. Neurosci Lett. 338, 9-12.

Dutschmann M and Paton JF (2003). Whole cell recordings from respiratory neurones in an arterially perfused in situ neonatal rat preparation. Exp Physiol. 88, 725-732.

Dunlop J, Beal McIlvain H, She Y and Howland DS (2003). Impaired spinal cord glutamate transport capacity and reduced sensitivity to riluzole in a transgenic superoxide dismutase mutant rat model of amyotrophic lateral sclerosis. J Neurosci. 23, 1688-1696.

Duprat F, Lesage F, Patel AJ, Fink M, Romey G and Lazdunski M (2000). The neuroprotective agent riluzole activates the two P domain K+ channels TREK-1 and TRAAK. Mol Pharmacol. 57, 906-912.

Essin K, Nistri A and Magazanik L (2002). Evaluation of GluR2 subunit involvement in AMPA receptor function of neonatal rat hypoglossal motoneurons. Eur J Neurosci. 15, 1899-1906.

Estevez AG, Stutzmann JM and Barbeito L (1995). Protective effect of riluzole on excitatory amino acid-mediated neurotoxicity in motoneuron-enriched cultures. Eur J Pharmacol. 280, 47-53.

Farber NB, Jiang XP, Heinkel C and Nemmers B (2002). Antiepileptic drugs and agents that inhibit voltage-gated sodium channels prevent NMDA antagonist neurotoxicity. Mol Psychiatry. 7, 726-733.

Fay RA and Norgren R (1997). Identification of rat brainstem multisynaptic connections to the oral motor nuclei using pseudorabies virus. III. Lingual muscle motor systems. Brain Res Brain Res Rev. 25, 291-311.

Feldman JL and Del Negro CA (2006). Looking for inspiration: new perspectives on respiratory rhythm. Nat Rev Neurosci. 7, 232-242.

Ferrante RJ, Browne SE, Shinobu LA, Bowling AC, Baik MJ, MacGarvey U, Kowall NW, Brown Jr. RH and Beal MF (1997). Evidence of increased oxidative damage in both sporadic and familial amyotrophic lateral sclerosis. J Neurochem. 69, 2064-2074.

Fray AE, Ince PG, Banner SJ, Milton ID, Usher PA, Cookson MR and Shaw PJ (1998). The expression of the glial glutamate transporter protein EAAT2 in motor neuron disease: an immunohistochemical study. Eur J Neurosci. 10, 2481-2489.

Frizzo ME, Dall'Onder LP, Dalcin KB and Souza DO (2004). Riluzole enhances glutamate uptake in rat astrocyte cultures. Cell Mol Neurobiol. 24, 123-128.

Fumagalli E, Funicello M, Rauen T, Gobbi M and Mennini T (2008). Riluzole enhances the activity of glutamate transporters GLAST, GLT1 and EAAC1. Eur J Pharmacol. 578, 171-176.

Funk GD, Smith JC and Feldman JL (1993). Generation and transmission of respiratory oscillations in medullary slices: role of excitatory amino acids. J Neurophysiol. 70, 1497-1515.

García Del Caño G, Millán LM, Gerrikagoitia I, Sarasa M and Matute C (1999). Ionotropic glutamate receptor subunit distribution on hypoglossal motoneuronal pools in the rat. J Neurocytol. 28, 455-468.

Gardiner PF (1993). Physiological properties of motoneurones innervating different muscle unit types in rat gasctrocnemius. J Neurophysiol. 69,1160-1170.

Gestreau C, Dutschmann M, Obled S and Bianchi AL (2005). Activation of XII motoneurons and premotor neurons during various oropharyngeal behaviors. Respir Physiol Neurobiol. 147, 159-176.

Green JD and Negishi K (1963). Membrane potentials in hypoglossal motoneurons. J Neurophysiol. 26, 835-856.

Greenway MJ, Andersen PM, Russ C, Ennis S, Cashman S, Donaghy C, Patterson V, Swingler R, Kieran D, Prehn J, Morrison KE, Green A, Acharya KR, Brown R. H and Hardiman O (2006). ANG mutations segregate with familial and 'sporadic' amyotrophic lateral sclerosis. Nat Genet. 38, 411-413.

Greer JJ, Smith JC and Feldman JL (1991). Role of excitatory amino acids in the generation and transmission of respiratory drive in neonatal rat. J Physiol. 437,727-749.

Groeneveld GJ, van Kan HJ, Lie-A-Huen L, Guchelaar HJ and van den Berg LH (2008). An association study of riluzole serum concentration and survival and disease progression in patients with ALS. Clin Pharmacol Ther. 83, 718-722.

Gurney ME, Pu H, Chiu AY, Dal Canto MC, Polchow CY, Alexander DD, Caliendo J, Hentati A, Kwon YW, Deng HX, Chen WJ, Zhai P, Sufit RL and Siddique T (1994). Motor neuron degeneration in mice that express a human Cu,Zn superoxide dismutase mutation. Science. 264, 1772-1775.

Guzmán-Lenis MS, Navarro X and Casas C (2009). Drug screening of neuroprotective agents on an organotypic-based model of spinal cord excitotoxic damage. Restor Neurol Neurosci. 27, 335-349.

Haddad GG, Donnelly DF and Getting PA (1990). Biophysical properties of hypoglossal neurons in vitro: intracellular studies in adult and neonatal rats. J Appl Physiol. 69, 1509-1517.

Hai T, Wolfgang CD, Marsee DK, Allen AE, Sivaprasad U (1999). ATF3 and stress responses. Gene Expr. 7, 321-335.

Hai T and Hartman MG (2001). The molecular biology and nomenclature of the activating transcription factor／cAMP responsive element binding family of transcription factors: activating transcription factor proteins and homeostasis. Gene. 273, 1-11.

Harvey PJ, Li Y, Li X and Bennett DJ (2006). Persistent sodium currents and repetitive firing in motoneurons of the sacrocaudal spinal cord of adult rats. J Neurophysiol. 96, 1141-1157.

Hay M, McKenzie H, Lindsley K, Dietz N, Bradley SR, Conn PJ and Hasser EM (1999). Heterogeneity of metabotropic glutamate receptors in autonomic cell groups of the medulla oblongata of the rat. J Comp Neurol. 403, 486-501.

He Y, Benz A, Fu T, Wang M, Covey DF, Zorumski CF and Mennerick S (2002). Neuroprotective agent riluzole potentiates postsynaptic GABAA receptor function. Neuropharmacol. 42, 199-209.

Heath PR and Shaw PJ (2002). Update on the glutamatergic neurotransmitter system and the role of excitotoxicity in amyotrophic lateral sclerosis. Muscle Nerve. 26, 438-458.

Heneka MT, Rodrìguez JJ abd Verkhratsky A (2010). Neuroglia in neurodegeneration. Brain Res Rev. 63, 189-211.

Horner RL, Innes JA, Morrell MJ, Shea SA and Guz A (1994). The effect of sleep on reflex genioglossus muscle activation by stimuli of negative airway pressure in humans. J Physiol. 476, 141-151.

Horner RD, Kamins KG, Feussner JR, Grambow SC, Hoff-Lindquist J, Harati Y, Mitsumoto H, Pascuzzi R, Spencer PS, Tim R, Howard D, Smith TC, Ryan MA, Coffman CJ and Kasarskis EJ (2003). Occurrence of amyotrophic lateral sclerosis among Gulf War veterans. Neurology. 61, 742-749.

Horner RL (2007). Respiratory motor activity: influence of neuromodulators and implications for sleep disordered breathing. Can J Physiol Pharmacol. 85, 155-165.

Horner RL (2008). Neuromodulation of hypoglossal motoneurons during sleep. Respir. Physiol. Neurobiol. 164, 179-196.

Horner RL (2009). Emerging principles and neural sub- strates underlying tonic sleep-state-dependent influences on respiratory motor activity. Phil Trans R Soc B. 364, 2553-2564.

Howland DS, Liu J, She Y, Goad B, Maragakis NJ, Kim B, Erickson J, Kulik J, DeVito L, Psaltis G, DeGennaro LJ, Cleveland DW and Rothstein JD (2002). Focal loss of the glutamate transporter EAAT2 in a transgenic rat model of SOD1 mutant-mediated amyotrophic lateral sclerosis (ALS). PNAS U S A. 99, 604-609.

Huang CS, Song JH, Nagata K, Yeh JZ & Narahashi T (1997). Effects of the neuroprotective agent riluzole on the high voltage-activated calcium channels of rat dorsal root ganglion neurons. J Pharmacol Exp Ther. 282, 1280-1290.

Huang WL, Robson D, Liu MC, King VR, Averill S, Shortland PJ and Priestley JV (2006). Spinal cord compression and dorsal root injury cause up-regulation of activating transcription factor-3 in large-diameter dorsal root ganglion neurons. Eur J Neurosci. 23, 273-278.

Huang WL, George KJ, Ibba V, Liu MC, Averill S, Quartu M, Hamlyn PJ, and Priestley JV (2007). The characteristics of neuronal injury in a static compression model of spinal cord injury in adult rats. Eur J Neurosci. 25, 362-372.

Hubert JP, Delumeau JC, Glowinski J, Premont J and Doble A (1994). Antagonism by riluzole of entry of calcium evoked by NMDA and veratridine in rat cultured granule cells: evidence for a dual mechanism of action. Br J Pharmacol. 113, 261-267.

Ihara Y, Nobukuni K, Takata H and Hayabara T (2005). Oxidative stress and metal content in blood and cerebrospinal fluid of amyotrophic lateral sclerosis patients with and without a Cu,Zn-superoxide dismutase mutation. Neurol Res., 27, 105-108.

Ikonomidou C and Turski L (1995). Excitotoxicity and neurodegenerative diseases. Curr Opin Neurol. 8, 487-497.

Ilieva H, Polymenidou M and Cleveland DW (2009). Non-cell autonomous toxicity in neurodegenerative disorders: ALS and beyond. J Cell Biol. 187, 761-772.

Ince PG, Stout N, Shaw PJ, Slade J, Hunziker W, Heizmann C and Baimbridge KG (1993). Parvalbumin and calbi- ndin D-28K in human motor system and in motor neuron disease. Neuropathol Appl Neurobiol. 19, 291-299.

Jaiswal MK and Keller BU (2009). Cu / Zn superoxide dismutase typical for familial amyotrophic lateral sclerosis increases the vulnerability of mitochondria and perturbs Ca^{2+} homeostasis in $SOD1^{G93A}$ mice. Mol Pharmacol. 75, 478-489.

Jean A (2001). Brain stem control of swallowing: neuronal network and cellular mechanisms. Physiol Rev. 81, 929-969.

Jordan AS and White DP (2008). Pharyngeal motor control and the pathogenesis of obstructive sleep apnea. Respir Physiol Neurobiol. 160, 1-7.

Kabashi E, Valdmanis PN, Dion P, Spiegelman D, McConkey BJ, Vande Velde C, Bouchard JP, Lacomblez L, Pochigaeva K, Salachas F, Pradat PF, Camu W, Meininger V, Dupre N and Rouleau GA (2008). TARDBP mutations in individuals with sporadic and familial amyotrophic lateral sclerosis. Nat Genet. 40, 572-574.

Kato S (2008). Amyotrophic lateral sclerosis models and human neuropathol- ogy: similarities and differences. Acta Neuropathol. 115, 97-114.

Kawamata T, Akiyama H, Yamada T and McGeer PL (1992). Immunologic reactions in amyotrophic lateral sclerosis brain and spinal cord tissue. Am J Pathol. 140, 691-707.

Krammer EB, Rath T and Lischka MF (1979). Somatotopic organization of the hypoglossal nucleus: a HRP study in the rat. Brain Res. 170, 533-537.

Kubin L and Fenik V (2004). Pontine cholinergic mechanisms and their impact on respiratory regulation. Respir Physiol Neurobiol. 143, 235-249.

Kühnlein P, Gdynia HJ, Sperfeld AD, Lindner-Pfleghar B, Ludolph AC, Prosiegel M and Riecker A (2008). Diagnosis and treatment of bulbar symptoms in amyotrophic lateral sclerosis. Nat Clin Pract Neurol. 4, 366-374.

Kuhse J, Betz H and Kirsch J (1995). The inhibitory glycine receptor: architecture, synaptic localization and molecular pathology of a postsynaptic ion-channel complex. Curr Opin Neurobiol. 5, 318-323.

Kuo JJ, Lee RH, Zhang L and Heckman CJ (2006). Essential role of the persistent sodium current in spike initiation during slowly rising inputs in mouse spinal neurones. J Physiol. 574, 819-834.

Kuzhandaivel A, Nistri A and Mladinic M (2010a.). Kainate-mediated excitotoxicity induces neuronal death in the rat spinal cord in vitro via a PARP-1 dependent cell death pathway (parthanatos). Cell Mol Neurobiol. 30, 1001-1012.

Kuzhandaivel A, Margaryan G, Nistri A and Mladinic M (2010b). Extensive glial apoptosis develops early after hypoxic-dysmetabolic insult to the neonatal rat spinal cord in vitro. Neuroscience. 169, 325-338.

Kwiatkowski Jr. TJ, Bosco DA, Leclerc AL, Tamrazian E, Vanderburg CR, Russ C, Davis A, Gilchrist J, Kasarskis EJ, Munsat T, Valdmanis P, Rouleau GA, Hosler BA, Cortelli P, de Jong PJ, Yoshinaga Y, Haines JL, Pericak-Vance MA, Yan J, Ticozzi N, Siddique T, McKenna-Yasek D, Sapp PC, Horvitz HR, Landers JE and Brown Jr. RH (2009). Mutations in the FUS/TLS gene on chromosome 16 cause familial amyotrophic lateral sclerosis. Science. 323, 1205-1208.

Lacomblez L, Bensimon G, Leigh PN, Guillet P and Meininger V (1996). Dose-ranging study of riluzole in amyotrophic lateral sclerosis. Amyotrophic Lateral Sclerosis/Riluzole Study Group II. Lancet. 347, 1425-1431.

Lamanauskas N and Nistri A (2006). Persistent rhythmic oscillations induced by nicotine on neonatal rat hypoglossal motoneurons in vitro. Eur J Neurosci. 24, 2543-2556.

Lamanauskas N and Nistri A (2008). Riluzole blocks persistent Na^+ and Ca^{2+} currents and modulates release of glutamate via presynaptic NMDA receptors on neonatal rat hypoglossal motoneurons in vitro. Eur J Neurosci. 27, 2501-2514.

Lape R and Nistri A (1999). Voltage-activated K^+ currents of hypoglossal motoneurons in a brain stem slice preparation from the neonatal rat. J Neurophysiol. 81, 140-148.

Lape R and Nistri A (2000). Current and voltage clamp studies of the spike medium afterhyperpolarization of hypoglossal motoneurons in a rat brain stem slice preparation. J Neurophysiol. 83, 2987-2995.

Lape R and Nistri A (2001). Characteristics of fast $Na^{(+)}$ current of hypoglossal motoneurons in a rat brainstem slice preparation. Eur J Neurosci. 13, 763-772.

Laslo P, Lipski J, Nicholson LF, Miles GB and Funk GD (2000). Calcium binding proteins in motoneurons at low and high risk for degeneration in ALS. Neuroreport. 11, 3305-3308.

Laslo P, Lipski J and Funk GD (2001a). Differential expression of Group I metabotropic glutamate receptors in motoneurons at low and high risk for degeneration in ALS. Neuroreport. 12, 1903-1908.

Laslo P, Lipski J, Nicholson LF, Miles GB and Funk GD (2001b). GluR2 AMPA receptor subunit expression in motoneurons at low and high risk for degeneration in amyotrophic lateral sclerosis. Exp Neurol. 169, 461-471.

Launey T, Ivanov A, Kapus G, Ferrand N, Tarnawa I and Gueritaud JP (1999). Excitatory amino acids and synaptic transmission in embryonic rat brainstem motoneurons in organotypic culture. Eur J Neurosci. 11, 1324-1334.

Li YQ, Takada M, Kaneko T and Mizuno N (1997). Distribution of GABAergic and glycinergic premotor neurons projecting to the facial and hypoglossal nuclei in the rat. J Comp Neurol. 378, 283-294.

Lindwall C, Dahlin L, Lundborg G. and Kanje M (2004). Inhibition of c-Jun phosphorylation reduces axonal outgrowth of adult rat nodose ganglia and dorsal root ganglia sensory neurons. Mol Cell Neurosci. 27, 267-279.

Lips MB and Keller BU (1998). Endogenous calcium buffering in motoneurones of the nucleus hypoglossus from mouse, J Physiol. 511, 105-117.

Liu AY, Mathur R, Mei N, Langhammer CG, Babiarz B and Firestein BL (2011). Neuroprotective drug riluzole amplifies the heat shock factor 1 (HSF1)- and glutamate transporter 1 (GLT1)-dependent cytoprotective mechanisms for neuronal survival. J Biol Chem. 286, 2785-2794.

Lowe AA (1980). The neural regulation of tongue movements. Prog Neurobiol. 15, 295-344.

Malaspina A, Ngoh SF, Ward RE, Hall JC, Tai FW, Yip PK, Jones C, Jokic N, Averill SA, Michael-Titus AT and Priestley JV (2010). Activation transcription factor-3 activation and the development of spinal cord degeneration in a rat model of amyotrophic lateral sclerosis. Neuroscience. 169, 812-827.

Marchetti C, Pagnotta S, Donato R and Nistri A (2002). Inhibition of spinal or hypoglossal motoneurons of the newborn rat by glycine or GABA. Eur J Neurosci. 15, 975-983.

Marchetto MC, Muotri AR, Mu Y, Smith AM, Cezar GG and Gage FH (2008). Non-cell-autonomous effect of human SOD1 G37R astrocytes on motor neurons derived from human embryonic stem cells. Cell Stem Cell. 3, 649-657.

Marder E and Calabrese RL (1996). Principles of rhythmic motor pattern generation. Physiol Rev. 76, 687-717.

Martin D, Thompson MA and Nadler JV (1993). The neuroprotective agent riluzole inhibits release of glutamate and aspartate from slices of hippocampal area CA1. Eur J Pharmacol. 250, 473-476.

Matyja E, Nagańska E, Taraszewska A and Rafałowska J (2005). The mode of spinal motor neurons degeneration in a model of slow glutamate excitotoxicity in vitro. Folia Neuropathol. 43, 7-13.

Matyja E, Taraszewska A, Nagańska E, Rafałowska J and Gebarowska J (2006). Astroglial alterations in amyotrophic lateral sclerosis (ALS) model of slow glutamate excitotoxicity in vitro. Folia Neuropathol. 44, 183-90.

Mazzone GL and Nistri A (2011). Delayed neuroprotection by riluzole against excitotoxic damage evoked by kainate on rat organotypic spinal cord cultures. Neuroscience. 190, 318-327.

Medina L, Figueredo-Cardenas G, Rothstein JD and Reiner A (1996). Differential abundance of glutamate transporter subtypes in amyotrophic lateral sclerosis (ALS)-vulnerable versus ALS-resistant brain stem motor cell groups. Exp Neurol. 142, 287-295.

Miles GB, Dai Y and Brownstone RM (2005). Mechanisms underlying the early phase of spike frequency adaptation in mouse spinal motoneurones. J Physiol. 566, 519-532.

Mizuta I, Ohta M, Ohta K, Nishimura M, Mizuta E and Kuno S (2001). Riluzole stimulates nerve growth factor, brain-derived neurotrophic factor and glial cell line-derived neurotrophic factor synthesis in cultured mouse astrocytes. Neurosci Lett. 310, 117-120.

Moritz AT, Newkirk G, Powers RK and Binder MD (2007). Facilitation of somatic calcium channels can evoke prolonged tail currents in rat hypoglossal motoneurons. J Neurophysiol. 98, 1042-1047.

Mosfeldt Laursen A and Rekling JC (1989). Electrophysiological properties of hypoglossal motoneurons of guinea-pigs studied in vitro. Neuroscience. 30, 619-637.

Nagy D, Kato T and Kushner PD (1994). Reactive astrocytes are widespread in the cortical gray matter of amyotrophic lateral sclerosis. J Neurosci Res. 38, 336-347.

Nakagomi S, Suzuki Y, Namikawa K, Kiryu-Seo S and Kiyama H (2003). Expression of the activating transcription factor 3 prevents c-Jun N-terminal kinase-induced neuronal death by promoting heat shock protein 27 expression and Akt activation. J Neurosci. 23, 5187-5196.

Nakamura Y and Katakura N (1995). Generation of masticatory rhythm in the brainstem. Neurosci Res. 23, 1-19.

Nani F, Cifra A and Nistri A (2010). Transient oxidative stress evokes early changes in the functional properties of neonatal rat hypoglossal motoneurons in vitro. Eur J Neurosci. 31, 951-966.

Neumann M, Sampathu DM, Kwong LK, Truax AC, Micsenyi MC, Chou TT, Bruce J, Schuck T, Grossman M, Clark CM, McCluskey LF, Miller BL, Masliah E, Mackenzie IR, Feldman H, Feiden W, Kretzschmar HA, Trojanowski JQ and Lee VM (2006) Ubiquitinated TDP-43 in fronto-temporal lobar degeneration and amyotrophic lateral sclerosis. Science. 314, 130-133.

Nicholls JG and Paton JF (2009). Brainstem: neural networks vital for life. Philos Trans R Soc Lond B Biol Sci. 364, 2447-2451.

Nishimura AL, Mitne-Neto M, Silva HC, Richieri-Costa A, Middleton S, Cascio D, Kok F, Oliveira JR, Gillingwater T, Webb J, Skehel P and Zatz M (2004). A mutation in the vesicle-trafficking protein VAPB causes late-onset spinal muscular atrophy and amyotrophic lateral sclerosis. Am J Hum Genet. 75, 822-831.

Nistri A, Taccola G, Mladinic M, Margaryan G and Kuzhandaivel A (2010). Deconstructing locomotor networks with experimental injury to define their membership. Ann N Y Acad Sci. 1198, 242-251.

Núñez-Abades PA, Spielmann JM, Barrionuevo G and Cameron WE (1993). In vitro electrophysiology of developing genioglossal motoneurons in the rat. J Neurophysiol. 70, 1401-1411.

O'Brien JA and Berger AJ (1999). Cotransmission of GABA and glycine to brain stem motoneurons. J Neurophysiol. 82, 1638-1641.

O'Brien JA, Isaacson JS and Berger AJ (1997). NMDA and non-NMDA receptors are co-localized at excitatory synapses of rat hypoglossal motoneurons. Neurosci Lett. 227, 5-8.

Pagnotta SE, Lape R, Quitadamo C and Nistri A (2005). Pre- and postsynaptic modulation of glycinergic and GABAergic transmission by muscarinic receptors on rat hypoglossal motoneurons in vitro. Neuroscience. 130, 783-795.

Palecek J, Lips MB, Keller BU (1999). Calcium dynamics and buffering in motoneurones of the mouse spinal cord, J. Physiol. 520, 485-502.

Parkinson N, Ince PG, Smith MO, Highley R, Skibinski G, Andersen PM, Morrison KE, Pall HS, Hardiman O, Collinge J, Shaw PJ and Fisher EM (2006). ALS phenotypes with mutations in CHMP2B (charged multivesicular body protein 2B). Neurology. 67, 1074-1077.

Parkis MA, Bayliss DA and Berger AJ (1995). Actions of norepinephrine on rat hypoglossal motoneurons. J Neurophysiol. 74, 1911-1919.

Paton JF, Ramirez JM and Richter DW (1994). Mechanisms of respiratory rhythm generation change profoundly during early life in mice and rats. Neurosci Lett. 170, 167-70.

Paton JF and Richter DW (1995). Role of fast inhibitory synaptic mechanisms in respiratory rhythm generation in the maturing mouse. J Physiol. 484, 505-521.

Paton JF (1996). The ventral medullary respiratory network of the mature mouse studied in a working heart-brainstem preparation. J Physiol. 493, 819-31.

Peever JH, Shen L and Duffin J (2002). Respiratory pre-motor control of hypoglossal motoneurons in the rat. Neuroscience. 110, 711-722.

Peluffo H, Estevez A, Barbeito L and Stutzmann JM (1997). Riluzole promotes survival of rat motoneurons in vitro by stimulating trophic activity produced by spinal astrocyte monolayers. Neurosci Lett. 228, 207-211.

Philips T and Robberecht W (2011). Neuroinflammation in amyotrophic lateral sclerosis: role of glial activation in motor neuron disease. Lancet Neurol. 10, 253-263.

Powers RK and Binder MD (2003). Persistent sodium and calcium currents in rat hypoglossal motoneurons. J Neurophysiol. 89, 615-624.

Pratt J, Rataud J, Bardot F, Roux M, Blanchard JC, Laduron PM and Stutzmann JM (1992). Neuroprotective actions of riluzole in rodent models of global and focal cerebral ischaemia. Neurosci Lett. 140, 225-230.

Purvis LK and Butera RJ (2005). Ionic current model of a hypoglossal motoneuron. J Neurophysiol. 93, 723-733.

Quitadamo C, Fabbretti E, Lamanauskas N and Nistri A (2005). Activation and desensitization of neuronal nicotinic receptors modulate glutamatergic transmission on neonatal rat hypoglossal motoneurons. Eur J Neurosci. 22, 2723-2734.

Ramirez JM, Quellmalz UJ and Wilken B (1997). Developmental changes in the hypoxic response of the hypoglossus respiratory motor output in vitro. J. Neurophysiol. 78, 383-392.

Rao SD and Weiss JH (2004). Excitotoxic and oxidative cross-talk between motor neurons and glia in ALS pathogenesis. Trends Neurosci. 27, 17-23.

Rao SD, Yin HZ and Weiss JH (2003). Disruption of glial glutamate transport by reactive oxygen species produced in motor neurons. J. Neurosci. 23, 2627-2633.

Reiner A, Medina L, Figuerdo-Cardenas G and Anfinson S (1995). Brainstem motoneuron pools that are selectively resistant in amyotrophic lateral sclerosis are preferentially enriched in parvalbumin: evidence from monkey brainstem for a calcium-mediated mechanism in sporadic ALS. Exp Neurol. 131, 239-250.

Rekling JC (1990). Excitatory effects of thyrotropin-releasing hormone (TRH) in hypoglossal motoneurons. Brain Res. 510, 175-179.

Rekling JC (1992). Interaction between thyrotropin-releasing hormone (TRH) and NMDA-receptor-mediated responses in hypoglossal motoneurones. Brain Res. 578, 289-296.

Rekling JC, Funk GD, Bayliss DA, Dong XW and Feldman JL (2000). Synaptic control of motoneuronal excitability. Physiol Rev. 80, 767-852.

Remmers JE, deGroot WJ, Sauerland EK and Anch AM (1978). Pathogenesis of upper airway occlusion during sleep. J Appl Physiol. 44, 931-938.

Roda F, Gestreau C and Bianchi AL (2002). Discharge patterns of hypoglossal motoneurons during fictive breathing, coughing, and swallowing. J Neurophysiol. 87, 1703-1711.

Rosen DR, Siddique T, Patterson D, Figlewicz DA, Sapp P, Hentati A, Donaldson D, Goto J, O'Regan JP, Deng HX, Rahmani Z, Krizus A, McKenna-Yasek D, Cayabyab A, Gaston SM, Berger R, Tanzi RE, Halperin JJ, Herzfeldt B, Van den Bergh R, Hung W, Bird T, Deng G, Mulder DW, Smyth C, Laing NG, Soriano E, Pericak-Vance MA, Haines J, Rouleau GA, Gusella JS, Horvitz HR and Brown Jr. RH (1993). Mutations in Cu/Zn superoxide dismutase gene are associated with familial amyotrophic lateral sclerosis. Nature. 362, 59-62.

Rothstein JD, Tsai G, Kuncl RW, Clawson L, Cornblah DR, Drachman DB, Pestronk A, Stauch BL and Coyle JT (1990). Abnormal excitatory amino acid metabolism in amyotrophic lateral sclerosis. Ann Neurol. 28:18-25.

Rothstein JD, Martin LJ and Kuncl RW (1992). Decreased glutamate transport by the brain and spinal cord in amyotrophic lateral sclerosis. N Engl J Med. 326, 1464-1468.

Rothstein JD, Jin L, Dykes-Hoberg M and Kuncl RW (1993).. Chronic inhibition of glutamate uptake produces a model of slow neurotoxicity. PNAS U S A. 90, 6591-6595.

Rothstein JD, Van Kammen M, Levey AI, Martin LJ and Kuncl RW (1995). Selective loss of glial glutamate transporter GLT-1 in amyotrophic lateral sclerosis. Ann Neurol. 38, 73-84.

Rothstein JD and Kuncl RW (1995). Neuroprotective strategies in a model of chronic glutamate-mediated motor neuron toxicity. J Neurochem. 65, 643-651.

Rowland LP and Shneider NA (2001). Amyotrophic lateral sclerosis. N Engl J Med. 344, 1688-1700.

Russo RE and Hounsgaard J (1999). Dynamics of intrinsic electrophysiological properties in spinal cord neurones. Prog Biophys Mol Biol. 72, 329-365.

Sasaki S, Komori T and Iwata M (2000). Excitatory amino acid transporter 1 and 2 immunoreactivity in the spinal cord in amyotrophic lateral sclerosis. Acta Neuropathol. (Berl). 100, 138-144.

Schwartz G and Fehlings MG (2002). Secondary injury mechanisms of spinal cord trauma: a novel therapeutic approach for the management of secondary pathophysiology with the sodium channel blocker riluzole. Prog Brain Res. 137, 177-190.

Schiffer D, Cordera S, Cavalla P and Migheli A (1996). Reactive astrogliosis of the spinal cord in amyotrophic lateral sclerosis. J Neurol Sci. 139 Suppl, 27-33.

Selvaratnam SR, Parkis MA and Funk GD. Developmental modulation of mouse hypoglossal nerve inspiratory output in vitro by noradrenergic receptor agonists. Brain Res. 805, 104-15.

Sen I, Nalini A, Joshi NB and Joshi PG (2005). Cerebrospinal fluid from amyotrophic lateral sclerosis patients preferentially elevates intracellular calcium and toxicity in motor neurons via AMPA/kainate receptor. J Neurol Sci. 235, 45-54.

Shao XM and Feldman JL (2005). Cholinergic neurotransmission in the preBötzinger Complex modulates excitability of inspiratory neurons and regulates respiratory rhythm. Neuroscience. 130, 1069-1081.

Sharifullina E and Nistri A (2006). Glutamate uptake block triggers deadly rhythmic bursting of neonatal rat hypo- glossal motoneurons. J Physiol. 572, 407-423.

Sharifullina E, Ostroumov K, Grandolfo M and Nistri A (2008). N-methyl-D-aspartate triggers neonatal rat hypo- glossal motoneurons in vitro to express rhythmic bursting with unusual Mg^{2+} sensitivity. Neuroscience 154, 804-820.

Shaw CA and Höglinger GU (2008). Neurodegenerative diseases: neurotoxins as sufficient etiologic agents? Neuromol Med. 10, 1-9.

Shaw PJ, Forrest V, Ince PG, Richardson JP and Wastell HJ (1995a). CSF and plasma amino acid levels in motor neurone disease: elevation of CSF glutamate in a subset of patients. Neurodegeneration. 4, 209–216.

Shaw PJ, Ince PG, Falkous G and Mantle D (1995b). Oxidative damage to protein in sporadic motor neuron disease spinal cord. Ann Neurol. 38, 691-695.

Shaw PJ, Williams TL, Slade JY, Eggett CJ and Ince PG (1999). Low expression of GluR2 AMPA receptor subunit protein by human motor neurons. Neuroreport. 10, 261-265.

Shaw PJ (2005). Molecular and cellular pathways of neurodegeneration in motor neurone disease. J Neurol Neurosurg Psychiatry. 76, 1046-1057.

Sheldon AL, and Robinson MB (2007). The role of glutamate transporters in neurodegenerative diseases and potential opportunities for intervention. Neurochem Int. 51, 333-355.

Silani V, Meininger V, Fornai F (2001a). Introducing Amyotrophic lateral sclerosis. Arch Ital Biol. 149, 1-4.
Silani V, Messina S, Poletti B, Morelli C, Doretti A, Ticozzi N and Maderna L (2011b). The diagnosis of Amyotrophic lateral sclerosis in 2010. Arch Ital Biol. 149, 5-27.

Singer JH, Bellingham MC and Berger AJ (1996). Presynaptic inhibition of glutamatergic synaptic transmission to rat motoneurons by serotonin. J Neurophysiol. 76, 799-807.

Singer JH and Berger AJ (2000). Development of inhibitory synaptic transmission to motoneurons. Brain Res Bull. 53, 553-560.

Smith JC and Feldman JL (1987). In vitro brainstem-spinal cord preparations for study of motor systems for mammalian respiration and locomotion. J Neurosci Methods. 21, 321-333.

Smith JC, Greer JJ, Liu GS and Feldman JL. (1990). Neural mechanisms generating respiratory pattern in mammalian brain stem-spinal cord in vitro. I. Spatiotemporal patterns of motor and medullary neuron activity. J Neurophysiol. 64, 1149-1169.

Smith JC, Ellenberger H, Ballanyi K, Richter DW and Feldman JL. (1991). Pre-Bötzinger complex: a brain stem region that may generate respiratory rhythm in mammals. Science. 254, 726-729.

Smith JC, Abdala AP, Koizumi H, Rybak IA, Paton JF. (2007). Spatial and functional architecture of the mammalian brain stem respiratory network: a hierarchy of three oscillatory mechanisms. J Neurophysiol. 98, 3370-3387.

Smittkamp SE, Spalding HN, Brown JW, Gupte AA, Chen J, Nishimune H, Geiger PC and Stanford JA (2010). Measures of bulbar and spinal motor function, muscle innervation, and mitochondrial function in ALS rats. Behav Brain Res. 211, 48-57.

Sokoloff AJ and Deacon TW (1992). Musculotopic organization of the hypoglossal nucleus in the cynomolgus monkey, Macaca fascicularis. J Comp Neurol. 324, 81-93.

Song JH, Huang CS, Nagata K, Yeh JZ and Narahashi T (1997). Differential action of riluzole on tetrodotoxin-sensitive and tetrodotoxin-resistant sodium channels. J Pharmacol Exp Ther. 282, 707-714.

Spreux-Varoquaux O, Bensimon G, Lacomblez L, Salachas F, Pradat PF, Le Forestier N, Marouan A, Dib M and Meininger V (2002). Glutamate levels in cerebrospinal fluid in amyotrophic lateral sclerosis: a reappraisal using a new HPLC method with coulometric detection in a large cohort of patients. J Neurol Sci. 193, 73-78.

Stefani A, Spadoni F and Bernardi G (1997). Differential inhibition by riluzole, lamotrigine, and phenytoin of sodium and calcium currents in cortical neurons: implications for neuroprotective strategies. Exp Neurol. 147, 115-122.

Strong MJ, Grace GM, Freedman M, Lomen-Hoerth C, Woolley S, Goldstein LH, Murphy J, Shoesmith C, Rosenfeld J, Leigh PN, Bruijn L, Ince P and Figlewicz D (2009). Consensus criteria for the diagnosis of frontotemporal cognitive and behavioural syndromes in amyotrophic lateral sclerosis. Amyotroph Lateral Scler. 10, 131-146.

Sumi T (1969). Functional differentiation of hypoglossal neurons in cats. Jpn J Physiol. 19, 55-67.

Suzue T (1984). Respiratory rhythm generation in the in vitro brain stem-spinal cord preparation of the neonatal rat. J Physiol. 354, 173-183.

Swash M and Ingram D (1988). Preclinical and subclinical events in motor neuron disease. J Neurol Neurosurg Psychiatry. 51, 165-168.

Taccola G, Margaryan G, Mladinic M and Nistri A (2008). Kainate and metabolic perturbation mimicking spinal injury differentially contribute to early damage of locomotor networks in the in vitro neonatal rat spinal cord. Neuroscience. 155, 538-555.

Takasu N and Hashimoto PH (1988). Morphological identification of an interneuron in the hypoglossal nucleus of the rat: a combined Golgi-electron microscopic study. J Comp Neurol. 271, 461-471.

Takata M (1993). Two types of inhibitory postsynaptic potentials in the hypoglossal motorneurons. Prog Neurobiol. 40, 385-411.

Talley EM, Sadr NN and Bayliss DA (1997). Postnatal development of serotonergic innervation, 5-HT1A receptor expression, and 5-HT responses in rat motoneurons. J Neurosci. 17, 4473-4485.

Talley EM, Lei Q, Sirois JE and Bayliss DA (2000). TASK-1, a two-pore domain K+ channel, is modulated by multiple neurotransmitters in motoneurons. Neuron. 25, 399-410.

Telgkamp P, Ramirez JM (1999). Differential responses of respiratory nuclei to anoxia in rhythmic brain stem slices of mice. J Neurophysiol. 82, 2163-2170.

Travers JB and Norgren R (1983). Afferent projections to the oral motor nuclei in the rat. J Comp Neurol. 220, 280-298.

Trotti D, Rossi D, Gjesdal O, Levy LM, Racagni G, Danbolt NC and Volterra A (1996). Peroxynitrite inhibits glutamate transporter subtypes. J Biol Chem. 271, 5976-5979.

Trotti D, Danbolt NC and Volterra A (1998). Glutamate transporters are oxidant vulnerable: a molecular link between oxidative and excitotoxic neurodegeneration? Trends Pharmacol Sci. 19, 328-334.

Trotti D, Rolfs A, Danbolt NC, Brown Jr. RH and Hediger MA (1999). SOD1 mutants linked to amyotrophic lateral sclerosis selectively inactivate a glial glutamate transporter. Nat. Neurosci. 2, 427-433.

Tsuchioka M, Hisaoka K, Yano R, Shibasaki C, Kajiatani N and Takebayashi M (2011). Riluzole-induced glial cell line-derived neurotrophic factor production is regulated through fibroblast growth factor receptor signaling in rat C6 glioma cells. Brain Res. 1384, 1-8.

Tsujino H, Kondo E, Fukuoka T, Dai Y, Tokunaga A, Miki K, Yonenobu K, Ochi T and Noguchi K (2000). Activating transcription factor 3 (ATF3) induction by axotomy in sensory and motoneurons: a novel neuronal marker of nerve injury. Mol Cell Neurosci.15, 170-182.

Umemiya M and Berger AJ (1994). Properties and function of low- and high-voltage-activated Ca2+ channels in hypoglossal motoneurons. J Neurosci. 14, 5652-5660.

Umemiya M and Berger AJ (1995a). Inhibition by riluzole of glycinergic postsynaptic currents in rat hypoglossal motoneurones. Br J Pharmacol. 116, 3227-3230.

Umemiya M and Berger AJ. (1995b). Presynaptic inhibition by serotonin of glycinergic inhibitory synaptic currents in the rat brain stem. J Neurophysiol. 73, 1192-1201.

Urbani A and Belluzzi O (2000). Riluzole inhibits the persistent sodium current in mammalian CNS neurons. Eur J Neurosci. 12, 3567-3574.

Valdmanis PN and Rouleau GA (2008). Genetics of familial amyotrophic lateral sclerosis. Neurology. 70, 144-152.

Van Damme P, Van Den Bosch L, Van Houtte E, Callewaert G and Robberecht W (2002). GluR2-dependent properties of AMPA receptors determine the selective vulnerability of motor neurons to excitotoxicity. J Neurophysiol. 88, 1279-1287.

Van Damme P, Bogaert E, Dewil M, Hersmus N, Kiraly D, Scheveneels W, Bockx I, Braeken D, Verpoorten N, Verhoeven K, Timmerman V, Herijgers P, Callewaert G, Carmeliet P, Van Den Bosch L and Robberecht W (2007). Astrocytes regulate GluR2 expression in motor neurons and their vulnerability to excitotoxicity. PNAS U S A. 104, 14825-14830.

Van Den Bosch L, Van Damme P, Bogaert E and Robberecht W (2006). The role of excitotoxicity in the pathogenesis of amyotrophic lateral sclerosis. Biochim Biophys Acta. 1762, 1068-1082.

Van Den Bosch L and Robberecht W (2008). Crosstalk between astrocytes and motor neurons: what is the message? Exp Neurol. 211, 1-6.

van Drongelen W, Koch H, Elsen FP, Lee HC, Mrejeru A, Doren E, Marcuccilli CJ, Hereld M, Stevens RL and Ramirez JM (2006). Role of persistent sodium current in bursting activity of mouse neocortical networks in vitro. J Neurophysiol. 96, 2564-2577.

Vanselow BK and Keller BU (2000). Calcium dynamics and buffering in oculomotor neurones from mouse that are particularly resistant during amyotrophic lateral sclerosis (ALS)-related motoneurone disease. J Physiol. 525, 433-445.

van Zundert B, Peuscher MH, Hynynen M, Chen A, Neve RL, Brown RH Jr, Constantine-Paton M and Bellingham MC (2008). Neonatal neuronal circuitry shows hyperexcitable disturbance in a mouse model of the adult-onset neurodegenerative disease amyotrophic lateral sclerosis. J Neurosci. 28, 10864-10874.

Viana F, Gibbs L and Berger AJ (1990). Double- and triple-labeling of functionally characterized central neurons projecting to peripheral targets studied in vitro. Neuroscience. 38, 829-841.

Viana F, Bayliss DA and Berger AJ (1993a). Multiple potassium conductances and their role in action potential repolarization and repetitive firing behavior of neonatal rat hypoglossal motoneurons. J Neurophysiol. 69, 2150-2163.

Viana F, Bayliss DA and Berger AJ (1993b). Calcium conductances and their role in the firing behavior of neonatal rat hypoglossal motoneurons. J Neurophysiol. 69, 2137-2149.

Viana F, Bayliss DA and Berger AJ (1994). Postnatal changes in rat hypoglossal motoneuron membrane properties. Neuroscience. 59, 131-148.

Vlug AS, Teuling E, Haasdijk ED, French P, Hoogenraad CC and Jaarsma D (2005). ATF3 expression precedes death of spinal motoneurons in amyotrophic lateral sclerosis SOD1 transgenic mice and correlates with c-Jun phosphorylation, CHOP expression, somato dendritic ubiquitination and Golgi fragmentation. Eur J Neurosci. 22, 1881-1894.

Volterra A, Trotti D, Tromba C, Floridi S and Racagni G (1994). Glutamate uptake inhibition by oxygen free radicals in rat cortical astrocytes. J Neurosci. 14, 2924-2932.

von Lewinski F, Fuchs J, Vanselow BK and Keller BU (2008). Low Ca^{2+} buffering in hypoglossal motoneurons of mutant SOD1 (G93A) mice. Neurosci Lett., 445, 224-228.

Vucic S and Kiernan MC (2006). Novel threshold tracking techniques suggest that cortical hyperexcitability is an early feature of motor neuron disease. Brain. 129, 2436-2446.

Wahl F and Stutzmann JM (1999). Neuroprotective effects of riluzole in neurotrauma models: a review. Acta Neurochir. 73, 103-110.

Wang F, Gerzanich V, Wells GB, Anand R, Peng X, Keyser K and Lindstrom J (1996). Assembly of human neuronal nicotinic receptor alpha5 subunits with alpha3, beta2, and beta4 subunits. J Biol Chem. 271, 17656-17665.

Wang SJ, Wang KY and Wang WC (2004). Mechanisms underlying the riluzole inhibition of glutamate release from rat cerebral cortex nerve terminals (synaptosomes). Neuroscience. 125, 191-201.

Wijesekera LC and Leigh PN (2009). Amyotrophic lateral sclerosis. Orphanet J Rare Dis. 3, 4-3.

Williams TL, Ince PG. Oakley AE and Shaw PJ (1996). An immunocytochemical study of the distribution of AMPA selective glutamate receptor subunits in the normal human motor system. Neuroscience. 74, 185-198.

Williams TL, Day NC, Ince PG, Kamboj RK and Shaw PJ (1997). Calcium permeable AMPA receptors: a molecular basis for selective vulnerability in motor neurone disease. Ann Neurol. 42, 200-207.

Wokke JH (1996). Riluzole. Lancet. 348, 795-799.

Wolfgang CD, Chen BP, Martindale JL, Holbrook NJ and Hai T (1997). gadd153/Chop10, a potential target gene of the transcrip- tional repressor ATF3. Mol Cell Biol. 17, 6700-6707.

Wu J, Tang T and Bezprozvanny I (2006). Evaluation of clinically relevant glutamate pathway inhibitors in in vitro model of Huntington's disease. Neurosci Lett. 407, 219-223.

Yasuda K, Robinson DM, Selvaratnam SR, Walsh CW, McMorland AJ and Funk GD (2001). Modulation of hypoglossal motoneuron excitability by NK1 receptor activation in neonatal mice in vitro. J Physiol. 534, 447-464.

Zeng J, Powers RK, Newkirk G, Yonkers M and Binder MD (2005). Contribution of persistent sodium currents to spike-frequency adaptation in rat hypoglossal motoneurons. J Neurophysiol. 93, 1035-1041.

Zona C, Siniscalchi A, Mercuri NB and Bernardi G (1998). Riluzole interacts with voltage-activated sodium and potassium currents in cultured rat cortical neurons. Neuroscience. 85, 931-938.